1. SPECTROMETER MEASUREMENTS OF THE RATES OF GAMMA RADIATION AND INTERNAL PAIR FORMATION FROM SOME NUCLEAR REACTIONS IN LIGHT NUCLEI

2. THEORY OF THE ENERGY LEVELS OF THE MIRROR NUCLEI, C^{13} AND N^{13}

Thesis by

Robert G. Thomas

In Partial Fulfillment of the Requirements

For the Degree of

Doctor of Philosophy

California Institute of Technology

Pasadena, California

1951

ACKNOWLEDGMENTS

The writer is grateful to Professor C. C. Lauritsen for being permitted to carry on research and study in his nuclear physics laboratory. He is particularly appreciative of the encouragement and active assistance of Professor T. Lauritsen with many of the experimental problems in this thesis and of the helpful suggestions and discussions from Professor R. F. Christy in connection with the theoretical problems. He is also indebted to Professors W. A. Fowler and C. C. Lauritsen for their helpful suggestions and discussions. He wishes to thank Mr. R. J. Mackin for his assistance with some of the experiments and calculations for Part II and Doctors V. K. Rasmussen and W. F. Hornyak for instructions in the techniques of beta-ray spectroscopy.

The writer was recipient of an AEC predoctoral fellowship, administered by the NRC, during the course of this work and is grateful to that organization for financial support. The laboratory work was assisted by the joint program of the ONR and AEC.

1. SPECTROMETER MEASUREMENT OF THE RATES OF GAMMA-RADIATION AND INTERNAL PAIR FORMATION FROM SOME REACTIONS IN LIGHT NUCLEI

ABSTRACT - PARTS I - III

In part III the measurements with a beta-ray spectrometer of the gamma-rays and internally-formed positrons from the reactions $C^{13}(dp)C^{14}$ and $C^{13}(dn)N^{14}$ are described; the energy levels of N^{14} and C^{14} are discussed. A measurement of the internally-formed positron spectra from the Be^{9} + d reactions is described, and an attempt is made to determine the multipolarity of the 2.87- and 3.38-Mev transitions from the ratio of the rates of pair emission to gamma radiation; the results are in agreement with electric-dipole assignments to the transitions. Also described is the measurement of the internal conversion electrons associated with the 0.871-Mev radiation from the $O^{16}(dp)O^{17}$ reaction; the result is shown to be consistent with an electric quadripole assignment to this transition.

In Part II methods are developed for analyzing the data of Part III. These include the measurement of absolute gamma-ray intensities by Compton conversion of the radiation in "thick" foils and photoelectric conversion in "thin" foils. Methods for analyzing internal-pair spectra and internal conversion spectra are given and several problems discussed. Measurements of the internal conversion coefficients of the 0.713-Mev transition of B^{10} and the 1.332-Mev transition of Ni^{60} are described.

Part I is concerned with the penetration of the secondary electrons through the converters in which they are produced. The effective stopping power of aluminum and beryllium are calculated for use in the Compton "thick" - converter method of measuring gamma-ray intensities developed in Part II. Also included is a discussion of the scattering of electrons in the converters.

2. ENERGY LEVELS OF THE MIRROR NUCLEI, N^{13} AND C^{13}

ABSTRACT PART IV

The low energy levels (< 6 Mev) of the mirror nuclei, N^{13} and C^{13}, are studied on the assumption that nn and pp nuclear forces are equal. By means of dispersion theory it is shown that the first excited states of these nuclei are $^2S_{1/2}$ and that the large displacement is due to their large reduced width and the difference in the extra-nuclear wave functions for the odd particle; the magnitude of the reduced widths suggests that a one-body type of interaction is involved between the odd particle and the C^{12} core. In particular, a square-well type of model gives a satisfactory account of the level shift, reduced widths, and the low-energy (< 1 Mev) scattering of neutrons by carbon. The $C^{12} + n$ s-wave interaction is also studied by means of the effective range theory. Some evidence is given that the second excited state of N^{13} is a doublet, one component of which appears at 3.68-Mev and the other at 3.90-Mev in C^{13}, and the 3.68-Mev component is most likely $^2P_{3/2}$ and the 3.90 ^2d. The reduced width of the ground states of N^{13} and C^{13}, as calculated from the knowledge of the s-wave $C^{12}(p\,\gamma)$ and $C^{12}(n\,\gamma)$ cross sections, is about 1/10 of the value expected for a familiar one-body type of interaction, but it is nearly equal to the reduced width of the 3.52-Mev level of N^{13}. This reduced width is used to calculate the ground-state level shift due to the difference in the extra-nuclear wave functions. The shift of the second pair of excited states, if they are $^2P_{3/2}$, can be about 1/3 accounted for as due to the difference of the extra-nuclear wave functions for the odd particle and about 1/3 as due to the difference in the electromagnetic spin-orbit interactions of the odd particle.

TABLE OF CONTENTS

TABLE OF CONTENTS

2. Energy Levels of the Mirror Nuclei, N^{13} and C^{13}

PART I.

The Passage of Fast Electrons Through Gamma-Ray Converters

1. Introduction

Gamma-radiation must be studied by the secondary effects which it produces. In the first two parts of this thesis we will develop methods for determining the energy and intensity of gamma-radiation by studying secondary conversion electrons with a beta-ray spectrometer. The second part will deal with the various processes by which gamma-radiation can produce secondary particles which can be counted. The first part will treat the kinetics of the conversion electrons in the converter material. It would seem logical to treat the conversion processes first; however, by treating the kinetics first it will be possible in the second part to derive, using the results of the first part, formulas which can be put to direct application for the analysis of the experimental data to be presented in the third and fourth chapters.

Figure (1) shows the geometry used to measure gamma-ray energies and intensities. Gamma-radiation from the source produces secondary electrons in a converter. These electrons are analyzed and detected by an axially symmetric beta-ray spectrometer. The spectrometer has been described by Hornyak, Lauritsen, and Rasmussen[1],[2],[3].

The efficiency of conversion is equal to

$$\sigma \, \Delta N \, \Omega \qquad , \Omega = \text{effective solid angle},$$

where σ is the cross section for the conversion process and N is the number of convertible electrons per unit area that can be accepted by the spectrometer at any particular field setting. If the effective spectrometer dispersion width in energy units is E, then, since

$$\Delta N = n \left(\frac{\Delta x}{\Delta E} \right) \Delta E$$

where Δx is the converter thickness from which electrons will reach the converter surface with the proper energy, and n is the number of convertible

electrons per unit volume, expression (1) becomes

$$\frac{\sigma}{\mu_{eff}} n \Delta E \Omega \qquad (3)$$

where $\mu_{eff} \equiv \frac{\Delta E}{\Delta x}$ is called the effective stopping power of the converter for the secondary electrons. From (3) it is apparent that a knowledge of the effective stopping power for conversion electrons is of fundamental importance in the study of gamma-radiation. In the second section we will determine the most-probable stopping power for beryllium and aluminum which are among the most appropriate materials in which to produce secondary Compton electrons; in the third section we will show how to determine an effective stopping power from the most-probable stopping power by means of Landau's theory of the distribution of energy losses; and in the fourth section we will consider the scattering of electrons in the converter and its possible influence on the determination of μ_{eff}.

2. Most-Probable Stopping Power for Fast Electrons.

The stopping power is defined as $\mu = \frac{\Delta E}{\Delta \ell}$ where ΔE is the amount of energy that an electron loses in traversing a distance $\Delta \ell$, which may not necessarily be straight. μ will have a distribution, and so it is necessary to characterize it by some feature such as average, median, or most-probable value. According to the straggling theory of Landau[4] or Bohr[5] the average energy loss will be roughly 35% greater than the most-probable energy loss; there is only a small probability for large energy losses but the net contribution of these large losses to the average is quite significant. For beta-ray spectrometer applications we will not be interested in these large losses so it will be more appropriate to consider the most-probable energy loss as the quantity of interest. Although we will eventually want an energy loss which is some effective value given by Landau's distribution theory, this value will lie closer to the most-probable value than to the average. Nearly all of the energy loss formulas treated in the literature pertain to the average loss; it happens to be the easiest quantity to compute. There are three

well-known formulas for the average energy loss: the Bethe-Bloch formula given in Heitler's book[6], the original Bohr formula[5], and the formula derived by Bethe in the Handbuch der Physik[6]. There is some uncertainty in the literature as to which of these formulas to use; according to Prof. Christy (unpublished) Bethe's derivation reduces to Bohr's formula if one is not interested in the violent energy losses. We will therefore use Bohr's formula, in particular, in the form that it is given in Landau's paper.

Bohr's stopping theory, as modified by Landau[7] to take into account straggling and by A. Bohr[8] to include polarization effects, gives for the most-probable stopping cross section

$$\mu_{mp}(\ell) \equiv \frac{\Delta E_{mp}}{\ell} = B\left[\ln \frac{B\ell 2m_0 v^2}{(I/\gamma)^2} - (1-F_p)\beta^2 + 0.37\right]$$

where

$$B = \frac{2\pi n e^4}{m_0 c^2 \beta^2} \quad ; \quad \beta = v/c \quad ; \quad \gamma = (1-\beta^2)^{-1/2} \quad ; \qquad (4)$$

and v = electron velocity;

I = average excitation potential including polarization effects,

t = electron path length,

F_p = fraction of atomic electrons which are essentially bound by polarization forces,

n = no. of electrons per unit volume, and

m_0 = electron rest mass.

Landau gives expression (4) with $F_p = 0$; A. Bohr has shown that the only modifications necessitated by the considerations of the polarization forces are the inclusion of the F_p term and the modification of I. If the length unit is [mg/cm^2], then $B\beta^2$ is nearly the same for all elements; some values of $B\beta^2$, together with other useful quantities, are listed in Table I.

Table I

Element	Z	A	ρ grams/cm^3	$B\beta^2$ kev/mg/cm^2	$\frac{\text{Atoms}}{\text{mg}}$
Beryllium	4	9.02	1.84	.0683	6.68×10^{19}
Carbon	6	12.01	2.25	.0770	5.01×10^{19}
Aluminum	13	27.0	2.70	.0741	2.23×10^{19}
Copper	29	63.6	8.9	.0702	9.47×10^{18}
Lead	82	207	11.0	.0610	2.91×10^{18}
Thorium	90	232	11.5	.0597	2.60×10^{18}

Evaluations, including polarization effects, of I and F_p have been made by Wick[9] for Pb, Fe, H_2O, air, C and by Halpern and Hall[10] for Pb, Fe, H_2O, C, air, He. Wick uses a rigorous formula of Fermi[11] for the evaluation of I . This method seems unnecessarily difficult so we will follow the approximate procedure of A. Bohr, which is essentially the same as that of Halpern and Hall; however, we will utilize X-ray data whenever possible, as was done by Wick.

When polarization effects in atomic interactions are neglected the average excitation potential is determined as

$$\log I = \sum_i f_i \log \hbar\omega_i \quad , \quad \sum_i f_i = 1 \tag{5}$$

where f_i is the oscillator strength for the i^{th} atomic transition of angular frequency ω_i . According to A. Bohr all of the atomic transitions will be affected by a polarization force due to the presence of nearby atoms in the medium, and this force may be characterized by a frequency,

$$\omega_p = \gamma (4\pi n F_p e^2/m_o)^{1/2} \quad , \quad F_p = \sum_{\omega_i < \omega_p} f_i \tag{6}$$

The energy-loss formula, Equation (4), will still apply when this effect is significant provided the expression (5) above is modified to (see the Appendix on page 21)

$$\log I = F_p \log \hbar\omega_p + \sum_{\omega_p < \omega_i} f_i \log \hbar\omega_i \qquad (7)$$

To obtain I from (7) one must know the f_i and $\hbar\omega_i$ for a free atom; then F_p, the fraction of oscillators that are polarized, and ω_p are found by the solution of the simultaneous equations (6). The main concern here is to determine the oscillator distributions for Al and Be.

The distribution of oscillators is related to the atomic absorption coefficient μ_a as (Ref. 12, page 291)

$$\mu_a \, d\omega = \frac{2\pi^2 e^2 Z}{m_o c} \, d f(\omega) \qquad (8)$$

In practical units and for a finite range of the distribution, (8) is

$$Z \int df = 1.875 \times 10^{-4} A \int \left(\frac{\mu_l}{\rho}\right) \frac{d\lambda}{\lambda^2} \qquad (9)$$

where (μ_l/ρ) is the mass absorption coefficient and λ is the wavelength of the transition in Angstroms. If absorption data, such as can be obtained in the X-ray region, were available for the entire spectrum of atomic transitions the problem of finding I would be straight forward. Unfortunately this is not the case as usually less than half of the oscillators fall in the spectral region that is accessible to accurate X-ray methods; hence additional information must be employed. For the determination of the distributions for Al and Be we use the following information.

(1) X-ray K- and L-shell absorption data,

(2) Wavelengths of discrete transitions,

(3) Non-relativistic $I_\gamma = 1$ as obtained from the measured value of the stopping cross section of the substance for protons,

(4) Theoretical K-shell oscillator distributions,

(5) Theoretical values of the total oscillator strengths for the K- and L-shells, and the sum rule $\sum_i f_i = 1$,

(6) Slater's empirical screening constants.

All of the above information is not sufficient for the construction of the complete spectrum of atomic transitions; however, the guesswork is minimized,

and we estimate that for Al and Be that it is possible to determine I with an error of not more than 15% so that μ_{mp} should not be in more than 2 1/2% error due to this source (the value of the logarithm in (4) is usually about 15).

Aluminum. The K-shell absorption spectrum is known from the work of Jönsson [13]. By substituting his data into equation (9) the total number of K-shell oscillators is found to be $Zf_K = 1.71$ and with an average excitation potential of $I_K = 2{,}750$ e.v. as obtained from the expression

$$I_K = \frac{1}{f_K} \int_{K\text{-shell}} \log(\hbar\omega)\, df \quad , \quad f_K = \int_{K\text{-shell}} df \, . \qquad (10)$$

This value of Zf_K agrees with a value that could have been read from a curve given by Wheeler and Bearden[14]. In the manner just described they determined Zf_K for a number of elements and found that the points when plotted as a function of Z fell on a smooth curve; however, they did not happen to use the Al data. The K-shell critical absorption wavelength is 7.94° so that $I_K/(\hbar\omega)_{K\text{-edge}} = 1.76$ which lies between the limits 1.95 and 1.65 suggested by Wick after his study of the empirical expressions for K-shell mass absorption coefficients. According to the theoretical considerations of Hönl[15] $Zf_{2s} = 1.82$ and $Zf_{2p} = 6.30$ so that $Zf_L = 8.12$, the sum. This leaves $13 - 8.1 - 1.7 = 3.2$ oscillators for the incomplete M-shell, which seems to be reasonable. The critical L-shell wavelength as observed in the X-ray photographic technique of Johnston[16] is 170 Å (73 e.v.). The effective polarization binding energy for Al is $\hbar\omega_p = 32.6\gamma F_p^{1/2}$ e.v. If all of the M-shell oscillators were polarized, this would give for $\gamma = 1$, $\hbar\omega_p = 16$ e.v. Hence, it seems likely that some of these oscillators are not polarized. We take the value of $I_M = 20$ ev. which, of course, is mostly a guess. For the L-shell there is continuous data up to 24 Å [17],[18],[19] in which $(\mu/\rho\lambda^2)$ ranges from 6 to 13 and an isolated point at 43 Å [20] with a value $(\mu/\rho\lambda^2) = 9.4$. By the photographic technique, which has only relative accuracy, Johnston[16] measured μ from 90 to 170 Å; aside from fluctuations his data shows that $(\mu/\rho\lambda^2)$ is constant to within about a factor of two over most of this range. So for the

L-shell we assume that $(\kappa/\rho\lambda^2)$ is a constant over the entire range of 8 to 170 Å; for 8.12 oscillators in the L-shell equation (9) gives 10.0 for this constant. A theoretical formula has been derived for the L-shell absorption[21]; however this formula neglects screening variation which clearly is not justified for such a light element as Al; the apparent constancy of $(\kappa/\rho\lambda^2)$ shows this variation to be important.

Now that we have specified a complete distribution of oscillators for the atomic transitions we must show that it is consistent with condition (3) listed above. Wilson[22] measured the stopping power for 3.5-Mev protons in Al, and from the data, which was analyzed by J. A. Wheeler, a value of $I_{\gamma=1} = 11.54$ Z was deduced. In obtaining this value he considered the correction of Bethe and Livingston[23] which takes into account the fact that K-shell orbital velocities are comparable with the incident particle velocity. However, in recent work of Hirschfelder and Magee[24] it is emphasized that an L-shell correction of the same nature is necessary. It is not known how to make such a L-shell correction accurately; following the suggestion of Bethe they do it in a manner similar to that for the K-shell (Ref. 23, Page 264). For Al the L-shell distribution of oscillators is very extended due to the variation of the screening; consequently such a correction may be inaccurate. Nevertheless, we roughly estimate, following their procedure, that including the K- and L-shell corrections I = 10.7 Z. A value I = 11.3 Z is calculated from the distribution that we have estimated; this can be considered in agreement with the observed value considering the uncertainties involved.

We have expressed I as a constant times Z since the theoretical work of Bloch (Ref. 6, Page 218) suggested this dependence; for a long time the constant was taken to be 13.5 e.v. Recent experiments[25] indicate that the constant decreases with increasing Z.

For values of $\gamma > 1$, the quantity I/γ is plotted as a function of γ, the circles in Figure (2), strictly following Equations (6) and (7). The calculated values are expected to be somewhat incorrect in the vicinity of absorption edges as a result of the approximate nature of these equations; we expect a smooth monotonic decreasing function passing near the calculated points to be more nearly correct. For very high particle energies the effective binding of the polarization forces is greater than all of the atomic binding forces; from (6) for Al

$$\lim_{\gamma\to\infty} \frac{I}{\gamma} = 32.6 \text{ e.v.} \quad , \quad \lim_{\gamma\to\infty} F_p = 1. \tag{11}$$

We thus have anchor points at $\gamma = 1$ and $\gamma = \infty$ between which I/γ varies by a factor of 5. Since we used oscillator distributions consistent with all available data we feel justified in claiming that intermediate values of I/γ should not be uncertain by more than $\pm$ 15% which means about $\pm$ 2 1/2% possible error in the stopping power from this source.

It may be possible to avoid the complications involved above and to obtain sufficient accuracy by representing the atomic oscillator distribution with a simple formula. A. Bohr[8] suggests the distribution

$$F = \frac{\chi^{1/2}}{1+\chi^{1/2}} \quad , \chi = \omega/\omega_o \quad , \quad F = \sum_{\omega_i < \omega} f_i \tag{12}$$

where ω_o is determined by requiring that this distribution give the observed average excitation potential for $\gamma = 1$. He shows that this distribution is consistent with some theoretical considerations, although he notes that only an approximate representation of the essential features of the problem is to be expected. With this distribution it can be shown that

$$I = \hbar\omega_p / F_p^2 \quad ; \tag{13}$$

ω_p and F_p are, as before, determined by the simultaneous Equations (6). For $I_{\gamma=1} = 11.3\ Z$ we obtain $F_p = .37$ and $\hbar\omega_o = 59$ ev; the former value seems unreasonable since, in view of what has been said, we expect not more than two electrons to be polarized when $\gamma = 1$, and therefore $F_p < .24$. I/γ

is plotted in Figure (2) for this distribution; there is considerable disagreement with the values calculated from absorption data. On the other hand, Prof. Christy (unpublished) finds that an oscillator strength distribution

$$F = \frac{x}{1+x} \quad , \quad x = \omega/\omega_o \quad , \quad F = \sum_{\omega_i < \omega} f_i \qquad (14)$$

is consistent with the measured X-ray absorption spectrum of Pt. The average excitation potential for this distribution can be shown to be

$$I = \hbar\omega_o + \hbar\omega_P \quad . \qquad (15)$$

If ω_o is adjusted to obtain $I_{\gamma=1} = 11.3$ Z, we find $F_p = .05$ and $\hbar\omega_o = 140$ ev. This value of F_p seems too small. Figure (2) shows I/γ plotted as a function of γ; the curve fits smoothly to the calculated absorption data values. This is very satisfactory and so (14) is probably the best distribution to use for other elements if one does not wish to bother with a study of the X-ray data. Using the distribution (14) we find $F_p = \dfrac{\sqrt{1+(2a\gamma)^2}-1}{\sqrt{1+(2a\gamma)^2}+1}$, and the most-probable stopping power, eq. (4), becomes

$$\mu m_p = B\left\{\ln\frac{\ell}{a_o} + 2\ln\left[\frac{\sqrt{1+(2a\gamma)^2}-1}{2a\gamma}\right] - \frac{2\beta^2}{1+\sqrt{1+(2a\gamma)^2}} + 0.37\right\}$$

where ℓ = foil thickness , $a_o = \hbar^2/m_o e^2$. , $a = \omega_P/\omega_o \gamma F_P^{1/2}$, (16)

The curves of Figure (4) were obtained from this expression.

Beryllium. This element has such a simple atomic structure, 2K- and 2L-electrons, that a rather accurate determination of I is possible using the theoretical K-shell absorption formula even though there is no X-ray data available other than the value of the wavelength of the $K\text{-}L_{II}$ transition ($115.7\ \text{Å}$)[12]. There is an accurate measurement of $I_{\gamma=1} = 64 \pm 5$ ev[26] (this includes the K-shell correction; no L-shell correction is necessary) together with an explanation by A. Bohr[8] that this rather large value of I (I = 16 Z) is due to the fact that the two L-electrons have an effective

polarization binding which is larger than an expected atomic binding of about 9 ev. Hence for all particle energies the L-electrons will be bound by an effective frequency ω_p, given by (6), of

$$\hbar\omega_p = 26.0\,\gamma\,F_p^{1/2} \quad \text{e.v.} \tag{17}$$

with $F_p = 1/2$ for $\hbar\omega_p < \hbar\omega_{K,L_{II}}$. When $\hbar\omega_p > \hbar\omega_{K,L_{II}}$, additional oscillators become polarized, and it is necessary to know the K-shell oscillator distribution in order to determine the extent. The formula for the K-shell atomic absorption coefficient is given by Bethe (Ref. (7), page 477); according to Slater's empirical screening rules[27] an effective charge $(Z - 0.3)$ should be used. Moreover, according to these rules the K-shell ionization potential is $E_K = \Theta(Z - 0.3)^2 R_y$ with $\Theta = .69$. This indicates that the theoretical absorption spectrum should be extrapolated to E_K from $(Z - 0.3)^2 R_y$ in order to take screening into account. This procedure yields a value of $Zf_{K,\text{cont.}} = 1.76$ for the total number of oscillators in the transitions from the K-shell into the continuum. Since the two valence electrons of Be are presumably in the L_I shell, none of the K-shell to L-shell transitions are forbidden by occupancy so that $Zf_{K,\text{cont.}} + Zf_{K,L_{II}L_{III}} = 2$. Hence $Zf_{K,L_{II}L_{III}} = 0.24$, this seems rather small so we used $\Theta = .715$ which results in $Zf_{K,L_{II}L_{III}} = 0.43$. Then from (7) we find $I_{\gamma=1} = 67$ ev which is in agreement with the observed value considering the uncertainties. With the oscillator distribution completely specified, I/γ and F_p as a function of γ are determined from (6) and (7); the results are plotted in Figure (3). From (17) it is seen that when $\gamma = 5.88$, $\hbar\omega_p = \hbar\omega_{K,L_{II}L_{III}}$ so that a discontinuity in the F_p curve occurs because the $K,L_{II}L_{III}$ oscillators suddenly become polarized according to the approximate expressions (6). Then F_p remains constant from $\gamma = 5.88$ up to $\gamma = 6.5$ where the K,cont. oscillators begin to become polarized. Such discontinuities are not expected to occur in actuality, and we expect I/γ to be a monotonic decreasing function with increasing energy; the smooth curves in Figure (3) are therefore to be preferred

to the calculated curves. According to (6), for high particle energies

$$\lim_{\gamma \longrightarrow \infty} I/\gamma = 26.0 \text{ ev} \qquad \text{and} \qquad \lim_{\gamma \longrightarrow \infty} F_p = 1$$

The anchor point values for I/γ at $\gamma = 1$ and $\gamma = \infty$ are only in the ratio 2.5 so that rather good over-all accuracy can be expected for the calculated most-probable stopping powers from equation (4) which are plotted in Figure (5).

At the time of this writing experiments are in progress at the University of Southern California for the determination of the most-probable stopping power for 624 kev electrons in Al, Be, and other materials. From these experiments it will be possible to calculate $I_\gamma = 2.22$, and thus obtain a check on the oscillator distributions that we have constructed. Should there not be agreement within the required accuracy, it will be necessary to alter the distributions in order to fit the measured values. It is evident from Figures (2) and (3) that a single determination of I/γ at an intermediate energy such as $\gamma = 2.22$ should make it possible to improve the accuracy of the determination of I/γ for all values of γ.

3. Distribution of Electron Energy Losses.

In the last section it was mentioned that in spectrometer work the most-probable energy loss is usually a more useful quantity than the average energy loss for electrons in converter foils. Actually the required effective loss is somewhat larger than the most-probable energy loss. Landau[4] has derived the distribution function for energy loss of fast electrons with which it is possible to obtain an effective energy loss for any particular problem. In this section we will show how to obtain an effective stopping power, to be used in an expression of the type (3), for Compton conversion in an "infinitely" thick converter. Actually the converter need only be a number of times thicker, in energy loss units, than the spectrometer resolution width in energy units.

According to Landau the probability that a monoenergetic beam of electrons

passing through a thickness x of stopping material suffers an energy loss Δ in the interval $d\Delta$ is $f(x, \Delta)d\Delta$, and

$$f(x, \Delta) = \frac{\varphi(\lambda)}{\chi B} \tag{18}$$

where $\phi(\lambda)$ is a universal function, which is plotted in his paper, with argument

$$\lambda = \frac{\Delta - \chi B\left(\ln \frac{\chi B}{\varepsilon'} + 0.42\right)}{\chi B} \tag{19}$$

and the normalization is

$$\int_0^\infty f(x,\Delta)\,d\Delta = \int_{-\infty}^{\infty} \varphi(\lambda)\,d\lambda = 1 .$$

The most-probable energy loss Δ_0 for this thickness x occurs, by definition, at the value of λ (= -.05) corresponding to the maximum of $\phi(\lambda)$. Hence

$$\Delta_0 = \chi B\left(\ln \frac{\chi B}{\varepsilon'} + 0.37\right) ; \tag{20}$$

$\ln\varepsilon'$ is an abbreviation for the additional terms appearing in the equivalent expression (4). Let the number of electrons generated (in a distance dx) by a conversion process with an energy E in the interval dE be

$$Q(E)\,dE\,dx.$$

These electrons will suffer an energy loss distribution so that the probability that an electron is generated between x and x+ dx with an initial energy between E and E + dE, and subjected to an energy loss from Δ to Δ+ $d\Delta$, is

$$Q(E)\,dE\,dx\,f(\Delta, x)\,d\Delta \quad .$$

If we substitute $\phi(\lambda)$ for $f(x, \Delta)$ and integrate over a converter of finite thickness t, we obtain

$$\frac{Q(E)\,dE\,d\Delta}{B} \int_0^t \frac{\varphi(\lambda)\,dx}{\chi} \quad . \tag{21}$$

Now we write (19) as

$$\lambda = \frac{\Delta}{\chi B} + \lambda' \quad ; \quad -\lambda' = \frac{\mu_{mp}}{B} + .05 \tag{22}$$

where μ_{mp} is the most-probable stopping power which, as is evident from Figures (4) and (5), is a slowly varying function of x. If we neglect this dependence x occurring in λ', the only assumption to be made, then

$dx/x = -d\lambda/(\lambda - \lambda')$,

and expression (21) becomes

$$\frac{Q(E)\,dE\,d\Delta}{\mu_{mp}}(-1)(\lambda' + .05)\int_{\lambda(t)}^{\infty}\frac{\varphi(\lambda)\,d\lambda}{\lambda-\lambda'} \qquad (23)$$

with $\lambda(t) = (\Delta/Bt) + \lambda'$;

or $t\,Q(E)\,dE\,f(\xi,\lambda')\,d\xi$

where $$f(\xi,\lambda') = -(\lambda' + .05)\int_{\lambda(t)}^{\infty}\frac{\varphi(\lambda)\,d\lambda}{\lambda-\lambda'} \qquad (24)$$

and $\xi = \Delta/\Delta_0(t)$; $\Delta_0(t) = t\mu_{mp}(t)$ is the most probable energy loss for a foil of thickness t. Consequently, for a converter of finite thickness t the total number of generated electrons with an energy E in the interval dE, tQ(E)dE , is redistributed in energy according to the probability distribution $f(\xi,\lambda')\,d\xi$.

Figure (6) shows a plot of $f(\xi,\lambda')$ for $\lambda' = -15$. For a Compton converter of finite thickness the generated distribution of electrons must be folded with this function in order to take into account the straggling in energy loss.

In the case of an "infinitely" thick converter we let $t \longrightarrow \infty$ in (23) and obtain $Q(E)\,dE\,\frac{F(\lambda')}{\mu_{mp}}\,d\Delta$

with $$F(\lambda') = -(\lambda' + .05)\int_{\lambda'}^{\infty}\frac{\varphi(\lambda)\,d\lambda}{\lambda-\lambda'} \quad ; \qquad (25)$$

the folding operation is no longer necessary. Let the electrons emerging from the converter have an energy E_0 in the interval dE_0 so that $E_0 = E - \Delta$; an integration over the primary distribution Q(E) gives the emerging distribution $$N(E_0)\,dE_0 = \frac{dE_0}{\mu_{eff}}\int_{E_0}^{E_{max}} Q(E)\,dE \qquad (26)$$

where $\mu_{eff} = \mu_{mp}/F(\lambda')$. We have now obtained an effective stopping cross section μ_{eff} to be used in an equation of the type (3). $F(\lambda')$ is plotted in Figure (7). This function was computed from the curve in Landau's paper for the function $\phi(\lambda)$, which is plotted up to $\lambda = 15$. The extension of this curve beyond $\lambda = 15$ cannot be neglected; the contribution to $F(\lambda')$ from

this region may be obtained with sufficient accuracy from the asymptotic expressions given by Landau; this was done in obtaining Figures (6),(7). The quantities $\mathcal{H}_{mp}(x)$ and λ' that enter into the determination of $\mathcal{H}_{eff}$ should be selected for a mean thickness of x which corresponds to the mean energy loss of the region of the emerging distribution that is the most important in the determination of absolute intensities. The best procedure is probably to use a value of x corresponding to an energy loss equal to one or two resolution widths of the spectrometer.

Two conditions must be met if the approximations used by Landau to derive the distribution function are to be valid:

$$\chi B \gg \varepsilon \quad , \quad \chi B \ll E \quad ;$$

ε is a quantity of the order of the mean atomic excitation energies and E is the energy of the penetrating electron. The most probable energy loss is usually about 13XB so that for a spectrometer of 3% resolution in energy units the above conditions reduce to

$$\varepsilon \ll .003\, E \ll E \,. \qquad (27)$$

The left side of this condition is probably only satisfied for the lightest elements, say up to aluminum. In addition, for elements heavier than aluminum scattering, for which there is no satisfactory treatment, is important for the determination of an effective stopping cross section. In these respects Be is the most satisfactory element to use as a Compton converter; however, there should be no objection to aluminum which is apt to be more convenient.

White and Millington[28] have measured the energy loss distribution of electrons in mica foils. Their experimental curve has a breadth which is about two times wider than expected from Landau's theory and also from a less rigorous theory of Williams[29]. They did find the universality of the distribution function as given by Landau in that the breadth of their curve increased very nearly linearly with the foil thickness. In any experiment all effects such as those due to finite resolution and scattering tend to introduce broadening; hence we feel that it is better to use the theory rather than the experimental

results.* A derivation of an effective stopping power, similar to the one given above but using the results of White and Millington, has been given by Ellis and Aston[27].

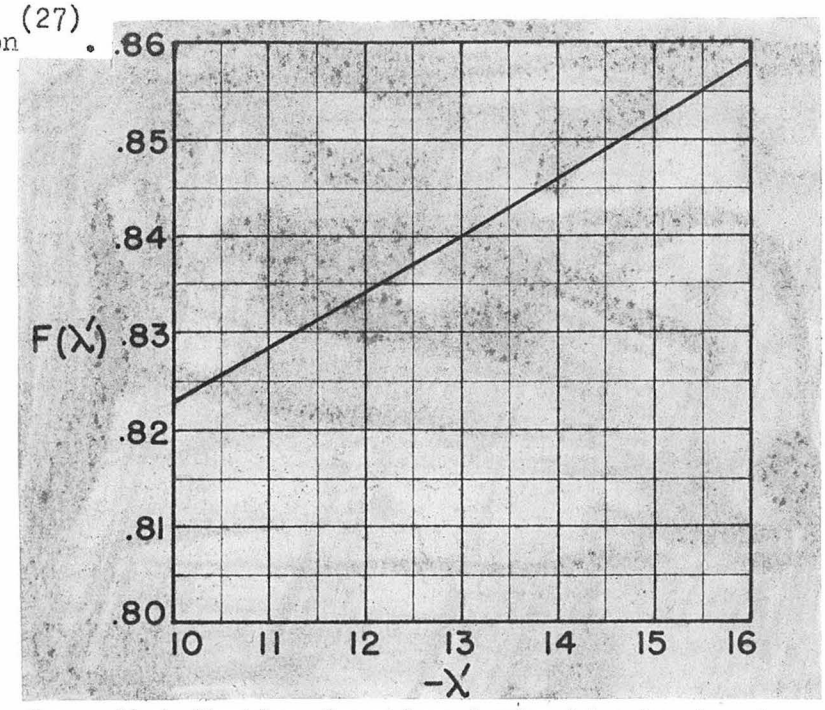

Figure (7)

The energy loss distribution function derived by Landau does not take into account the fact that there is a certain probability that an electron traversing a foil will lose no energy. As a result Landau's distribution should include a delta function at the origin to represent this probability, and the rest of the distribution should be renormalized accordingly. The following argument, due to Professor Christy, shows that in our spectrometer work this effect is insignificant. A rough measure of the energy transferred in the distant resonance collisions is the average excitation potential I. The average distance between energy-loss collisions is $t_o \approx I/\mu$, and the probability that an electron suffers no loss of energy in a distance t is e^{-t/t_o}. For $\frac{\Delta E}{E} \approx$ 2% spectrometer resolution, electrons will be accepted by the spectrometer from a distance $t \approx \frac{.02E}{\mu}$; so the ratio $t/t_o \approx .02E/I$ which is always very large. The energy spectrum of electrons emerging from a converter will be modified at the high energy limit of the spectrum over an energy interval many times less than the resolution width, and so there will be no detectable change.

* See Appendix B, page 22a.

4. Scattering of Fast Electrons

For two reasons elastic scattering of electrons in the converter material can affect absolute gamma-ray intensity determinations: (1) There may be an increase or decrease in the number of electrons emerging from the converter into the spectrometer acceptance solid angle due to the change in the angular distribution of the conversion electrons, (2) The electron paths will not be straight, and this fact will affect the determination of an effective stopping cross section to be used in an expression such as Equation (3). The Coulomb scattering cross section is proportional to Z^2; however in spectrometer work one is concerned with the ratio of scattering to atomic stopping cross section, and this ratio is approximately proportional to Z.

There are many papers on the scattering of electrons, and none are very satisfactory for our purposes, especially in regard to reason (2) above; some of the most useful are References (5), (31), (32), (33), and (34); Ref. (35) gives a summary of work on this subject. We will give here a few results, mainly from Ref. (31), which we need. These results will be principally qualitative; it is hoped that they will provide some indication of the uncertainties from multiple scattering to be expected in intensity determinations. It should be emphasized that in all of the theories on multiple scattering (except that of Ref. (32)) the electron path length is the basic parameter, and it is necessary, therefore, to interpret the results in terms of the component distance along the axis of symmetry, which is usually taken to be perpendicular to the scattering foil.

Let the initial distribution f_o of conversion electrons before scattering be symmetrical about the axis $\theta = 0$, and therefore representable in terms of Legendre polynomials as

$$f_o(\cos\theta_o)\, d\cos\theta_o\, d\varphi_o = \sum_{n=0}^{\infty} a_n P_n(\cos\theta_o)\, d\cos\theta_o\, d\varphi_o \quad ; \qquad (28)$$

the normalization $\int_0^{4\pi} f_o\, d\Omega_o = 1$ requires that $a_o = (4\pi)^{-1}$.

These conversion electrons are subjected to an axially symmetric angular redistribution probability which can also be expressed in terms of Legendre polynomials. The probability that an electron is multiply scattered by an angle ω into the solid angle $d\cos\omega\, d\psi$ is

$$\mathcal{G}(\cos\omega)\, d\cos\omega\, d\psi = \frac{1}{4\pi}\sum_{n=0}^{\infty} G_n\,(2n+1)\,P_n(\cos\omega)\, d\cos\omega\, d\psi \tag{29}$$

where

$$G_n = 2\pi \int_{-1}^{1} \mathcal{G}(\cos\omega)\, P_n(\cos\omega)\, d\cos\omega \ .$$

We want to know the final distribution, $f_1(\theta_1)$, after the redistribution by the scattering law $\mathcal{G}$. It is given by the integral

$$f_1(\cos\theta_1)\, d\cos\theta_1\, d\varphi_1 = \int_{\Omega_0} f_0(\cos\theta_0)\, d\Omega_0\, \mathcal{G}(\cos\omega)\, d\cos\theta_1\, d\varphi_1$$

where

$$\cos\omega = \cos\theta_0\cos\theta_1 + \sin\theta_0\sin\theta_1\cos(\varphi_0-\varphi_1) \ . \tag{30}$$

By substituting (28), and (29) into (30) and using the addition theorem for Legendre polynomials,

$$P_n(\cos\omega) = P_n(\cos\theta_0)\,P_n(\cos\theta_1) + 2\sum_{m=0}^{n}\frac{(n-m)!}{(n+m)!}\,P_n^m(\cos\theta_0)\,P_n^m(\cos\theta_1) \times \cos m(\varphi_0-\varphi_1), \tag{31}$$

and the orthogonality property of the Legendre functions, we obtain

$$f_1(\cos\theta_1)\, d\Omega_1 = \sum_{n=0}^{\infty} a_n\, G_n\, P_n(\cos\theta_1)\, d\Omega_1 \ . \tag{32}$$

This result is general; it can be extended to any number of axially symmetric redistribution laws such as $\mathcal{G}, \mathcal{H}, \mathcal{J}$ with the result

$$f(\cos\theta)\, d\Omega = \sum a_n G_n H_n J_n \cdots P_n(\cos\theta)\, d\Omega \ . \tag{33}$$

In the case of multiple scattering the coefficients G_n are evaluated in the paper of Goudsmit and Saunderson; they give the following approximate expression

$$G_n = e^{-\frac{\ell}{\lambda} n(n+1)\left[1-\left(\frac{1}{2}+\frac{1}{3}+\cdots+\frac{1}{n}\right)/\log\xi\right]} \tag{34}$$

where ℓ is the electron path length, and we have introduced the scattering length

$$\lambda = [2\pi K^2 N \log \xi]^{-1} \; ; \; K = \frac{Ze^2}{m_0 c^2} \frac{(1-\beta^2)^{\frac{1}{2}}}{\beta^2} \; ; \; N = \frac{\text{atoms}}{\text{cm}^3} \; ; \qquad (35)$$

Z = charge of scattering nucleus.

The quantity $\log \xi$ depends upon the specific single scattering law and the method that is used for obtaining the single scattering probability. For the Born-approximation solution in the Thomas-Fermi atomic field they find

$$\log \xi = \log \frac{150}{Z^{1/3}} \left(\frac{P}{m_0 c}\right) \quad , \text{ where } P \text{ is}$$

the electron momentum. The multiple scattering experiments of Kulchitsky and Latyschev[36] are in excellent agreement with the theory, except for lead, when the above expression is used for $\log \xi$. Using (35) and (36) $\frac{Z^2\lambda}{A}$ is plotted in Figure (8) for a range of values of Z. In the case of lead we expect the Born approximation to be invalid, and the experimental results indicate that λ should be increased about 25% from Equation (35) for the heavy elements.

If we have initially a beam of electrons in the direction $\theta = 0$, then $a_n = (2n+1)/4\pi$ which, if substituted into (32), gives Equation (4) of Ref. (31). For such a beam

$$\langle \sin^2 \tfrac{\theta}{2} \rangle_{AV} = \tfrac{1}{2} (1 - G_1) ,$$

and so for thin foils,

$$\langle \theta^2 \rangle_{AV} \approx 4\ell/\lambda , \qquad (37)$$

which is the mean-square scattering angle to be used in the approximate Gaussian representation of the scattering at small angles.

The coefficients G_n are expressed in terms of path length rather than foil thickness X. For an initial beam of particles Rose[37] has derived an approximate expression for the "Umweg" factor, $\langle \ell \rangle_{AV} / X$. In the first approximation his result reduces to

$$\langle \ell \rangle_{AV} / X \approx 1 + (X/\lambda) \quad , \; X \ll \lambda . \qquad (38)$$

Such an expression was used by Oleson, Chao, and Crane[38] to interpret their

multiple scattering data. The effective stopping power used in absolute intensity measurements should contain this factor as electron energy loss is proportional to the path length.

We can obtain this result for the Umweg factor in another way which will provide qualitative information about the angular redistribution due to scattering in a case where $f_o(\cos\theta_o)$ is not a beam but fairly uniform. The Fokker-Planck approximation to the Boltzmann diffusion equation applied to multiple scattering gives for the equation to be satisfied by the distribution function, $f(\mu, x, \ell)\, d\Omega$ (32),

$$(1-\mu^2)\frac{\partial^2 f}{\partial \mu^2} = 2\mu\frac{\partial f}{\partial \mu} + \mu\frac{\partial f}{\partial x} + \frac{\partial f}{\partial \ell} \quad , \mu = \cos\theta \; ; \tag{39}$$

ℓ is the path length and x is the component distance along the axis of symmetry $\theta = 0$; the lengths are expressed in units of λ . For $\mu \approx 1$ and if $\left(\frac{\partial^2 f}{\partial \mu^2}\right)_{\mu\approx 1} << \left(\frac{\partial f}{\partial \mu}\right)_{\mu\approx 1}$, we set the term on the left of (39) equal to zero. What remains is first order, and therefore not a diffusion equation; it will only give some mean value for $f(\mu, x, \ell)$ rather than a distribution. A unique solution as given by LaGrange's method[39] is

$$f = f(\mu - 2x, \mu e^{-2\ell}) \tag{40}$$

The boundary condition, which occurs at $\ell = 0$, is

$$f(\mu, x, 0) = \delta(x)\, f_o(\mu) \tag{41}$$

where $f_o(\mu)$ is the initial angular distribution. All solutions which satisfy (40) and (41) reduce to

$$f = f_o(\mu - 2x)\, \delta\left[\frac{\mu e^{-2\ell} - (\mu - 2x)}{2}\right]. \tag{42}$$

f is non-zero when

$$\ell = -\tfrac{1}{2}\ln\left(1 - \frac{2x}{\mu}\right).$$

This expression is only valid for $x << 1$, and so just the first term in an expansion is significant; it is (reintroducing λ)

$$\ell \approx \frac{x}{\mu}\left(1 + (x/\lambda\mu)\right) \tag{43}$$

which is similar to (38) except for the $\mu\,(\approx 1)$ term. Equation (42)

gives the additional information

$$f(\mu, x) \approx f_o\left(\mu - \frac{2x}{\lambda}\right), \tag{44}$$

which is of qualitative value if $f_o(\mu)$ is fairly uniform at small angles. This result shows that for thin foils and at small angles if $f_o(\mu) \approx \mu^{-1}$, as it would be if an isotropic distribution of gamma-radiation is converted in a flat foil, then $f(\mu, x) \approx \mu^{-1}\left(1 + \frac{2x}{\lambda\mu}\right)$, $x << \lambda$; scattering will increase the number of electrons into the spectrometer acceptance solid angle, and such an increase has actually been observed experimentally. In the case that $x >> \lambda$ Bethe, Rose, and Smith[29] give for the Umweg factor

$$\langle \ell \rangle / x \approx x/\lambda ,$$

which is consistent with (38) indicating that (38) may be reasonably valid for larger thickness than claimed.

In addition to the effects due to multiple scattering, there may be attenuation in the beam of conversion electrons due to single large-angle scatterings. These collisions will follow the Rutherford scattering law; the probability that in a distance t an electron is scattered once through an angle greater than θ_o is

$$P_{\theta > \theta_o} = \pi K^2 N t \cot^2\left(\frac{\theta_o}{2}\right),$$

which may be expressed in terms of λ as

$$P_{\theta > \theta_o} = \frac{t \cot^2\left(\frac{\theta_o}{2}\right)}{2\lambda \log \xi} . \tag{45}$$

APPENDIX - PART I

The following analysis, which is due to Professor Christy, shows how to take into account the polarization forces in the stopping-power formula, eq. (4).

According to N. Bohr[5] the energy-loss problem may be treated by an impact-parameter method using the classical Coulomb scattering formula. The range of permissible impact parameters is divided into two groups corresponding to the free and resonance-type of collisions. The average stopping power, M_f, resulting from the free encounters with energy transfers to the atomic electrons less than a certain W_{max}, which is less than the kinetic energy of the penetrating electron, is given by (eq. 3.314 of reference (5))

$$M_f = B \sum_i f_i \log \frac{W_{max}}{I_i}$$

where f_i is the oscillator strength and I_i the excitation energy of the i^{th} atomic transition, and B is the quantity defined in connection with (4). The average stopping power due to the resonance-type collisions is given by (eq. 3.3.15 of ref. (5))

$$M_r = B \sum_i f_i \log e^{-\beta^2} \left(\frac{d_{max}}{d_{min}}\right)^2$$

where d_{min} is an impact parameter equal to $\hbar/(2m_o I_i)^{1/2}$, the 'size' of the i^{th} atomic oscillator, and $d_{max}(\text{adiabatic}) = \gamma v \hbar / I_i$ is the maximum impact parameter which corresponds to the adiabatic limit.

For large particle velocities ,v, A. Bohr[8] shows that in order to include polarization effects, we must use the lesser (an approximation) of $d_{max}(\text{adiabatic})$ and $d_{max}(\text{polarization}) = \frac{\gamma v \hbar}{(\hbar \omega_p)}$ where ω_p is given by (6); furthermore, he shows that the term $e^{-\beta^2}$ in the argument of the logarithm for the resonance

collisions is not to be included when d_{max} is determined by the polarization forces. Thus, for the stopping cross section due to resonance collisions we obtain

$$\mu_r = B\left[\sum_{\omega_i<\omega_P}{}' f_i \log\frac{2m_0v^2\gamma^2 I_i}{(\hbar\omega_P)^2} + \sum_{\omega_i>\omega_P}{}' f_i\left(\log\frac{2m_0v^2\gamma^2}{I_i} - \beta^2\right)\right],$$

and by combining this expression with that for the free collisions, we obtain the total average stopping power for energy transfers less than W_{max}, viz. equation (4) provided that we use (7) for logI rather than (5), and furthermore if, according to Landau[4], we set $W_{max} = Ble^{0.37}$ in the case that we are interested in the most-probable stopping power.

B. Recent Results Concerning Straggling in Energy Loss

A measurement of the distribution of energy losses of the 0.663-Mev internal conversion electrons from Cs^{137} passing through a 13.4-mg/cm^2 aluminum foil has been reported by R. D. Birkhoff, Phys. Rev. 82, 448 (1951), using a beta-ray spectrometer of 0.5% resolution. His result does not appear in satisfactory agreement with theoretical distributions of either Landau or Blunck-Leisegang (see below) although it is not clear to me whether it would require any significant change in $F(\lambda')$ appearing in fig. (7). Furthermore, Birkhoff states that there is a 23% attenuation of the beam in the foil due to scattering; this is surprising since the scattering length for this foil was large compared to the foil thickness, viz. $\chi/\lambda = .04$, and the angular distribution involved was essentially isotropic. He plans future experiments with improved equipment.

A recent theoretical paper by Blunck and Leisegang, Zeits. für Physik 128, 500 (1950), extends the range of validity of Landau's result by approximately taking into account the second moment of the resonance energy losses in individual encounters; Landau considered only the first moment of these collisions although he considered all moments of the free encounters. The effect of the inclusion of the second moment of the resonance collisions is to broaden Landau's distribution and, in fact, to such an extent that agreement is obtained with the experimental results of White and Millington. This additional broadening will probably not affect the determination of $F(\lambda')$ by more than a few percent.

PART II

Processes for Conversion of Gamma-Radiation

1. Introduction

With the geometry of fig. (1), the following conversion processes may be utilized for studying gamma-radiation of moderate energies:

1) Compton conversion
2) External photoelectric conversion
3) External pair formation
4) Nuclear photo-disintegration
5) Internal conversion
6) Internal pair formation
7) Internal scattering

We will be concerned here with only the first two of the external conversion processes. The cross section for external pair formation is larger than that of the first two processes at sufficiently high energies; however, the line shape features are not pronounced enough to make it as satisfactory as the first two for quantum energies up to about 6 Mev. In using a spectrometer for process 4, one might detect charged photo-disintegration products, such as protons from the photo-disintegration of the deuteron. The cross section for this process is sufficiently high for certain gamma-ray energies; unfortunately, the converter stopping cross section is much higher for slow nuclear charged particles than for the fast electrons that are ejected in the other external conversion processes. Processes 5 and 6 are similar; in one case an atomic electron is ejected by an interaction with the nuclear radiation field; in the other an electron from the sea of occupied negative energy states is ejected from the surroundings of the nucleus, the positron of the pair appearing as the resultant hole in

the negative energy states. We will now mention all that need be said about process 7.

At one time some experimenters found an unusually large number of electrons in energy regions just below strong K-photoelectric lines in heavy elements, in particular in the region just below the 2.62-Mev gamma-ray of ThC". None of the processes that we have listed, with the exception of 7, could energetically account for these electrons, and even 7 seemed unlikely since it is second order in $e^2/\hbar c$. Theoretical calculations of internal scattering were made by Cooper and Morrison (40), who showed that the number of such processes is almost negligible even in the heaviest nuclei, and so it was not possible to account for the spurious electrons in the ThC" spectrum in this way. Later experimental investigations showed that the source of these electrons was of instrumental origin.

We will discuss the external processes 1 and 2 for thick and thin converters, the dividing line for such a classification being whether the converter is thicker or thinner in electron energy loss units than the spectrometer dispersion width in energy units. We will discuss processes 5 and 6 to the extent necessary for the analysis of some data to be given in this thesis.

2. Converter Geometry Considerations

In order to determine intensities by means of the external conversion processes using an axially symmetric spectrometer it is necessary to understand the converter geometry. A

geometry that is frequently used is shown in fig. (9). The shape of the converter is usually conveniently taken as flat, although some mention will be made of the use of hemispherical converters.

Let the total yield of radiation from the source be Y; if its distribution is isotropic, the number of quanta converted from the gamma-ray direction solid angle $2\pi\, d\cos\theta_o$ is, for a flat converter (neglecting attenuation),

$$\begin{aligned} &(Y/4\pi)\,\sigma N t \sec\theta_o\, 2\pi\, d\cos\theta_o && \text{if } \theta_o < \delta \\ &\text{and} \qquad 0 && \text{if } \theta_o > \delta \end{aligned} \tag{46}$$

where N is the number of atoms per unit volume, t is the converter thickness, and σ is the total atomic cross section for conversion. Let the probability that in the conversion process a secondary electron is ejected at an angle ω with the gamma-ray direction and into the solid angle $d\Omega = d\cos\omega\, d\psi$ be

$$S(\cos\omega)\, d\cos\omega\, d\psi \qquad \text{with} \quad \int_0^{4\pi} S\, d\Omega = 1$$

where ψ is the azimuthal angle about the gamma-ray direction. We need to know the angular distribution of the conversion electrons in order to know how many will enter the spectrometer acceptance solid angle. In the case of photoelectric conversion in heavy elements there may be an angular redistribution of the electrons due to multiple or pronounced single scattering. In case the gamma-radiation comes from the compound or recoil nucleus in a nuclear reaction, the radiation may not be isotropic. In general this problem can be approached by means of eq. (33), in which additional redistributions or asymmetry of

Fig. (9). Converter Geometry.

The converter is a circular disc centered on the spectrometer axis and perpendicular to it; it subtends an angle 2δ at the source. The limiting angles of the spectrometer acceptance solid angle are θ_a and θ_b. If the source is produced in a nuclear reaction, the path of the incident beam is coincident with the spectrometer axis.

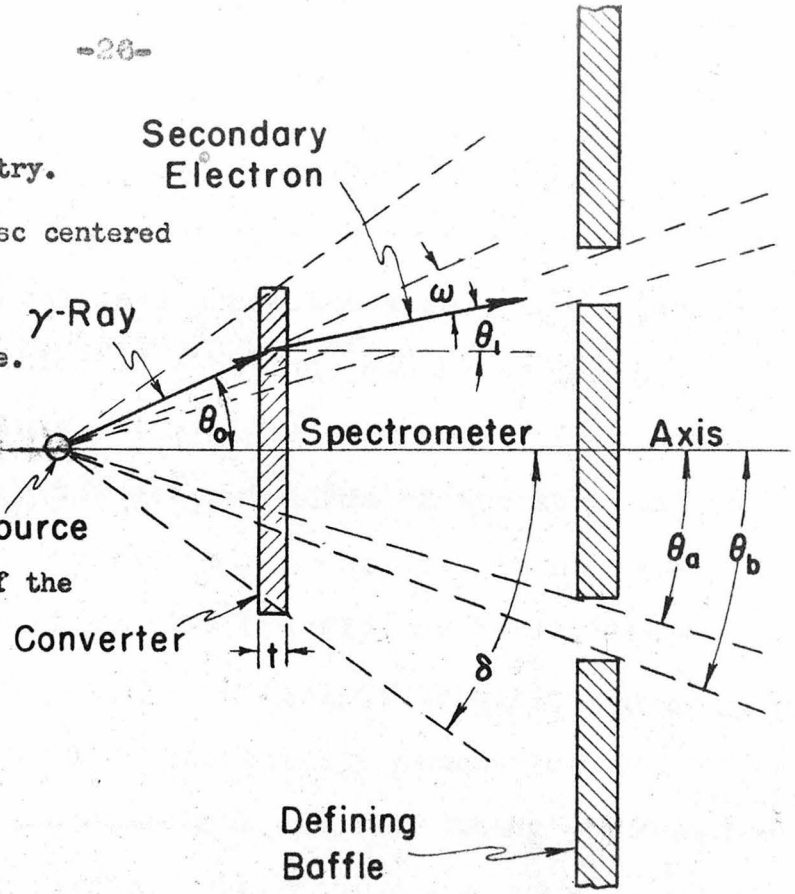

Fig.(10)

The solid angles $2\pi d\cos\omega$ and $2\pi d\cos\theta_1$ are shown as zones on the surface of a sphere. For $\theta_0 < \delta$ the contribution to the solid angle $2\pi d\cos\theta_1$ from the conversion into the solid angle $2\pi d\cos\omega$ is shaded.

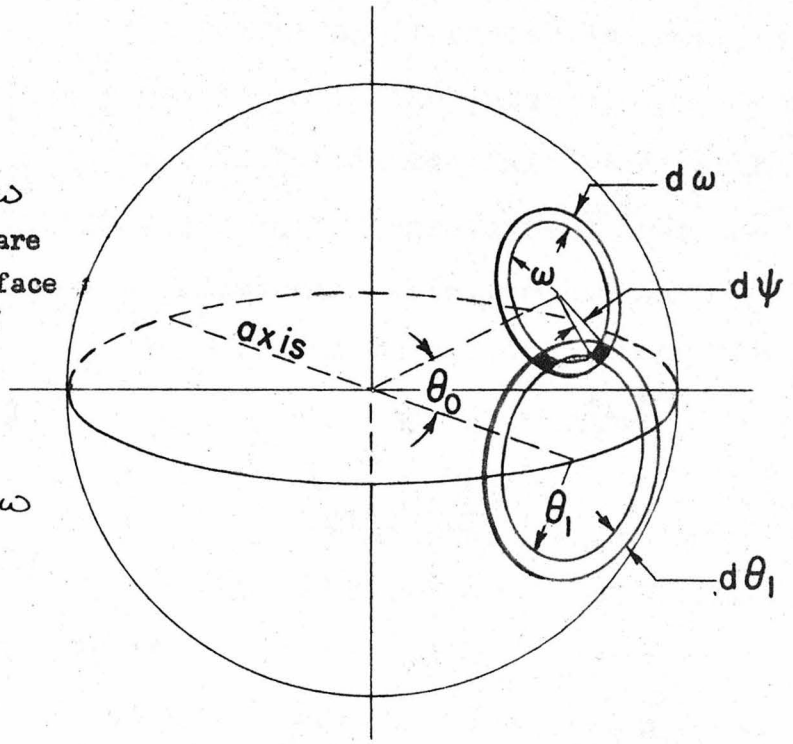

the radiation do not appreciably increase the complications of the problem. We will neglect scattering for the time being and assume that the quanta are converted according to (46), for which the distribution of electrons can be obtained by a direct integration. This solution is essentially that given by Hornyak [1],[41] for the determination of the angular distribution of Compton conversion electrons. It is necessary to extend his result so that we give briefly the basic steps involved. As in eq. (28) let the initial distribution $f_o(\cos\theta_o)d\cos\theta_o d\phi$ be redistributed according to the axially symmetric law $\delta(\cos\omega)\times d\cos\omega d\psi$. We can integrate over the azimuthal angle using for the relation between the angles $\cos\theta_1 = \cos\theta_o\cos\omega + \sin\theta_o\sin\omega\cos\psi$. After some algebra we find

$$\frac{2\pi f_o(\cos\theta_o)\, d\cos\theta_o\, \delta(\cos\omega)\, d\cos\omega\, d\cos\theta_1}{\left\{\left[\cos(\theta_1-\omega)-\cos\theta_o\right]\left[\cos\theta_o-\cos(\theta_1+\omega)\right]\right\}^{1/2}} \qquad (47)$$

for the probability that a gamma-ray is converted from the solid angle $2\pi\, d\cos\theta_o$ through an angle ω in the interval $d\cos\omega$ into the interval $d\cos\theta_1$. For a flat foil the initial distribution $f_o(\cos\theta_o)$ is given by (46). We can integrate (47) over the angle θ_o which, for a fixed ω, has the following ranges:

$$|\theta_1-\omega| \text{ to } |\theta_1+\omega| \quad \text{if} \quad \omega+\theta_1 \le \delta,$$

$$|\theta_1-\omega| \text{ to } \delta \quad \text{if} \quad 2\theta_1+\delta > \omega+\theta_1 > \delta.$$

The integral is zero if $\omega > \theta_1+\delta$. Fig. (10) may be of assistance in visualizing the angles. For the distribution emerging from the foil we may write

$$f_1(\cos\theta_1)\, d\Omega_1 = (Y/4\pi)\,\sigma N t\, d\Omega_1\, 2\pi \int \delta(\cos\omega)\langle \sec\theta_o(\omega,\theta_1)\rangle_{Av} \times d\cos\omega, \qquad (48)$$

the kernel $\langle \sec\theta_o(\omega,\theta_1)\rangle_{Av}$ assumes various values depending on the

limits of integration; it may be interpreted as the average value of $\sec\theta_0$ for electrons converted through an angle ω into the differential element $d\cos\theta_1$. The expressions for $\langle \sec\theta_0(\omega,\theta_1)\rangle_{AV}$ are the following:

Case I: $\theta_1 + \omega < \delta$,

$$\langle \sec\theta_0(\omega,\theta_1)\rangle_{AV} = (\cos^2\theta_1 - \sin^2\omega)^{-1/2};$$

Case II: $\theta_1 + \omega = \delta$,

$$= \left[\cos\delta\,\cos(\theta_1-\omega)\right]^{-1/2};$$

Case III: $|\omega-\theta_1| < \delta < \theta_1+\omega < \pi/2$,

$$= (\cos^2\theta_1-\sin^2\omega)^{-\frac{1}{2}}\left[\frac{1}{2}+\frac{1}{\pi}\sin^{-1}\frac{\cos^2\theta_1-\sin^2\omega-\cos\omega\cos\theta_1\cos\delta}{\cos\delta\sin\omega\sin\theta_1}\right];$$

Case IV: $|\omega-\theta_1| < \delta < \theta_1+\omega = \pi/2$,

$$= (2/\pi\cos(\omega-\theta_1))\left[(\cos(\omega-\theta_1)/\cos\delta)-1\right]^{1/2}; \qquad (49)$$

Case V: $\pi/2 < \omega+\theta_1 < 2\theta_1+\delta$, $\delta > |\omega-\theta_1|$,

$$= (1/\pi)(\sin^2\omega-\cos^2\theta_1)^{-1/2}\times$$

$$\log\frac{(\sin^2\omega-\cos^2\theta_1)\left[1+\sqrt{1+\cos\delta\left(\frac{2\cos\omega\cos\theta_1-\cos\delta}{\sin^2\omega-\cos^2\theta_1}\right)}\right]+\cos\omega\cos\theta_1\cos\delta}{\sin\omega\sin\theta_1\cos\delta};$$

Case VI: $|\omega-\theta_1| > \delta$,

$$\langle \sec\theta_0(\omega,\theta_1)\rangle_{AV} = 0.$$

If the redistribution law is known, then (48) may be integrated to give an expression of the form

$$f_1(\cos\theta_1)\,d\Omega_1 = (Y/4\pi)\sigma Nt\langle\sec\theta_0(\theta_1)\rangle_{AV}\,d\Omega_1 \qquad (50)$$

Here $\langle\sec\theta_0(\theta_1)\rangle_{AV}$ is to be interpreted as the average value of $\sec\theta_0$ for electrons converted into the solid angle $d\Omega_1$.

The distribution is written in this manner in order to show the resemblance to (46).

3. Compton Conversion

The cross section for Compton conversion decreases less rapidly with gamma-ray energy than does that of the photoelectric process, and so for energies greater than 2 or 3 Mev it is the more sensitive method of detection. However, the main advantage in the use of the Compton process is for intensity determinations because the conversion cross section and angular distribution are theoretically known with accuracy, which is not the case with the photoelectric process. Below about 1 Mev the Compton process is not very useful since its spectral features are broad; consequently, it may be difficult to distinguish the Compton electrons from background electrons.

For the determination of energies and intensities by means of external conversion processes it is useful to classify the converter according to its thickness in energy loss units relative to the spectrometer dispersion width. The thicker the converter the more knowledge of the electron stopping process is required. For a very thin converter one need only know the foil surface density, for moderately thick foils one must make a correction for the distribution of energy losses, and for very thick foils the effective electron stopping power is a factor in the intensity formula.

Thin-Converter Method

According to the Klein-Nishina formula (ref. (6), eq. (51),

page 155) the differential cross section for scattering a gamma-ray by a free electron into the solid angle $d\Omega$ is

$$d\sigma = \frac{r_0^2}{2} \frac{k^2}{k_0^2} \left(\frac{k_0}{k} + \frac{k}{k_0} - \sin^2\theta \right) d\Omega \qquad (51)$$

where k = energy of the scattered quantum,
k_0 = energy of the incident quantum,
$r_0 = e^2/m_0c^2$, and $d\Omega = 2\pi d\cos\theta$;

the angles involved are shown in fig. (11). For this process there is the relation (ref. (6), eq. (4), page 146):

$$k_0/k = 1 + \gamma(1 - \cos\theta) , \quad \gamma = k_0/m_0c^2 . \qquad (52)$$

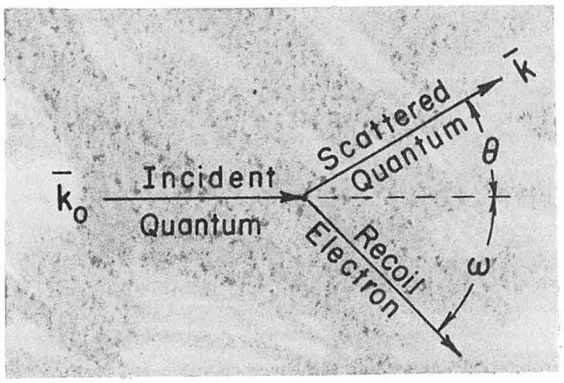

Fig. (11)
Compton Scattering
Angles

If we take $x = k/k_0$ as the independent variable and eliminate the angle from (51) by means of (52), we obtain

$$d\sigma = \pi r_0^2 f(x)\, dx/\gamma , \qquad (53)$$

$$f(x) = \frac{1}{\gamma^2 x^2} + \frac{1}{x}\left[1 - \frac{2(1+\gamma)}{\gamma^2}\right] + x + \frac{1+2\gamma}{\gamma^2} .$$

By means of the relation between θ and ω ,

$$\cot\left(\frac{\theta}{2}\right) = -(1+\gamma)\tan\omega , \qquad (54)$$

and eq. (52) we find, after some algebra, the relation between ω and x, viz.,

$$\sin^2\omega = \left[x(1+2\gamma) - 1\right] / \left[\gamma^2(1-x) + 2\gamma\right] \qquad (55)$$

Assuming the gamma-ray distribution to be isotropic, the number of electrons ejected into the solid angle $2\pi\, d\cos\theta$, is

obtained from (48). We are dealing with a spectrum of conversion electrons, and there is a fixed relation between dx and $d\cos\omega$ given by (55); hence the integrand factor $\delta(\cos\omega)$ in (48) is a delta function and (50) becomes, in the case $\theta_1 + \omega < \delta$,

$$(Y/4\pi) \Sigma \, d\sigma \, Nt \, (\cos^2\theta_1 - \sin^2\omega)^{-1/2} \, 2\pi \, d\cos\theta_1 \, . \qquad (56)$$

Expression (56) may be integrated between the limits θ_a and θ_b of the spectrometer acceptance solid angle. If q is a transmission and counting efficiency factor for the solid angle defined by these limits, then the total number of electrons which will be counted in the interval dx is

$$(Y/4) \Sigma \, Nt \, r_0^2 \, f(x) \, q \, \langle \sec\theta_0 \rangle_{AV} \, \Omega_1 \, dx / \gamma \qquad (57)$$

where

$$\langle \sec\theta_0 \rangle_{AV} \, \Omega_1 = 2\pi \left\{ \log\left(\frac{\cos\theta_b}{\cos\theta_a}\right) + \log\left(\frac{1 + \sqrt{1 - \frac{\sin^2\omega}{\cos^2\theta_b}}}{1 + \sqrt{1 - \frac{\sin^2\omega}{\cos^2\theta_a}}} \right) \right\} .$$

The second term in the brace may be neglected compared to the first for large γ and small x ; it may be regarded as an angular distribution correction term.

The energy of the ejected electron is $T = k_0 - k$ so that $\frac{T}{k_0} = 1 - \chi$. The maximum value of T, or the minimum value of x, occurs when $\theta = \pi$; thus, from (52),

$$\chi_{min} = (1 + 2\gamma)^{-1} \, , \quad \text{and}$$
$$T_{max}/k_0 = 2\gamma/(1 + 2\gamma) \, . \qquad (58)$$

T_{max} is less than k_0 by an energy Δ which is

$$\Delta = \frac{T_{max}}{2} \left[\left(1 + \frac{2m_0c^2}{T_{max}} \right)^{\frac{1}{2}} - 1 \right] \qquad (59)$$

Expression (57) must be corrected for the energy loss distribution in the converter in accordance with the method indicated

by eq. (24), and the spectrometer dispersion must be taken into account before a comparison is made between the experimental and theoretical spectra. A detailed account of the application of the thin-converter method has been given by Rasmussen[2], so we will not discuss it any further.

Thick-Converter Method

When t is large, the distribution in energy of the secondary electrons can be obtained from (26). For simplicity we neglect the rather small angular distribution effects by essentially considering the converter surface to be spherical. We find for the number of electrons in the interval dx

$$Y z N r_0^2 k_0 q \Omega_1 F(x)\,dx/4\pi\mu_{eff}\,, \quad F(x)=\int_{x_{min}}^{x} f(x)\,dx, \tag{60}$$

and

$$F(x)=\frac{2}{\gamma}-\frac{1}{2(1+2\gamma)^2}+\frac{1+2\gamma}{\gamma^2}x+\left(1-2\frac{1+\gamma}{\gamma^2}\right)\ln x(1+2\gamma)+x^2/2-1/(\gamma^2 x)$$

Expression (60) assumes that the yield of gamma-radiation is isotropic. If this is not the case, it will nevertheless be a good approximation when x is small, since the direction of the converted electrons is then nearly the same as that of the incident quantum; Y would then be 4π times the differential cross section for gamma emission in the direction of the spectrometer acceptance solid angle.

The spectrometer data is usually plotted as a function of the field strength which is often expressed in terms of the voltage (millivolts - abbreviated here as mv) across a shunt through which the field current passes. The spectrometer field calibration constant is the field strength in units of gauss-cm

divided by the shunt voltage, viz., $G' = \text{gauss-cm/mv}$.

The relativistic relation between kinetic energy and momentum p is

$$dT = \beta c\, dp \quad , \text{or} \quad dT(kev) = 0.300 \beta\, d\,H\rho(\text{gauss-cm}). \tag{61}$$

In most cases $\beta = \frac{v}{c}$ may be regarded as a constant over the interesting high energy region of the Compton spectrum, so instead of (61) we can simply write

$$\Delta x = -\, 0.300 \beta G' \Delta mv / k_0 \,, \quad k_0 \text{ in kev}. \tag{62}$$

It is customary to express the effective solid angle as the fraction of a sphere, $\Omega_{eff} = \frac{q\Omega_1}{4\pi}$. Using (60) and (61) we obtain for the number of converted Compton electrons which will be detected in the field interval dmv

$$Y \Omega_{eff} \pi Z N r_0^2 (m_0c^2/\mu_{eff})(0.300\beta/k_0) G' F(x)\, d\,mv. \tag{63}$$

In order to compare an experimental distribution with this formula we must take into account the spectrometer dispersion. It is adequately represented by a Gaussian

$$P(\Delta mv) = e^{-(1.67 \Delta mv/W)^2} \,; \quad \int_{-\infty}^{\infty} P(\Delta mv)\, d\,\Delta mv = 1.063\, W, \tag{64}$$

where $\Delta mv = mv_0 - mv$ is the number of millivolts that the field mv_0 is set from a line source at mv, and W is the full width (in mv units at $\frac{1}{2}$ maximum) of the dispersion curve. W increases with the field as $W = (mv_0)p$ where p is the fractional width of the dispersion curve. Over a limited spectral region it is permissible to treat W as a constant. The expected number of Compton electrons counted as a function of the field setting mv_0 is evidently given by

$$Y \Omega_{eff} \pi Z N r_0^2 (m_0c^2/\mu_{eff})(0.300 \beta G'/k_0) \times \int_{-\infty}^{\infty} F(x)\, e^{-(1.67 \Delta mv/W)^2}\, d\,\Delta mv \,. \tag{65}$$

Several resolution widths below the edge of the Compton distribution, it is a fairly good approximation to regard F(x) as linear so that it may be taken outside of the integral of (65). The slope of the distribution on a mv plot is then (in practical units)

$$1.220 \times 10^{-23}\, Y \Omega_{eff} \beta^2 G^2 W f(x) Z \left(\frac{\text{atoms}}{\text{mg}}\right) / H_{eff.} k_0^2, \qquad (66)$$

with k_0 in kev, H_{eff} in kev/mg/cm²

and f(x) is given by (53).

The energy and yield of gamma-radiation may be determined in the following manner. The energy is first estimated from the value of the end point of the spectrum, and then, using a nominal value of γ corresponding to this energy, the spectrum (65) is plotted on the same abscissa scale as the experimental data. The experimental data should be corrected for the variation of the dispersion W by dividing the data through by mv_2/mv, where mv_2 is a reference field setting which should be taken at the most interesting part of the spectrum, say several resolution widths from the edge. The yield and an accurate gamma energy are found as the values which give the best fit of the theoretical to the experimental curve. An approximate method for finding the yield is to compare slopes using (66). The variation of W is most easily taken into account by using for the true slope of the experimental spectrum (less background) the expression

$$\left(\frac{dE(mv)}{d\,mv}\right)_{mv_2} - \frac{E(mv_2)}{mv_2}$$

where $E(mv)$ is the number of counts at mv.

In the determination of the effective stopping power to

use in (65), it is necessary to make a correction for the effects of scattering in addition to the straggling correction (26). Scattering can cause a change in the intensity of the emerging electrons as a function of the depth within the converter from which they were created, and it can cause their paths to deviate from a straight line (umweg) which was assumed in (26).

Since the angular distribution of the converted electrons is roughly isotropic at small angles, the change in intensity due to scattering should be negligible in the light elements that are used as Compton converters. The effect of the umweg can be estimated from the approximate expression (38) if we neglect the straggling of the umweg, for which there is no available treatment in the literature of even an approximate nature. The number of electrons emerging from the foil with a loss in energy Δ in the interval $d\Delta$ is proportional to the thickness of the converter in which they were generated, viz., $N(\Delta)d\Delta \sim dt$. The energy loss is $\Delta = \mu_{eff}\, l$ where μ_{eff} is the effective stopping power which includes energy-loss straggling, and l is the path length. Combining these two expressions with the approximate umweg factor (38) we obtain for the emerging distribution in energy loss

$$N(\Delta)\, d\Delta \sim \frac{d\Delta}{\mu_{eff}\sqrt{1+(4\Delta/\lambda\mu_{eff})}} \qquad (67)$$

If we write $\mu_{eff} = B\log\alpha$ and use (35) for λ , we have

$$4\Delta/\lambda\mu_{eff} = \frac{4Z}{\gamma}\,\frac{\log\xi}{\log\alpha}\,\frac{\Delta P}{P} \quad , \quad \gamma = (1-\beta^2)^{-1/2},$$

where Δp is the momentum loss of the electrons whose initial

momentum was p. For low-Z converters an approximate <u>average</u> correction factor f_{AV} by which the effective stopping power is to be multiplied is

$$f_{AV} \approx 1 + \frac{2Z}{\gamma} \frac{\log \xi}{\log \alpha} \frac{\Delta P}{P} . \qquad (68)$$

For example, for aluminum $\log \xi \approx 4.5$, $\log \alpha \approx 15$ and as a mean value for $\frac{\Delta P}{P}$ we take .02; thus, $f_{AV} \approx 1 + (.16/\gamma)$, which is a significant factor at low energies.

The advantages of the thick-converter method for intensity and energy determination are simplicity and the fact that it is often difficult to satisfy the geometrical requirements for a thin converter. All substances are about equally efficient as Compton converters, so that one may expect secondary electrons coming from the spectrometer baffles and the source itself; hence, it may be difficult to determine the effective thickness of a 'thin' converter. Moreover, if it is required to place an absorber between the source and the converter, the only alternative is the thick-converter method. Although this method requires the additional knowledge of the electron stopping power, we have shown in Part I how this quantity may be determined with rather good accuracy, certainly to within 10% even considering straggling effects. From the point of view of counting statistics the thick-converter method is also superior since the counting rate will be higher. For energy determinations the thin-converter method is to be preferred. It should be mentioned that the thick-converter method developed here is very similar in principle to the well-known Geiger counter methods for finding gamma-radiation intensities (42).

4. Photoelectric Conversion

The photoelectric conversion process is useful at low energies, in particular for energies less than about 2 Mev, where the cross section is higher and the spectral features sharper than the corresponding qualities for the Compton process. In fact, the line shape is monoenergetic aside from broadening due to energy loss in the converter and spectrometer dispersion. The most useful paper for gamma-ray spectroscopy on the external photoelectric effect is the one of Hulme et al [43]. They made calculations which enable one to obtain fairly accurate cross sections for any element for gamma-ray energies greater than about 300 kev. In this section we will survey this paper and develop a method for measuring intensities by photoelectric conversion. Information on the photoelectric effect at high energies can also be found in references (6), (44), and (45).

In the limit as the atomic number Z of the converter material goes to zero, the photoelectric cross section is given exactly in the relativistic region by the equation of Sauter and Hulme [46]. For finite Z , the Born approximation, which is used in the derivation of the Sauter-Hulme equation, leads to a significant error, and cross sections can only be obtained by difficult calculations. Hulme et al numerically calculated photoelectric cross sections for two energies, 1.13 and .354 Mev, and for three values of atomic charge, Z 26, 50, and 84. These six calculated values are plotted in fig. (12) together with the values from Sauter's equation for Z 0; the two curves are interpolations on these points which enable one to obtain crosssections

at these two energies for any value of Z . A third point for the cross section at infinitely high energies can be obtained from a theoretical formula, presumed to be valid at high energies, derived by H. Hall [47] . Hulme et al remark that a certain step in Hall's derivation may not be justified. However, their rigorous calculations seem to approach this limiting formula in the proper manner so that they accept it as being correct, or at least a good approximation, in the high energy limit. The K-shell photoelectric cross section for thorium is plotted in fig. (13) from the two values of fig. (12) and Hall's formulae for infinity and 2.5 Mev. Shown dotted in fig. (13) is the empirical formula of L. H. Gray [48] . For lead this formula is

$$\sigma_K = 1.35 \times 10^{-25} \lambda^{1 + 0.48 \log_{10} \lambda} \quad cm^2 \qquad (69)$$

with λ in X.U.; we have converted it to thorium by means of the theoretical ratios from fig. (12) and Hall's formula. Gray's formula, which is in excellent agreement with the calculated points, was used as a guide for interpolating through these distant points.

Hulme et al make two approximations in their work; they neglect electron exchange and screening by the outer shells. These approximations are presumably quite good; they say that their overall results should be accurate to within 8%, and possibly 4% for Pb in view of the agreement with Gray's formula. Fig. (14) is obtained drectly from their paper except that we have plotted the total K-shell cross section rather than the atomic absorption cross section. For the relation between these two quantities they used $\sigma_{atom} = \frac{5}{4} \sigma_K$.

In order to determine gamma-ray yields from a flat converter it is necessary to know the angular distrigution factor in eq. (50). Unfortunately, the angular distribution of photoelectrons for relativistic energies is known only in the limit by Sauter's equation, viz.,

$$S(\mu)\,d\mu = \text{constant} \times \frac{(1-\mu^2)}{(1-\beta\mu)^3}\left[\frac{\sqrt{1-\beta^2}}{(1-\beta\mu)} + \frac{3(1-\sqrt{1-\beta^2})-2\beta^2}{2(1-\beta^2)}\right]d\mu \quad (70)$$

where $\mu = \cos\omega$, $\beta = v/c$, and v is the electron velocity. A noteworthy feature of (70) is that the distribution is concentrated in the forward direction with a maximum at about $\cos\omega = \beta$. According to fig. (14) the Born approximation applied to Pb would be in error by a factor of about three at all high energies, so it is not expected that (70), also derived by the Born approximation, is correct for the heavy elements. However, it was anticipated that the angular distribution might be less affected by this approximation for high Z than the total cross section, and so $\langle \sec\theta_0(\theta_1)\rangle_{AV}$ was computed from (50) using (70) as a function of the angle 2δ subtended by the converter at the source. Actually, if the distribution is predominantly in the forward direction, the evaluation of $\langle \sec\theta_0(\theta_1)\rangle_{AV}$ would not be sensitive to the details of $S(\cos\omega)$. The results are shown in figs. (150, (16), and (17) for three photoelectron energies. According to (50), $\langle \sec\theta_0(\theta_1)\rangle_{AV}$ is proportional to the distribution per unit solid angle $d\Omega$, of converter electrons; the figures show that this distribution is not isotropic so that multiple scattering will affect the results. An approximate scattering correction may be made by using (44). The mean spectrometer acceptance which we used

corresponds to $\cos\theta_1 = .94$. Since expression (44) is not accurate, it should serve as an indication of the uncertainties involved as well as a correction factor. From figs. (15) - (17) it is apparent that for minimizing these uncertainties the most suitable converter angle δ is about 60°. The results of some experiments described below show that the use of the distribution (70) for Z 90 is incorrect; the curves of figs. (15) - (17) are reproduced here for their qualitative value.

Thin-Converter Method

In order to avoid the complications due to scattering, intensity determinations by means of photoelectric conversion should be performed with as thin a converter as allowed by the considerations of counting statistics, background, etc. It has not been possible to account for the observed thin-converter line shapes in a quantitative manner, the difficulty being due to the lack of knowledge of the angular distribution in the conversion process and the effects of scattering. Hence, the best procedure is to take the total area under the line spectrum as a measure of the gamma-ray intensity. For the Gaussian dispersion curve (64) the relation between the yield and the area under the K-conversion spectrum is

$$Y\,\Omega_{eff}\,\sigma_K\,N\,t\,\langle \sec\theta_0(\theta_1)\rangle_{AV} = (.940/P)\int_0^\infty E(m_0c)\,d(h\nu/m_0c) \quad (71)$$

where Ω_{eff} is the solid angle expressed as a fraction of a total sphere, p is the fractional width of the dispersion curve at $\frac{1}{2}$ maximum, and σ_K is the K-shell conversion coefficient.

Some experiments were performed with radioactive sources in

order to find the correct value of $\langle \sec\theta_o \rangle_{AV}$ to be used in (71). Actually there may be some error in the value of σ_K taken from fig. (13); nevertheless, it is just as well to regard σ_K as known, and to consider $\langle \sec\theta_o \rangle_{AV}$ as a combined angular distribution and correction factor which we will find empirically. The most direct procedure is to measure $Y\Omega_{eff}$ for the source by means of the presumably accurate Compton thick-converter method;** then $\langle \sec\theta_o \rangle_{AV}$ is determined from the area of the photoelectric line spectrum as a function of the converter thickness t and the converter angle δ . The results for $\langle \sec\theta_o \rangle$ as a function of cos δ are shown in fig. (18) for the 1.275-Mev gamma-ray of Na^{22} using a 22 mg/cm^2 ($t/\lambda \approx .1$) thorium converter. Typical photoelectric and thick-converter (55 mils Al) Compton spectra are shown in figs. (19) and (20). The calculated curve of fig. (18) was obtained from fig. (15), and an estimate of the effects of scattering in the converter was made with (44) as a guide. It is quite apparent from the results that the use of (70) for the angular distribution in heavy elements is not satisfactory.

Fig. 21 shows the observed effect* of converter thickness on the determination of $\langle \sec\theta_o \rangle_{AV}$ together with the estimated effect due to scattering, using fig. (15) and eq. (44). Again the theory is not correct but at least the proper trend is predicted. That is, for small cosδ scattering will actually increase rather than decrease the number of electrons emerging in the direction of the spectrometer acceptance solid angle as

* Figures (21a) and (21b) show the observed spectrometer distributions from the Na^{22} 1.275-Mev gamma-ray for cosδ = .32 and cos$\delta \approx$ .08.

** The experimental points in figures (18), (21), (22), and (23) were evaluated from eq. (71) using an inaccurate measurement of the

mentioned in Section 4 of Part I. On the other hand, for a larger value of $\cos\delta$ there are not so many electrons from gamma-radiation in directions near $\pi/2$ which can be scattered into the spectrometer solid angle; it is evident from fig. (21) that for $\cos\delta = .32$ about as many electrons are scattered into as out of this direction.

Fig. (22) shows a plot of $\langle \sec\theta_0 \rangle$ calculated from (71) using hemispherical converters of various thicknesses (the converter being situated between the source and the spectrometer. According to (70), in the limit $Z = 0$ there are very few electrons converted at angles $\omega > \pi/2$ so that $\langle \sec\theta_0 \rangle$ should be nearly unity, whereas it is found to be about 20% less for a very thin converter. The difficulty apparent in figs. (22) and (18) is very likely that the angular distribution for $Z = 90$ is not nearly as pronounced in the forward direction as it is in (70). This explanation would also account for the fact that the calculated values of fig. (18) are greater than observed for $\cos\delta > .2$ and less than observed for $\cos\delta < .2$. With the hemispherical converter $\langle \sec\theta_0 \rangle$ drops rapidly with the converter thickness probably because the electrons have to travel a large effective distance through the converter in order to get out, contrary to the situation in a flat converter. Fig. (23) shows the results for the annihilation radiation from the positrons of Na^{22}. Not much data was taken but it is seen to be in disagreement with the predictions of (70). It is interesting to note that the curve for $\langle \sec\theta_0 \rangle$ from the distribution (70) for 400 kev electrons fits

solid angle, viz. $\Omega_{eff} = .024$. A more accurate value, $\Omega_{eff} = .0203$ (from page 64 - see also page 47) requires that all experimental points be raised by a constant factor 1.18.

rather closely to the experimentally observed curve, fig. (18), for the conversion electrons from the 1.275-Mev gamma-ray; this observation is compatible with the above conclusion that at a particular energy the photoelectric angular distribution is not as pronounced in the forward direction for high Z as it is for $Z = 0$.

We will describe now a scheme which was developed by Professor T. Lauritsen for finding relative values of $\langle \sec \theta_o \rangle$. It is apparent from figs. (18) and (23) that $\langle \sec \theta_o \rangle_{Av}$ is rather sensitive to $\cos \delta$ but not to the energy of the gamma-ray. On this account it was decided to standardize for all energies on a value of $\cos \delta = .32$, in particular a 3/8" diameter flat converter at 1/16" from the source.*

Co^{60} decays to Ni^{60}, which subsequently emits a gamma-ray of 1.33 Mev in cascade with one of 1.17 Mev. Since the 1.33-Mev gamma-ray has almost the same energy as the 1.28-Mev gamma-ray of Na^{22}, it was possible by means of the beta-ray spectrometer to determine accurately the relative strengths of these two sources. This was done by comparing the areas of the photoelectric conversion spectra, making the appropriate correction for the variation of the total photoelectric cross section, using fig. (13), but otherwise assuming $\langle \sec \theta_o \rangle_{Av}$ to be the same in each case (this turns out to be a very good approximation). The efficiency of an aluminum-walled Geiger counter for the annihilation radiation of Na^{22} was found by comparing the counting rates for the two sources. The relative efficiencies for the two Ni^{60}

*Fig. (23a) shows the constructional details of the radioactive source holders used in the following experiments.

gamma-rays are 0.86 and 0.74% for an aluminum-walled counter according to the curve of Bradt et al[49]. Good et al[50] found that the percentage K-capture in the 1.28-Mev transition of Na^{22} is less than 5% so that there will be nearly two annihilation quanta for every gamma-quantum from Na^{22}, the probability of one-quantum or no-quantum annihilation in light elements being negligible[6]. With this information and making appropriate corrections for source and wall absorption, the counter efficiency for annihilation radiation was found to be 0.25%, relative to the above-mentioned values, which is about 20% higher than the figure given by the curve of Bradt et al. The Geiger counter efficiency is then assumed to be linear between this value for annihilation radiation and 0.86% for the Ni^{60} 1.33-Mev gamma-ray; it is very nearly so according to the curve of Bradt et al. The strengths of Cs^{137} and Cs^{134} sources, which emit radiations in this energy range, were found relative to Co^{60} by means of the counter. The photoelectric lines from these other sources were observed in the spectrometer using a thin (5.75 mg/cm^2) thorium foil with a geometrical factor $\cos\delta = .32$. Relative to the Na^{22} 1.275-Mev gamma-ray the value of $\langle \sec\theta_D \rangle_{AV}$ for 0.51-Mev radiation was found to be $0.92 \pm .02$; for the .67-Mev γ-ray of Cs^{137} and the .79-Mev γ-ray of Cs^{134} it was 0.97 relative. Another useful source for obtaining relative converter efficiency factors is Na^{24} which emits a 2.76-Mev gamma-ray in cascade with a 1.38-Mev gamma-ray; no cross-over radiation has been observed. From the areas under the photoelectron line spectra from a 22-mg/cm^2 Th converter

and using eq. (71) we found $\langle \sec\theta_0 \rangle_{1.38} / \langle \sec\theta_0 \rangle_{2.76} = 1.01$. The strength of the Na^{24} source relative to the Co^{60} source was determined by comparing the photoelectric line shapes of the adjacent 1.38 and 1.33 radiations in exactly the same manner as in the comparison of Na^{22} with Co^{60}. By a Geiger counter comparison of the radiations from Na^{24} and Co^{60}, it was possible to determine the efficiency of the counter for 2.76-Mev radiation relative to the efficiency for Co^{60} gamma-radiation; a value of 2.1 ± 0.2 % for 2.76-Mev radiation relative to the above-mentioned values for Co^{60} was obtained. Fig. (24) is a plot of the Geiger counter efficiency from these data and an extrapolation of high-energy data[42]; the absolute normalization of this curve is somewhat arbitrary since it depends on how the counter solid angle is measured; in this figure a solid angle about 10 % larger than the geometrical value was used.*

The absolute strength of the Co^{60} source can be found by a counter comparison with a calibrated standard source furnished by the National Bureau of Standards. Furthermore, the solid angle of the spectrometer may be accurately obtained by a spectrometer measurement of the Co^{60} internal conversion electron spectrum as described in the next section; by this prodedure we obtained an effective solid angle of $\Omega_{eff.}$ .0203. Knowing the Co^{60} source strength and the spectrometer solid angle, eq. (71) may be used to solve for the absolute value of the efficiency factor $\langle \sec\theta_0 \rangle_{AV}$; from the photoelectron line spectrum from 21.8-mg/cm^2 Th, which is shown in fig. (24'), a

* An extensive bibliography and recent measurements of low-energy Geiger counter efficiencies are given by G. A. Renard, Annales de Physique 5-12, 25 (1950).

value $\langle \sec\theta_o \rangle_{Av} = 1.36$ is obtained. With this absolute value, the above-mentioned relative values of $\langle \sec\theta_o \rangle_{Av}$ may be made absolute.

An additional value of $\langle \sec\theta_o \rangle_{Av}$ for 3.1 Mev can be obtained by an analysis of the photoelectron conversion spectrum from the strong radiation from the nuclear reaction $C^{12}(dp)C^{13*}$. There is good reason to believe that this radiation is isotropic (see Appendix F of Part IV) so it is possible to compare measurements at various angles and to regard the yield per unit solid angle as independent of angle. A Geiger counter was placed at 90° to the beam direction and the rate of emission from this reaction (after filtering out the annihilation radiation with lead shielding) was compared with that observed from a Co^{60} source of known strength placed at the target position in the spectrometer. The relative Geiger counter efficiencies for these two radiations was obtained from fig. (24). In this way the absolute yield of the 3.10 radiation from 1.41-Mev deuteron bombardment of a thick carbon target was found to be $Y = 12.3 \times 10^{-6}$ γ/d which is in satisfactory agreement with a value of 13.3×10^{-6} obtained in another experiment (Appendix F of Part IV) for a slightly higher energy, $E_d = 1.46$ Mev. The rate of change of the $C^{12}(dp)C^{13*}$ thick-target yield in the range from 1.2 to 1.4 Mev has been measured to be 22 γ/d x Mev so that the above difference is accountable. Fig. (25) shows the photoelectron spectrum from a 22-mg/cm^2 Th converter having a geometrical factor of $\cos\delta = .32$; also shown is the Compton spectrum from a 50-mil Al converter. The thorium converter was placed over the Al converter in order to facilitate the determination of the background. Using the solid-angle value .0203 and from the area under the photo-

electron spectrum, a value of $\langle \sec\theta_0 \rangle_{AV} = 0.77$ was obtained from eq. (71). The results of the absolute measurements of sec for a geometrical factor of cos .32 are the following:

Gamma-Ray Energy	Source	$\langle \mathrm{Sec}\,\theta_0 \rangle_{AV}$
.51 Mev	Na^{22} annihil. rad.	1.25
.66	Cs^{137}	1.32
.79	Cs^{134}	1.32
1.33	Co^{60}	1.36
2.76	Na^{24}	1.01
3.10	$C^{12}(dp)C^{13*}$	.77

The solid angle of the spectrometer may also be computed from the Compton spectra from these various sources since we know their absolute strengths. These evaluations provide some indication of the accuracy of this procedure for determining intensities. Using the slope method described in Appendix A for determining the absolute intensity from the Compton thick-converter spectra, the quantity $\Omega_{eff.}$ was evaluated in eq. (90) for the various sources. The results are the following:

Gamma-Ray Energy	Source	Ω_{eff} from (90)
1.33	Co^{60}	2.10×10^{-2}
1.28	Na^{22}	2.06
.51	Na^{22} annihil. rad.	1.96
.66	Cs^{137}	2.12
1.38	Na^{24}	2.09
2.76	Na^{24}	2.43
3.10	$C^{12}(dp)C^{13*}$	1.99

Aside from the Na^{24} 2.76-Mev value, which is somewhat high, the above values appear to be in satisfactory agreement with one another and with the value $\Omega_{eff} = .0203$ obtained from the Co^{60} internal conversion measurement.

Thick-Converter Method

As in the case of Compton conversion, it is desirable to have a thick converter method for measurement of radiation intensities by the photoelectric process; in fact, such a method has been discussed by Richardson[51] and applied by Martin and Richardson[52]. In their intensity determination procedure they considered straggling using the White and Millington data[28], but neglected scattering effects, asserting that it is unimportant in regard to attenuation of the beam. They overlooked the umweg factor which is easily shown to be essential to the determination of the converter efficiency. It is apparent from fig. (6) that the effect of straggling in an infinitely thick converter is merely to reduce the intensity and not to alter the distribution in energy of the emerging electrons. The line-shape features which they observed were not at all flat but rather qualitatively resembled (except for their Th X-line data) the distribution (67) which arises from just the consideration of the umweg effect. According to (67) the momentum distribution of emerging electrons will drop to one-half its maximum initial value when

$$\left(\frac{\Delta P}{P}\right)_{\frac{1}{2}\,max} = \frac{3\gamma \log\alpha}{4Z \log\xi} . \qquad (72)$$

Using values of the constants appropriate to thorium, this expression becomes $\left(\frac{\Delta P}{P}\right)_{\frac{1}{2}\,max} \approx .03\,\gamma$.

In the low energy region where the photoelectric conversion process is applied, this momentum loss is only several spectrometer dispersion widths. Expression (72) is in reasonable agreement with the thick converter (3 mil Th) spectra for Au^{198} ($E_\gamma = 411$ kev)

and B^{10*} ($E_\gamma = 713$ kev) observed by Hornyak, Lauritsen, and Rasmussen[3].

We conclude, contrary to Martin and Richardson, that scattering is important; since our treatment is approximate as well as incomplete, it is not possible to obtain thick-converter efficiency factors other than by empirical methods.

5. Internal Conversion

The internal conversion of gamma-radiation is proportional to the K-electron probability density at distances from the nucleus of the order of the Compton wave length of the electromagnetic field; therefore it is roughly proportional to Z^3, which makes it useful for determining the character of radiative transitions in the heavy elements. Nevertheless, we have been able to detect the internal conversion electrons associated with the 713-kev gamma-ray of B^{10} which was produced in the nuclear reaction $Be^9(dn)B^{10*}$. We will describe here an attempt to determine the multipolarity of this gamma-ray. Two difficulties which arise in the interpretation of conversion data in nuclear reactions will be considered; some of this discussion will also be pertinent to the interpretation of internal pair formation data (section 6).

Using the Born approximation and neglecting the binding of the K-electrons, the K-shell probability density was taken to be everywhere $(Z\alpha)^3/\pi$ where $\alpha = e^2/\hbar c$, Dancoff and Morrison[53] computed the 2^ℓ-pole electric, α_K^ℓ, and magnetic, β_K^ℓ, internal comversion coefficients by relativistic quantum electrodynamics;

their results for 2 K-electrons are :

$$\alpha_K^{\ell} = \frac{2Z^3\alpha^4}{k^3}\left(\frac{k+2}{k}\right)^{\ell-\frac{1}{2}}\left[\frac{(\ell+1)k^2+4\ell}{\ell+1}\right],$$

$$\beta_K^{\ell} = \frac{2Z^3\alpha^4}{k}\left(\frac{k+2}{k}\right)^{\ell+\frac{1}{2}}; \quad k = h\nu/m_0c^2. \tag{73}$$

Recently Rose et al (54) calculated these coefficients numerically, making no approximations other than the neglect of screening. We have plotted in figs. (26), (27), and (28) the ratio of these exact values to those of (73); it is apparent that the expressions (73) are considerably in error even for Z as low as ten, the error being first order in . It is possible to show by a relativistic calculation that the error due to the neglect of the binding of the K-electrons is second order in so that the first order error of (73) must arise from the use of the Born approximation. This deduction is important for our consideration of internal pair formation, a process which is very similar to internal conversion, since the only calculations available (there are a few exceptions) make use of the Born approximation.

Angular Distributions for Internal Conversion Electrons

The radiations from a nuclear reaction may not be isotropic since the incident beam is polarized with zero angular momentum about the beam direction, $\theta=0$. With an axially aymmetric spectrometer, we can measure at the spectrometer acceptance angle θ the rate of internal conversion $I_i(\theta)$ and the rate of emission $I_e(\theta)$ of electrons from external conversion of the gamma-radiation

associated with the internal conversion electrons. In the case of external Compton conversion the most energetic electrons are ejected in the same direction as the gamma radiation so that for these energetic electrons $I_e(\theta)$ will be proportional to the rate of emission of gamma-radiation $I_\gamma(\theta)$ at the angle θ. As we have seen in section 4, in the case of external photoelectric conversion the angular distribution problem is complicated so that it is probably not possible to determine accurately the relation between $I_\gamma(\theta)$ and $I_e(\theta)$. Nevertheless, if we use the Compton process to measure $I_\gamma(\theta)$, there is no assurance that the internal conversion coefficient $\int_{4\pi} I_i \, d\Omega / \int_{4\pi} I_\gamma(\theta) \, d\Omega$ is equal to $I_i(\theta)/I_\gamma(\theta)$ since the angular distributions may not be isotropic or not the same, in case that they are not isotropic; consequently the interpretation of the data may be complicated. Calculations given below show that the angular distributions of the electric dipole and quadripole conversion electrons do indeed differ from the associated gamma-radiation distributions for each magnetic-axis component transition but that the distributions are the same in the case of the magnetic dipole and quadripole fields.

This calculation is essentially a repetition of the original one of Dancoff and Morrison in order to determine the angular distributions which they did not give.

A convenient gauge for describing the 2^ℓ-pole radiation field is given by Rose[55] as

$$\vec{A}_{\ell m} = \left(2/\pi\ell(\ell+1)\right)^{1/2} \chi_{\ell-1}(kr)\left(r\,\overrightarrow{\text{grad}} + \frac{\ell \vec{r}}{r}\right) Y_\ell^m(\theta,\phi),$$

$$V = i\left(2\ell/\pi(\ell+1)\right)^{1/2} \chi_\ell(kr)\, Y_\ell^m(\theta,\phi)$$

for electric multipole fields and

$$\vec{A}_{lm} = -(2/\pi l(l+1))^{1/2} \chi_l(kr) i\vec{r} \times \overrightarrow{\text{grad}}\, Y_l^m(\theta,\phi), \quad (74)$$
$$V = 0$$

for magnetic multipole fields, where χ_l is the spherical Hankel function of the first kind

$$\chi_l(x) = (\pi/2x)^{1/2} H^{(1)}_{l+\frac{1}{2}}(x)$$

and $k = h\nu/m_0c^2$. With this normalization the number of quanta per second is $1/\pi k^2$. If the unperturbed Hamiltonian is taken as

$$H = -\vec{\alpha}\cdot\vec{P} - \beta$$

the interaction of an electron with the radiation field is

$$e(V + \vec{\alpha}\cdot\vec{A})$$

With the use of the Born approximation and the neglect of the binding of the K-electrons, the calculation is facilitated by means of the projection operators for K-electron and ejected electron, viz.,

$$G_K = (-\beta+1)/2 \qquad \text{and} \qquad G_- = (-\vec{\alpha}\cdot\vec{P} - \beta + W)/2W$$

where W is the total energy of the ejected K-electron and $|\vec{P}| = P$ is its momentum. The differential conversion coefficient for the solid angle $d\Omega$ is then given by

$$d\gamma_{lm} = \frac{\alpha^4 k P W Z^3}{4\pi} \text{Spur}(\Lambda G_K \Lambda^* G_-)\, d\Omega,$$

$$\text{with} \quad \Lambda = (\vec{\alpha}\cdot\vec{f}) + g \quad , \quad \text{and}$$

$$\vec{f}_{lm} = \int e^{-i\vec{P}\cdot\vec{r}} \vec{A}_{lm}\, d\tau, \quad (75)$$

$$g_{lm} = \int e^{-i\vec{P}\cdot\vec{r}} V_{lm}\, d\tau.$$

A straightforward evaluation of the spur leads to:

$$\text{Spur}(\Lambda G_K \Lambda^* G_-) = \quad (76)$$

$$[g g^*(k+2) + (\vec{f}\cdot\vec{f}^*)k - \vec{P}\cdot(g\vec{f}^* + g^*\vec{f})]/(k+1).$$

The computation of $\vec{f}$ and g is performed by means of the relation

$$\int e^{-i\vec{P}\cdot\vec{r}} B_{\ell m}(\vec{r})\, d\tau = 4\pi(-i)^{\ell} Y_{\ell}^{m}(\Theta,\Phi)\sqrt{\tfrac{\pi}{2}}\int_{0}^{\infty}\frac{r^{2}}{\sqrt{Pr}} J_{\ell+\frac{1}{2}}(Pr) R_{\ell}(r)\, dr \qquad (77)$$

where $B_{\ell m}(\vec{r}) = Y_{\ell}^{m}(\theta,\varphi)\, R_{\ell}(r)$;

$J_{\ell+\frac{1}{2}}$ is the Bessel function of $\frac{1}{2}$-integer order; the angles θ, φ describe the direction of $\vec{r}$; and Θ, Φ describe $\vec{P}$ with respect to the axis of quantization $\theta = 0$. It is necessary to use a convergence factor for the radial integration in (77).

The internal conversion angular distributions were calculated from (75) for just the $m = 0$ component. According to Falkoff and Uhlenbeck[56] the angular distributions of the other components of the transition may be obtained from any one component. From symmetry considerations they find that angular distribution intensity components $F_{\ell}^{m}(\theta)$ have the following general parametric forms:

$$\begin{aligned}
\ell = 1 \quad ; \quad & F_{1}^{0}(\theta) = (1+\lambda) - 2\lambda\cos^{2}\theta, \\
& F_{1}^{\pm 1}(\theta) = 1 + \lambda\cos^{2}\theta ; \\
\ell = 2 \quad ; \quad & F_{2}^{0}(\theta) = \mu_{1} + \cos^{2}\theta + \mu_{2}\cos^{4}\theta, \\
& F_{2}^{\pm 1}(\theta) = (\mu_{1}+\tfrac{1}{6}) + (\mu_{2}+\tfrac{1}{2})\cos^{2}\theta - \tfrac{2}{3}\mu_{2}\cos^{4}\theta, \\
& F_{2}^{\pm 2}(\theta) = (\mu_{1}+\tfrac{1}{2}\mu_{2}+\tfrac{2}{3}) - (\mu_{1}+1)\cos^{2}\theta + \tfrac{1}{6}\mu_{2}\cos^{4}\theta .
\end{aligned} \qquad (78)$$

The parameters for the internal conversion distributions are given in Table II, which also includes the parameters for the radiation[57] and spherical harmonic fields.

From Table II it is apparent that the magnetic-pole internal conversion electron distributions are the same as the distribu-

ℓ	Parameter	Internal Conversion		γ-Radiation Elect.& Mag.	Spherical Harmonic
		Electric	Magnetic		
1	λ	$\frac{(k^2-4)}{(k^2+4)}$	1	1	-1
2	μ_1	$\frac{4}{(9k^2-24)}$	0	0	$-\frac{1}{6}$
	μ_2	$\frac{(12-3k^2)}{(3k^2-8)}$	-1	-1	$-\frac{3}{2}$

Table II

tions of the associated radiation fields. The electric-pole conversion distributions are the same as the radiation distributions when $k=\infty$ and the same as the spherical harmonic (particle of spin zero) distributions when $k=0$. In the case of the 713-kev transition of B^{10}, k 1.39 so that

$$\lambda = -1/3 \quad \text{and} \quad \mu_1 = -2/3 \,, \; \mu_2 = -3 \,.$$

Thus we can expect conversion distributions differing from the radiation distributions unless the conditions favor isotropy.

Probability that the K-shell of the Recoil Nucleus is Occupied

Another complication to the finding of internal conversion coefficients from transitions produced by nuclear reactions is the determination of the probability that the recoiling nucleus has any K-electrons at the time it radiates. The time it takes

to emit a low-energy quadrupole quantum ($\sim 10^{-12}$ sec. for .7-Mev transition) is estimated to be of the order of magnitude of the time that it takes to stop a recoil nucleus in a solid material. In the case of electric or magnetic dipole radiations, which are faster, we would expect that the recoil nucleus radiates before it loses much velocity. In order to give a minimum estimate of the K-shell occupation probability at the time of radiation, we need to know the number of K-electrons that the nucleus has before it is slowed down in the target material.

There are three aspects to the history of the K-electrons of a recoil nucleus. First of all, there is a certain probability that the incident particle, deuteron in the case of interest, will ionize the two K-electrons of the target nucleus; it has a well-defined orbit since a disintegration is observed. The ionization probability will be of the order of the ratio of the classical cross section for ionization to the 'area' of the K-shell, $\pi a_0^2/Z^2$; this ratio is $4(e^2/\hbar v)^2$ where v is the incident particle velocity. For 1-Mev deuterons this probability is nearly unity. Secondly, at the instance of recoil from the nuclear reaction, the probability that a K-electron, initially bound to a nucleus of charge Z_1, will attach itself to the residual nucleus, which is suddenly moving with a velocity v' and with a new charge Z_2, is given by the absolute square of the Fourier coefficient for the sudden change, viz.,

$$2^6 Z_1^3 Z_2^3 (Z_1+Z_2)^2 / [(Z_1+Z_2)^2 + (a_0 K)^2]^4 \qquad (79)$$

$$K = m_0 v'/\hbar .$$

For 1-Mev deuterons in the reaction $Be^9(dn)B^{10}$ this probability is nearly unity.

Finally, as the recoil nucleus proceeds through the target material, there will occur capture and loss of the orbital electrons. From the estimates of Bohr[5] on the cross sections for these processes, it can be shown that the average charge of the nucleus will reach the equilibrium value given by capture and loss considerations before the nucleus has a significant probability of radiating; hence, the two first two aspects are rather unimportant. At equilibrium the ratio of the probability that an ion has one K-electron to the probability that it has two is $\sigma_\ell^{1-2}/\sigma_c^{1-2}$ where σ_ℓ^{1-2} and σ_c^{1-2} are the cross sections for loss and capture in the exchange from one to two K-electrons; for the exchange from one to no K-electron the ratio of the probabilities is similarly $\sigma_\ell^{1-0}/\sigma_c^{1-0}$. For the case $E>>E_0$, where E_0 is the ion energy for which its velocity is equal to the classical velocity of the atomic orbital involved in the exchange, Bohr[5] obtains the approximate relation

$$\sigma_\ell^{1-0}/\sigma_c^{1-0} \sim \frac{Z_m^{1/3}}{4Z_i^\ell}\left(\frac{E}{E_0}\right)^{5/2} \qquad (80)$$

where Z_m is the charge of the material being penetrated, and Z_i^ℓ is the net charge of the ion when it has lost the electron in concern. Fig. (29) shows the experimental results of T. Hall[58] on the capture and loss ratio for protons in various materials, and fig. (30) shows the early results on measurements of the ratio of singly- to doubly-charged helium ions in mica. The insensitivity of (80) to Z_m is borne out by the measurements of Hall

and the early measurements of the capture and loss ratio for helium ions in various materials (63). An examination of figs. (29) and (30) shows that for $E > E_o$, eq. (80) is at least correct to within a factor of two; no greater accuracy is to be expected considering the nature of the derivation.

In an attempt to estimate the capture and loss ratio for the K-shell of other ions it is probably more accurate to use instead of (80) the relation

$$\sigma_\ell / \sigma_c \sim f(E/E_o) \tag{81}$$

where $f(E/E_o)$ is given by the experimental curves of figs. (29) and (30). We are interested in the capture and loss ratio for the exchange '1-2', whereas figs. (29) and (30) are for the exchange '1-0'. In view of the lack of information on the former ratio we estimate that it is simply

$$\sigma_\ell^{1-2} / \sigma_c^{1-2} \sim 4 f_{1-0} \left(\frac{I_{1-0}}{I_{2-1}} \cdot \frac{E}{E_o} \right) \tag{82}$$

where I_{2-1} and I_{1-0} are the ionization potentials for removal of the first and second K-electrons respectively, and E_o is the ion energy at which its velocity is $Z_2 e^2/\hbar$, where Z_2 is the nuclear charge of the ion. The factor of 4 in (82) is obtained from the considerations that the probability of capture of a second K-electron is reduced by a factor of 2 since the exclusion principle requires its spin to be opposite to that of the other K-electron, and the probability of loss is twice as great from a completely occupied K-shell as from a singly occupied K-shell.

We are interested in the state of ionization of the residual nucleus B^{10} produced in the reaction $Be^9(dn)B^{10*}$. With deuterons of 1 Mev the mean energy of motion of the residual nucleus will be about $E/E_0 = .08$. Using (82) and fig. (30) we find $\sigma_\ell^{1-2}/\sigma_c^{1-2} \sim .04$. As the recoil nucleus slows down this ratio diminishes rapidly so that we can be fairly certain that there is a high probability of B^{10} having two K-electrons at the time it radiates, even though our estimate may be incorrect by several factors of two.

Actually the experimental curves of figs. (29) and (30) refer to the exchange of charge for the total of all of the shells of the penetrating ion while we have assumed that practically the entire exchange observed involves the K-shell. This assumption is justified by the classical velocity-dependence arguments of Bohr[5] and by the detailed born-approximation calculations of Brinkman and Kramers[64].

Internal Conversion Coefficient of the 713-kev Gamma-Ray of B^{10}

The 713-kev gamma-ray observed in the $Be^9(dn)B^{10*}$ reaction is very strong; according to Rasmussen[2] the thick-target yield at 1.2-Mev bombarding energy is 13.7×10^{-6} γ per deuteron making it one of the most intense of the radiations observed in light nuclear reactions at low energies. On this account it was possible to observe with a spectrometer the electrons from the inefficient internal conversion process.

A beryllium target of about 1-mg/cm^2 thickness consisting

of thin evaporated foils was bombarded by a 0.97-Mev deuteron beam of about 1/4-μamp intensity. The exact field setting for the internal conversion electrons was calculated from the knowledge of the gamma-ray energy and the spectrometer field constants, and it was found that at this setting the counting rate was about 5.6 counts/sec. as compared to 4.8 counts/sec. for a field setting 3.3% higher or lower than the predicted internal conversion line setting (the spectrometer resolution was 2.0%). A cursory observation was made of the line shape, but, clearly, the statistics were so poor that not enough time was available to permit finding the internal conversion line peak from the line shape. A total of about 1700 counts above background was found at the field setting predicted for the IC electrons. The intensity of the associated gamma-ray was measured by the Compton thick-converter method using a 10-mil Al foil; otherwise the geometry and experimental conditions were identical with those of the measurement of the IC electrons. Assuming that the ratio of IC to gamma-ray differential cross sections at the mean spectrometer acceptance angle ($\theta_1 = 20^\circ$) is equal to the ratio of the respective total cross sections, a value of 1.8×10^{-6} is obtained for the IC coefficient with an uncertainty of $\pm 0.8 \times 10^{-6}$ (standard deviation) which is mostly due to statistics. According to Rose et al (54) the expected K-shell IC coefficients for the lowest radiation multipoles are :

$$\alpha_K^1 = 1.49 \times 10^{-6} \quad , \quad \alpha_K^2 = 4.25 \times 10^{-6}$$

$$\beta_K^1 = 1.92 \times 10^{-6} \quad , \quad \beta_K^2 = 4.68 \times 10^{-6} ;$$

the higher multiposes have coefficients which increase with the order. It appears that our datum is consistent with only mag-

netic or electric dipole assignments provided the important assumptions that we have made concerning the angular distribution and the K-shell occupation probability due not lead to significant errors.

It would seem to be possible to increase the total counting time by a factor of four in a day without losing reproducibility so that it may be possible to narrow the assignment to one multipole. However, a computational investigation should be made of the possible errors that can be expected from angular distribution anisotropies to determine if it is worthwhile to have more statistical accuracy.

The suggestion of this experiment that the 713-kev transition is magnetic or electric dipole is not compatible with the finding (not absolutely certain) that the $C^{10}-\beta^{+}$ decay proceeds with an allowed value $ft \sim 2000$ to this state. We would expect that C^{10} has $J=0$ (even) so that the 713-kev state would be $J=1$ (even) on Gamow-Teller selection rules and $J=0$ (even) on Fermi rules; the radiation to the ground state $J=3$ (even) would be of higher order than dipole.

Internal Conversion Coefficient of the Ni^{60} 1.33-Mev Gamma-Ray

The energy level diagram of Ni^{60}, as given by Mitchell[66], is shown in fig. (31). The spin and parity assignments of the levels are determined from the assumption that the ground state, being an even-even nucleus, is $J=0$ (even) and the measurements of the angular[67] and polarization-directional correlation[68]

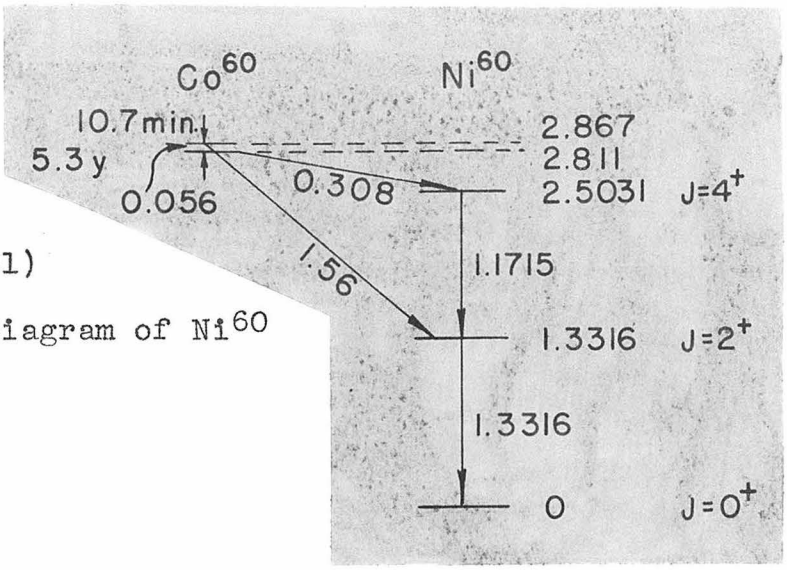

Fig. (31)

Energy Level Diagram of Ni^{60}

of the cascade radiations. The measurements by Waggoner, Moon, and Roberts[69] of the internal conversion coefficients of the two gamma-rays show that they are both electric quadripole; this finding is consistent with the level assignment of fig. (31). Deutsch and Siegbahn[70] also measured the IC coefficients and obtained values which are not in good agreement (about 40% difference) with those of Waggoner *et al.* Both groups using a beta-ray spectrometer obtained the IC coefficient from the ratio of the number of IC electrons to the total number of beta particles in the 0.308-Mev decay spectrum of Co^{60}; that is, they assumed that there is one Ni^{60} cascade transition for each Co^{60} decay. They found the part of the beta spectrum which they could observe to be of an allowed shape, and so they assumed it to have an allowed shape over the entire range in order to determine the total number of decays.

It seemed worthwhile to measure the IC coefficient of the 1.33-Mev gamma-ray by a different method in order to see if the

above discrepancy could be resolved. By the Compton thick-converter method we directly measured with the spectrometer the rate of emission of the 1.33-Mev gamma-ray from a 11.65 rutherford source and compared it with the rate of internal conversion. Fig. (32) shows the spectrum from a bare Co^{60} source (about 3/8" in diameter). The rate of internal conversion was measured from the area under the line spectrum using expression (71) in which the external conversion efficiency factor, $\sigma_K N t \langle \sec \theta_o \rangle_{AV}$, is replaced by the IC coefficient, α, viz.,

$$Y \Omega_{eff} \alpha = (.940/P) \int_0^\infty E(mv)\, d\ln(mv) \qquad (83)$$

Fig. (33) shows the Compton spectrum from 20 mils of Al. Our result, which is shown in Table III together with the other two, agrees within the estimated accuracy of 10% with the measurement of Waggoner et al, but not with that of Deutsch and Siegbahn.

Experiment	$\alpha_{total} \times 10^4$	Theory - Rose et al.		
		Z	EQ	MD
Waggoner, Moon, Roberts	1.286±.035	27	1.17	1.03
Deutsch and Siegbahn	1.83	28	1.30	1.14
This thesis	1.26± .10			

Table III. Internal conversion coefficient of the Ni^{60} 1.332-Mev gamma-ray

The theoretical values of Rose et al[54] are shown in Table III; we have included a 10% correction for the estimate of the L, M contribution[53] and screening effects[71]. Only the EQ

and MD theoretical conversion are listed as the others differ by a factor of two or more from the observed coefficients. The IC coefficients vary nearly as Z^3, and there is some uncertainty as to whether to use $Z = 27$ or $Z = 28$. Immediately after the beta-decay the K-shell wave function in the vicinity of the nucleus, where the internal conversion takes place, is undisturbed so that for very fast nuclear radiation one should use $Z = 27$. The K-shell electronic wave function will adjust itself in a time of the order of atomic-radiation times for a K-L transition which is estimated to be about 10^{-15} sec. in this case.* This time is usually regarded as shorter than EQ radiation times, so that it would seem preferable to use $Z = 28$.

A possible source of error in our determination of the IC coefficient is that there may have been some contribution due to external conversion in the source itself; these external conversion electrons will have very nearly the same energy in the spectrometer as the internally converted electrons. Our source was mostly $CoCl_2$, so by knowing its approximate thickness from the broadening or shift of the IC line spectrum and using the appropriate photoelectric cross section from fig. (14) we estimate that there was at the most a 2% contribution due to external conversion.

The rate of emission of gamma-radiation from the source was also determined using an external thorium photoelectric converter (12.9 mg/cm^2) of hemispherical shape. In order to facilitate the determination of the Compton background the converter was placed

* In the case of low-Z elements, a more accurate estimate of the time for readjustment of the K-shell wave function is given by the time for auto-ionization (Auger-electron emission) which is about 10^{-15} sec. for all elements (ref. 12, page 491).

over a thick Compton converter (20 mils Al). A typical photoelectric spectrum obtained in this manner is shown in fig. (33). Since the energy of this Ni^{60} gamma-ray is nearly the same as the Na^{22} 1.275-Mev gamma-ray, we used fig. (21) for the converter geometrical efficiency factor (0.80). This procedure yielded a value of 1.31×10^{-4} for the IC coefficient of the 1.33-Mev gamma-ray, which is in satisfactory agreement with the value obtained from the Compton spectrum.

Once the IC coefficient of a Ni^{60} transition is known, a convenient method is available for determining the spectrometer solid angle. The absolute strength Y of the Co^{60} source can be obtained by a Geiger counter comparison with a calibrated Bureau of Standards source, and Ω_{eff} in (83) can be found. Using the value α of Waggoner et al, which is the most accurate, we found $\Omega_{eff} = .0203$ with a spectrometer resolution of 2.1% and with the particular spectrometer adjustments at the time of this experiment.

6. Internal Pair Formation

The process of internal pair formation is similar to internal conversion; from a quantum-mechanical viewpoint it is a first order transition for an electron going from one state to another as induced by a radiation field. The efficiency of this process is independent of Z in the approximation of representing the wave functions by plane waves, so that it is just as useful in light nuclear work as in heavy, contrary to the case with internal conversion. Some experimental studies of this process in heavy

elements are described by Latyshev[72].

With the radiation field (74), the ratio of the number of pairs per second with electron and positron traveling in the solid angles $d\Omega_-$ and $d\Omega_+$ and the positron energy between W_+ and $W_+ + dW_+$ to the number of quanta per second is[55]

$$d\gamma = \frac{\alpha k}{32\pi^3} P_+ P_- W_+ W_- \, \mathrm{Spur}\,(\Lambda G_+ \Lambda^* G_-)\, d\Omega_+ \, d\Omega_- \, dW_+ \; ; \tag{84}$$

instead of G_K in (75) we have the positron projection operator

$$G_+ = (-\vec{\alpha}\cdot\vec{P_+} + \beta + W_+)/2W_+ \; .$$

The evaluation of the spur gives*

$$\mathrm{Spur}\,(\Lambda G_+ \Lambda^* G_-) = \frac{1}{W_+ W_-}\Big\{ g g^* [W_+ W_- + (\vec{P_+}\cdot\vec{P_-}) - 1] + (\vec{f}\cdot\vec{f}^*)[W_+ W_- + 1] - (\vec{P_+} W_- + \vec{P_-} W_+)\cdot(g\vec{f}^* + g^*\vec{f}) + (\vec{f}\cdot\vec{P_+})(\vec{f}^*\cdot\vec{P_-}) + (\vec{f}\cdot\vec{P_-})(\vec{f}^*\cdot\vec{P_+}) - (\vec{f}\cdot\vec{f}^*)(\vec{P_+}\cdot\vec{P_-})\Big\} \; . \tag{85}$$

The expressions for f and g are the same as in internal conversion except here $\vec{P} = \vec{P_+} + \vec{P_-}$. Rose[55], [73] has evaluated (84) for all multipoles. However, in the case that the pair formation is induced by a nuclear reaction in which the incident beam is polarized with zero angular momentum about the beam axis, it is necessary to know the angular distribution properties of the formation process. That is, as in the measurement of internal conversion induced in a nuclear reaction, one can only measure the differential cross section for pair formation and for gamma-radiation at the spectrometer acceptance angle, and then only if the differential cross sections have the same ratio as the total cross sections, is the pair formation coefficient

* I am indebted to Mr. M. Ruderman for this evaluation.

readily obtained. It is rather necessary to use a spectrometer to achieve the required resolution, and it does not seem to be at all possible to measure the total cross section integrated over angles of either of the spectra. The angular distributions for pair formation have not been calculated; the effort required would probably be prohibitive. In experiments to be described in Part III only the high-energy portion of the positron spectrum is studied. We can get some idea of the angular distributions to be expected if in (85) we set $\vec{P}_- = 0$ and $W_- = 1$; then the spur simplifies to

$$\underset{\vec{P}_- = 0,\ W_- = 1}{\text{Spur}} (\Lambda G_+ \Lambda^* G_-) = \tag{86}$$

$$[g g^* (k-2) + (\vec{f} \cdot \vec{f}^*) k - \vec{P}_+ \cdot (g \vec{f}^* + g^* \vec{f})] / (k-1).$$

This expression is similar, but not identical, to expression (76). When it is considered that there is a different relation between k and p in the pair formation case, it is found that the distribution given by (86) are indeed the same as those listed in Table II for internal conversion. Hence, we can expect distributions differing from the associated gamma-radiation distributions making the interpretation of the data difficult in some cases. Of course, if k is large enough, the distributions are nearly the same. For example, in the experiment in Part III, $k = 6$ so that for electric dipole emission $\lambda = .8$ as compared to $\lambda = 1$ for gamma-radiation.

Since the process of internal pair formation resembles that of internal conversion, we may expect the same errors in the use of the Born approximation as shown in figs. (26 - 28). Thus,

for $Z=6$, there may be a 10% error due to this approximation. Methods which do not use the Born approximation near the edges of the pair spectra are given in a paper of Rose and Uhlenbeck.[74] If one is able to integrate the entire pair spectrum over the momentum distribution, some of this error disappears, as noted by Rose[55], since the errors are of opposite sign at each end of the spectrum. In most nuclear reactions spurious radiations will prevent the use of all but a small portion of the spectrum for the determination of the formation coefficient.

For computational purposes the positron (or electron) internal formation distributions, as given by Rose, and Rose and Uhlenbeck, are most conveniently written in the following manner:

$$\gamma(P^+)\,dP^+ = (\alpha/\pi k^3)\beta^+ Q\,dP^+ \qquad (87)$$

where k = gamma-ray energy in units of m_0c^2,

p (or p^-) = positron (or electron) momentum in units of m_0c,

β^+c (or β^-c) $=v^+$ (or v^-) positron (or electron) velocity,

and for the various multipoles (E = electric, M = magnetic, D = dipole, Q = quadripole)

$$Q(ED) = 2P^+P^- + (P_+^2+P_-^2)\log b + 2\log b,$$

$$Q(EQ) = \frac{2P_+P_-[(k^2-4)-(P_+^2+P_-^2)]}{(3k^2/2)} + (P_+^2+P_-^2)\log b,$$

$$Q(MD) = (P_+^2+P_-^2)\log b,$$

$$Q(MQ) = (P_+^2+P_-^2)\log b - 2\log b + P_+P_- - \frac{(P_+P_-)(P_+^2+P_-^2)}{(k^2/3)},$$

and

$$\log b = \log[k^2-(P_+^2+P_-^2)+(2P_+P_-)] - \log 2k.$$

The quantities P_+, P_- are tabulated as a function of the electron kinetic energy, or momentum in units of Gauss-cm, in the WPA table of electronic functions.[75]

In Part III we study the high-energy portion of some positron distributions, and so we need to consider the end-point correction formulas given by Rose and Uhlenbeck, which are valid when $p^- \ll 1$ and therefore only very close to the end point p^+_{max}. In the limit $p^- = 0$ or $p^+ = p^+_{max} = \sqrt{k(k-2)}$, they are, for ED and EQ:

$$Q(ED) = 2\pi\alpha Z (k^2+2)[k(k-2)]^{1/2}/k^2,$$
$$Q(EQ) = 2\pi\alpha Z (3k^2+8)[k(k-2)]^{3/2}/3k^3 \qquad (88)$$

where Z is the nuclear charge.

If we neglect the quadratic and higher variations in the positron distribution over the width of the spectrometer dispersion curve, the number of observed spectrometer counts divided by millivolts, which can be obtained from expressions (61), (83), and (87), is, in terms of the associated γ-ray yield Y,

$$\frac{\text{Spectrometer counts}}{\text{millivolts}} = 6.25\times10^{-4}\,\gamma(P^+)\,Y\,\Omega_{eff}\,P\,C' . \qquad (89)$$

Appendix - Part II

A. Determination of Gamma-Ray Intensities from the Slope of the Thick-Converter Compton Distribution

It has been satisfactory to use the slope method discussed on page 32 to obtain intensities of gamma-rays of low and moderate energies. To facilitate computation it is desirable to standardize on the number of resolution widths from the high-energy edge of the Compton distribution at which one measures the observed slope and computes the theoretical slope of the distribution in order to determine Y from (66). Here we take 1.0 resolution width (that is, $\Delta mv = -pmv_0$) from the end point (calculated end point - not the extrapolated edge). The quantity $f(x)$ which enters into (66) is then to be evaluated for a value

$$x' = x_{min}\left[1 + 2\gamma p(1+\sqrt{1-\beta^2})\right], \quad x_{min} = (1+2\gamma)^{-1}.$$

The function $f(x')$ is plotted in fig. (34), for $p = .020$, together with $f(x_{min}) = x_{min} + x_{min}^{-1}$, in order to show the variation of $f(x)$ over the first resolution width from the front edge of the distribution. It is apparent from the figure that the slope method loses accuracy at high energies since the variation of $f(x)$ becomes significant.

We can group some of the factors in (66); for Al we have

$$S/(mv)_r = 3.54 \times 10^{-12} C' p Y \Omega_{eff} G(k_0)/k_0 \qquad (90)$$

where k_0 = gamma-ray energy in kev, S = distribution slope in (counts/mv) at the reference value $(mv)_r$ corresponding to x', and

$$G(k_0) = \beta^2 f(x')/\mu_{eff} f_{AV} k_0 \; ;$$

f_{AV} is given by (68) and μ_{eff} is to be evaluated from fig. (4), (7) for an energy loss corresponding to $x' - x_{min}$.

For aluminum the quantity $G(k_0)$ is plotted in fig. (36).

Part III

Radiations from the C^{13}+d, Be^{9}+d, and O^{16}+d Reactions

1. Introduction

In this part we study by means of the beta-ray spectrometer the gamma-radiation and internally-formed positron spectra from the bombardment of a carbon target, enriched to 50% in C^{13}, with 1- to 1½-Mev deuterons from the Cal-Tech electrostatic generator. The C^{13}+ d reactions produce C^{14} and N^{14} in excited states which can emit γ-radiation or internally formed pairs; an attempt to ascribe the observed radiations to energy levels in these nuclei will be made and the positron component of the internal pair distributions will be discussed. The positron spectra associated with the 3.38- and 2.87-Mev gamma-rays from Be^{9}+ d are also studied, and an attempt is made to determine the multipolarity of these gamma-rays by comparing the intensities of the positron spectra with those of the associated spectra of Compton electrons from the external conversion of the radiations. In the last section of this part we describe a measurement of the internal conversion line spectrum associated with the 0.871-Mev gamma-ray from the $O^{16}(dp)O^{17*}$ reaction. The methods developed in Part II are used to analyze the spectrometer data of this part of the thesis.

2. Gamma-Radiation and Internally-Formed Positrons from C^{13}+ d

When C^{13} is bombarded with 1.5-Mev deuterons, the following reactions are energetically possible:

1) $C^{13} + d \longrightarrow N^{14} + n$, $Q_1 = 5.312$,
2) $C^{13} + d \longrightarrow C^{14} + p$, $Q_2 = 5.940$,
3) $C^{13} + d \longrightarrow B^{11} + \alpha$, $Q_3 = 5.164$,
4) $C^{13} + d \longrightarrow C^{12} + t$, $Q_4 = 1.310$;

the ground-state Q values which are given are from Li's thesis.[76] Due to the fact that our targets contained 50% C^{12}, there also occured the reactions

5) $C^{12} + d \longrightarrow C^{13} + p$, $Q_5 = 2.716$,

6) $C^{12} + d \longrightarrow N^{13} + n$, $Q_6 = -0.280$,

$N^{13} \longrightarrow \beta^+ + C^{13}$, $\beta^+_{max} = 1.20$.

Only the reaction 1) and 2) of the first four appear to leave the residual nucleus to any significant extent in other than the ground state so that this work will only provide information concerning the energy levels of N^{14} and C^{14}.

Theoretical interest in these two nuclei lies in the fact that they are mirrors in regard to the interchange of the pair of odd nucleons nn to pn. Thus, if nn and pn nuclear forces are equal in the same quantum states, in addition to the rather well established equality of nn and pp nuclear forces, we should expect to find a correspondence between the energy level diagrams with regard to the states that are not forbidden in C^{14} by the exclusion principle, which operates in the case of the odd pair of identical nucleons nn but not in the case of the non-identical pair pn of N^{14}. In other words, on the above assumption as to the equality of nuclear forces we expect to find corresponding states in N^{14} and C^{14} having charge supermultiplet quantum number $T \geq 1$ whereas those states having $T = 0$ would appear only in N^{14}. The theoretical aspects of this problem are treated in the review article by Wigner and Feenberg[77] and in the books by Devons[78] and Rosenfeld[79] so that there is no need to elaborate here. At the present time there exists excellent evidence as to the equality of nn and pp nuclear forces from the study of the odd iso-

baric light nuclei; in particular from the fact that the energy differences of the ground states of pairs of such nuclei are well accounted for by the Coulomb energy. On the other hand, there is not much information of a similar nature for the nuclei with $A = 4n+2$ with regard to possible equality of nn and pn nuclear forces. The ground state of N^{14} is probably $T = 0$ since its total nuclear binding energy is several Mev greater than that of C^{14} when proper account is taken of the additional Coulomb energy of N^{14}; that is, on account of the exclusion principle, the ground state of N^{14} cannot occur in C^{14}. There is some evidence that the 2.3-Mev level of N^{14} is the $T = 1$ level which corresponds to the ground states of C^{14} and O^{14} (80). In the case of the analogous nuclear triad with $A = 10$, it is not yet clear which level of B^{10} is the $T = 1$ level corresponding to the ground states of Be^{10} and C^{10}. Recently, Day and Walker(81) have obtained experimental evidence that there is a 3.6-Mev level of Li^6 which may be the $T = 1$, $J = 0$ counterpart to the ground states of He^6 and Be^6. One of the main interests in the levels of the nuclei C^{14} and N^{14} is to try to establish such corresponding levels and to determine the relative densities of $T = 0$ levels as compared to $T \geq 1$ levels.

A carbon target enriched to 50% in C^{13}, which was obtained from Eastman CO, was mechanically pressed into a thin flake about 10-mils thick, which is thick enough to constitute a thick target for the incident deuteron beam. This target was mounted on a 2-mil Cu support over which was placed a thin thorium photo-

electric converter or a beryllium Compton converter. The secondary electrons arising from these converters were studied by means of the beta-ray spectrometer when the target was bombarded by 1½-Mev deuterons. The secondary electrons from the thorium converters were observed in the range of energies from .4 to 4 Mev using foils of thickness 14.3 mg/cm^2 in the low-energy range and 28.5 and 57 mg/cm^2 for higher gamma-ray energies; the converter thickness was selected so that the loss of energy of the secondary electrons passing through it was comparable to the width of the spectrometer dispersion curve in energy units, thus providing optimum sensitivity without significant loss in overall resolution. The spectra from the various thorium converters are shown in fig. (36) for a 1.58-Mev bombarding energy. The energies of the observed gamma-rays were determined by the procedure developed by Hornyak, Lauritsen, and Rasmussen[3], and the results are listed in column 1 of Table IV; no Doppler shift correction to the energy was made since we do not know whether the residual nucleus radiates before or after it is significantly slowed down in the target material. The maximum possible Doppler shifts due to the forward motion of the center-of-mass system are listed in column 2 of Table IV. If at some future time there is reason to believe that the Doppler shift correction should be made, then the correction listed in column 2 is to be subtracted from the observed energy value listed in column 1; otherwise it is probably best to regard the possibility of such a shift as an additional source of uncertainty which is to be added to

the inherent uncertainty in the determination of energies with the spectrometer.

This study was performed prior to the work described in Part II on the efficiency of photoelectric converters; as a result a rather unfortunate choice of a converter geometry with $\cos\delta = .1$ was made for which it is difficult to estimate the efficiency. The intensities of the gamma-rays were obtained from the areas under the photoelectron lines. We estimate the efficiency factor for converters with small $\cos\delta$ by assuming that the electrons are all ejected at an angle ω, where $\cos\omega = v/c$ (see page 37), with respect to the gamma-ray direction; then, if the spectrometer acceptance angle is θ_1 ($=20^\circ$), the final distribution of secondary electrons is approximately given by eq. (44) of Part I. The initial distribution of electrons is given by Case I of eq. (49), and so the <u>average</u> converter efficiency factor for a foil of thickness x becomes

$$\langle \sec\theta_0(\omega,\theta_1)\rangle_{AV} = \left[\left(\cos\theta_1 - \frac{x}{\lambda}\right)^2 - \sin^2\omega\right]^{-1/2}$$

Considering the approximate character of this expression, only the first term of a power series expansion in x/λ is significant, viz.,

$$\langle \sec\theta_0\rangle_{AV} \approx (\beta^2 - \sin^2\theta_1)^{-1/2}\left(1 + \frac{\cos\theta_1}{\beta^2 - \sin^2\theta_1}\cdot\frac{x}{\lambda}\right). \qquad (91)$$

Column 3 of Table IV gives the values for the gamma-ray intensities from (71) with $\langle \sec\theta_0\rangle_{AV} = 1$ and column 4 gives the values using (91); it is probably best to regard the factor (91) as providing a measure of the uncertainty in the calculation of intensities as well as a correction factor. The yields were calculated assuming the angular distribution of the radiation to be isotropic.

Table IV

Energies and intensities of $C^{13}_{(50\%)}$+d, C^{12}+ d gamma-rays from photoelectric conversion in thorium. E_d = 1.580 Mev. $\Omega/4\pi$ = .020.

Energy kev	Max. Possible Doppler shift	Yield $\langle \sec\theta_0 \rangle_{AV} = 1$	Yield $\langle \sec\theta \rangle_{AV}$ by (91)	Radiating Nucleus
.729 ± .004	.004 kev	2.5×10^{-6} γ/d	1.6×10^{-6} γ/d	?
1.643 ± .008	.009	2.1	1.8	N^{14}
2.318 ± .016	.013	6.9	5.6	N^{14}
3.102 ± .020	.017	6.2	7.7	C^{13}
3.390 ± .020	.019	2.1	1.8	N^{14}

For gamma-rays whose energies are greater than about 3 Mev the Compton conversion process is a more sensitive method of detection than the photoelectric process. Fig. (37) shows for 1.42-Mev bombarding energy the Compton spectra from 94 mg/cm^2 Be in addition to the 2-mil Cu target support and the 10-mil carbon target which also contribute Compton electrons. These distributions were analyzed by the Compton thick-converter method described in Section 3 of Part II; the experimental curves were fitted by an integral Compton distribution in order to obtain the energy as well as the intensity of the radiation, the dispersion of the spectrometer being considered by folding the Gaussian dispersion curve with the theoretical primary spectrum. The results are given in Table V. A rise occurring at a potentiometer reading of about 38 millivolts, which would correspond to a gamma-ray of 3.9 Mev, is not believed to be due to Compton electrons as there is no corresponding photoelectric line in fig. (36); the rise may consist of electrons from internal pair formation accompanying the emission of the 5.056-

Mev gamma-rays. The uncertainties of the thick-target yields listed in column are estimated to be about ±30% except for the 3.10 line which is apt to be less certain due to the sloping background and the 5.69 radiation which is less certain due to its weakness.

Table V

Energies and intensites of the C^{13}(50%),C^{12}+ d γ-rays from Compton conversion in 94 mg/cm^2 of Be and in the target and target support. E_d = 1.42 Mev. The γ-ray distribution is assumed to be isotropic in the yield determination. $\Omega/4\pi$=.020.

Energy kev	Yield γ/d	Radiating Nucleus
6.115 ± .030	2.5 x 10^{-6}	C^{14}
5.69 ± .05	.7	N^{14}
3.393 ± .020	2.1	N^{14}
5.056 ± .025	1.5	N^{14}
3.088 ± .020	3.9	C^{13}

In the last columns of Tables IV and V we list the probable source of the radiation. As already mentioned, there are four possible reactions when C^{13} is bombarded with deuterons; of these the (dt) reaction need not be considered in our work since not enough bombarding energy was available to excite any levels in C^{12}. There is sufficient energy available in the C^{13}(dα)B^{11} reaction to permit excitation of fairly high levels in B^{11}; however, not until recently has there been any evidence of a short range alpha particle group in this reaction. Li and Whaling[81] have observed an alpha particle group from the bombardment of C^{13} with deuterons which they attribute to

leaving B^{11} in an excited state at 2.107 ±.017 Mev. Therefore, we should have observed a gamma-ray of this energy from the deexcitation of this level. In fact, inspection of fig. (36) reveals that there is some indication of a photoelectric conversion line at about the expected field setting, 42 millivolts; furthermore the Compton spectrum from the 2.32-Mev gamma-ray appears more intense than one might expect due possibly to the presence of the B^{11} gamma-ray.Other spectrometer runs over this spectral region show a similar behaviour; however the interference from the Compton spectrum from the 2.32 line makes it difficult to draw a conclusion as to the existence of such a gamma-ray.

The 6.115 gamma-ray we assign to C^{14} since a small but definite yield was observed with a bombarding energy of 650 kev which is below the threshold for such a level in either B^{11} or N^{14}; at least 925-kev deuterons would be required to excite such a level if it were to belong to N^{14} and still more energetic deuterons for such a level in B^{11}. Recently Buechner's group has confirmed this assignment by their observation of the energy of the proton group to this level in C^{14};[82] they find the level position to be 6.096± .015 Mev above the ground state in good agreement with our value. They found no other proton groups which could correspond to levels in C^{14} from 5.2 to 6.1 Mev with an intensity of greater than 0.2 of that of the proton group associated with the 6.096 level. This observation is valuable in that it rules out a level at 5.24 Mev reported by Humphreys and Watson[83] from range mea-

surements of the proton groups. It also excludes a level at 5.59 ± .04 Mev recently reported by Curling and Newton[84] from their range measurements of the charged particle groups. In Energy Levels III[85] our 5.69 gamma-ray was assigned to C^{14} on the basis that it was a radiation from the 5.59 level reported by Curling and Newton; from the results of Buechner's group we can say that this gamma-ray probably arises from a level in N^{14}.

We do not believe that the results of Humphreys and Watson are capable of providing any information concerning energy levels in C^{14} above 3 Mev since any groups corresponding to such levels would have been obscured by the presence of the intense proton group from $C^{12}(dp)C^{13}$; however, their results do show that there are probably no C^{14} states below 3 Mev. Now from magnetic spectrometer studies of the charged particle groups from the bombardment of C^{13} by 1.0-Mev deuterons, Li and Whaling[76] found no evidence for energy levels in C^{14} from 1.4 to 4.5 Mev. Thus, with the exception of the range of excitation energies from 4.5 to 5.2 Mev, one may say from the results of the three above-mentioned groups of experimenters that there are no levels in C^{14} below 6.1 Mev which can be excited by the bombardment of C^{13} with deuterons of moderate energies. Concerning the unexplored range from 4.5 to 5.2 Mev, we note that the 5.056-Mev gamma-ray which we observed is unambiguously assigned to N^{14} on the basis of the finding of a neutron group to such a level (see below). It therefore appears that the 6.1-Mev level may

be the first excited state of C^{14} which is indeed of interest since it indicates that all of the low-lying levels of N^{14} have isotopic spin quantum number $T = 0$ with the exception of the 2.3 level which probably corresponds to the ground state of C^{14}.

Aside from the 3.10-Mev gamma-ray, which is already known to arise from the $C^{12}(dp)C^{13*}$ reaction, and the 6.115 radiation which we have assigned to C^{14}, all of the other radiations listed in Tables IV and V are presumably from levels in N^{14}. There is considerable experimental literature on the low levels of N^{14}, and it is reviewed in Energy Levels III and by T. Lauritsen[80]. Recent work contributing to our knowledge of these levels is the study of the neutrons in the $C^{13}(dn)N^{14}$ reaction by Swann and Mandeville[87]; using their measurement of $5.17 \pm .05$ for the ground state Q, they report levels at $2.19 \pm .07$, $3.47 \pm .07$, $3.87 \pm .07$, and $4.90 \pm .07$ from the energies of the neutron groups. Their ground-state Q value differs significantly from the accurate value Q_1 obtainable from Li's mass table. If we use $Q_1 = 5.312$ rather than 5.17 to determine the level positions from the neutron energies, then our 2.32- and 5.05-Mev gamma-rays agree in energy with the positions of their N^{14} levels. Table VI summarizes their results with this change and includes our estimate of the relative intensities of the neutron groups. It is noteworthy that the level at 4.01, which is associated with a strong neutron group, leads to a very weak, if not absent, 3.9-Mev gamma-ray. This situation may be resolved by postulating that the 4.0 level decays by the emission of a 1.643-Mev

Table VI

Energy levels of N^{14} as determined from the observations of Swann and Mandeville of neutron groups from $C^{13}(dn)N^{14}$ using a 1.43-Mev deuteron beam on a carbon target enriched to 53% in C^{13}. We have used a more accurate ground-state Q value to determine the energy levels from the neutron energies.

N^{14} level	Relative Intensity of the Neutron Group
2.33 Mev	Weak
3.61	Weak and partially obscured by the group to the 4.01 level
4.01	Strong
5.04	Strong

gamma-ray to the 2.32 level rather than to the ground state. Since they observed only a weak neutron group to the 2.32 level, this proposal requires that the intensity of the 2.32 and 1.64 radiations be about equal; according to Table IV the 2.32 gamma-ray is about 3-times stronger than the 1.64 gamma-ray indicating that if our proposal is correct, there must be other transitions to the 2.32 level from higher states of N^{14}. A possibility is that the 3.39 gamma-ray is a cascade from the 5.69 level to the 2.32 level; the energy difference is correct to within the estimated error of the measurement. Thus, the intensity of the 2.32 level should be $Y(1.64) + Y(3.39) = 3.6$ as compared to the observed value of 5.6×10^{-6} γ/d. The discrepency may be due to the fact that some neutrons go directly to the 2.32 level and that our measurement of the intensity of the 2.32 radiation may be inaccurate on account of the rising background. If this proposed decay scheme is correct, Swann and Mandeville should have observed a moderately strong neutron group to the 5.69-Mev level. Upon exam-

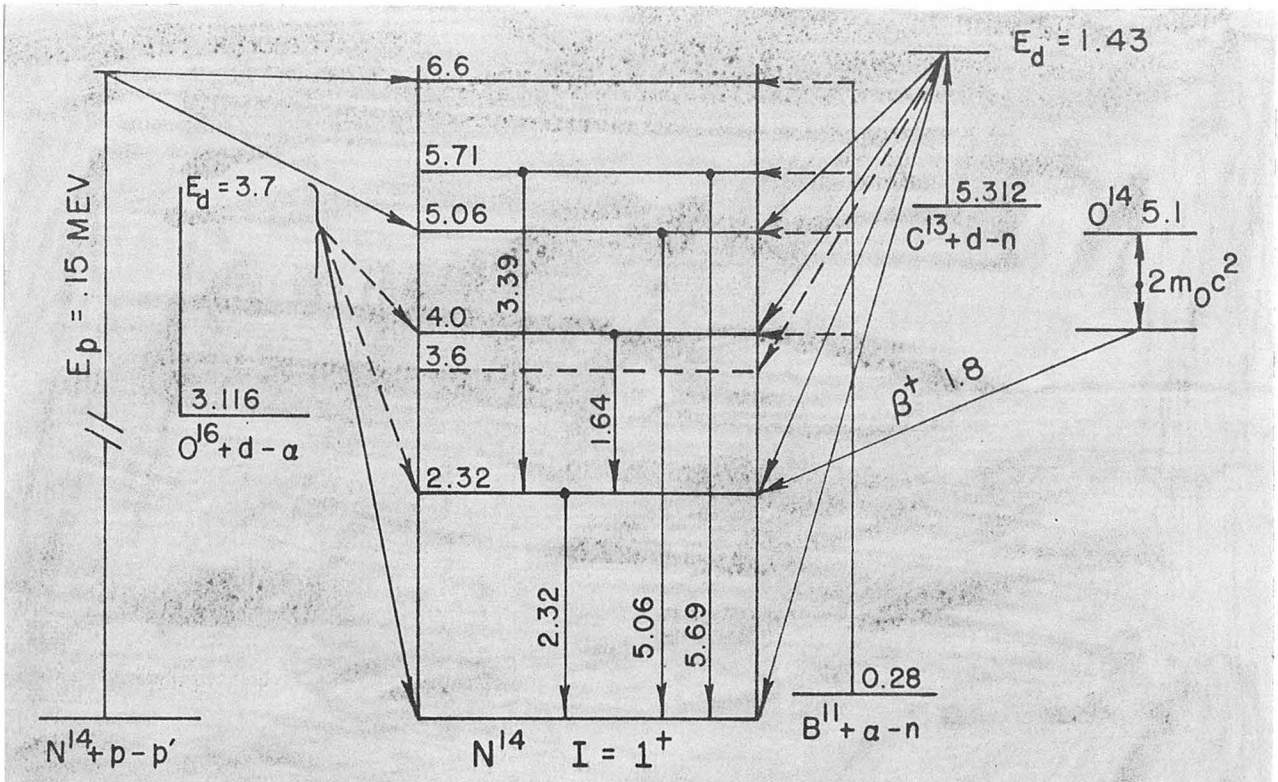

FIG. 38. ENERGY LEVELS OF N^{14} BELOW 7 MEV

ining fig. (1) of their paper, one sees that such a group would have about the same energy as a very strong group from the competing $C^{12}(dn)N^{13}$ reaction, so that their failure to report such a group is understandable. Fig. (38) shows a N^{14} level scheme which is based on the above analysis.

An alternative decay scheme is the one given in Energy Levels III in which the 5.056 level cascades by emission of the 1.64 gamma-ray to a 3.39 level of N^{14}. Either decay scheme is equally acceptable in the light of present experimental evidence and accounts for all of the radiations which we observed with exception of the .729-Mev gamma-ray.

A possible assignment of the .729 radiation is based upon the experiments of Seagrave[88] on the resonance energy levels of N^{14} from C^{13}+p and the mirror-nuclei considerations

mentioned above. He finds, in addition to the well known .55-Mev $C^{13}(p\gamma)N^{14}$ resonance, a broad resonance ($\Gamma \sim .50$ Mev) whose maximum occurs at a proton bombarding energy of about 1.25 Mev. When one considers the effect of the barrier factors on the widths, it is apparent that both of the resonances are too broad to be attributed to other than s-wave protons. In fact Devons and Hine[89] found the angular distribution of the radiation from the .55-Mev resonance to be isotropic which indicates that the level is probably formed by s-wave protons; the angular distribution from the 1.25-Mev resonance has not yet been measured. If one computes the reduced widths of these two levels by the procedure outlined in Part IV of this thesis, taking into account the variation of the level shift with respect to proton energy, the following values are obtained using a nuclear radius of 3.9×10^{-13} cm for s-wave protons:

Proton Resonance	Observed Width	θ^2-Reduced Width
$E_p = .554$ Mev	.0325 Mev	.68
$E_p = 1.25$ Mev	.50 Mev	.8

It is interesting that the two reduced widths are equal within the uncertainty of the measurements and the computations involved. Moreover, these reduced widths are about $\frac{1}{2}$ of the value expected for a single-particle type of interaction and found for the first excited states of N^{13}, C^{13}, and O^{17} as reported in Part IV. A possible explanation is that the compound system exists in a symmetrical way one-half of the time as $C^{13}+p$ and the other half as $N^{13}+n$ but otherwise that the interaction of theodd particle with the core is a simple one-body type. When

s-wave protons interact with $C^{13}(J=\frac{1}{2}^-)$, the compound states of N^{14} so formed can have $J=0^-$ or $J=1^-$. The reduced widths for the above-mentioned C^{13}+ p levels correspond to a level spacing of the order of 8 Mev (see Appendix B of Part IV) so that they are surely not of the same spin, provided that they are both s-wave resonances. Hence, one would expect to find corresponding $J=0^-$ and $J=1^-$ levels in C^{14} since, on the shell-structure model at least, such levels would not be excluded from C^{14}. In fact if one computes at what energy in C^{14} the level corresponding to the .55 resonance level of N^{14} should appear, one finds 6.1 Mev, in agreement with the actual position of the known level. The method of this computation is similar to that used in Part IV to obtain the boundary-condition level shifts of the excited states of N^{13} and C^{13} or Li^7 and Be^7 in Appendix G of Part IV; it is reasonably accurate to neglect here the contribution to the level shift from the differences of the electromagnetic spin-orbit interactions and nuclear volume expansion with excitation. Using the reduced width $\theta^2=.68$ for the lower resonance, we find a boundary-condition shift of .415 Mev. Now Sherr, Muether, and White[90] show from their study of the beta decay of O^{14} that it is very likely that the 2.32 level of N^{14} corresponds to the ground states of O^{14} and C^{14} if one takes into account the Coulomb and proton-neutron mass difference in the usual manner. If this is the case, then we expect to find the state of C^{14} which corresponds to the .554 resonance level of N^{14} at

$$7.542 + .554(13/14) - 2.318 + .415 = 6.153 \text{ Mev},$$

where the energy value 7.542 is the binding energy of a proton in the ground state of N^{14}. This predicted value for the C^{14} level position agrees within the accuracy of the method of computation with the level position, 6.115 Mev.

If the above agreement is not the result of a fortuity, then we must expect to find a level of C^{14} which corresponds to the 1.25-Mev level of N^{14}. The boundary-condition shift for such a pair of states is calculated to be .53 Mev so that we should find a level in C^{14} at about

$$7.542 + 1.25\ (13/14) - 2.318 + .53 = 6.91 \text{ Mev.}$$

We observed no radiation of this an energy although the bombarding energy in our experiments was sufficiently above the threshold for such a level. However, we have concluded that one of the two s-wave resonance levels of N^{14} may be $J = 0^-$; if it is the 1.25 resonance level, its counterpart in C^{14} at about 6.9 Mev could not radiate to the ground state of C^{14}, which is probably $J = 0^+$ since it is an even-even nucleus, and so it would have to radiate to the 6.1 level since there do not appear to be any other lower levels in C^{14}. Therefore, we considered the possibility that the unassigned .729-Mev radiation is from such a transition. This proposal was checked by observing whether the threshold for producing the .729 radiation is above or below the anticipated threshold for a level at $.729 + 6.115 = 6.844$ Mev in C^{14}. Fig. (39) shows on arbitrary scales the excitation functions for the low-energy gamma-rays from $C^{13} + d$; the results may be made absolute by means of the intensities listed in Table IV. The threshold for

a 6.844 level should occur above a deuteron bombarding energy of $(15/13)x(6.844 - 5.940) = 1.04$ Mev. Fig. (39) shows that the .729 radiation although very feeble is still evident at this energy, thus invalidating our proposal.

Internally-Formed Positrons from C^{13}+ d

If the 6.115 level of C^{14} corresponds to the .554 resonance level of N^{14}, then it must have $J = 0^-$ or 1^-. If it has $J = 0^-$, the radiation to the ground state would be forbidden contrary to observation. If it has $J = 1^-$, it would radiate by electric dipole emission. Here we describe an attempt to measure with the spectrometer the multipolarity of this radiation and of the other high-energy C^{13}+ d gamma-rays from the intensity of the internally-formed positrons using the theory discussed in Section 6 of Part II.

A self-supporting target of carbon was made by mechanically squeezing together some soot which was enriched to 50% in C^{13}; its thickness was estimated to be about 30 mg/cm^2 which is sufficient to stop the incident deuteron beam and yet thin enough so as not to constitute a significant source for formation of external pairs which might be confused with those internally formed. Due to the presence of 50% C^{12} in this target, there was a constant production of gaseous positron-emitting N^{13} which resulted in a field insensitive but somewhat time-dependent background. On this account, alternate runs were taken at each field setting with the beam off and the background counts thus obtained were subtracted from the

beam-on count reading for the same time interval. The spectrometer is provided with a helical baffle which permits observation of either positron or electron spectra individually. The positron distribution is shown in fig. (40); we have plotted the counts divided by the millivolt reading corresponding to the field setting in order to obtain the counts per constant momentum interval; this is the proper procedure in this case since the field-insensitive background was rather negligible after subtraction of the beam-off counts. Shown dotted are the theoretical distributions predicted on the basis of the intensity of the associated gamma-rays for electric dipole (E.D.) and electric quadripole (E.Q.) internal positron formation distributions; these were added to an assumed background from the higher-energy distributions. Of particular importance in making the comparison between the theoretical and experimental distributions is the estimation of this background; of course, we have no assurance that the ones which we have assumed are correct. The distributions for all other multipole orders follow immediately below that of E.Q.. Fig. (41) shows the complete positron (or electron, except at the end point) momentum distributions for E.D., E.Q., M.D. (magnetic dipole), and M.Q. (magnetic quadripole) when $E_\gamma = 6.115$ and 5.056 Mev. Electric octopole, which is not included in this figure, has a total pair formation coefficient between that of M.D. and M.Q. so that its momentum distribution probably falls between that of the M.D. and M.Q. multipoles. All higher multipoles, both magnetic and electric, have,

according to figures (3) and (4) of the paper of Rose, total pair formation coefficients which are less than these four so that their distributions probably lie below those shown in our fig. (41). It is quite evident from figures (40) and (41) that, considering the experimental accuracy, the most one can hope to determine from an experiment of this kind is whether or not the transition is electric dipole, the differences between the other distributions being too small; however, in some cases such information is valuable.

In order to draw the theoretically predicted positron distributions using eq.(89), it is necessary to know the absolute yield of the associated gamma-radiation. Under the same experimental conditions as described above for measuring the positrons, the gamma-ray intensity was obtained by the slope method (eq. (90)) applied to the secondary electron distributions from a thick aluminum converter; the results are given in Table VI.

Table VI

C^{13}(50%),C^{12}+ d gamma-radiation yields for E_d = 1.21 Mev. The radiation distributions are assumed to be isotropic.

Energy-Mev	Yield - γ/d
6.115	2.30×10^{-6}
5.69	.69
5.056	1.56
3.39	1.85
3.10	3.81

The yield of the 3.10 radiation is apt to be rather inaccurate because of the uncertain background from the high-energy lines.

Due to the multitude of high-energy gamma-rays in this reaction which produce overlapping distributions, it is not possible to make any multipolarity assignments. Although the

6.115 distribution is best fitted by an E.D. assignment up to the point where the 5.69 positrons may appear with about 1/3 of the intensity of those from the 6.115 transition, the accuracy is insufficient to make this definite. The rise in the positron intensity occuring just below p_{max}, 5.056 Mev appears somewhat greater than predicted for an E.D. transition. Near p_{max} for a 3.9-Mev transition there appears a rather abrupt rise that is not at all understood since there is no gamma-ray, or only a very weak one, of this energy. However, there is definitely a level in N^{14} at this energy as shown in fig. (38) which is fed by an intense neutron group. Finally, at p_{max} corresponding to the 3.10 gamma-ray of C^{13} which is produced in the $C^{12}(dp)C^{13}$ reaction there appears a rise in positron intensity which is within satisfactory agreement with that anticipated for an E.D. transition although in this particular experiment there is some uncertainty as to the behaviour of the background. The internally-formed positrons from this transition as produced in a normal carbon target have been studied and the results are given in Appendix F of Part IV; good agreement with the observed distribution is obtained with an E.D. assignment to the transition. In this experiment the intensity was strong and the background negligible.

The internally-formed electron distributions were also observed but in a cursory manner; they appeared to be qualitatively the same as the positron distributions. In observing the electrons one encounters a rather strong additional background of Compton secondary electrons from the source itself,

and so a less quantitative comparison with the theoretical spectra is possible.

3. Internally-Formed Positrons from $Be^9 + d$

The gamma-rays from this reaction have been carefully studied by Rasmussen.[2] There are two moderately intense high-energy radiations whose associated internally-formed positrons we have measured. We will be interested in the gamma-rays listed in Table VII; the yields were determined for a deuteron bombarding energy of 1.19 Mev both by Rasmussen and in the measurements described below.

Table VII

$Be^9 + d$ gamma-ray intensities for $E_d = 1.19$ Mev.
The radiations are assumed to be isotropic.

Reaction	γ-Energy	Yield - Rasmussen	Yield - This thesis
$Be^9(dn)B^{10}$	2.87	2.4×10^{-6} γ/d	$(2.4) \times 10^{-6}$ γ/d
$Be^9(dp)Be^{10}$	3.38	2.1	2.12
$Be^9(dn)B^{10}$	3.60	.9	.96

Figure (42) shows the thick-converter Compton spectrum from 50 mils of aluminum for the 3.38- and 3.69-Mev radiations. The background from the 3.38 gamma-ray was too intense to permit an accurate determination of the intensity of the 2.87 gamma-ray. Using eq. (90) we obtained the values in Table VII for the intensities of the two high-energy radiations. Our values are in agreement with Rasmussen's, which were obtained using a 'thin' Compton converter, so that we used his value in eq. (89) for the intensity of the 2.87 gamma-ray in order to obtain the theoretically-expected E.D. and E.Q. internally-formed positron distributions. Figure (43) shows

the predicted (dotted lines) and observed spectra from a 15-mg/cm^2 Be target; fig. (44) shows the complete theoretical momentum distributions for E.D., E.Q., M.D., and M.Q. as given by eq. (87). As with the positron spectra from C^{13}+ d, the main difficulty in making a comparison is the estimation of the behaviour of the background. Since the background which appears above 55 mv is field insensitive and fairly large (possibly due to neutrons), we have plotted counts rather than counts per constant momentum interval; therefore the theoretical spectra were multiplied throughout by the millivolt reading in order to take into account the variation of the spectrometer dispersion width with momentum. The rapid rise of the positron intensity below 30 mv is due to the production of N^{13} from the deuteron bombardment of the carbon contamination on the surface of the beryllium target.

It is apparent that the positron distributions for the 2.87 and 3.38 radiations are best fitted by electric dipole assignments although this observation can not be considered as conclusive in view of the background problem. There is no significant rise associated with the 3.60 gamma-ray so that we can say nothing about its multipole order.

It is of interest to see how the first two assignments fit with the known information about the energy levels from which these radiations occur. The 3.38 radiation is from the first excited state of Be^{10} so that it is of particular interest. The ground state of Be^{10}, being an even-even nucleus, is presumably spin zero with even parity; thus, the first

excited state of Be^{10} must have $J = 1^-$ if it is to radiate by electric dipole emission to the ground state. If one examines the low-energy $Be^9 + n$ scattering data[91], it is seen that the cross section is about 5 barns near zero energy and then gradually diminishes with increasing neutron energy. This cross section is considerably larger than potential scattering which is expected to be less than 1 barn at these energies; hence, there must be a bound state of Be^{10} which is associated with this low-energy s-wave interaction. S-wave neutrons interacting with Be^9, which has $J = 3/2^-$,[86] produce a compound nucleus in a state of either $J = 1^-$ or 2^- so that we should be able to find a state of Be^{10} with less than 6.7-Mev excitation energy which has either of these assignments. It is plausible that the 3.38 level could be the 1^- state as the only other known bound state of Be^{10} below the threshold for $Be^9 + n$ instability is at 6.3 Mev which is so close to the threshold that one would expect an even larger low-energy neutron scattering cross section.

The most recent information on the energy levels of B^{10} is the study of the neutron groups from the reaction $Be^9(dn)B^{10}$ by Ajzenberg[92] who attributes the 2.87-Mev gamma-ray to a transition from the 3.59 to the 0.72-Mev level. There is no evidence concerning the spins of these levels except what has been included in Part II in regard to the internal conversion electrons associated with the 0.72 radiation. There, some evidence was presented that the 0.72 level is either $J = 1^+$ or 2^+; thus if the radiation from the 3.59-Mev level is electric

dipole, the 3.59 level could have J = 3, 2, 1, or 0, all of odd parity. Although this deduction is not very informative, it is nevertheless interesting that there can be low-lying levels of opposite parity contrary to the usual surmises made about the light nuclei (see also Part IV, concerning N^{13} - C^{13}).

4. Internal Conversion Electrons from the 0.871-Mev Level of O^{17}

It was mentioned in Section 5 of Part II that the internal conversion coefficients of radiative transitions are approximately proportional to Z^3. Thus we expect that the strongest source of internal conversion electrons from the light nuclei would be the intense 0.871 radiation from the first excited state of O^{17} which can be produced in the $O^{16}(dp)O^{17}$ reaction. We describe below a preliminary attempt to measure the internal conversion coefficient of this radiation.

A target of about 8 mg/cm^2 of SiO_2, which is thick enough to stop the incident beam, was bombarded with 1.35-Mev deuterons. On account of the insulation property of quartz, the target became highly charged during the bombardment and so it was not possible to use the current integrator; instead an external monitor counter was used to control the bombarding period of each run. The spectrometer field expected for these internal conversion electrons, 23.4 mv, was calculated from the known energy of the gamma-radiation. The spectrum which was observed in the vicinity of this field is reproduced in fig. (45); it it is qualitatively of the proper shape for a monochromatic source, the slight shift of the maximum from the expected value being due to the energy loss of the electrons in emerging from the target. The intensity of the associated gamma-radiation

was obtained by measuring the distribution of the secondary electrons from a 'thick' 20-mil aluminum converter; this spectrum is also shown in fig. (45) with the same arbitrary ordinate scale as for the internal conversion electrons for a definite number of monitor counts. The radiation intensity was computed from eq. (90) and the internal conversion coefficient calculated from eq. (83). The accuracy of the counting statistics is rather low so that about all we can do is to put limits on the conversion coefficient; we find $\alpha = (8 \pm 4) \times 10^{-6}$. The theoretical values expected for various multipole transitions are the following (see Section 5 of Part II):

$\alpha_K' = 3.76 \times 10^{-6}$, $\beta_K' = 4.87 \times 10^{-6}$,

$\alpha_K^2 = 9.15$, $\beta_K^2 = 11.90$,

$\alpha_K^3 = 21.2$, $\beta_K^3 = 27.2$.

The data is in best agreement with an E.Q. assignment but it is also consistent with M.D., M.Q. and certain possible mixtures. The theoretical conversion coefficients increase with increasing multipole order so that we have not listed any higher multipoles. This transition is anticipated to be E.Q. since the spin of the ground state of O^{17} is now known to be $J = 5/2$ and even parity and the excited state is known to be $J = \frac{1}{2}$, even parity. A detailed discussion of the theory of the 0.87 level of O^{17} is given in Appendix H of Part IV.

Since the excited state of O^{17} is $J = \frac{1}{2}$, both the angular distribution of the radiation and the conversion electrons will be isotropic; hence the problem that was discussed in Section 5 of Part II in regard to possible differences of the respective angular distributions, does

not apply to this measurement. Furthermore, because of the relatively large charge of the radiating nucleus, we can be certain that the K-shell occupation probability of O^{17} is almost unity at the time of radiation, especially in the case of an E.Q. transition which is apt to be rather slow.

References

1. W. F. Hornyak, PhD Thesis, Calif. Inst. of Tech. (1949).
2. V. K. Rasmussen, PhD Thesis, Calif. Inst. of Tech. (1950).
3. Hornyak, Lauritsen, and Rasmussen, Phys. Rev. 76, 731 (1949).
4. L. Landau, J. Phys. USSR 8, 201 (1944).
5. N. Bohr, DKDVS, Mathematisk-fysiske Meddelelser XVIII, 8 (1948).
6. W. Heitler, Quantum Theory of Radiation, Oxford Univ. Press, (1936).
7. H. Bethe, Handbuch der Physik, Vol. 24/1 (1933).
8. A. Bohr, DKDVS, Mathematisk-fysiske Meddelelser XXIV, 19 (1948).
9. G. C. Wick, Ric. Scient. 12, 858 (1941), and Il Nuovo Cimento 1, 302 (1943).
10. Halpern and Hall, Phys. Rev. 73, 477 (1948).
11. E. Fermi, Phys. Rev. 57, 485 (1940).
12. Compton and Allison, X-Rays in Theory and Experiment, D. Van Nostrand Co. (1935).
13. E. Jönsson, Thesis, Uppsala (1928).
14. Wheeler and Bearden, Phys. Rev. 46, 755 (1934).
15. H. Hönl, Zeits. für Physik 84, 1 (1933).
16. J. E. Johnston, Proc. Camb. Phil. Soc. 35, 108 (1939).
17. Bandopadhyaya and Maitra, Phil Mag. 21, 869 (1936).
18. H. H. Biermann, Ann. der Physik 26, 740 (1936).
19. R. D. Hill, Proc. Roy. Sec. 161A, 284 (1937).
20. Dershem and Schein, Phys. Rev. 37, 1238 (1931).
21. H. Hall, Rev. Mod. Phys. 8, 358 (1936).
22. Robert R. Wilson, Phys. Rev. 60, 749 (1941).
23. Livingston and Bethe, Rev. Mod. Phys. 9, 245 (1937).
24. Hirschfelder and Magee, Phys. Rev. 73, 207 (1948).
25. Bakker and Segrè, Bull. Am. Phys. Sec. 25-5, K12 (1950).

26. Madsen and Venkateswarlu, Phys. Rev. 74, 648 (1948).

27. J. C. Slater, Phys. Rev. 36, 57 (1930).

28. White and Millington, Proc. Roy. Sec. A120, 701 (1928).

29. E. J. Williams, Proc. Roy. Soc. A125, 420 (1929).

30. Ellis and Aston, Proc. Roy. Soc. 129, 180 (1930).

31. Goudsmit and Saunderson, Phys. Rev. 57, 24 (1940), and Phys. Rev. 58, 39 (1940).

32. Bethe, Rose, and Smith, Proc. Am. Phil. Soc. 78, 573 (1938).

33. W. T. Scott, Phys. Rev. 76, 212 (1949).

34. Snyder and Scott, Phys. Rev. 76, 220 (1940).

35. Mott and Massey, The Theory of Atomic Collisions, Oxford Univ. Press (1949), pages 193-199.

36. Kulchitsky and latyschev, Phys. Rev. 61, 260 (1942).

37. M. E. Rose, Phys. Rev. 58, 90 (1940).

38. Oleson, Chao, and Crane, Phys. Rev. 378 (1941).

39. F. Miller, Partial Differential Equations, Wiley and Sons, (1941).

40. Cooper and Morrison, Phys. Rev. 57, 862 (1940).

41. Rasmussen, Hornyak, Lauritsen, and Lauritsen, Phys. Rev. 77, 617, (1950).

42. Fowler, Lauritsen, and Lauritsen, Rev. Mod. Phys. 20, 236 (1948).

43. Hulme, McDougall, Buckingham, and Fowler, Proc. Roy. Soc. 149A (1935).

44. Harvey Hall, Rev. Mod. Phys. 8, 358 (1936).

45. A. Sommerfeld. Wellenmechanik, Frederic Unger (1939).

46. F. Sauter, Ann. der Physik 9, 217 (1931) and 11, 454 (1931).

46. H. Hall, Phys. Rev. 45, 620 (1934).

48. L. H. Gray, Proc. Camb. Phil. Soc. 27, 103 (1931).

49. Bradt, Gugelot, Huber, Medicus, Preiswerk, and Scherrer, Helv. Phys. Acta. 18 II, 77 (1946).

50. Good, Peaslee, and Deutsch, Phys. Rev. 69, 313 (1946).

51. H. O. W. Richardson, Proc. Phys. Soc. London 63, 234 (1950).

52. Martin and Richardson, Proc. Phys. Soc. London 63,223 (1950).

53. Dancoff and Morrison, Phys. Rev. 55, 122 (1939).

54. Rose, Goertzel, Spinrad, Harr, and Strong, Phys. Rev. 76, 1883 (1949).

55. M. E. Rose, Phys. Rev. 76, 678 (1949).

56. Falkoff and Uhlenbeck, Phys. Rev. 79, 323 (1950).

57. Ling and Falkoff, Phys. Rev. 76, 1639 (1949).

58. T. Hall, Phys. Rev. 79, 504 (1950).

59. E. Rutherford, Phil. Mag. 47, 277 (1924).

60. G. H. Briggs, Proc. Roy Soc. A114, 341 (1927).

61. G. H. Henderson, Proc. Roy. Soc. 109, 157 (1925).

62. Chr. Gerthsen, Phys. Z. S. 31, 948 (1930).

63. Rutherford, Chadwick, and Ellis, Radiations from Radioactive Substances, MacMillan Co. (1930).

64. Brinkman and Kramers, K. Wet. Amst. 33, 973 (1930).

65. Sherr, Muether, and White, Phys. Rev. 75, 282 (1949).

66. Allan C. G. Mitchell, Rev. Mod. Phys. 72, 36 (1950).

67. Brady & Deutsch, Phys. Rev. 74, 1541 (1948) and 78,558(1950)

68. Metzger and Deutsch, Phys. Rev. 78, 551 (1950).

69. Waggoner, Moon, and Roberts, Phys. Rev. 80, 420 (1950).

70. Deutsch and Siegbahn, Phys. Rev. 77, 680 (1950).

71. John R. Reitz, Phys. Rev. 77, 10 (1950).

72. G. Latyshev, Rev. Mod. Phys. 19, 132 (1947).

73. M. E. Rose, Phys. Rev. 78, 184 (1950).

74. Rose and Uhlenbeck, Phys. Rev. 48, 211 (1935).

75. Miscellaneous Physical Tables (Electronic Functions), National Bureau of Standards, 1941.

76. C. W. Li, Thesis, Calif. Inst. of Tech. (1951).

77. Wigner and Feenberg, Rep. Progr. Phys. 8, 274 (1942).

78. S. Devons, Excited States of Nuclei, Cambridge University Press (1949).

79. Rosenfeld, Nuclear Forces, Interscience Publishers (1949).

80. T. Lauritsen, Energy Levels of Light Nuclei, Nuclear Science Review (1950).

81. Walker and Day, Bull. Amer. Phys. Soc. 26-3, 12 (1951).

82. Sperduto, Holland, Van Patter, and Buechner, Phys. Rev. 80, 769 (1950).

83. Humphreys and Watson, Phys. Rev. 60, 542 (1941).

84. Curling and Newton, Nature 165, 609 (1950).

85. Hornyak, Lauritsen, Morrison, and Fowler, Energy Levels of Light Nuclei, III, Rev. Mod. Phys. 22, 291 (1950).

86. Gutowsky, McClure, and Hoffman, Phys. Rev. 81, 635 (1951).

Shuster and Pake, Phys. Rev. 81, 886 (1951).

87. Mandeville and Swann, Phys. Rev. 79, 787 (1950).

88. John Seagrave, Thesis, Calif. Inst. of Tech. (1951).

89. Devons and Hine, Proc. Roy. Soc. A199, 56 (1949).

90. Sherr, Muether, and White, Phys. Rev. 75, 282 (1949).

91. C. K. Bockelman, Phys. Rev. 80, 1011 (1950).

92. Fay Ajzenberg, Phys. Rev. 82, 43 (1951).

PART IV

2. Energy Levels of the Mirror Nuclei, N^{13} and C^{13}

1. Introduction

The assumptions of equality of *nn* and *pp* nuclear forces and a uniform distribution of electrostatic charge throughout a nuclear volume of radius $R_c = 1.46\ A^{1/3} \times 10^{-13}$ cm provide a satisfactory account of the ground state energy differences of the pairs of light odd nuclei of charges Z, Z + 1 and mass 2Z + 1. If the Coulomb energy differences of these mirror nuclei remain the same in the excited states, then we might expect to find corresponding energy levels at the same nuclear excitation energies. However, in the pairs of such nuclei for which there is sufficient experimental data on the excited states, Be^{7} - Li^{7} and N^{13} - C^{13} for instance, it is apparent that there is a displacement of the levels. The following possible sources of energy level shifts will be examined in order to see if they can account for the shifts observed in the excited states of N^{13} and C^{13} with the same assumptions that are made in regard to the energy differences of the ground states. (1) If there is not a sharply defined nuclear radius for the odd particle (proton or neutron for N^{13} or C^{13} respectively), then the nuclear excitation energies required for the interior wave function to join onto the exterior proton or neutron wave function will be different*.

*In an abstract on the C^{13} -N^{13} excited-state level shift (R.G. Thomas, Phys.Rev.80,136(1950)) it was stated that the shift was due to the fact that the odd proton of N^{13} spends time outside of the nucleus so that its average Coulomb interaction is diminished. This statement can be justified but is not strictly correct in such simple terms. J.B. Ehrman(Phys.Rev.81,412(1951) interprets this shift as being due to the difference of the boundary conditions for the odd particle at the nuclear surface. We have adopted this interpretation, which is strictly correct, and we have also used here some details of Ehrman's method of calculation which we found to be more suitable than those which

This difference may be particularly large if the level of one member of the mirror pair is in the continuum, that is, unstable to particle emission, whereas that of the other member is not. A measure of the sharpness of the definition of the nuclear radius for a particular nuclear particle is the smallness of the reduced width for that particle (for bound as well as unbound particles). (2) Due to the difference of the neutron and proton magnetic moments, the electromagnetic spin-orbit interaction of the odd particle may not be the same in the two nuclei in different states of excitation. (3) Even considering the nuclear radius as sharply defined, a volume expansion with nuclear excitation is expected. As a result of this expansion the average Coulomb interaction will diminish, the diminution being greater for the member of the mirror pair with charge $Z+1$.

The first source will be shown to account for the large shift of the first excited states of C^{13} and N^{13}. The observed shift of the second excited states may be almost accounted for with about equal contributions from sources 1 and 2. The third source is estimated to have a smaller effect than the first two and to be almost negligible. Inglis[1] has shown that the 49-kev shift of the first excited states of Be^{7} and Li^{7} is about one-half accounted for by source 2 and one-quarter by source 3.

2. Experimental Data

The energy levels of C^{13} and N^{13} below 6-Mev excitation are shown in Figure (1). The levels of N^{13} are found from observations of resonances for gamma-radiation[2],[3] and elastic

---

we originally used. I am indebted to Mr. Ehrman for having sent to me his manuscript before publication.

scattering of protons [4], and also by the neutron groups from $C^{12} + d$ [5]. The positions and widths of these two levels as found in the different experiments are essentially in agreement. However, the elastic proton scattering anomaly associated with the 3.52 level shows peculiar interference effects on each side of the main resonance which cannot be understood as a single resonance interfering with a constant background. The level at 3.10 in C^{13} is well established by spectrometer measurement of the proton group to it [6] and the resulting gamma-radiation [7]. In addition to the level at 3.10, Rotblat finds by range measurements of the proton groups from $C^{12} + d$ levels at 3.77 and 3.90 Mev [8]. By precision magnetic spectrometer analysis of the α-particle groups from $N^{15} + d$ a level is found at 3.68 in addition to the one at 3.10 [9]. We assume that this 3.68 level is the same as the one reported by Rotblat at 3.77 and that the level reported by him at 3.90 was not observed in the $N^{15} + d$ reaction because it would have occurred at the same spectrometer field setting as a broad group from the competing $N^{14}(d\alpha)C^{12*}$ reaction and so could have been obscured. A possible level at 1 Mev in C^{13} reported by some experimenters, is thought to be due to an impurity [10]. In addition to the observations of discrete levels in C^{13}, there is also much data, which is summarized by Adair [11], on the scattering of neutrons by carbon. This scattering cross section at low energies is too large to be attributed to potential scattering alone; actually it appears as the tail of a resonance. The Q values in Figure (1) are calculated from the compilation of Tollestrup, Fowler, and Lauritsen [12].

We will assume the level scheme of Figure (1) to be correct and attempt to show the following. (1) The 2.37-Mev resonance level of N^{13} is formed by s-wave protons and corresponds to the 3.10 level of C^{13}; the large reduced scattering width is responsible for the large level shift and suggest that a simple one-body type of interaction between the odd particle and the C^{12} core is involved. (2) In view of the peculiar interference observed at the 3.52 level of N^{13} in the elastic scattering experiment, this level may possibly be a doublet one component of which appears at 3.68 and the other at 3.90 in C^{13}, and the 3.68 component is most likely $^2p_{3/2}$ and the 3.90 ^2d*.

3. Reduced Level Widths

At a particular nuclear excitation energy a measure of the probability that the nucleus is decomposed into a pair of constituents s, which are separated by a distance R, is the reduced level width $\gamma^2_{\lambda s l}$ introduced in the dispersion theory of Wigner and Eisenbud (13). Here we shall consider the reduced widths to be energy dependent and therefore omit the level subscript λ. The pair s will be $C^{12} + p$ for N^{13} and $C^{12} + n$ for C^{13} with a relative orbital momentum l.

The reduced width may be written as

$$\gamma^2 = \theta^2 \hbar^2 / 2MR \quad , \quad \theta^2 = R|u(R)|^2 / \int_\tau |\phi|^2 d\tau \qquad (1)$$

where ϕ is the complete wave function within the nuclear volume of radius R, u is r times the radial part of the wave function describing the separated pair s, and M is their reduced mass. We

---

*In the use of the l_s notation we refer to exterior region. Since C^{12} has zero spin, the relative orbital momentum l between the odd particle and the C^{12} core and the spin s are good quantum numbers.

shall use θ^2, which will be a function of R as well as energy, as a convenient dimensionless measure of the reduced width. The radius R is somewhat arbitrary; according to dispersion theory it is usually desirable to use the smallest value beyond which the nuclear forces do not significantly extend.

Following the dispersion theory of Feshbach, Peaslee, and Weisskopf[14] we introduce f(E) which is

$$f(E) = R\left[(d\mathcal{U}/dr)/\mathcal{U}\right]_{r=R} . \qquad (2)$$

The theory of WE relates this quantity to the reduced width as

$$(-df/dE)^{-1} = \theta^2\hbar^2/2MR^2. \qquad (3)$$

The accuracy of the experimental cross section data is usually only sufficient to determine the value of θ^2 at the resonance where the cross section is relatively large. At the resonance energy E_r the relationship between the reduced width and the observed scattering width Γ' may be found by means of Equation (41) of FPW. Taking into account the variation of the level shift with respect to energy[15], we have

$$-(df/dE)_{E_r} = -(dg/dE)_{E_r} + 2\chi/(F^2+G^2)\Gamma',$$
$$g = \left[d\ln(F^2+G^2)^{1/2}/d\ln\chi\right]_{\chi} , \quad \chi = kR . \qquad (4)$$

The wave number for the pair is k; F(x) and G(x) are the usual regular and irregular solutions to the wave equation in the region external to R. For $C^{12} + p$ the values and derivatives of F and G, which are the Coulomb wave functions provided nuclear forces do not extend beyond R, may be obtained from Breit's tables[16]. The quantity $(dg/dE)_{E_r}$ is positive, and in the case of the 2.37-Mev resonance level of N^{13} it is of the same order of magnitude as the second quantity on the right side of (4); hence any error in the experimental determination of Γ', due possibly

to target thickness uncertainties and dispersion effects, or in the determination of $d\gamma/dE$, would make a significant error in the determination of θ^2 from (3) and (4). This sensitivity to error is an indication that the strong Coulomb barrier for the incident proton makes it difficult to extract accurate information about the nuclear interaction.

For incident proton energies sufficiently below the top of the Coulomb barrier $G \gg F$, $dG/dx \gg dF/dx$, and we may use the approximation $\gamma = x(dG/dx)/G$ for the required quantity in (4). In this case and for s-wave protons*

$$E\frac{d}{dE}\left[x\,(dG/dx)/G\right]_x = x\,\Theta_0^{-2}(x)\left[H(\eta) - \int_0^x \Theta_0^2(x)\,dx\right], \qquad (5)$$

where $\Theta_0(x) = C_0 G(x)$, $C_0 = \left(\frac{2\pi\eta}{e^{2\pi\eta}-1}\right)^{1/2}$, $H(\eta) = \eta - 2\eta^3 \sum_{\nu=1}^{\infty} \nu/(\nu^2+\eta^2)^2$

$x = kR$, (16) $\eta = Ze^2M/\hbar^2 k$.

The quantity $\Theta_0(x)$ is tabulated as an auxiliary function for G.

Column 5 of Table I gives the reduced widths for the two $C^{12} + p$ resonances for various possible assumptions as to the partial wave involved and for four evenly spaced radii. Expression (5) was used to evaluate $d\gamma/dE$ at the 2.37 resonance level; otherwise it was obtained from the slope of a plot of γ as a function of energy. The only possible assignments are s-wave to the 2.37 level and s-, p-, or d-wave to the 3.52 level; other partial waves yield negative values for the (positive-definite) reduced with or violate Wigner's criterion (17), $\theta^2 \lesssim 3$, for reasonable values of the radius.

Figure (2) shows a plot of $^{P}\theta_{\ell}^{-2}$ ** as a function of

*This expression can be readily obtained by setting $\delta_1 = \delta_2 = \pi/2$ in equations (49) and (50) of Ref. (19) and then taking the limit as $E_2 \to E_1$.

**The following notation is used in referring to energy levels:

TABLE I

Calculated level shifts due to the difference of the boundary conditions at R$_o$. The energy unit is Mev in the center-of-mass system.

(a)

$E_r^p = 2.37$; $E_b^n = 3.10$; $\Gamma' = .032$; s-wave

R x 10^{13} cm	g	dg/dE	$F^2 + G^2$	$p_{\theta_r}^2$	n_{θ}^2 o-b	$E_b^n - E_r^p$			$p_{\theta_r}^2$
						Model 1	Model 2	Model 3	Model 3
3.34	-.784	.47	49.0	4.4	3.42	1.18	1.21		
3.86	-.832	.58	38.8	2.5	1.88	.77	.81	.88	2.20
4.39	-.866	.70	31.8	1.8	1.19	.54	.59	.72	1.70
4.92	-.897	.82	26.2	1.4	.74	.33	.39	.58	1.36

(b)

$E_r^p = 3.52$; $E_b^n = 3.68$; $\Gamma' = .068$; p-wave

R x 10^{13} cm	g	dg/dE	$F^2 + G^2$	$p_{\theta_r}^2$	$E_b^n - E_r^p$	
					Model 1	Model 2
3.34	-1.069	.256	9.50	.200	.114	.112
3.86	-1.016	.302	7.01	.167	.106	.104
4.39	-.954	.321	5.44	.144	.097	.093
4.92	-.887	.324	4.41	.129	.089	.086

(c)

$E_r^p = 3.52$; $E_b^n = 3.90$; $\Gamma' = .068$; d-wave

R x 10^{13} cm	g	dg/dE	$F^2 + G^2$	$p_{\theta_r}^2$	$E_b^n - E_r^p$	
					Model 1	Model 2
3.34	-2.062	.158	126.0	10.7	2.02	1.99
3.86	-2.038	.214	69.2	3.1	.77	.77
4.39	-1.995	.280	41.7	1.6	.49	.49
4.92	-1.931	.363	26.7	1.0	.36	.36

radius for the 2.37-Mev resonance. The radial dependence is due to the variation of the penetrability factor, F^2+G^2, and $d\gamma/dE$ with respect to R. The plot crosses the axis indicating that θ^2 has been improperly evaluated, at least for the smaller radii. The difficulty lies in the fact that we used Coulomb wave functions at a radius R, and it is possible that the nuclear forces extend beyond this radius. One should actually use the wave functions pertaining to the problem which includes any extension of the nuclear forces as well as the Coulomb potential. The net effect of using the improper functions at R is to make F^2+G^2 and $d\gamma/dE$ too large; as a result df/dE is made too small in absolute magnitude and eventually, for small enough R, of the wrong sign. From the plot of Figure (2) one cannot say anything about the radius of the nuclear interaction other than that the criterion $\theta^2 \lesssim 3$ requires that $R \gtrsim 3.6 \times 10^{-13}$ cm. Nuclear radii for carbon obtained in various ways are indicated at the top of the graph.

Column 6 of Table Ia lists the reduced widths of the s-wave C^{12} + n interaction as a function of the radius. These reduced widths, $\hat{\theta}^2_{o-b}$, are obtained by setting in (3) $df/dE = (f_o^n - f_b^n)/(E_o^n - E_b^n)$; f_o^n is given in terms of the zero-energy scattering length a as $-f_o^n = R/(a-R)$, and for the bound state $-f_b^n = [2MR^2(E_o^n - E_b^n)/\hbar^2]$. Using these reduced widths the one-level dispersion formula gives a good fit to the low-energy neutron scattering data.

---

subscripts g, b, r and o denote respectively the ground state, bound excited state, resonance level, and the excitation level corresponding to zero-energy protons or neutrons incident on C^{12}; the superscripts n and p refer to $C^{12}+n$ and $C^{12}+p$.

It is evident from Table I that for the s-wave interactions $^{p}\theta_{\ell}^{2}$ and $^{n}\theta_{0\text{-}b}^{2}$ are of the same order of magnitude and about equal to the reduced widths expected for a simple one-body potential interaction. For example, it follows from the definition (1) that $\theta^2=2$ is the maximum possible value for a square-well interaction. Hence, there is no particular evidence for the formation of a compound nucleus in which the incident particle remains within the nucleus longer than the time that it takes for a particle of the velocity of the incident particle to cross the nucleus. The ^{12}C + p,n reduced widths listed differ somewhat; it is not necessary for them to be equal, even if the interactions are the same, since they are evaluated at different nuclear excitation energies.

The assumption that the 3.52 resonance level is a d-state also gives a large reduced width with essentially the same radial dependence as that of the lower s-state. If the 3.52 level is a p-state, its reduced width is not very sensitive to the radius and about 1/10 of the value expected for the familiar one-particle type of model.

4. Analysis of The ^{12}C + n S-Wave Interaction By Means of The Effective Range Theory

For interactions having large reduced widths an alternative to the dispersion theory is to analyze the data by means of the effective range theory, which has been very useful in the study of the pn and pp interactions [18),(19)]. In this theory the effective range is analogous to the reduced width of the dispersion theory, and the reciprocal of the scattering length is the analogue to the quantity f at some particular reference energy.

The s-wave $C^{12} + n$ interaction resembles the s-wave triplet np interaction; the 3.10 level of C^{13} is the analogue of the ground state of the deuteron and the scattering cross sections at low energies have a similar behaviour. The s-wave $C^{12} + p$ cross sections differ significantly from the pp cross sections because the Coulomb barrier is much greater in the former case.

According to BJ the s-wave neutron scattering phase shift may be expressed in terms of the wave number as

$$k \cot \delta = -1/a + \tfrac{1}{2} r_0 k^2 - P r_0^3 k^4 + \ldots . \qquad (6)$$

where a is the scattering length, r_0 the effective range, and P is the shape factor; they show that for familiar potentials the third and higher terms of (6) are small for a rather large energy range. Expression (6) also applies to the bound state with the substitutions $\cot \delta = -i$ and $k = -i\gamma$ where $\gamma = [2M(E_0^n - E_b^m)/\hbar^2]^{1/2}$.

An accurate determination of the $C + n$ total cross section from .02 to 1.36 Mev has been made by Miller[20]; his values are in excellent agreement with those of Lampi, Freier, and Williams[21] where measured. Up to about 0.8 Mev the cross section may be considered as almost entirely due to s-wave scattering; potential scattering of the higher partial waves is estimated to be at the most 3% of the total at this energy and negligible below 0.4 Mev. In making a $k \cot \delta$ plot of this data we subtracted potential scattering of the partial waves $p, d, ..$ from a sphere of radius 3.86×10^{-13} cm according to the formula of FPW,

$$\sigma_0' = (4\pi/k^2) \sum_{l=1}^{\infty} (2l+1) F_l^2/(F_l^2 + G_l^2) \quad ;$$

the prime on σ_0 is to indicate that the term $\ell=0$ is omitted from the summation. The potential scattering correction may not be accurate since the proper radius to use is not certain; furthermore, there is a resonance, probably p-wave, for 3.5-Mev neutrons[11]. The $k\cot\delta$ plot is shown in Figure (3). We wish to emphasize that this sort of plot exaggerates the scatter of the points which is only a few per cent on the cross section plot, at least for energies greater than 0.4 Mev. The points at 0.4, 0.6, 0.8, and 1.0 Mev have vertical lines through them to indicate the possible uncertainty of the potential scattering correction; the top of the line corresponds to a 30% increase of the potential scattering over that of a sphere of radius 3.86×10^{-13} cm, and the bottom of the line corresponds to no potential scattering correction. It is apparent that the correction improves the straightness of the plot. The plotted $k\cot\delta$ value for E_n = 10 ev is from the slow neutron velocity spectrometer cross section, $4.70 \pm .05$ barns, obtained by Havens and Rainwater[22]; this datum is in agreement with that of Jones[23].

From the $k\cot\delta$ plot*, together with the datum corresponding to the bound state at 3.10 Mev, we find the interaction parameters to be $r_0 = (3.23 \pm .35) \times 10^{-13}$ cm, $a = (6.14 \pm .04) \times 10^{-13}$ cm, $P = -.03 \pm .05$; the uncertainties in these quantities are not independent. The

*We disregard the presence of C^{13} in ordinary carbon. We have reason to believe that the low-energy C^{13} (n n) cross section is not significantly different from the C^{12} (n n) cross section.

curves of BJ enable one to say something about the shape of the interaction; according to Figures (10) and (6) of their paper the long-tailed interactions would be excluded and a square-well interaction would have a rather large radius, 4.88×10^{-13} cm. The lower curve of Figure (3) is a plot of $k \cot \delta$ for a square well of this radius, and shown above it is the straight line corresponding to $P=0$. If we assume that the 3.68-level of C^{13} is the bound s-state associated with the scattering, we obtain $P = -.14 \pm .05$ with about the same effective range values. These possible values would seem to be unreasonable on the basis of Figure (10) of BJ.

In connection with the use of the curves of BJ with this data it should be noted that according to both the shell-structure model[24] and the alpha-particle model[25] the internal s-wave function for the $C^{12} + n$ interaction would have a node. Consequently, these curves may not apply exactly to this case although we would not expect very much change, other than in the determination of well depths, if the node were included in the calculations. We have verified that a square-well wave function with a node gives a $k \cot \delta$ plot that is almost the same as shown in Figure (3) for the case without the node. However, the radius of the well is smaller, viz 4.03×10^{-13} cm.

5. Level Shift Calculations

(1). Level Shift Due to the Boundary Condition Difference

Information about the nuclear interaction of C^{12} with low-energy incident protons can be obtained only in the vicinity of the resonances where the cross section is sufficiently large

for accuracy. According to dispersion theory this information may be the value of f and df/dE at the resonance energy; usually no additional information is provided by the data. In the case of the bound C^{13} levels the binding energy for the pair $C^{12} + n$ determines the value of f_b^n provided their relative orbital momentum is known for $r > R$; expressions for f_b^n are

$$\begin{aligned} &\ell = 0, && -\chi \\ &\ell = 1, && -(1+\chi+\chi^2)/(1+\chi) \\ &\ell = 2, && -(6+6\chi+3\chi^2+\chi^3)/(3+3\chi+\chi^2), \end{aligned} \qquad (7)$$

where

$$\chi = [2MR^2(E_o^n - E_b^n)/\hbar^2]^{1/2}.$$

The low-energy neutron scattering data furnishes a value f_o^n for the s-state.

A necessary condition for the equality of the $C^{12} + p$ and $C^{12} + n$ nuclear interactions is the equality of the respective values of f and θ^2 at the same nuclear excitation energy, taking into account the presence of the non-nuclear forces. Rather than comparing f values we will compare calculated with observed level shifts. In order to do this it is necessary to employ a model for the interaction in order to extrapolate the $C^{12} + n$ information to the same nuclear excitation energy as the $C^{12} + p$ information. The following simple models should cover a reasonable range of possibilities:

1. $\Delta f = \text{constant} \times \Delta E$,
2. $f = KR \cot[(\pi/D^*)(E - E')]$, $K \approx 1.2 \times 10^{+13}\ cm^{-1}$

The first model is the basis of the one-level dispersion formula. The second is a model used by FPW for a statistical analysis of cross section data; D* is an effective distance between energy levels, and K is a wave number corresponding to the kinetic energy of a particle within the nucleus. The third model with

$R' = 0$ represents an ordinary square-well of depth V.

Another possible way of comparing the broad s-wave interactions would be to extend the effective range theory to the $C^{12} + p$ interaction as was done with $C^{12} + n$. (26) Because of the rather large Coulomb field of C^{12}, this method loses the simplicity for which it was designed. We believe that the above models are adequate.

It was shown in Section 3 that the first excited states of N^{13} and C^{13} must be s-states and that their reduced widths are so large as to suggest a simple one-body type of interaction; consequently, it is appropriate to use model 3 for this case. From the knowledge of f_o^n and f_b^n for a particular radius R, the parameters V and R' are found. The predicted shift of the levels, $E_b^n - E_\ell^p$ can then be solved for since at the resonance $f_\ell^p = g_\ell^p$ according to Equation (40) of FPW; the results are given in column 9 of Table 1a. The reduced widths $^p\theta_\ell^2$ at E_ℓ^p as predicted by this model, are given in column 10. The parameter R' turns out to be positive and so we assumed in the calculation of the reduced width zero probability for the odd particle being in the range $0 \leq r \leq R'$; this will perhaps represent the repulsion that is anticipated over part of the range of the $C^{12} + p$, n interactions. The values listed in Table 1a are for a nodeless wave function; inclusion of a node does not significantly alter the results.

The procedure is essentially the same in the use of models 1 and 2. In the case of the upper levels, which are probably p- or d - orbitals, there is no information provided by the neutron scattering data. Therefore the model parameters are

determined from the knowledge of ${}^{p}\theta_r^2$ and $f_r^p = g_r^p$ at the N^{13} resonance; $E_b^n - E_r^p$ is calculated using the known value of given by (7). The results are tabulated in columns 7 and 8 of Table 1a and columns 6 and 7 of Tables 1b and 1c.

The reduced width of model 1 is constant with nuclear excitation, and so this model will not account for the difference between ${}^{p}\theta_r^2$ and ${}^{n}\theta_{o-b}^2$ shown in columns 5 and 6 of Table Ia. On the other hand, model 3 with $R = 4.4 \times 10^{-13}$ cm gives the proper shift and the observed value of ${}^{p}\theta_r^2$.

There may also be an energy level shift due to the difference in the ground-state boundary conditions although it is expected to be less due to the greater binding energy. The energy level diagrams of Figure (1) are drawn with the ground states at the same level so that this shift would appear as a displacement of the excited states in the opposite direction.

For the bound system $C^{12} + p$ outside of the range of nuclear forces the wave function u_g^p is Whittaker's function $W_{-\eta,\mu}(2x)$, and[27] where

$$-f_g^p = (\eta + x) + [\mu^2 - (\eta + \tfrac{1}{2})^2] W_{-\eta-1,\mu}(2x) / W_{-\eta,\mu}(2x),$$

$$x = [2MR^2(E_o^p - E_g^p)/\hbar^2]^{1/2}, \quad \mu = \ell + \tfrac{1}{2}, \quad \eta = Ze^2MR/x\hbar^2 \qquad (9)$$

We have found the WKB-$(\ell+\frac{1}{2})^2$ approximation to be accurate for the determination of f_g^p for negative-energy protons. This approximation is discussed by Yost, Wheeler, and Breit[28] for the positive-energy case. If the WKB-$(\ell+\frac{1}{2})^2$ approximation is used for f_g^p, it should also be used for f_g^n.

In order to predict the level shift of the ground states using the models (8), it is necessary to know their reduced width.

In Section 6 we obtain a value $\theta_g^2 = .19$ (assumed to be the same in N^{13} and C^{13}) from the s-wave radiative capture cross section data. Using models 1 and 2 and this reduced width the ground-state shifts are -50 and -43 kev* with $R = 4.0 \times 10^{-13}$ cm.

(2) Level Shift Due to the Differences of the Spin-Orbit Interactions

Using a reasonable model for the mirror nuclei Be^7 and Li^7 Inglis[1] has shown that most of the level shift of the first excited states can be accounted for as the differences of the electromagnetic spin-orbit interactions of the various states involved. Assuming a uniform charge distribution over a volume of radius R_c, the electromagnetic spin-orbit interaction for the odd particle is

$$-Ze^2(g_s - \tau^-)\vec{l}\cdot\vec{s}/2(Mc)^2R_c^3 \qquad (10)$$

where Z is the core charge, $\tau^- = 1$, or 0 for an odd proton or neutron respectively, and g_s is the spin g-factor for the odd particle. The fact that the magnetic moment of C^{13} in the ground state falls near to the Schmidt line for the moment of a single odd particle whose spin and orbital momentum are oppositely directed suggests that the orbital motion is essentially carried by one nucleon[29]; the shifts listed in Table II are for such a case using the Coulomb radius $R_c = 1.46\ A^{1/3} \times 10^{-13}$ cm. If some of the orbital motion is shared by nucleons within the core, we would expect shifts smaller in absolute value.

It appears to be contradictory that the magnetic moment

---

*The sign convention (except for Table II) for level shifts is the following. The shift is taken to be positive if it is such as to lower the position of the N^{13} level with respect to the corresponding C^{13} level, the ground-state levels being taken as a common reference level (as in Figure (1)).

of the ground state can be interpreted in terms of the single-particle model whereas the reduced width which we have found for the ground state is about 1/10 of the value expected for the familiar one-particle models. This paradox is not new; a possible resolution of it has been given by Weisskopf[30].

(3) Level Shift Due to Nuclear Volume Expansion with Excitation

It is possible that some contribution to the observed level shifts be due to the volume expansion with nuclear excitation. The average Coulomb energy for the nucleus with charge Z + 1 will diminish more with expansion than that of the nucleus with charge Z. Feenberg has derived the following expression for the volume expansion with nuclear excitation[31];

$$E_x / k_v U_v \leq \Delta R/R \leq 2E_x / k_v U_v \qquad (11)$$

TABLE II

Level shift in kev due to the electromagnetic spin-orbit interaction.

LEVEL	N^{13}	C^{13}
$^2d_{5/2}$	-21	18
$^2d_{3/2}$	32	-27
$^2p_{3/2}$	-11	9
$^2p_{1/2}$	21	-18

where U_v is the total nuclear potential energy, ΔR is the increase in radius with excitation energy E_x, and k_v is the volume compressibility coefficient. For a nucleus with A = 13 we take k_v = 2 1/2 and U_v = 350 Mev; for E_x = 3 Mev this gives $.003 \leq \Delta R/R \leq .006$. If we assume a uniform Coulomb charge

distribution in the excited as well as the ground state, then

$$\Delta_x E_c / E_c \approx \Delta R / R \qquad (12)$$

where $\Delta_x E_c$ is the change with excitation in the difference of the Coulomb energies E_c for the mirror levels. In the case of C^{13} and N^{13} $E_c = 3.0$ Mev, so that

$$-10 < \Delta_x E_c < -20 \quad \text{kev.} \qquad (13)$$

For the s-states of C^{13} and N^{13}, which have unusually large reduced widths, it is possible that the charge distribution may be entirely different from that of the ground states, and so expression (12) may not be valid. Some idea of the possible variation of the Coulomb energies may be obtained by an examination of the table in a paper of Stephens[37] which summarizes the theoretical calculations. It appears that we can expect a Coulomb difference from the ground state for this s-state up to several hundred kev.

Total Shifts and Comparisons with Experiments

Table III summarizes the various shifts for the assumed level schemes and a nuclear radius of 4.0×10^{-13} cm. For the first excited states the calculated shift appears to be correct within the large possible uncertainty in not knowing accurately the average Coulomb energy and within the range of values provided by the various models. It is not possible to obtain this sort of agreement if the 3.68 level is assumed to be the s-state corresponding to the 2.37 level of N^{13}.

The gamma-radiation from the 3.10-Mev state has been found to be electric dipole by a measurement of the internal pair-formation coefficient of the radiation[33]; furthermore, the

angular distribution of the capture radiation at the 2.37 state in N^{13} is isotropic [34]. Both of these observations are in accord with a $^2S_{1/2}$ assignment to these states.

TABLE III

Level shift summary for $R=4.0\times10^{-13}$cm. The energy unit is Mev.

N^{13} Energy Level	2.37	3.52	3.52	
C^{13} Energy Level	3.10	3.68	3.90	
Level assignment	$^2S_{1/2}$	$^2P_{3/2}$	$^2d_{3/2}$	$^2d_{5/2}$
(1) Shift due to boundary-condition differences *	.65-.80	.05	(.65)	
(2) Shift due to spin-orbit interaction differences *	.04	.06	-.02	+.08
(3) Estimate of shift due to change in nuclear Coulomb energy.	($\pm$ .2)	$\sim$.02	($\pm$ .2)	
Total level shift	.8 $\pm$ .3	.13	(.7 $\pm$ .2)	
Observed shift	.73	.16	.38	

* Ground-state shift included.

The calculated shift for a $^2P_{3/2}$ assignment to the 3.52- and 3.68-Mev states is in reasonable agreement with the observed shift. The measured radiation width of the 3.52 resonance level of N^{13} is 1.3 ev [3]. A calculation of the expected magnetic-dipole radiation width from the flipping of the moment of a single odd proton in a $^2P_{3/2}\rightarrow{}^2P_{1/2}$ transition, assuming that the radial parts of the wave functions are the same in the initial and final states, yields a value of 1.6 ev. A possible similarity of the 3.68 and ground states of C^{13} is suggested by the fact that the particle groups to these two states observed in the $N^{15}(d\alpha)C^{13}$ reaction are of nearly the same intensity [9]. It will be shown in Section 6 that from the $C^{12}+p$, n s-wave radiative capture cross sections that the reduced width of the ground states can be deduced, though not very accurately, and that it is nearly equal to

that for a p-wave assignment to the 3.52 resonance level. The angular distribution of the $C^{12} + p$ radiation at this level has been measured and found to be in agreement with a $J = 3/2$ assignment but with d-wave giving the best fit to the energy dependence of the $\cos^2\theta$ coefficient[35]. The total level shift calculated for a s-wave assignment to the pair of levels at 3.52 and 3.68 is about 50 kev which is too small. Moreover, it would be surprising to find another s-state so near to the lower s-state whose reduced width suggests a level spacing of the order of 20 Mev.

The suggestion that the 3.52 N^{13} resonance level is a doublet was offered as a possible explanation of the peculiar interference in the elastic scattering and the fact that two closely spaced levels are found in C^{13} which might correspond to the levels of such a doublet in N^{13}. From Table Ic it is apparent that the shift calculated for a d-wave assignment to this resonance level does not agree with the observed shift; however, if there is a doublet at 3.52 Mev, then we could very well have used too large a level width in this calculation and therefore have obtained too large a level shift. The gamma-ray resonance curve is fitted well by the one-level Breit-Wigner formula, there being no evidence for complexity[3]. Nevertheless, if one component of this presumed doublet were $^2d_{5/2}$, its radiation to the lower states would be by quadripole or slower emissions which are expected to be weak compared to magnetic-dipole radiation for the likely $^2p_{3/2}$ component of the doublet.

6. S-Wave Capture Radiations

The s-states of C^{13} and N^{13} radiate by electric dipole emission to the ground states ($J = 1/2$). The reduced widths of

the C^{12} + p, n s-wave interactions suggest that a simple one-body model is involved in the initial state, and in the ground state the measured magnetic moment of C^{13} suggests that the orbital motion is carried by the odd particle about a C^{12} core. Neglecting interaction effects in the radiation, the transition probability for a single-particle $^2S_{1/2} \rightarrow {}^2P_{1/2}$ transition is given by the usual expression $(\frac{4}{9})(h\nu)^3(e^2/\hbar^4c^3)\,C_{ed}^2 \left| \int_0^\infty u_i\, r\, u_g\, dr \right|^2$ (14) where u_i/r and u_g/r are the radial parts (angular and spin parts being normalized to unity) of the initial and ground-state wave functions for the odd particle; C_{ed} is the reduced charge number for electric-dipole emission, 6/13 for both $C^{12}(p\gamma)$ and $C^{12}(n\gamma)$, and $h\nu$ is the radiation energy.

The radial integral of (14) may be separated into a nuclear part $r<R$, and an extra-nuclear part $r>R$, where R is a radius beyond which the nuclear forces may be regarded as negligible. For $r<R$ the wave functions of the initial and final states are not known aside from the normalization requirement of the final state and the reduced-width relationship of the initial state. When $r>R$, the p-state wave function for C^{12} + n in the ground state is

$$u_g^n = N_n^{-1/2}\,[1 + (1/\chi)]\,e^{-\chi}\,, \quad \chi = r\,[2M(E_o^n - E_g^n)/\hbar^2]^{1/2}, \tag{15}$$

and for C^{12} + p it is

$$u_g^p = N_p^{-1/2}\,W_{-\eta,3/2}(2\chi)\,, \quad \chi = r\,[2M(E_o^p - E_g^p)/\hbar^2]^{1/2}, \tag{16}$$

where $W_{-\eta,\mu}(2\chi)$ is Whittaker's function, N is the normalization factor. The initial-state wave function, normalized to unit flux so that the transition probability becomes equal to the radiative cross section, is (17)

$$u_i = (4\pi/v)^{1/2}\,(F\cos\delta + G\sin\delta)/kr\,, \quad r \geq R,$$

where δ is the phase shift; F and G represent the usual regular and irregular solutions for the proton and neutron wave functions when $r > R$. Considering the large reduced widths of the initial states we can use Wigner's first assumption [26] (which is that the radial integration for $r < R$ is merely proportional to $u_i(R)$) in the 3-Mev range of nuclear excitation energies with which we are concerned. The contribution to the integral for $r > R$ is different in N^{13} and C^{13} and is a function of the phase shift. The normalization constant N can be expressed by means of (1) in terms of the ground-state reduced width θ_g^2, which we assume to be the same in each case, viz.,

$$1 = R\theta_g^{-2} N^{-1} / N^{1/2} u_g(R) /^2 + \int_R^\infty /u_g/^2 dr + \int_R^\infty /u_g'/^2 dr + \ldots . \quad (18)$$

Here u_g', u_g'' are the wave functions for other pairs s in the external region, for instance $Be^9 + \alpha$ or $B'' + d$;formally, the relations between the $u_g(R)$ are given by the R-matrix of WE. We know nothing about the reduced widths of these other modes of decomposition aside from the restriction of the sum rule [17] $\sum_s \theta_s^2 \approx 3$; however, we expect that their contribution to (18) is small since their binding energies are large and so they will be neglected. Even the $C^{12} + n$ alternative contributes in the external region only about 5% to the normalization.

The C^{12} thermal neutron absorption cross section is 3.5×10^{-3} barns [37] which we assume to be due entirely to radiation to the ground state. The radiative capture cross section of protons by C^{12} at the 2.37 resonance level is 1.2×10^{-4} barns[2]. With this information in Equation (14) we can solve for the value of the nuclear radial integral and the ground-state

reduced width. Using $R = 3.86 \times 10^{-13}$ cm we find that the only permissible solution is for the nuclear and extra-nuclear contributions to have the same sign and that

$$\theta_g^2 = 0.19 \quad , \quad \theta_i \left| \int_0^R u_i r u_g \, dr \right| / R^{1/2} |u_i(R)| = 0.26 R. \qquad (19)$$

This reduced width is close to the value $^{P}\theta_r^2$ obtained for the same nuclear radius at the 3.52 level in N^{13} assuming it to be formed by p-wave protons, and the value of the radial integral seems reasonable.

In the capture of thermal neutrons by C^{12} the extra-nuclear contribution to the radial integral of the electric-dipole moment is small compared to the nuclear contribution because the initial-state wave functin in the region $r > R$ changes sign at $r = a$ (6.1×10^{-13} cm) with the result that the contributions on each side of a are nearly equal in magnitude but opposite in sign, and so the net contribution is small. On the other hand, at the $C^{12} + p$ resonance the extra-nuclear wave function does not change sign in a region where contributions to the radial integral are significant, and so a much larger value of the integral is obtained; in fact, the nuclear and extra-nuclear contributions are about equal*.

---

*Another example in the light nuclei where the extra-nuclear contribution to the electric-dipole matrix element is important is in the capture of thermal neutrons by Li^7. Hughes, Hall, Eggler, and Goldfarb (Phys. Rev. 72, 646 (1947)) found the cross section for production of Li^8 by thermal neutrons to be 0.033 barns and noted that this was about ten-times larger than the maximum intensity expected for electric-dipole emission as given by the usual estimates. The recent Li^7 (n n) data of Adair (Phys. Rev. 79, 1018 (1950)) shows that the zero-energy scattering length is negative suggesting that (contrary to the C^{12} (n γ) case) a large extra-nuclear contribution

As a check on the values (19) we can calculate from (14) the $C^{12}(p\gamma)N^{13}$ cross section for 120-kev incident protons and compare the result with the accurately measured cross section of Hall and Fowler, viz., $(6.1 \pm 0.6) \times 10^{-10}$ barns (38). At this proton energy the phase shift is nearly zero so that the ratio of extra-nuclear to nuclear contribution becomes even larger than at the resonance. The phase shift required in (17) is obtained by using model 1 in which the constant is given by the reduced width at the resonance. This is equivalent to using the one-level dispersion formula, although here it is necessary to take into account the variation of δ, as well as F^2+G^2, with respect to the proton energy (15). A value of 4.8×10^{-10} barns is obtained which is in satisfactory agreement with the observed value considering the assumptions and that there are possible uncertainties in the thermal-neutron and proton resonance capture cross sections. If the extra-nuclear contribution is ignored in this calculation, a value of 2.5×10^{-10} barns is obtained for the 120-kev $C^{12}(p\gamma)$ cross section.

We have assumed that the radiation at 120-kev proton energy is due entirely to the s-wave interaction. The tails of the other known $C^{12}(p\gamma)$ resonances should not contribute significantly to this cross section.

---

*is possible in $Li^7(n\gamma)$. The reduced width of the ground state of Li^8, which enters into an exact calculation of the extra-nuclear contribution of the matrix element, is not known, but if it is assumed to be the same as the reduced width for the p-wave resonance which Adair finds at $E_n = 0.27$ Mev, then it is possible to account for this large cross section. See Appendix E.

APPENDIX

A. ON THE DETERMINATION OF REDUCED WIDTHS FROM THE ONE-LEVEL DISPERSION FORMULA

A common approximation used in applying the one-level nuclear dispersion formula to the determination of reduced level widths may be unjustified in the case of broad levels, which are numerous in light nuclei.

The one-level dispersion formula as given by Equation (57) of the paper of Wigner and Eisenbud[13] for the λ th energy level is

$$\sigma^{ss'} = \frac{\pi}{(2j_s+1)k_s^2} \sum_{\ell\ell'} \frac{(2J+1)\,\Gamma_{\lambda s\ell}\,\Gamma_{\lambda s'\ell'}}{(E_\lambda + \Delta_\lambda - E)^2 + \frac{1}{4}\Gamma_\lambda^2} \quad , \tag{20}$$

and according to Equations (58a) and (58b), in their notation,

$$\tfrac{1}{2}\Gamma_{\lambda s\ell} = (B\gamma_{\lambda s\ell})^2/(1+C_{s\ell}^2) \quad , \quad \Gamma_\lambda = \sum_{s\ell} \Gamma_{\lambda s\ell} \; ;$$

$$\Delta_\lambda = \sum_{\ell} \Delta_{\lambda s\ell} \quad ; \quad \Delta_{\lambda s\ell} = \tfrac{1}{2} C_{s\ell}\,\Gamma_{\lambda s\ell} \; ;$$

ℓ is the relative orbital momentum of the pair of particles s ; B and C are related to the values and derivatives of the extra-nuclear wave functions at the nuclear radius R_s . The common approximation in applying these formulas to the determination of reduced level widths, $\gamma_{\lambda s\ell}^2$, is to neglect the variation of the level shift, Δ_λ , with respect to the energy of the incident particle with the result that Γ_λ is interpreted as the observed level width. It is not hard to calculate this variation, and it will be shown to be important in some cases. In the notation of YWB the regular solution to the wave equation in the region external to the nucleus is F(x) and the irregular solution is G(x), the argument x being equal to kr; then

$$\Delta_{\lambda s\ell} = -(\gamma_{\lambda s\ell}^2/R_s)(\mathcal{S}_{s\ell} + \ell),$$

where

$$\mathcal{S}_{s\ell} = \left[d\ln (F_{s\ell}^2 + G_{s\ell}^2)^{1/2}/d\ln x \right]_{x=kR_s} \tag{21}$$

By expanding Δ_λ linearly with respect to energy about the resonance, usually a good approximation, the one-level formula may be written as

$$\sigma^{ss'} = \frac{\pi}{(2j_s+1)k_s^2} \sum_{\ell\ell'} \frac{(2J+1)\,\Gamma'_{\lambda s\ell}\,\Gamma'_{\lambda s'\ell'}}{(E-E_r)^2 + \frac{1}{4}\Gamma_\lambda'^2} \tag{22}$$

where the primed widths, which may be called the observed widths, are

$$\Gamma'_{\lambda s\ell} = \Gamma_{\lambda s\ell}\left[1 + \sum_{s\ell}{}' (\gamma_{\lambda s\ell}^2/R_s)(d\mathcal{S}_{s\ell}/dE)_{E=E_r}\right]^{-1} ; \tag{23}$$

E_r is the observed resonance energy and satisfies the equation

$$E_\lambda + \Delta_\lambda(E_r) - E_r = 0 . \qquad (24)$$

The same consideration applies to the dispersion theory of Feshbach, Peaslee, and Weisskopf[14]. All of the Γ_λ's in expressions (42) and (43) of FPW should be primed; in the notation of their paper, with the exception of φ which is defined in Equation (21) above and with F^2+G^2 now equal to the $|v|^2$ of their paper, we have

$$\Gamma_n' = -(2k/|v|^2)\left[(df_0/dE)-(d\varphi/dE)\right]^{-1}_{E=E_r}, \quad \Gamma_a' = -2k\left[(df_0/dE)-(d\varphi/dE)\right]^{-1}_{E=E_r}; \qquad (25)$$

f_0/R is the real part of the logarithmic derivative of the wave function at the nuclear surface. The unprimed Γ_λ of expressions (41) and (12) remain unchanged.

In applying the one-level dispersion theory at energies considerably off resonance, formulas (20) above or (38) and (39) of FPW should be used rather than the more approximate expression (22); that is, f_0 may be approximately a linear function of E (basic assumption of the one-level formula) over a wider range of energies than φ.

In the case of s-wave neutron reactions φ is zero so that there is no correction. For higher partial waves $d\varphi/dE$ can be calculated from the penetrability factors $|v|^2$ given by Equations (45a) of FPW; in the case of p neutrons $Edg/dE = (kR)^2\left[1+(kR)^2\right]^{-2}$. For example, if the resonance at 1.2 Mev in the scattering of neutrons by He^4 is p-wave, then $d\varphi/dE = .16\ \text{Mev}^{-1}$. Supposing $\gamma^2 = \hbar^2/MR$, R being taken as 2.5×10^{-13} cm, then the observed width at resonance would be $\Gamma' = .76$ Mev. Were γ^2 infinite, the observed width would be only 1.2 Mev.

An exact criterion for applying this correction cannot be given. It is probably not negligible for resonances for which $\gamma^2 \gtrsim \hbar^2/10MR$ (s-wave neutron resonances being excepted).

B. DESCRIPTIONS OF REDUCED WIDTHS OF ENERGY LEVELS

Reduced widths of nuclear energy levels have been described in the literature in a variety of different ways. The relations between them are given here. The nuclear radius R is in units of 10^{-13} cm, M is the reduced mass, and A_r is the reduced mass number.

1. Wigner and Eisenbud[13] introduce the quantity γ^2 which is described in Section III. In terms of the dimensionless quantity θ^2,

$$\gamma^2 = (20.7\,\theta^2/A_r R)\times 10^{-13}\ \text{Mev}\cdot\text{cm}. \qquad (26)$$

2. In terms of the quantity $(\Gamma/\sqrt{E}\,P)$, which Christy and Latter[39] call the width-without-barrier at 1 Mev,

$$\theta^2 = 0.110\,R\,(\Gamma/\sqrt{E}\,P)\ ,\quad P = 1/(F^2+G^2)_{\rho=R}, \qquad (27)$$

where Γ is the center-of-mass level width (corrected for the variation of the level shift with respect to energy), E is the bombarding energy in Mev as measured in the laboratory. The quantity $\sqrt{E}\,P$ is plotted in their paper.

3. The reciprocal of θ^2 is equal to the number of times that a classical particle of velocity V within the nucleus must traverse the nucleus before getting out. From (3) and (4)

$$\theta^2 = \Gamma R/\hbar v P \qquad (28)$$

where $\Gamma = -2\chi P(df_0/dE)^{-1}$, $\chi = kR$, v is the velocity of the incident particle, and the relation between Γ and the observed width Γ' is given by (23). In addition to the combined Coulomb and centrifugal-force field barrier factor P, there is at the nuclear surface an effective barrier, $P' = 4vV/(v+V)^2 \approx 4v/V$, due to the reflection at the potential discontinuity there[35]. It is this barrier factor P' that is responsible for the well-known velocity proportionality of level widths. The ratio of the time that is required to form within the nucleus the particle that is to be emitted, $\hbar PP'/\Gamma$, to the time that it takes for a classical particle of velocity V to traverse a distance 4R is then

$$(\hbar PP'/\Gamma)/(4R/V) \approx 1/\theta^2. \qquad (29)$$

4. According to FPW the relation between Γ and an effective spacing D^* between levels of the same character is

$$\Gamma = (2/\pi)(v/V)\, P D^*. \qquad (30)$$

Thus, the relation between D^* and the reduced width is

$$D^* = 310\beta\theta^2/R \ \text{MEV}, \ \beta = V/c. \qquad (31)$$

C. EXTRA-NUCLEAR WAVE FUNCTIONS FOR BOUND CHARGED PARTICLES

The wave equation for r times the radial part of the wave function of a negative-energy charged particle in a Coulomb field with orbital momentum l is

$$\frac{d^2G}{dx^2} - \left\{1 + \frac{2\eta}{x} + \frac{l(l+1)}{x^2}\right\} G = 0,$$

where

$$x = kr, \quad k = (2MB/\hbar^2)^{1/2}, \quad \eta = zz'e^2M/k\hbar^2; \qquad (32)$$

B is the binding energy, M is the reduced mass. With the substitutions $z = 2x$, $\mu = l + \frac{1}{2}$, $\kappa = -\eta$ Equation (32) can be recognized as Whittaker's equation for $W_{\kappa,\mu}(z)$ [27], viz.

$$\frac{d^2W}{dz^2} + \left\{-\frac{1}{4} + \frac{\kappa}{z} + \frac{\frac{1}{4}-\mu^2}{z^2}\right\} W = 0. \qquad (33)$$

The solution which vanishes at infinity can be expressed as [27]

$$W_{\kappa,\mu}(z) = \frac{z^{\kappa} e^{-\frac{z}{2}}}{\Gamma(\mu+\frac{1}{2}-\kappa)} \int_0^{\infty} t^{\mu-\kappa-\frac{1}{2}} e^{-t} \left(1+\frac{t}{z}\right)^{\mu+\kappa-\frac{1}{2}} dt \qquad (34)$$

or

$$W_{\kappa,\mu}(z) = \frac{(-1)^{2\mu} z^{\mu+\frac{1}{2}} e^{-\frac{z}{2}}}{\Gamma(\frac{1}{2}-\kappa-\mu)\Gamma(\frac{1}{2}-\kappa+\mu)} \left\{ \sum_{n=0}^{\infty} \frac{\Gamma(\mu+\frac{1}{2}+n-\kappa)}{n!\,(2\mu+n)!} z^n \right.$$

$$\cdot \left[\psi(n+1) + \psi(n+1+2\mu) - \psi(n+\tfrac{1}{2}+\mu-\kappa) - \ln z\right] \qquad (35)$$

$$\left. + (-z)^{-2\mu} \sum_{n=0}^{2\mu-1} \frac{\Gamma(2\mu-n)\,\Gamma(\frac{1}{2}+n-\mu-\kappa)}{n!} (-z)^n \right\}$$

where

$$\psi = d\ln\Gamma(x)/dx.$$

For obtaining accurate logarithmic derivatives at the nuclear surface it was expedient to use (35) together with the relation (9); for obtaining $W_{K,M}^{(2)}$ as a function of r, which was required in (14) for the radiation calculations, it was simplest to use (34). In view of the difficulty in evaluating (35), it is worthwhile to investigate the approximate WKB methods.

The applicability of the WKB method to the positive-energy solutions is discussed in detail by YWB. The irregular (at the origin) function G of their paper is the solution which vanishes at infinity in the negative-energy case. Thus

$$G = Q^{-\frac{1}{2}} \exp\left\{ \int_x^{x_0} Q(x')\, dx' \right\} \qquad (36)$$

where

$$Q = \left[\frac{(\ell+\frac{1}{2})^2}{x^2} + \frac{2\eta}{x} \pm 1 \right]^{\frac{1}{2}} ;$$

x_0 is an arbitrary constant, which is conveniently taken as the solution of the equation Q = 0 (the classical turning point) in the positive-energy case; the upper sign in Q and in the expression below applies to the negative-energy solutions and the lower sign to the positive-energy solutions. The quantity f is given directly from (36) as

$$f \equiv x\,(dG/dx)/G = \frac{1}{2} - \frac{x\eta \pm x^2}{2(xQ)^2} - xQ . \qquad (37)$$

Table IV gives the exact values of f for the case $\eta = .653$, $\ell = 1$, $B = 1.95$ Mev ; the approximate values from (37) with either $(\ell+\frac{1}{2})^2$ or $\ell(\ell+1)$ in the expression (36) for Q are also listed for comparison. The WKB - $(\ell+\frac{1}{2})^2$ approximation appears to be good and better than the WKB - $\ell(\ell+1)$ approximation in accord with the findings of YWB for positive energies. For the case $\eta = 0$ (uncharged particles) and $\ell = 1$, the difference between the exact values of f from (7) and the approximate values from (37) are plotted in Figure (4); again the WKB- $(\ell+\frac{1}{2})^2$ method is superior to the WKB - $\ell(\ell+1)$ method.

If it is necessary to use the WKB method at all for a level shift calculation, it is important to consistently use it throughout the calculation. For instance,

it is apparent from Table IV and Figure (4) that it is accurate to use the WKB-$(\ell+\frac{1}{2})^2$ method for calculating the difference of f for the N^{13} and C^{13} ground states, but it would be less accurate to use the simpler exact expression (7) for f of C^{13} together with the WKB-$(\ell+\frac{1}{2})^2$ method for f of N^{13}.

TABLE IV

$f = x(dG/dx)/G$ for the odd proton of the ground state of N^{13}.

R x 10^{-13} cm	Exact- Eq. (35)	WKB- $(\ell+\frac{1}{2})^2$	WKB- $\ell(\ell+1)$
3.33	-1.821	-1.809	-1.750
2.34	-1.555	-1.534	-1.472

D. DERIVATION OF THE DISPERSION FORMULA FOR THE CASE OF WEAK ABSORPTION

When there is only weak absorption, such as radiative, it is possible to give a derivation of the dispersion formula in which it is easy to see the nature of the assumptions involved.

Wigner's "first assumption"[36] is that over a limited energy range the shape of the wave function within the nucleus is energy independent though its amplitude will be proportional to the value of the wave function at the nuclear surface. An incident partial wave function for ℓ-wave which is normalized to unit flux, is[40]

$$\psi_\ell = (4\pi/v)^{1/2}(2\ell+1)^{1/2}[(G\sin\delta + F\cos\delta)/kr]Y_\ell^0(\theta,\phi). \quad (38)$$

From (39) we obtain the quantity f at the nuclear surface R, viz.,

$$f = x\,\frac{(dG/dx) + (dF/dx)\cot\delta}{G + F\cot\delta}\,, \quad x = kR\,. \quad (39)$$

Now it is merely assumed that the radiative absorption cross section is proportional to the square of the amplitude of the wave function (38) at the nuclear surface (and, therefore, also inside); that is,

$$\sigma_a \sim \phi^2(R) \quad (40)$$

where $\phi(r)$ is the radial part of the wave function. By means of (39) the phase shift δ can be replaced by f in (40). After some algebra, in

which the Wronskian relation $\left(G\frac{dF}{dx} - F\frac{dG}{dx} = 1\right)$ is used, we obtain the dispersion formula as it is given in Equation (38) of FPW except that the radiative absorption term in the denominator is missing; thus,

$$\sigma_a \sim \frac{(2l+1)}{k^2} \frac{\chi P}{(\chi P)^2 + (f-\delta)^2}, \quad \chi = kR, \tag{41}$$

$$P = (1/F^2+G^2), \quad \delta = [d\ln(F^2+G^2)^{1/2}/d\ln\chi]_{\chi=kR}.$$

The derivation of the one-level dispersion formula follows by assuming constancy of the reduced scattering width θ^2, or from (3), constancy of df/dE as in FPW. From (1) it is apparent that the assumption of constancy of θ^2 is equivalent to the "first assumption" above.

According to (41) exact resonance (maximum absorption) occurs when $f = \delta$ or, from (39), $\cot\delta = F/G$ which, evidently from (38), is the phase shift corresponding to $\varphi^2_{max}(R)$. Since F is not zero, the resonance will not occur at the energy corresponding to $\delta = \pi/2$ for which $f = \chi(dG/d\chi)/G$. The difference,

$$f_{res} - f_{\delta=\pi/2} = \chi F/G(F^2+G^2) \approx \chi F/G^3 \ (\text{if } G \gg F). \tag{42}$$

The energy shift corresponding to this difference is

$$\Delta E = E_{res.} - E_{\delta=\pi/2} \approx \frac{f_{res} - f_{\delta=\pi/2}}{(df/dE)_{reo.}} \approx -E_p\left(F\theta^2_{res.}/\chi G^3\right) \tag{43}$$

where E_p is the incident proton energy.

The C^{12} + p gamma-ray resonance is reported[2] at 0.456-Mev proton energy whereas the $\pi/2$ phase shift occurs at 0.475 Mev in the experiment on the elastic scattering of the protons[4]. For a large nuclear radius, $R = 7 \times 10^{-13}$ cm, Equation (43) gives $\Delta E \approx -3$ kev which shows that (43) is in the right direction but much too small to account for the observed 19-kev difference.

E. RADIATION CALCULATIONS

1. Magnetic Dipole - $C^{12}(p\,\gamma)N^{13}$

It is possible to calculate the radiative cross section for a single particle $^2P_{3/2} \rightarrow {}^2P_{1/2}$ magnetic-dipole transition if it is assumed that the radial

parts of the initial and final state wave functions are identical to within a multiplicative constant which can be determined. In Section V some evidence was given for the 3.52-Mev level of N^{13} being the $^2P_{3/2}$ member of ^2P term of which the ground state is the $^2P_{1/2}$ level; if this is the case, this assumption would be a reasonable one.

According to Equation (5[4]13) of Condon and Shortley[4] the magnetic-dipole transition probability from the initial state i to the final ground state g is given by

$$\tau(i,g) = \frac{1}{2J_i+1}\,\frac{64\pi^4\nu^3}{3hc^3}\sum_{m_i,m_g}|(i|\bar{M}|g)|^2 \qquad (44)$$

where $|(i|\bar{M}|g)|^2 = |(i|M_x|g)|^2 + |(i|M_y|g)|^2 + |(i|M_z|g)|^2$

$\bar{M} = (e/2Mc)(g_l\bar{L} + g_s\bar{S})$,

g_l, g_s = g-factors for orbital and spin motion,

$(e\hbar/2Mc)$ = nuclear magneton,

m_i, m_g = J-component substates of the initial and final states.

The matrix element of the magnetic-dipole moment can be simplified if we use the relation $\bar{J} = \bar{L} + \bar{S}$; then $\bar{M} = (e/2Mc)[g_l\bar{J} + (g_s - g_l)\bar{S}]$.

The transition matrix elements for J are zero, so we simply use

$$\bar{M} = (e/2Mc)(g_s - g_l)\bar{S}\,. \qquad (45)$$

With an incident wave function normalized to unit flux,

$$\psi_i = \nu^{-\frac{1}{2}} e^{ikz}$$

the transition probability becomes equal to the radiative cross section. A partial wave function so normalized and which includes incident and scattered parts is given by (38). At exact resonance $\cot\delta = (F/G)_{r=R}$ so that at the nuclear radius, r = R,

$$\psi_i = (u_i/R)\bar{Y}_l^0 = (4\pi/\nu)^{\frac{1}{2}}(2l+1)^{\frac{1}{2}}[(F^2+G^2)^{\frac{1}{2}}/kR]\,\bar{Y}_l^0(\theta,\varphi). \qquad (46)$$

The radiative absorption isweak so that the total reaction width is very nearly equal to the observed proton width, Γ' ; at exact resonance the observed radiative width, Γ_γ' , is given by the Breit-Wigner formula as

$$\omega \Gamma_\gamma' = \sigma_\gamma k^2 \Gamma'/4\pi \qquad (47)$$

where ω is the statistical factor.

In order to take into account the polarization of the incident beam, $l_z = 0$ and $S_z = \pm \frac{1}{2}\hbar$, the transition probability must be multiplied by a factor which gives the fractional content in the incident beam of the compound nucleus total angular momentum. This factor can be obtained from Table 1[3] of CS; it is

$$\frac{l + \frac{1}{2} \pm \frac{1}{2}}{(2l+1)} , \qquad (48)$$

the upper sign applies if $J = l + \frac{1}{2}$ and the lower sign if $J = l - \frac{1}{2}$.

When (45) and (46) are substituted into (44), there occur angular, spin, and radial integrations. Let $u_i(r)$ and $u_g(r)$ be r times the radial part of the wave functions, the angular and spin parts being normalized to unity. The angular and spin part can be evaluated by means of the formulas of CS; for a $^2p_{3/2} \rightarrow {}^2p_{1/2}$ transition it is $\frac{1}{3}(g_s - g_\ell)^2 (e\hbar/2Mc)^2$. The radial part can only be evaluated if we know something about u_i and u_g. We assume that $u_g = \gamma u_i$, $r < R$ where γ is a constant which can be determined. For the sake of simplicity we also assume $u_g = \gamma u_i$, $r > R$. It is not necessary to treat accurately the extra-nuclear wave functions as their contribution to the radial integration is only a few percent.

Let us write:

$$\begin{aligned} u_g &= \gamma u_i(R)\, u(r), \\ u_i &= u_i(R)\, u(r), \end{aligned} \qquad (49)$$

so that $u(R) = 1$.

The radial integration is

$$\gamma u_i^2(R) \left[\int_0^R u^2(r)\, dr + \int_R^\infty u^2(r)\, dr \right],$$

and by (1) (if we neglect other modes of decomposition in the external region) this becomes

$$\gamma u_i^2(R) R\theta^{-2} \left[1 + (\theta^2/R) \int_R^\infty u^2(r)\, dr \right] \qquad (50)$$

where $\theta^2 = \theta_i^2 = \theta_g^2$ on the above assumption (49).

The normalization factor for the square of the ground-state wave function (with the same assumption as in (50)) is the reciprocal of

$$r^2 u_i^2(R) R\theta^{-2}\left[1 + (\theta^2/R)\int_R^\infty u^2(r)\,dr\right] \qquad (51)$$

The ratio of the square of (50) to the normalization factor (51) enters into (44); it is

$$u_i^2(R) R\theta^{-2}\left[1 + (\theta^2/R)\int_R^\infty u^2(r)\,dr\right]. \qquad (52)$$

Using (28) for the θ^{-2} factor of (52) and (46) for $u_i^2(R)$, expression (52) becomes

$$4\pi(2\ell+1)(\hbar/pk^2)\left[1 + (\theta^2/R)\int_R^\infty u^2(r)\,dr\right]. \qquad (53)$$

Substituting (53), (48), (44) into (47) we obtain

$$\omega\Gamma_\gamma' = \frac{2}{9}\left(\frac{h\nu}{m_0c^2}\right)^3\left(\frac{m_0}{M}\right)^2\alpha\left(\frac{\Gamma'}{\Gamma}\right)\left[1+(\theta^2/R)\int_R^\infty u^2\,dr\right](g_s-g_\ell)^2 m_0c^2 \qquad (54)$$

where $\alpha = e^2/\hbar c$, m_0 is the electron mass. With the values $h\nu = 3.52$ Mev, $g_s = 5.58$, $g_\ell = 0.96$ (reduced from unity by reduced-mass considerations), $\theta^2 = 0.167$ for the p-wave resonance at 3.52 Mev, $\left[1+(\theta^2/R)\int_R^\infty u^2(r)\,dr\right] = 1.05$ as found by numerical integration using the Whittaker function (34) for $u(r)$ and $\Gamma'/\Gamma = 0.91$ from (23), we finally obtain $\omega\Gamma_\gamma' = 1.6$ ev as compared to the observed value of 1.3 ev[3].

2. Electric Dipole - Nuclear Contribution to the Matrix Element.

If the two-body model is accurate, then it should be possible to calculate the electric-dipole radiation intensity from the capture of s-wave neutrons and protons by C^{12}. Such calculations for the capture of protons by C^{12} have been made by Breit and Yost[42]; however, at the time of their paper the experimental information was inaccurate and the dispersion theory of nuclear reactions had not yet been formulated. In the following we ignore interaction or exchange effects[43].

The expression for the electric-dipole transition probability for a single-particle transition is the same as (44) for magnetic dipole except that $\bar{M}$ is replaced by $\bar{P}$,

$$\bar{P} = e C_{ed} \bar{r}$$

where $\bar{r}$ is the relative coordinate position vector and C_{ed} is the reduced charge number for electric-dipole emission. The effective charge eC_{ed} is determined thus. Let eZ_1, A_1, x_1 and eZ_2, A_2, x_2 be the charges, mass numbers, and coordinate positions as measured from the center of mass of the two particles. Then the electric-dipole moment is

$$P_x = e(Z_1 x_1 + Z_2 x_2).$$

By substituting into this expression the center-of-mass condition,

$$x_1 A_1 + x_2 A_2 = 0$$

and the relative coordinate, $x = x_1 - x_2$, we obtain

$$P_x = ex\left(\frac{Z_2 A_1 - A_2 Z_1}{A_1 + A_2}\right) = ex\, C_{ed}$$

and similarly for the y and z coordinates. For C^{12}(p γ) and C^{12}(n γ), C_{ed} = 6/13; this shows that the electric-dipole moment is considerably reduced in the relative coordinate system as pointed out by Bethe[44].

From (44) we obtain the nuclear contribution to the radiative cross section for s-wave capture,

$$\sigma_\gamma(i,g) = \frac{4}{3}\left(\frac{h\nu}{m_0c^2}\right)^3 \alpha^4 (c/r_0^3)\, \tilde{F}\, C_{ed}^2 \left|\int_0^R u_i\, r\, u_g\, dr\right|^2, \quad r_0 = e^2/m_0c^2; \tag{55}$$

the ground-state wave function u_g is normalized radially, and the angular integration factor $\tilde{F}$ can be obtained from CS for a single-particle transition. For $^2S_{1/2} \longrightarrow {}^2P_{1/2}$, $\tilde{F}$ = 1/3; for $^2S_{1/2} \longrightarrow {}^2P_{3/2}$, $\tilde{F}$ = 2/3. A convenient dimensionless measure of the radial moment of the radiating system is a quantity D which is defined by the relation

$$\theta_i^2 \left|\int_0^R u_i\, r\, u_g\, dr\right|^2 / R\,|u_i(R)|^2 = (DR)^2; \tag{56}$$

according to (1) the inclusion of the factor θ_i^2 in (56) makes D independent of the initial-state reduced width. Substituting (56) into (55) and using (46) with ℓ = 0 for $u_i^2(R)$, we obtain

$$\tilde{\sigma}_\gamma = \frac{4}{3}\left(\frac{h\nu}{m_0c^2}\right)^3 \alpha^4 \left(\frac{c}{v}\right)\left(\frac{R}{r_0}\right)^3 \tilde{F}\, C_{ed}^2 \left(\frac{4\pi R^2}{\theta_i^2 \chi_0^2}\right) \psi^2 D^2, \qquad (57)$$

where $\psi = \cos\delta\, F(R) + \sin\delta\, G(R)$ and $\chi_0 = kR$.

3. Electric Dipole - Extra-Nuclear Contribution to the Matrix Element

The reduced widths of the energy levels of the light nuclei are rather large so that the extra-nuclear contribution to the matrix element of the electric-dipole transition moment may be significant.

The electric-dipole radiative cross section is given by (55) with the radial integration running from R to infinity. In the case of capture of thermal neutrons the initial state wave function is

$$u_i(r) = (4\pi/v)^{\frac{1}{2}} [1 - (r/a)] \sin\delta/k \,, \quad r > R, \qquad (58)$$

where a is the zero-energy scattering length, and the phase shift is given in terms of the zero-energy scattering cross section by

$$\sigma_{sc} = 4\pi \sin^2\delta / k^2 .$$

The extra-nuclear part of a p-orbital ground-state wave function for the odd neutron (normalized to unit amplitude at R) is

$$u_g(r) = \left(\frac{\chi_0 e^{\chi_0}}{1+\chi_0}\right)\left(\frac{1+\chi}{\chi}\right) e^{-\chi},$$

$$\chi_0 = k_g R \,, \quad k_g = \left[2M(E_o^n - E_g^n)/\hbar^2\right]^{\frac{1}{2}}. \qquad (59)$$

The normalization factor (18) is then (neglecting in the external region all modes of decomposition except "core + n")

$$\frac{R}{N} = \theta_g^2 \left[1 + \theta_g^2 \frac{(\chi_0+2)}{2(\chi_0+1)^2}\right]^{-1}. \qquad (60)$$

After evaluating the radial integral we obtain the result

$$\sigma_\gamma(i,g) = \frac{4}{3}\left(\frac{h\nu}{m_0c^2}\right)^3 \alpha^4 \left(\frac{c}{v}\right)\left(\frac{R}{r_0}\right)^3 \chi_0^{-4}\, \tilde{F}\, C_{ed}^2\, \sigma_{sc} \left(\frac{R}{N}\right) S^2 \qquad (61)$$

where

$$S = \left(\frac{\chi_0}{1+\chi_0}\right)\left[(2+\chi_0) - \frac{(3+3\chi_0+\chi_0^2)}{(a/R)\,\chi_0}\right]. \qquad (62)$$

$Li^7(n\,\gamma)Li^8$

Hughes, Hall, Eggler, and Goldfarb( ) found the cross section for production of Li^8 by thermal neutrons to be 0.033 barns and noted that this value is about ten times larger than the maximum intensity expected for electric-dipole emission as given by the usual estimates in which the radiation is regarded as taking place within the nucleus. It is possible qualitatively to account for this large cross section if the extra-nuclear contribution to the matrix element of the dipole moment is taken into consideration.

There is a triplet and a quintet s-wave phase shift for $Li^7(n\,n)Li^7$. In the low-energy scattering of neutrons by Li^7, as reported by Adair[46], there appears a broad s-wave resonance at about 1-Mev with J = 2 and the "zero"-energy cross section is 1.1 barn. This cross section is about equal to the potential scattering for a radius $R = \sqrt{\sigma/4\pi} = 3 \times 10^{-13}$ cm. The effective scattering length

$$a = \frac{I}{2I+1} a_1 + \frac{I+1}{2I+1} a_2 ,$$

where I is the nuclear spin of the target nucleus and a_1, a_2 are the respective s-wave scattering lengths, has been measured by Fermi, and Marshall[47] who obtained $a = -(7/8) \times 0.59 \times 10^{-13}$ cm. Considering the requirement $|a| \leq \sqrt{\sigma/4\pi}$, this value is not consistent with the cross section measurement of Adair (extrapolating his result from about 20 kev to zero energy). Nevertheless, it appears likely from the work of Adair and Fermi-Marshall that both scattering lengths are negative and a large extra-nuclear contribution to the matrix element is to be expected since the second term in the bracket of the quantity S above has the same sign as the first.

We can attempt a qualitative calculation by assuming both scattering lengths to be negative and equal to one another which would be the case if there were no triplet-quintet splitting. Then $a = -\sqrt{\sigma/4\pi} = -2.96 \times 10^{-13}$ cm, and for θ_g^2 in (60) we use the value $\theta^2 = 0.45$ found by Adair[46]

for a p-wave Li^7 + n resonance at $E_n = 0.27$ Mev (corrected here for the variation of the level shift with respect to energy). With $R = 2.8 \times 10^{-13}$ cm the result is $S^2 = 19.9$ and $\sigma_\gamma = 80.5 \tilde{F}$ millibarns. The angular integration factor is unknown since we do not know the character of the extra-nuclear wave function for the ground state of Li^8 other than it is probably a p-state from shell structure model considerations; we would expect $\frac{1}{3} < \tilde{F} < 1$.

$C^{12}(n\,\gamma)C^{13}$

Radiation to the ground state from the capture of thermal neutrons by C^{12} is expected to be an electric-dipole $^2S_{1/2} \longrightarrow {}^2P_{1/2}$ transition in the external region. There is only one s-wave phase shift so that the scattering length is known from the "zero"-energy scattering cross section. From (61) we obtain, for $R = 3.86 \times 10^{-13}$ cm and $\tilde{F} = 1/3$ for the indicated transition, $S^2 = 0.37$ and $\sigma_\gamma = 1.36\ \theta_g^2 \times 10^{-3}$ barns. The quantity S^2 is small because the scattering length is positive and of such a value that the two terms in expression (62) are nearly equal in magnitude but opposite in sign. We will show below that $\theta_g^2 = 0.19$ so that the extra-nuclear contribution to the radiation is very small compared to the observed value of 3.5 millibarns[37].

$C^{12}(p\,\gamma)N^{13}$

In this case the ground-state extra-nuclear wave function is the Whittaker function which can be obtained by numerical integration of (34). The initial-state function is given by (38); F and G can be obtained from Breit's tables[16],[28]. For proton energies well below the s-wave resonance at 0.456 kev, $\delta \approx 0$ and one can approximate $\cos\delta = 1$; from (39)

$$G \sin\delta + F\cos\delta \approx$$

$$C_0 \left\{ \left[\frac{x\Phi_0}{\mathcal{H}_0} \left(\frac{1}{\mathcal{H}_0 \Phi_0 \left(f - \frac{\mathcal{H}_0^*}{\mathcal{H}_0}\right)} - 1 \right) \right]_{x=x_0} \mathcal{H}_0(x) + x\Phi_0(x) \right\} \qquad (63)$$

where $C_0, \Phi_0, \mathcal{H}_0, \mathcal{H}_0^*$ are the tabulated auxiliary functions of YWB for F_0 and G_0. The extra-nuclear radial integral was evaluated by numerical integration.

4. Determination of the Ground-State Reduced Width

The results of Section 2 and 3 of this Appendix on the s-wave neutron and proton radiative capture by C^{12} are listed in columns 4 and 5 of Table V; the following data was used:

$$a = 6.1 \times 10^{-13} \text{ cm}, \quad R = 3.86 \times 10^{-13} \text{ cm}, \quad \theta_i^2 = 2.0, \quad \tilde{F} = \frac{1}{3}.$$

Column 3 gives the observed cross sections.

TABLE V

Capture	Energy		σ_γ (i,g) - barns	
		Observed	Calculated-Nuclear	Calculated-Extra-nuclear
$C^{12} + p$	E_p = .456 Mev	1.2×10^{-4}	$2.94\ D^2 \times 10^{-4}$	$2.20\ \theta_g^2 \times 10^{-4}$
$C^{12} + p$	E_p = .120 Mev	$(6.1 \pm .6) \times 10^{-10}$	$7.21\ D^2 \times 10^{-10}$	$1.165\ \theta_g^2 \times 10^{-9}$
$C^{12} + n$	E_n = 1/40 ev	3.5×10^{-3}	$26.9\ D^2 \times 10^{-3}$	$1.362\ \theta_g^2 \times 10^{-3}$

The quantities θ_g^2 and D are found as the solutions to the simultaneous equations

$$3.5 = \left| (1.362\,\theta_g^2)^{\frac{1}{2}} \pm (26.9\,D^2)^{\frac{1}{2}} \right|^2$$

$$1.2 = \left| (2.20\,\theta_g^2)^{\frac{1}{2}} \pm (2.94\,D^2)^{\frac{1}{2}} \right|^2$$

The only permissible solution occurs with the + sign, and it is

$$D = 0.264, \quad \theta_g^2 = 0.19.$$

With these values the cross section for capture of 120-kev protons is predicted to be

$$\left[(1.165\theta_g^2 \times 10^{-9})^{\frac{1}{2}} + (7.21\,D^2 \times 10^{-10})^{\frac{1}{2}}\right]^2 = (1.488 + .709)^2 \times 10^{-10} = 4.8 \times 10^{-10} \text{ barns},$$

which is in reasonable agreement with the observed value. It is noteworthy that the amplitude of the extra-nuclear contribution is about twice as large as the nuclear contribution at this energy.

We have taken D and θ_i^2 to be the same at these different excitation energies; this is equivalent to Wigner's "first assumption"[36].

F. MULTIPOLARITY OF THE 3.10-MEV GAMMA-RAY OF C^{13}

The internally-formed pairs from the 3.10-Mev gamma-ray of C^{13} were first observed by Dougherty, Hornyak, Lauritsen, and Rasmussen[7] who reported the conversion coefficient to be of the order of 10^{-3} pair per gamma-quantum. We have shown in Section III that the 2.37-Mev state of N^{13} must be formed by s-wave protons incident upon C^{12} and so the radiation to the $^2p_{1/2}$ ground state would occur by electric-dipole emission; calculations of the radiation intensity in Appendix E and the observed isotropy of the gamma-radiation are consistent with this conclusion. A check on the correspondence of this level of N^{13} to the 3.10-Mev level of C^{13} would be the measure of the gamma-ray multipolarity from the internal pair formation coefficient. The measurement of IPFC hinges on the measure of the absolute gamma-ray intensity, which can be done by means of the methods developed in Part II.

A 17-mg/cm^2 carbon target was bombarded with 1.46-Mev deuterons, and the pairs and converted electrons from the reaction $C^{12}(d\,p)C^{13*}$ were observed with the beta-ray spectrometer. The absolute gamma-ray yield was measured in three ways. (1) The photoelectrons from a thin 22.4-mg/cm^2 Th converter with a geometrical factor $\cos\delta \approx .1$ were observed. The $\langle \sec\theta_o \rangle_{AV}$ factor required for Equation (50) of Part II was calculated by assuming that all of the photo-electrons are ejected at an angle of $\cos\omega = v/c$ (where v is taken as the velocity of the ejected photoelectron) with respect to the direction of the gamma-ray so that the angular distribution factor $\langle \sec\theta_o \rangle_{AV} = \left[\left(\frac{v}{c}\right)^2 - \sin^2\theta_1\right]^{-1/2}$ according to Case I, Equation (49) of Part II; the effect of scattering in the converter was estimated by means of Equation (44) of Part I. This procedure should be moderately accurate for this high gamma-ray energy; it yielded a value $\langle \sec\theta \rangle_{AV} = 1.11$. (2) The gamma-ray yield was calculated using the thin-converter Compton method described in Section 3 of Part II. Straggling in energy loss was taken into account by means of Equation (24) of Part I using Landau's distribution function. In order to avoid errors due to spurious

sources of Compton electrons such as from the source and the spectrometer baffles, the difference between the no-converter and the thin 27.2-mg/cm^2 Al converter spectrum was used to compute the absolute intensity. (3) The absolute intensity was measured by the thick-converter Compton method using a 360-mg/cm^2 aluminum strip (for which the gamma-ray attenuation is 1%). The method of computation was as described in Section 3 of Part II. The results are the following for the thick-target yield using a spectrometer resolution of 1.98% and a solid angle (as determined by the Co^{60} method described in Section 5 of Part II) of 2.2% of a sphere.

(1) Photoelectric conversion is a thin foil, 13.4×10^{-6} γ/d,

(2) Compton conversion in a thin foil, 13.3×10^{-6} γ/d,

(3) Compton conversion in a thick foil, 13.2×10^{-6} γ/d.

The absolute intensity of the gamma-radiation was also determined from the observed positron spectrum of the pairs by a comparison with the theoretical spectra calculated by Rose and Uhlenbeck for the various multipoles. The intense positron spectrum from the decay of the N^{13} produced in the accompanying reaction $C^{12}(d\ n)N^{13}$ prevented observation of all but the high-energy portion of the pair positron spectrum. The yield of internally-produced positrons was observed at $p/m_o c = 4.26$ with a statistical counting rate error of 3%; fewer counts were taken at the other points of the spectrum. The absolute yields calculated for the various multipoles are

electric dipole,	13.2×10^{-6} γ/d
electric quadrupole	20.6×10^{-6} γ/d,
magnetic dipole,	23.8×10^{-6} γ/d.

The higher multipoles have lower IPFC and so would predict even higher gamma-ray yields. It is apparent that the assignment of electric dipole to the transition is in excellent agreement with the gamma-ray intensity measurements. The good agreement is probably somewhat fortuitous; the over-all error is probably not greater than 10%. A plot of the IPFC using the Compton data for

the absolute yield is shown in Figure (5).

We need not be concerned with the angular distribution problem discussed in Section 6 of Part II, since the radiating state is almost surely spin 1/2 so that both pair and gamma-radiation distributions should be isotropic. However, we might expect a 10% error in the theoretical values for the positron distribution due to the use of the Born approximation.

G. LEVEL SHIFT OF THE FIRST EXCITED STATES OF Be^7 - Li^7 DUE TO THE DIFFERENCES OF THE EXTRA-NUCLEAR WAVE FUNCTIONS

There is a 49-kev shift of the first excited states of Li^7 and Be^7[48]. Part of this shift may be due to the differences of the extra-nuclear wave functions for the various modes of decomposition. The most loosely bound mode is $H^3 + \alpha$ in the case of Li^7 and $He^3 + \alpha$ in the case of Be^7. In order to estimate the shift due to these particular modes in the external region, it is necessary to know their probability or reduced width. There is no available information of this kind, so for an upper limit we take $\theta^2 = 2$ which corresponds roughly to a pure model of $\alpha + He^3$, or H^3, in the internal region.

The logarithmic derivatives at the nuclear surface, which we arbitrarily assume to have a radius $R = 3.4 \times 10^{-13}$ cm, can be obtained fairly accurately from the WKB-$(\ell+\frac{1}{2})^2$ approximation, Equations (36) and (37). We assume the reduced widths of the four levels in concern to be equal; according to (3) with $\theta^2 = 2$,

$$(-df/dE)^{-1} = \hbar^2/MR^2,$$

and the apparent shift of the first excited states is approximately

$$\Delta E \approx \frac{f_{Li^7}^* - f_{B\ell}^*}{(df/dE)} - \frac{f_{Li^7} - f_{Be^7}}{(df/dE)} = 0.26 - 0.27 \text{ Mev.}$$

with $\ell = 1$ for the relative orbital momentum. This shift is of the wrong sign and negliglble compared to the observed shift. Some error is expected from the WKB method, and a relatively small difference of the reduced widths for the excited and ground states could result in a significant shift.

The observed shift has been accounted for by Inglis[1]* as due in part to the differences of the electromagnetic spin-orbit interactions for the odd particles and in part to nuclear volume expansion with excitation.

---

* See also E. Feenberg, Phys. Rev. 81, 644 (1951).

H. S-WAVE PROTON AND NEUTRON INTERACTIONS WITH O^{16}

The s-wave proton and neutron interactions with O^{16} are similar to the respective interactions with C^{12}. The energy levels of F^{17} and C^{17} below 5-Mev are shown in fig. (6); the thresholds for decomposition into O^{16} n, p are obtained from the Q values of the reactions

$$O^{16} + d \rightarrow O^{17} + p + 1.920 \pm .006 \text{ (49)},$$
$$O^{16} + d \rightarrow F^{17} + n - 1.610 \pm .010 \text{ (50)}, \qquad (64)$$
$$n + p \rightarrow d + 2.225 \pm .002 \text{ (49)}, \text{ Mev.}$$

The Q value of the dn reaction is consistent with the less accurate F^{17} β^+-decay end-point determination (51). The data on the scattering of protons by O^{16} is from the work of Laubenstein et al (52). The position of the first excited state of O^{17} was found by measurement with a beta-ray spectrometer (1.9% resolution) of the electrons from a 25-mg/cm^2 thorium photoelectric converter ejected by the gamma-radiation from the bombardment of SiO_2 with deuterons; the spectrum is shown in fig. (7) together with the L-line spectrum from the 713-kev gamma-ray of B^{10}. The energy of the gamma-ray was determined to be $0.871 \pm .003$ Mev, no Doppler shift correction being made as it is not known whether or not the radiation takes place on the average before or after the recoil nucleus stops in the target material. The thick-target (SiO_2) yield from 1.36-Mev deuterons is about 6×10^{-6} γ/d as determined by the thick-converter Compton method. The measurement by Buechner et al (7) of the energy of the O^{16} (dp) O^{17} proton groups yields $0.876 \pm .009$ Mev for the level position. Further details concerning the level diagrams are given in the survey article of Hornyak et al (53).

By means of an analysis of the angular distribution of

protons from the bombardment of O^{16} with 8-Mev deuterons (54), Butler concludes that the ground state of O^{17} is a d-state* and the first excited state is an s-state (55). There is no published measurement of the ground-state spin although the weak quadrupole moment observed by Low and Townes indicates $J = \frac{1}{2}$, but they admit that $J = 3/2$ cannot be excluded (55),**. Fig. (8) is a reproduction from the survey article by Adair (11) of the O^{16} low-energy neutron scattering data. There is apparantly a non-resonant background scattering that is larger than potential scattering (~1 barn) similar to the situation with $C^{12} + n$. The most acurate slow-neutron scattering cross section is the velocity spectrometer measurement of Melkonian (57), $\sigma = 3.73 \pm .04$ barns from 1 to 500 ev., which gives a value of $a = \sqrt{\frac{\sigma}{4\pi}} = 5.45 \times 10^{-13}$ cm for the zero-energy scattering length and -3.54 for the respective value of $f_o^n = -\frac{R}{a-R}$ at a nuclear radius of 4.25×10^{-13} cm. Since $df/dE \leq 0$ and for a bound s-state $f_b^n = -\frac{[2MB/\hbar^2]^{1/2}}{R^{-1}}$ where B is the binding energy, there must be a bound s-state associated with this scattering. If it is the 0.871 level, then $f_b^n = -1.629$. The rate of variation of f^n with respect to excitation energy is approximately $(f_o^n - f_b^n)/(E_o^n - E_b^n) = -.583\ \text{Mev}^{-1}$ which corresponds to a reduced width of $\theta^2_{o-b} = 1.395$ according to (26); this reduced width is nearly the same as that obtained for $C^{12} + n$ using the same nuclear radius which indicates that a potential type of interaction is also involved with $O^{16} + n$ in an s-state. Using for the variation of f with respect to excitation energy,

$$f^n(E) = -1.629 - .583\,(E - .871), \qquad (65)$$

---

*See footnote on page 102.

** The ground-state spin of O^{17} has recently been determined to be $J = 5/2$ by Alder and Yu, Phys. Rev. 81, 1067 (1951).
See also: Geschwind, Gunther-Mohr, Townes, Bull. Am. Phys. Soc. 26-3.

and the s-wave scattering formula of FPW,

$$\sigma_{sc} = 4\pi R^2 \left(\cos x - f\frac{\sin x}{x}\right)^2/(x^2+f^2), \quad x = kR, \qquad (66)$$

the neutron scattering cross section is determined and plotted in fig. (8). The fit to the 'non-resonant' background is seen to be satisfactory.

If nn and pp nuclear forces are equal, we would expect that the quantity f(E) is the same in F^{17} at the same nuclear excitation energies provided that we have selected for R the proper nuclear radius beyond which the nuclear forces may be neglected and within which the Coulomb potential can be considered as a constant which is equal to the ground-state Coulomb energy difference for O^{17} and F^{17}. From the Q values (64) this ground state energy difference is 3.53 Mev; on the assumption of a uniform distribution of Coulomb charge throughout a volume of radius $R = r_o A^{1/3}$, this corresponds to a value $r_o = 1.52 \times 10^{-13}$ cm which is somewhat larger than the value 1.46 that best fits most of the ground-state Coulomb energy difference data of the light nuclei with $Z > 5$. This increase of r_o corresponds to a Coulomb energy diminution of about 150 kev so that we might expect an anomalous ground-state shift of this amount and the relations between the O^{17} and F^{17} excitation energies correspondingly uncertain. Nevertheless, we will simply assume the ground states to be unshifted by any of the effects mentioned in the discussion of the C^{13}-N^{13}; consequently the quantity $f^p(E)$ for F^{17} is assumed to be the same as $f^n(E)$ given by (65) for O^{17}, viz,

$$f^p(E) = -1.629 - .583\,(E - .871). \qquad (67)$$

By using this expression we can compute the s-wave scattering cross section for O^{16} + p and the expected position of the bound or virtual s-state which has not been observed.

From (39) the phase shift of the scattering is given by $\cot\delta = \frac{(xG' - fG)}{(fF - xF')}$ where the prime denotes differentiation with respect to the argument $x = k\ell$. If G is eliminated by means of the Wronskian relation, $F'G - G'F = 1$, this phase shift may be expressed in terms of Breit's tabulated auxiliary functions as

$$\cot\delta_0 = -\left\{(\Theta_0\Phi_0) + \left(f - \frac{\Phi_0^*}{\Phi_0}\right)^{-1}\right\} / C_0^2 x\, \Phi_0^2 \quad , x = kR. \tag{68}$$

If we neglect the spins of the colliding particles by considering only one phase shift for each partial wave which is scattered, the nuclear scattering amplitude is given in terms of the phase shift as (58)

$$\tilde{f}_{nuc.} = (2ik)^{-1} \sum_{\ell=0}^{\infty} (2\ell+1) \exp(2i\sigma_\ell)\left[\exp(2i\delta_\ell) - 1\right] P_\ell(\cos\theta) \tag{69}$$

where $2i\sigma_\ell = (\ell + i\eta)!/(\ell - i\eta)!$, $\eta = zz'e^2M/k\hbar^2$,

and the Coulomb scattering amplitude is

$$\tilde{f}_{coul.} = -(e^2/2mv^2)\csc^2(\theta/2)\exp\left[-2i\eta \log\sin(\theta/2) + 2i\sigma_0\right]. \tag{70}$$

The total differential scattering cross section, which is obtained by adding the above amplitudes, is given by

$$d\sigma = \left|\tilde{f}_{nuc.} + \tilde{f}_{coul.}\right|^2 d\Omega . \tag{71}$$

Only the relative Coulomb phase shift enters into (71); it may be written as (59)

$$\sigma_\ell - \sigma_0 = \sum_{s=1}^{\ell} \tan^{-1}(\eta/s). \tag{72}$$

Neglecting all but the s-wave nuclear scattering, the ratio of total to Rutherford scattering is (73)

$$\frac{\left|\tilde{f}_{nuc.} + \tilde{f}_{coul}\right|^2}{\left|\tilde{f}_{coul.}\right|^2} = 1 - 2\left|\frac{\tilde{f}_{nuc.}}{\tilde{f}_{coul}}\right| \cos\left[\delta_0 + 2\eta \log\sin(\theta/2)\right] + \left|\frac{\tilde{f}_{nuc.}}{\tilde{f}_{coul}}\right|^2.$$

The scattering of protons by oxygen has been measured by Brown and Fowler (unpublished) at two energies with a heavy particle magnetic spectrometer at 138° (laboratory). The experimental results and the cross sections calculated using (68), (67), and (73) are:

$4\pi d\sigma(lab)$ - barns

Ep(lab)	Observed	Calculated	Rutherford
.600	(4.5)	3.91	3.76
1.240	1.83	1.43	.885

The p-wave and higher phase shifts have been neglected in the above calculation since they are not known. For potential scattering from a hard sphere of radius R, the phase shift is $\cot\delta_\ell = -\left(\frac{G_\ell}{F_\ell}\right)_{kR}$, and the p-potential scattering amplitude is about 1/10 th of the s-wave amplitude at these energies and shifted about 90° in phase so that it can be neglected.

The calculation of the quantity f_b^P for the bound s-state of F^{17} is simplified by using the approximate WKB formula, eq. (37). The position of the bound state is given as the solution of the equation

$$f^P(E) = f_b^P(B)$$

where the binding energy, B = 0.615-E Mev according to fig. (6), and $f^P(E)$ is given by (67) with $R = 4.25 \times 10^{-13}$ cm. The solution to this equation is E = 0.40 Mev above the ground state. No such state in F^{17} has been observed, although it is not clear whether any experiment has been performed which could have detected it if it actually exists. Since the calculated ratio of total to Rutherford cross section at $E_p = 1.24$ Mev is below the observed value, it is probable that there is a significant ground-state level shift, and this would put the s-state at a higher excitation energy by perhaps several hundred kev.

We have plotted in figs. (9) and (10) the ratio of total to Rutherford cross section for $\theta = 138^\circ$ at the two proton energies as a function of the quantity f at a nuclear radius which we take to be $R = 4.25 \times 10^{-13}$ cm. The curves are typical portions of resonance functions with interference effects. Fig (11) is a plot of f_b^P (for $E-.615<0$) or f_ℓ^P (for $E-.615>0$) using the WKB approximation, eq. (37). From the observed cross section

of 1.83 barns at $E_p = 1.24$ Mev, one finds $f = -1.39$. Assuming a linear variation of f with $df/dE = -.583$ Mev as suggested by the s-wave neutron data, the position of the bound or resonant s-state is found as the intersection with curve $f^P_{b,r}$ of the straight line of slope -.583 which passes through the point $(f = -1.39, E = (\frac{16}{17})1.24\ Mev)$. The solution in this case is approximately E-0.615 = 0.6 Mev; no such resonant state has been found with incident protons of energy greater than .600 Mev (52), and the scattering cross section has not been studied below this energy. Actually the approximation of assuming df/dE a constant may not be very good; rather, we would expect the reduced width to be larger, and therefore $|df/dE|$ smaller, at the lower nuclear excitation energies where $|f|$ is smaller.

REFERENCES

1. D. R. Inglis, Phys. Rev. 82, 181 (1951).
2. Fowler, Lauritsen, and Lauritsen, Rev. Mod. Phys. 20,236(1948).
3. D. M. Van Patter, Phys. Rev. 76, 1264 (1949).
4. Goldhaber, Williamson, Jackson, and Laubenstein, Bull. Amer. Phys. Soc. 25-5,22 (1950).
5. J. C. Grosskreutz, Phys. Rev. 76, 482 (1949).
6. Buechner, Strait, Sperduto, and Malm, Phys. Rev. 76, 1543(1949).
7. Dougherty, Hornyak, Lauritsen, and Rasmussen, Phys. Rev.74, 712 (1948).
8. J. Rotblat, Proceedings of the Harwell Conference (1950).
9. Malm and Buechner, Phys. Rev. 81. 519 (1951).
10. Blundell and Rotblat, Phys. Rev. 81, 144 (1951).
11. Robert K. Adair, Rev. Mod. Phys. 22, 249 (1950).
12. Tollestrup, Fowler, and Lauritsen, Phys. Rev. 78, 372 (1950).
13. Wigner and Eisenbud, Phys. Rev. 72, 29 (1947), referred toas WE.
14. Feshbach, Peaslee, and Weisskopf, Phys. Rev. 71-, 145 (1948) referred to as FPW.
15. R. G. Thomas, Phys. Rev. 81, 148 (1951).
16. Bloch, Hull, Broyles, Bouricius, Freeman, and Breit, Phys. Rev. 80, 553 (1950).
17. E. P. Wigner, Amer. J. of Phys. 17, 99 (1949).
18. Blatt and Jackson, Phys. Rev. 76, 18 (1949), referred to as BJ.
19. H. A. Bethe, Phys, Rev. 76, 38 (1949).
20. D. W. Miller, Phys. Rev. 78, 806 (1950).
21. Lampi, Freier, and Williams, Phys. Rev. 80, 853 (1950), and Freier, Fulk, Lampi, and Williams, Phys. Rev. 78,508 (1950).
22. Havens and Reinwater, Phys. Rev. 75, 1296 (1949).

23. W. B. Jones, Phys. Rev. 74, 364 (1948).

24. M. G. Mayer, Phys. Rev. 78, 16 (1950).

25. Hafstad and Teller, Phys. Rev. 54,681 (1938).

26. R. G. Thomas, Phys. Rev. 81, 661 (1951).

27. Magnus and Oberhettinger, Formeln und Sätze für die Speziellen Funktionen der Mathematischen Physik,Kap. VI 2, J. Springer (1948).

28. Yost, Wheeler, and Breit, Phys. Rev. 49, 174 (1936).

29. L. W. Nordheim, Phys. Rev. 75, 1894 (1949).

30. V. F. Weisskopf, Helv. Phys. Acta. 23, 187 (1950).

31. E. Feenberg, Rev. Mod. Phys. 19,239 (1947).

32. W. E. Stephens, Phys. Rev. 57, 938 (1940).

33. R. G. Thomas, Phys. Rev. 80, 138 (1950). See Appendix F.

34. Devons and Hine, Proc. Roy. Soc. A199, 56 (1949).

35. Day and Perry Phys. Rev. 81, 662 (1951).

36. E. P. Wigner, Phys. Rev. 70, 15 (1946).

37. Way and Haines, AECD 2138 (1948).

38. Hall and Fowler, Phys. Rev. 77, 197 (1950).

39. Christy and Latter, Rev. Mod. Phys. 20, 185 (1948).

40. Mott and Massey, The Theory of Atomic Collisions, Oxford University Press (1933), Chapter III.

41. Condon and Shortley, Theory of Atomic Spectra, Cambridge University (1935).

42. Breit and Yost, Phys. Rev. 48, 203(1935).

43. A. J. F. Siegert, Phys. Rev. 52, 787 (1937).

44. H. A. Bethe, Rev. Mod. Phys. 9, 222 (1937).

45. Hughes, Hall, Eggler, and Goldfarb, Phys. Rev. 72, 646 (1947).

46. R. K. Adair, Phys. Rev. 79, 1018 (1950).

47. Fermi and Marshall, Phys. Rev. 71, 666 (1947).

48. Brown, Chao, Fowler, and Lanritsen, Phys. Rev. 78, 88 (1950). Lauritsen and Thomas, Phys. Rev. 78, 88 (1950).

49. C. W. Li, Thesis, California Institute of Technology (1951).

50. Heydenberg and Inglis, Phys. Rev. 73, 230 (1948).

51. Perez-Mendez and Lindenfeld, Phys. Rev. 80, 1097 (1950)

52. Laubenstein, Laubenstein, Mobley, and Koester, Bull. Am. Phys. Soc. 25-6, 11 (1950).

53. Hornyak, Lauritsen, Morrison, and Fowler, Rev. Mod. Phys. 22, 291 (1950).

54. Burrows, Gibson, and Rotblat, Phys. Rev. 80, 1095 (1950).

55. S. T. Butler, Phys. Rev. 80, 1095 (1950).

56. Low and Townes, Phys. Rev. 75, 529 (1949).

57. E. Melkonian, Phys. Rev. 76, 1750 (1949).

58. Jackson and Blatt, Rev. Mod. Phys. 22, 82 (1950).

59. E. R. Cohen, Thesis, California Institute of Technology (1949).

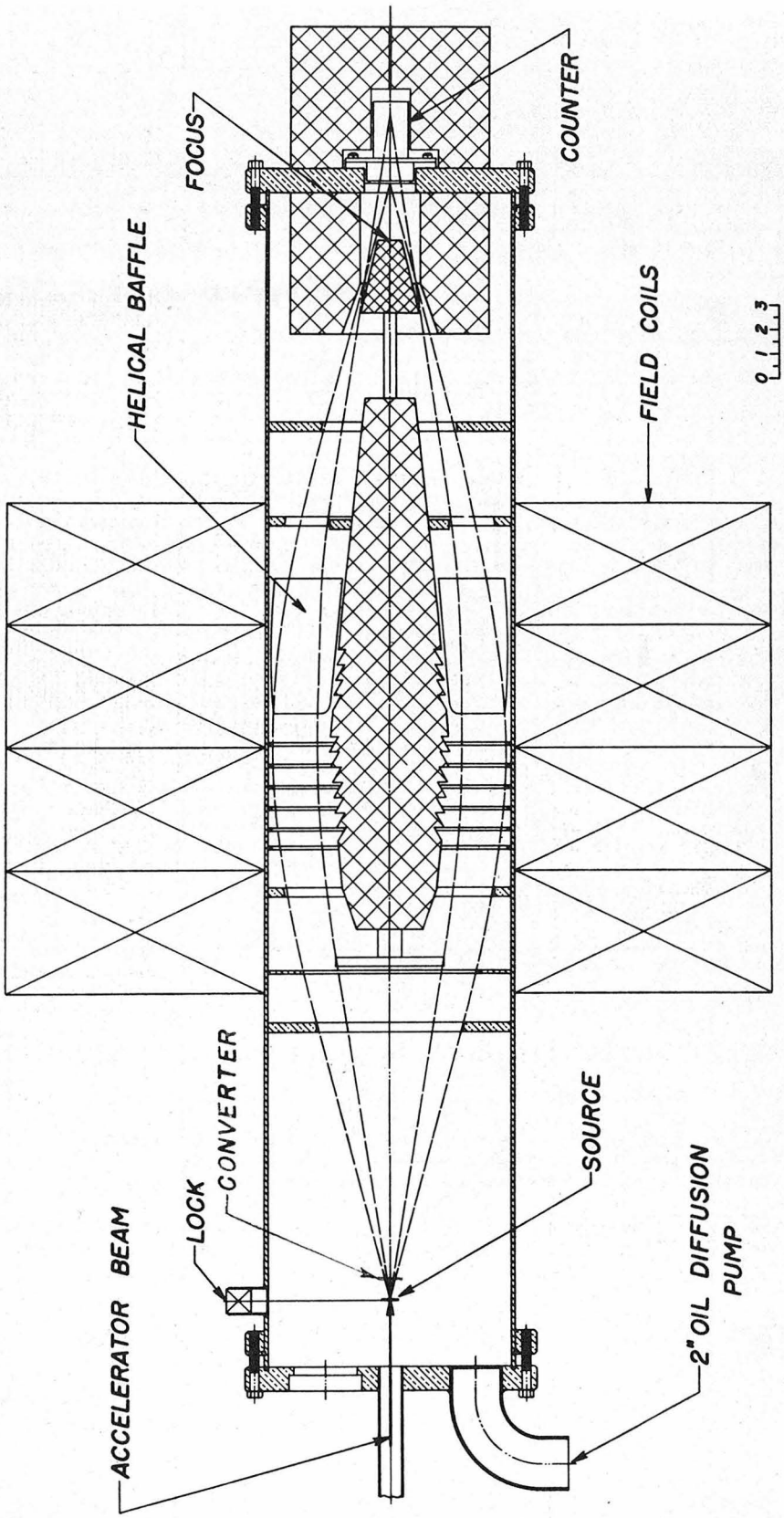
FOCUS
COUNTER
HELICAL BAFFLE
FIELD COILS
0 1 2 3
INCHES
CONVERTER
LOCK
SOURCE
ACCELERATOR BEAM
2" OIL DIFFUSION PUMP

FIG 1

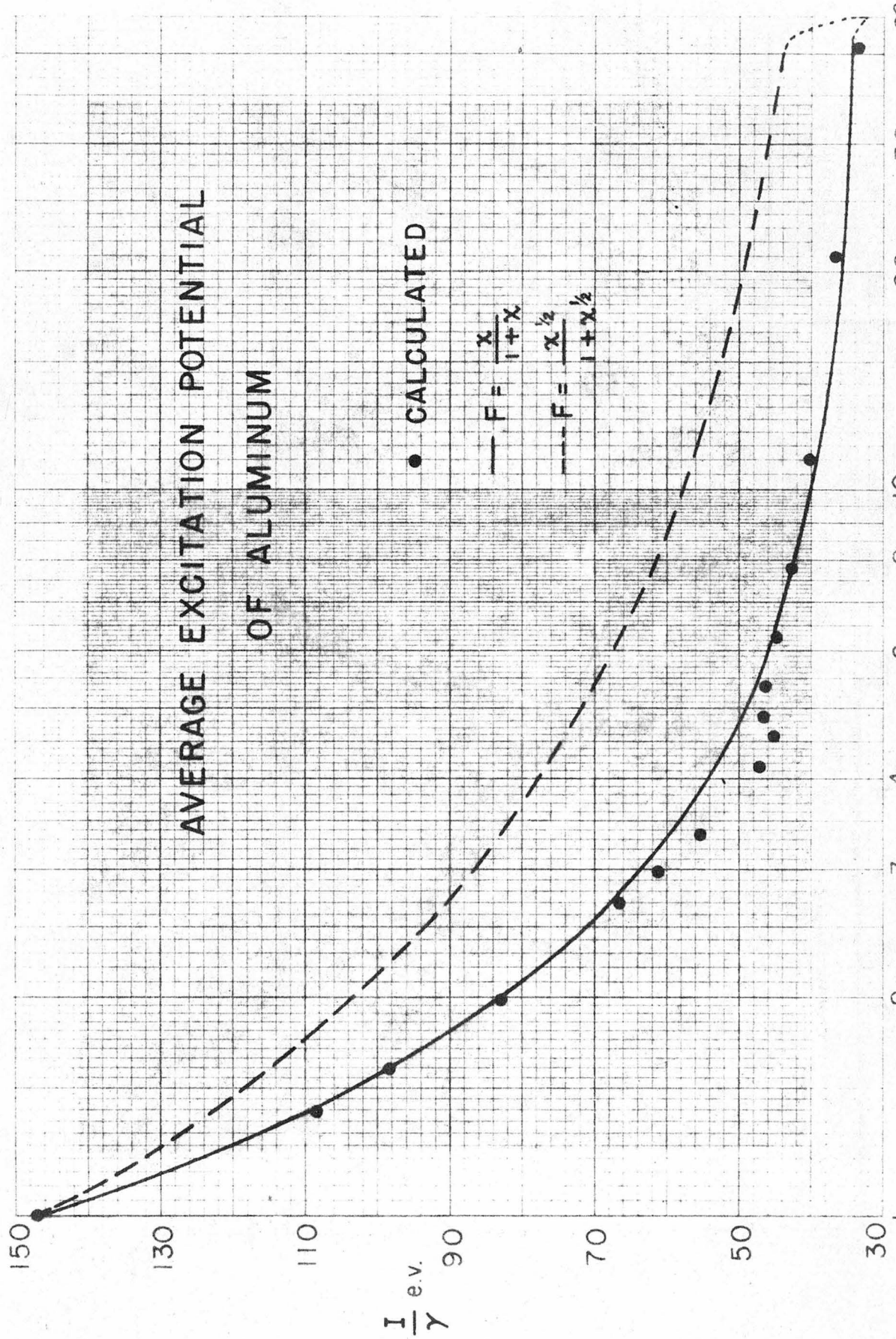
AVERAGE EXCITATION POTENTIAL
OF ALUMINUM
• CALCULATED
— $F = \frac{\chi}{1+\chi}$
--- $F = \frac{\chi^{1/2}}{1+\chi^{1/2}}$
$\frac{I}{Y}$ e.v.
150
130
110
90
70
50
30
1
2
3
4
6
8
10
20
30
∞
γ

FIG. (2)

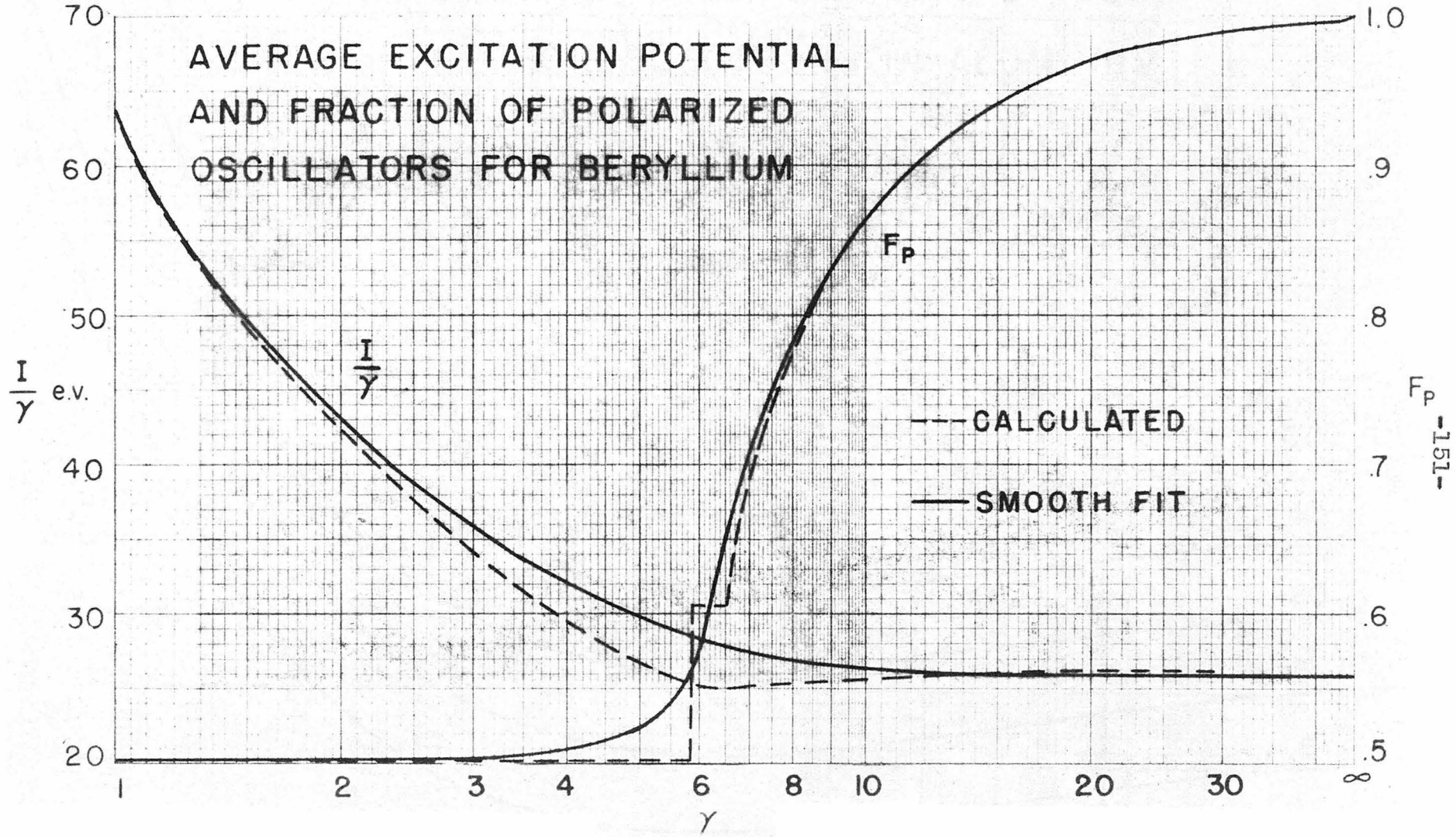
AVERAGE EXCITATION POTENTIAL
AND FRACTION OF POLARIZED
OSCILLATORS FOR BERYLLIUM
70
60
50
40
30
20
I/γ e.v.
I/γ
F_P
---CALCULATED
—SMOOTH FIT
1.0
.9
.8
.7
.6
.5
F_P
1
2
3
4
6
8
10
20
30
∞
γ

FIG. (3)

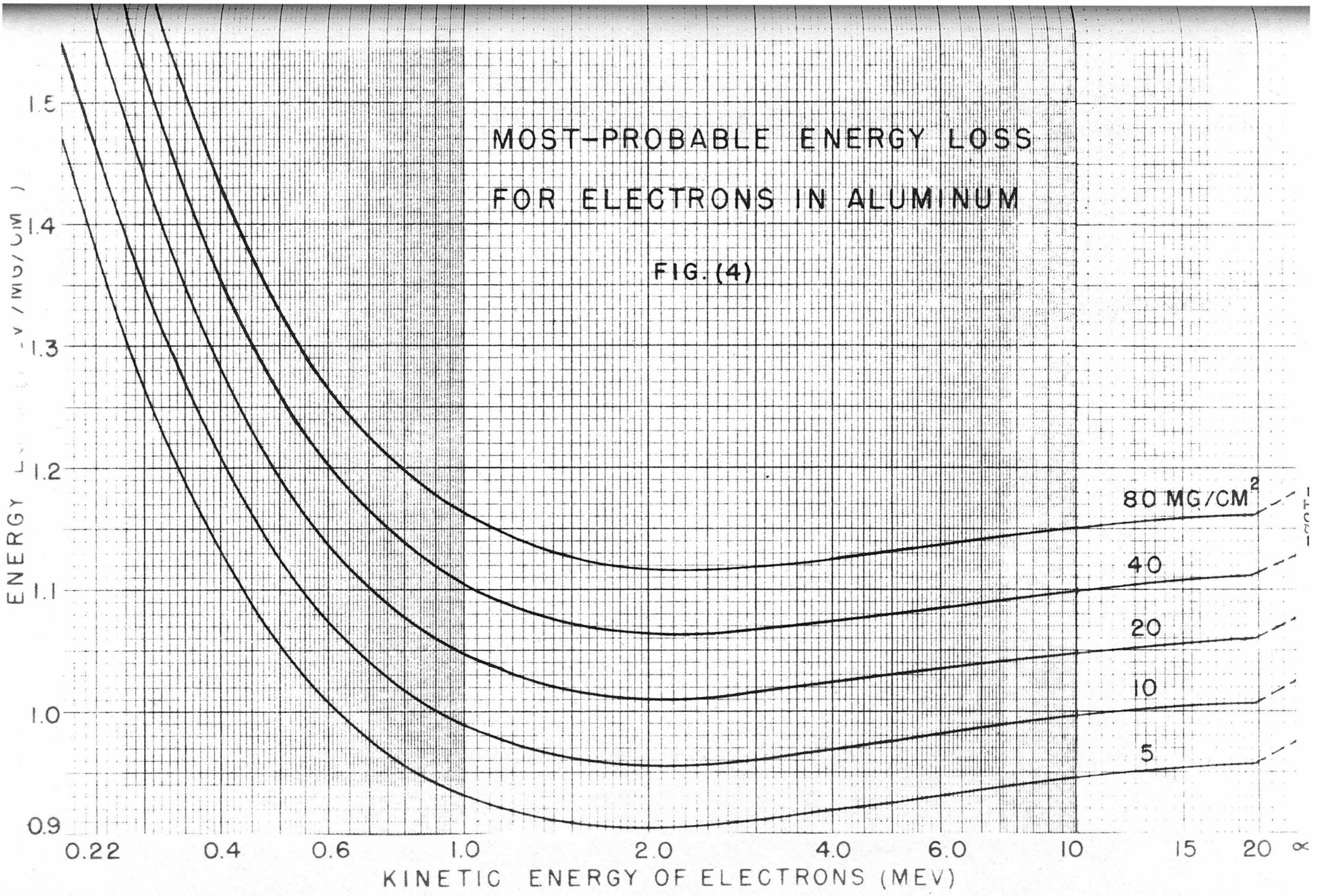
MOST-PROBABLE ENERGY LOSS
FOR ELECTRONS IN ALUMINUM
FIG. (4)
ENERGY
1.5
1.4
1.3
1.2
1.1
1.0
0.9
80 MG/CM²
40
20
10
5
0.22
0.4
0.6
1.0
2.0
4.0
6.0
10
15
20
KINETIC ENERGY OF ELECTRONS (MEV)

MOST-PROBABLE ENERGY LOSS

FOR ELECTRONS IN BERYLLIUM

FIG. (5)

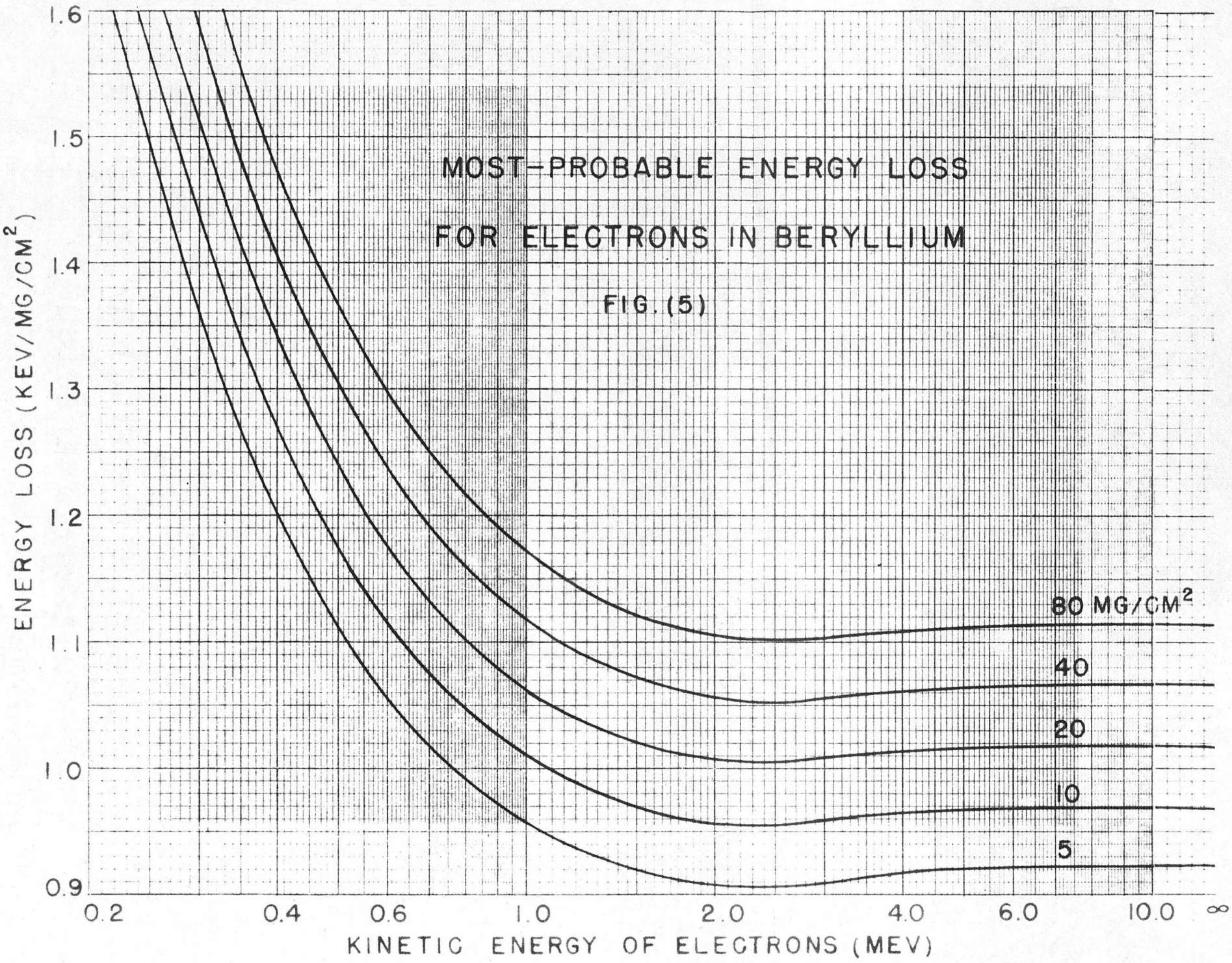

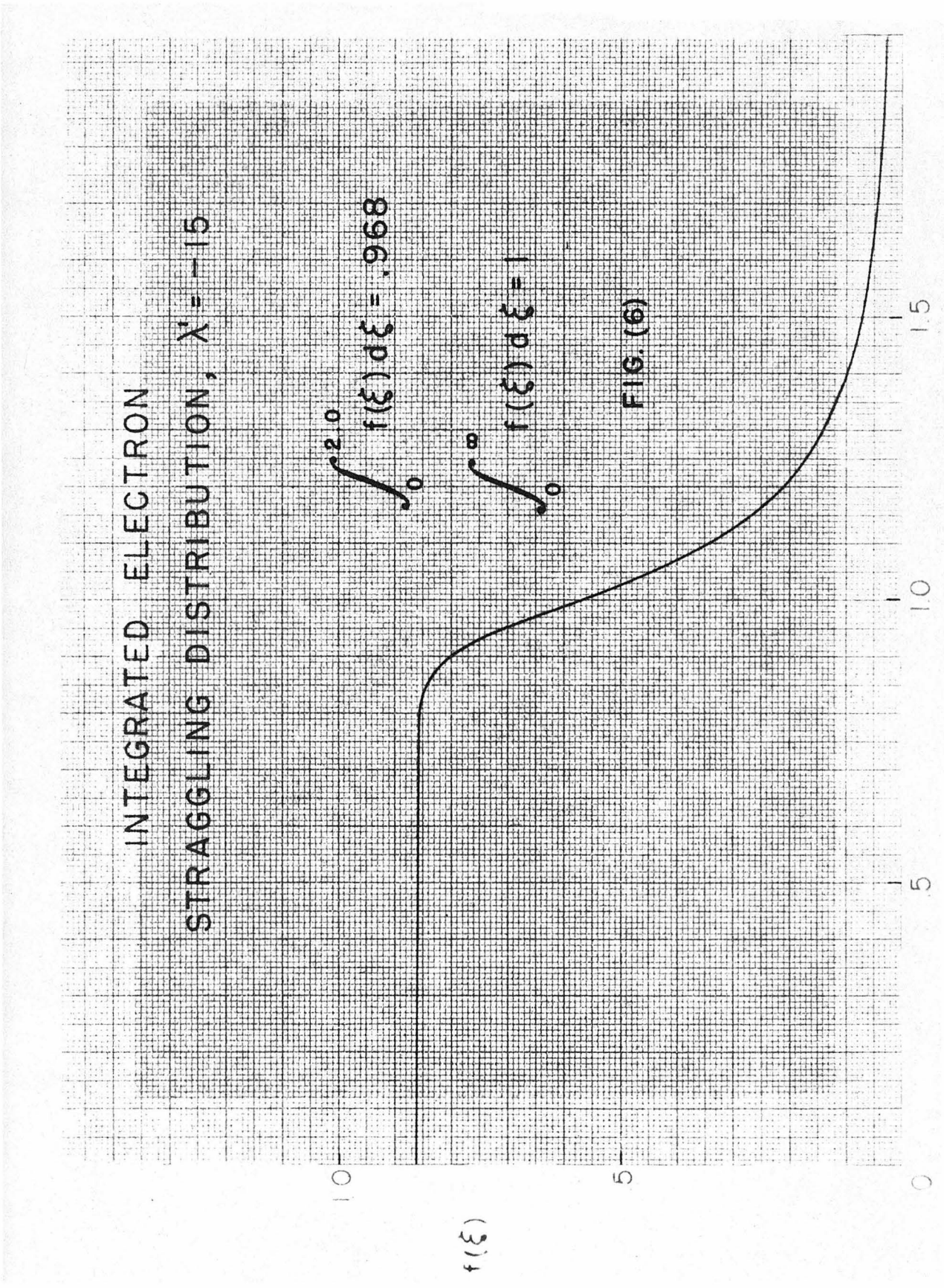
INTEGRATED ELECTRON
STRAGGLING DISTRIBUTION, λ' = -1.5
$\int_0^{2.0} f(\xi)\,d\xi = .968$
$\int_0^{8} f(\xi)\,d\xi = 1$
0
5
1.0
1.5
$\xi = \frac{\Delta}{\Delta_0(t)}$
$f(\xi)$

FIG. (6)

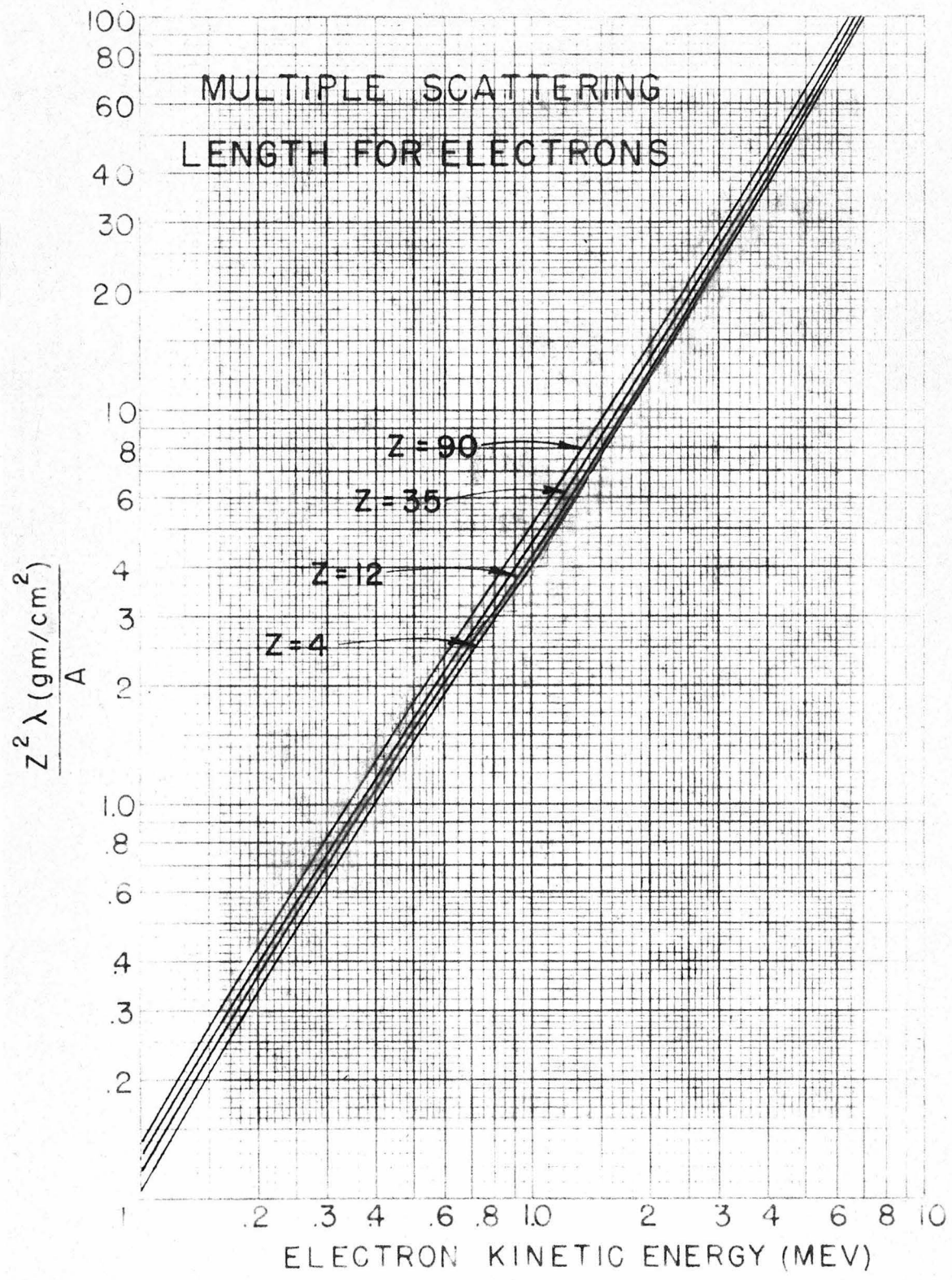
MULTIPLE SCATTERING
LENGTH FOR ELECTRONS
Z = 90
Z = 35
Z = 12
Z = 4
$\frac{Z^2 \lambda (gm/cm^2)}{A}$
100
80
60
40
30
20
10
8
6
4
3
2
1.0
.8
.6
.4
.3
.2
1
.2
.3
.4
.6
.8
1.0
2
3
4
6
8
10
ELECTRON KINETIC ENERGY (MEV)

FIG. (8)

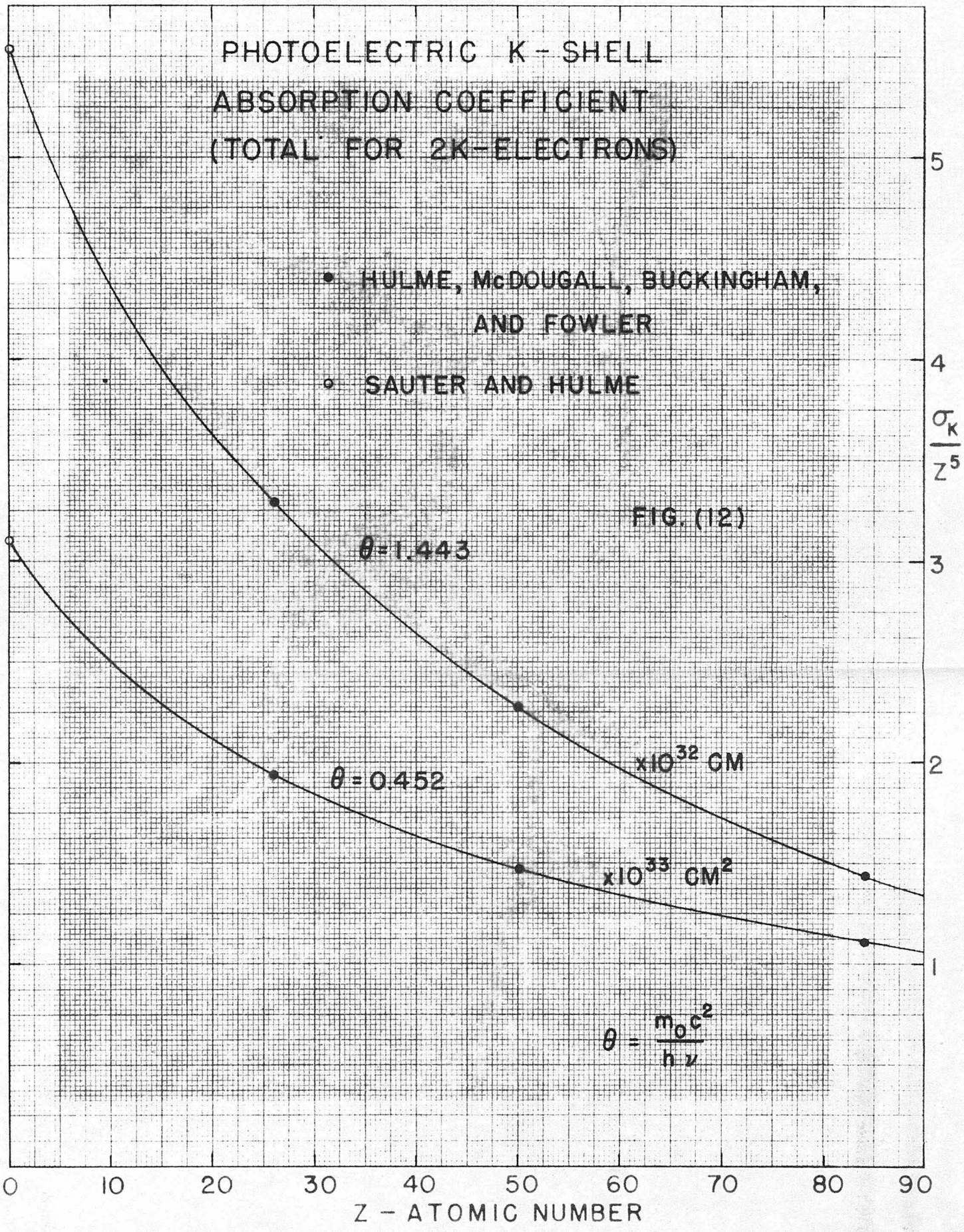
PHOTOELECTRIC K-SHELL
ABSORPTION COEFFICIENT
(TOTAL FOR 2K-ELECTRONS)
• HULME, McDOUGALL, BUCKINGHAM, AND FOWLER
○ SAUTER AND HULME
θ=1.443
θ = 0.452
×10^32 CM
×10^33 CM^2
θ = m0c^2 / hν
σK / Z^5
5
4
3
2
1
0
10
20
30
40
50
60
70
80
90
Z - ATOMIC NUMBER

FIG. (12)

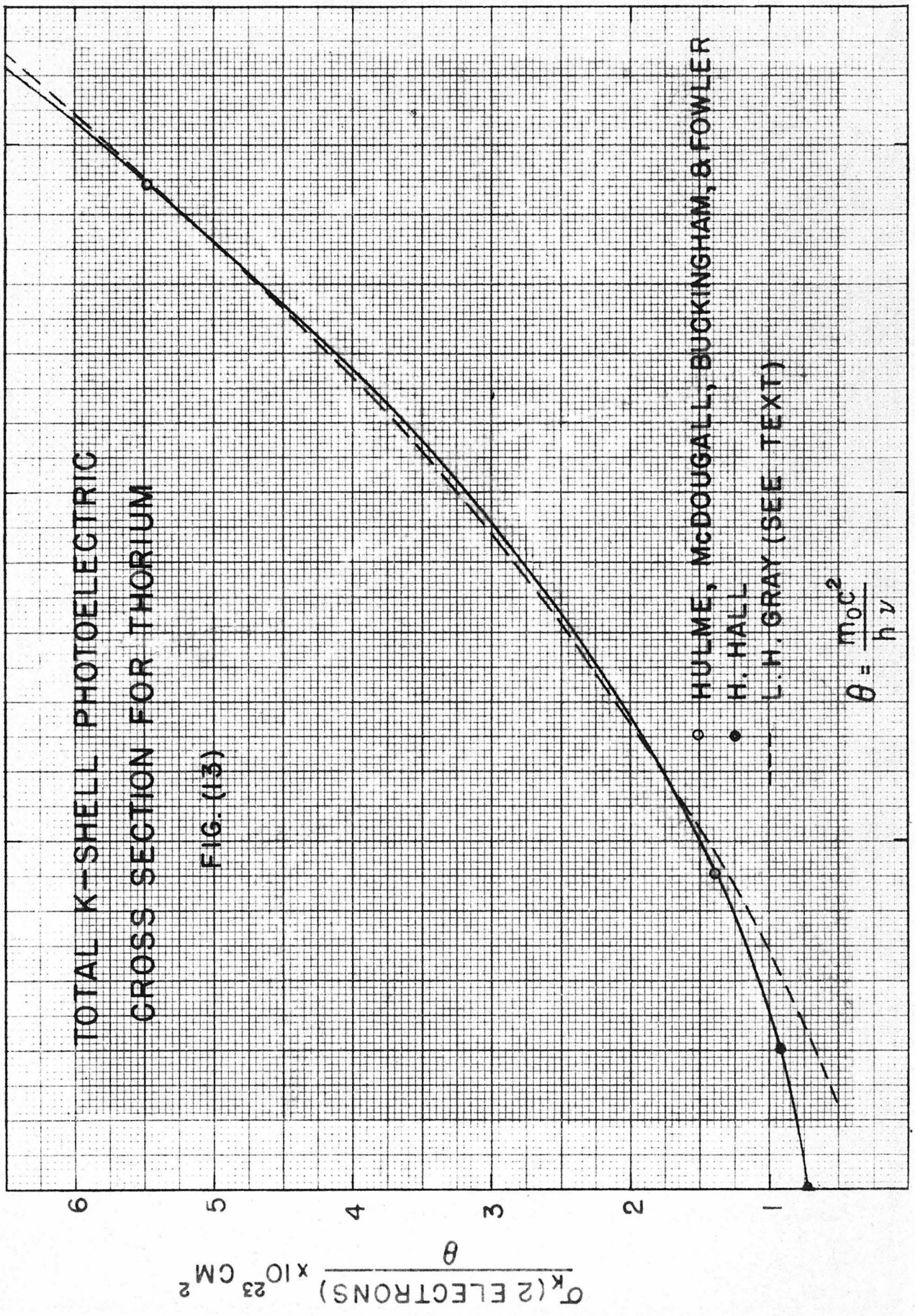
TOTAL K-SHELL PHOTOELECTRIC
CROSS SECTION FOR THORIUM
FIG. (13)
○ HULME, McDOUGALL, BUCKINGHAM, & FOWLER
● H. HALL
— L.H. GRAY (SEE TEXT)
$\theta = \frac{m_0c^2}{h\nu}$
$\frac{\sigma_K(2\ \text{ELECTRONS})}{\theta} \times 10^{23}\ \text{CM}^2$
0
0.5
1.0
1.5
1
2
3
4
5
6

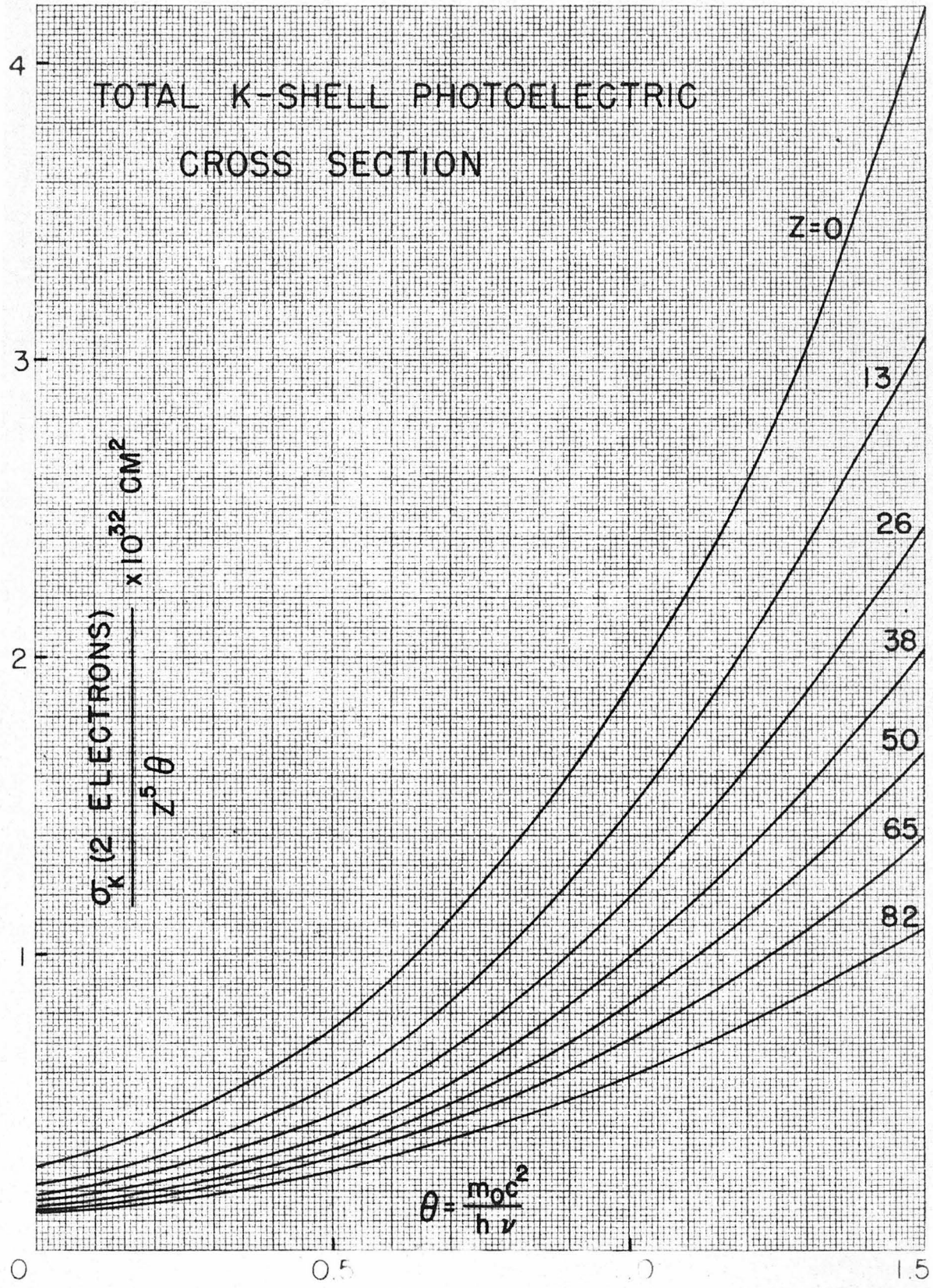
TOTAL K-SHELL PHOTOELECTRIC
CROSS SECTION
Z=0
13
26
38
50
65
82
$\frac{\sigma_K (2 \text{ ELECTRONS})}{Z^5 \theta} \times 10^{32} \text{ CM}^2$
$\theta = \frac{m_0 c^2}{h \nu}$
0
0.5
1.0
1.5
1
2
3
4

FIG. 14

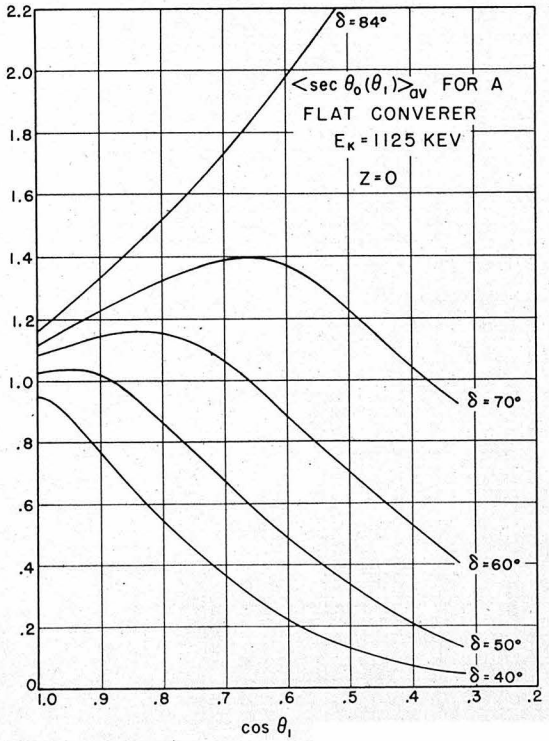

FIG. (15)

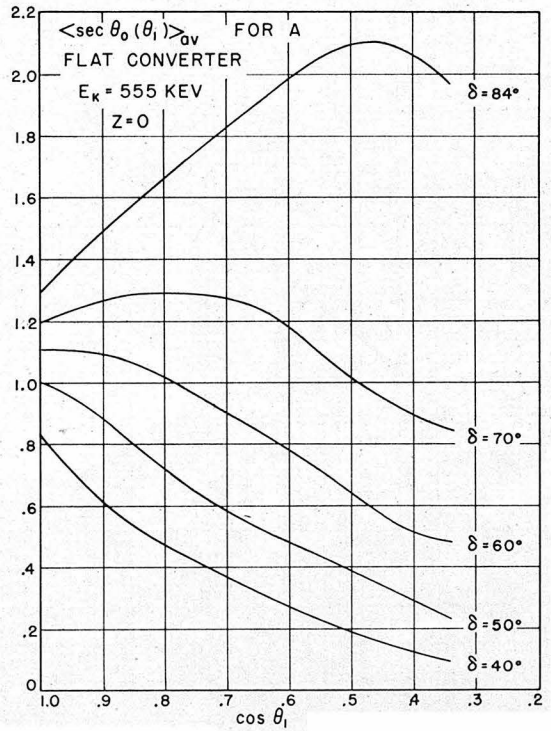

FIG. (16)

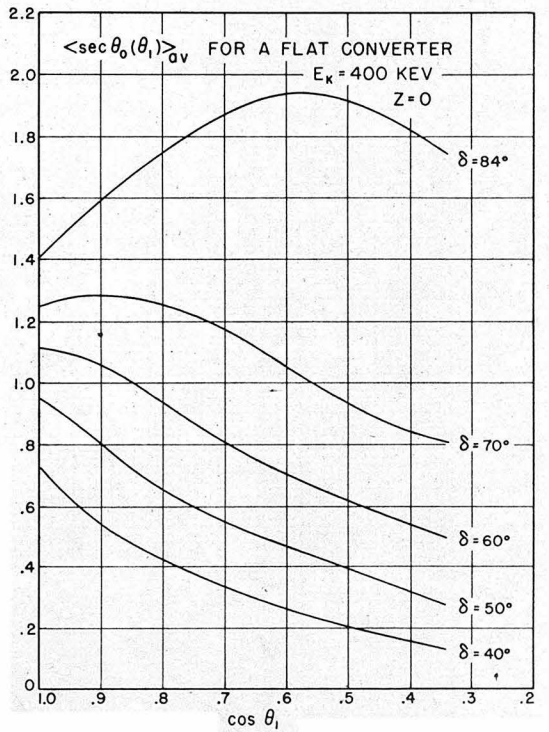

FIG. (17)

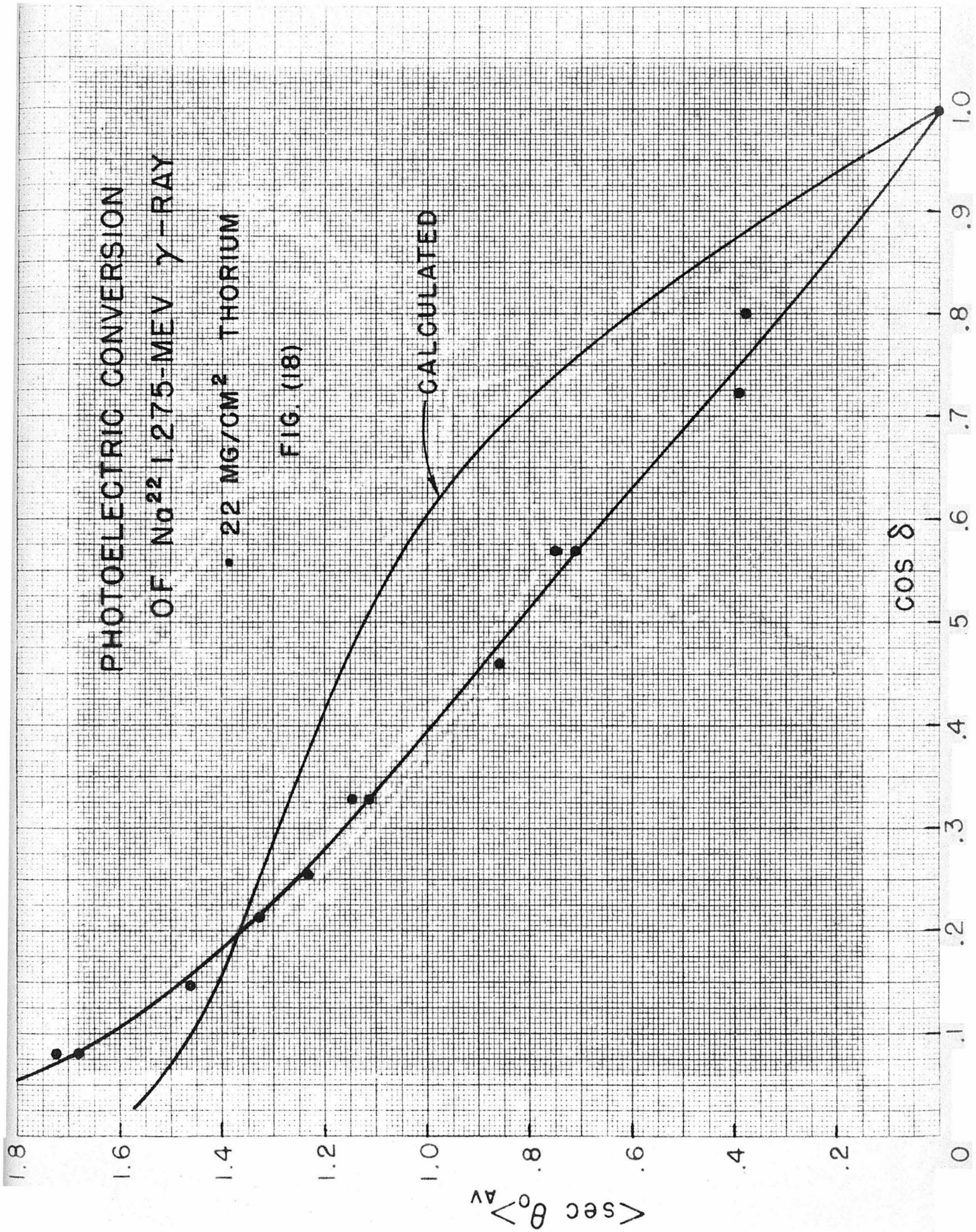
PHOTOELECTRIC CONVERSION
OF Na^{22} 1.275-MEV γ-RAY
• 22 MG/CM² THORIUM
FIG. (18)
CALCULATED
$\cos\delta$
$\langle \sec\theta_o \rangle_{av}$
0
.2
.4
.6
.8
1.0
1.2
1.4
1.6
1.8
.1
.3
.5
.7
.9

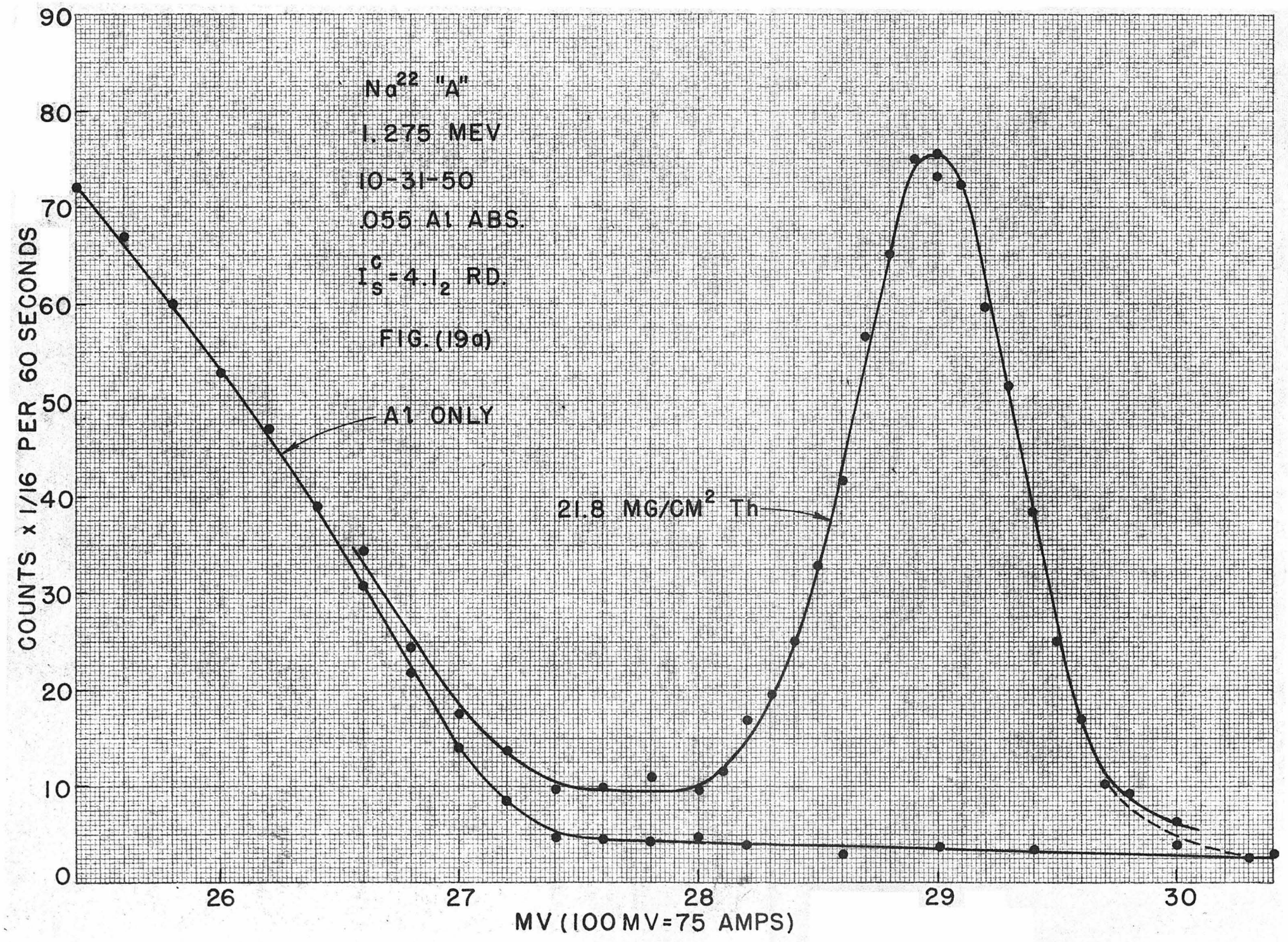

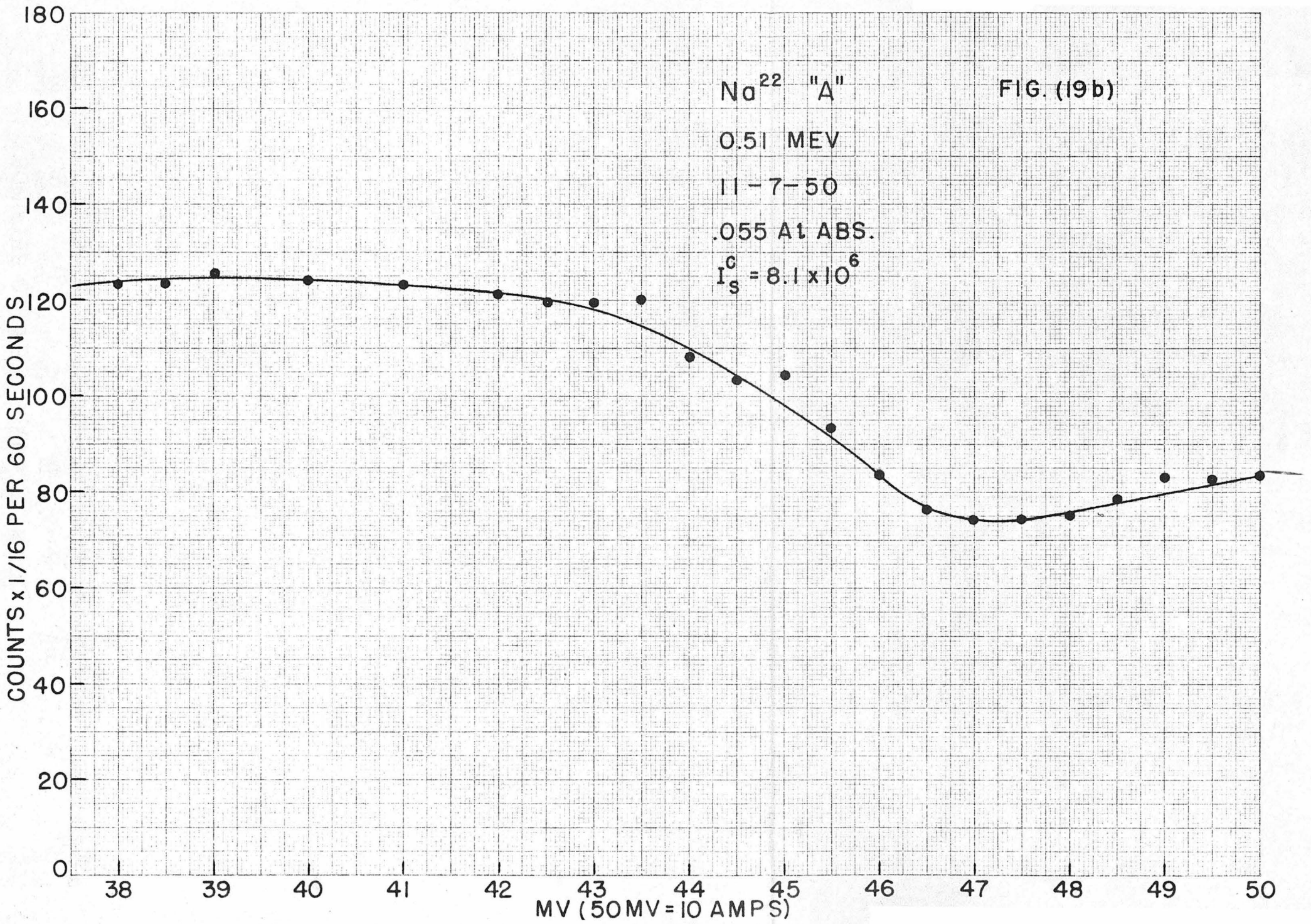

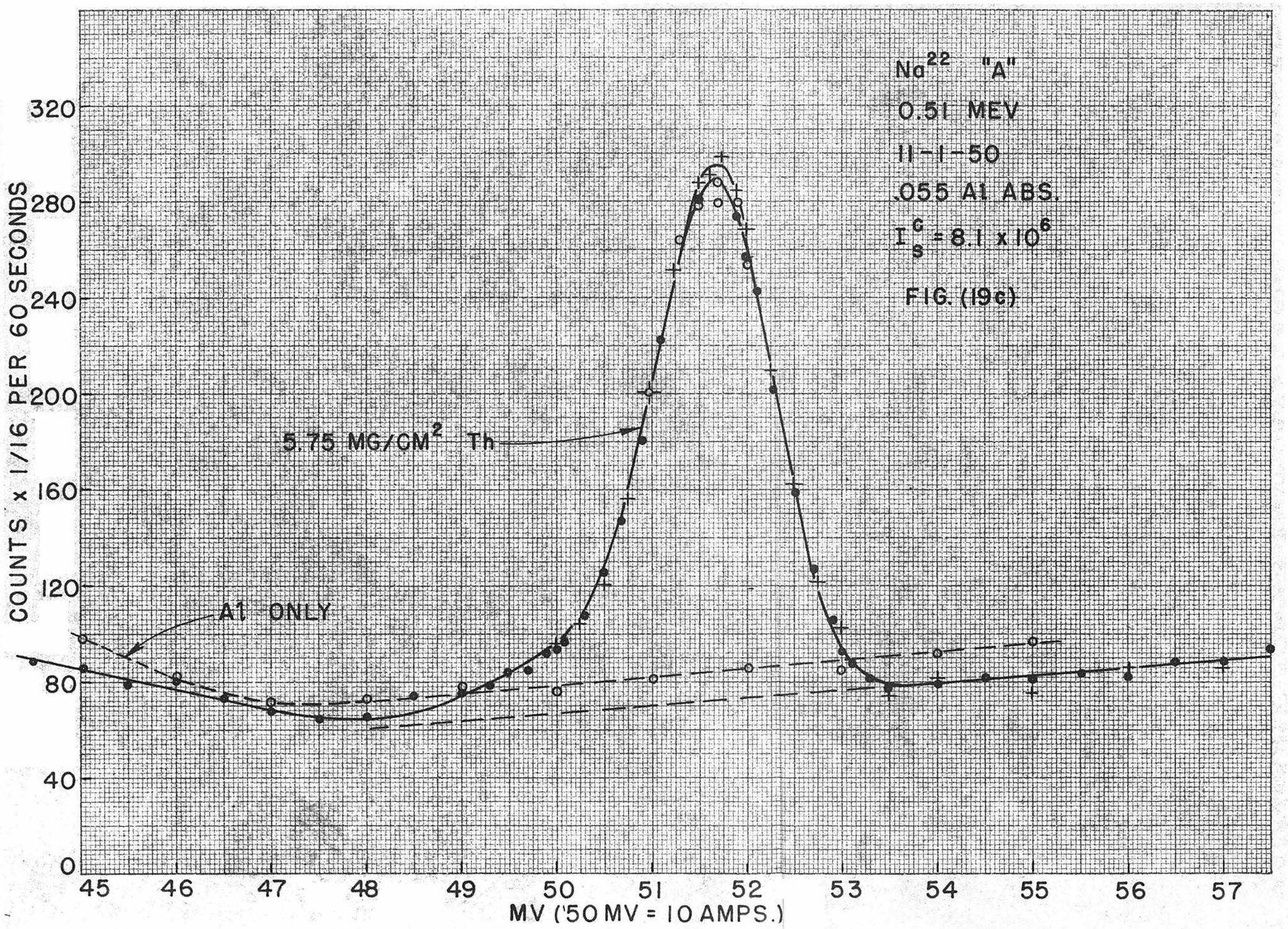

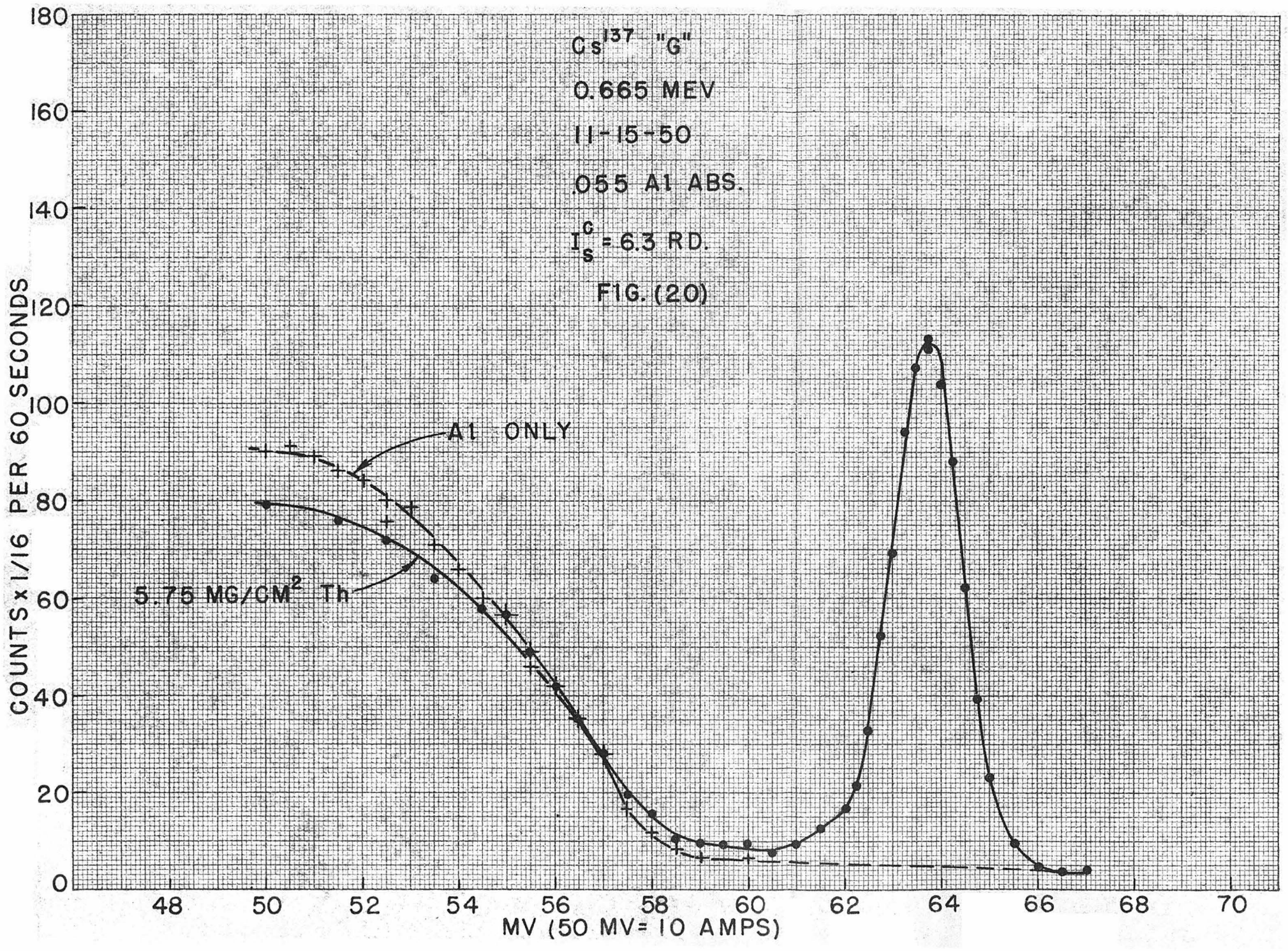

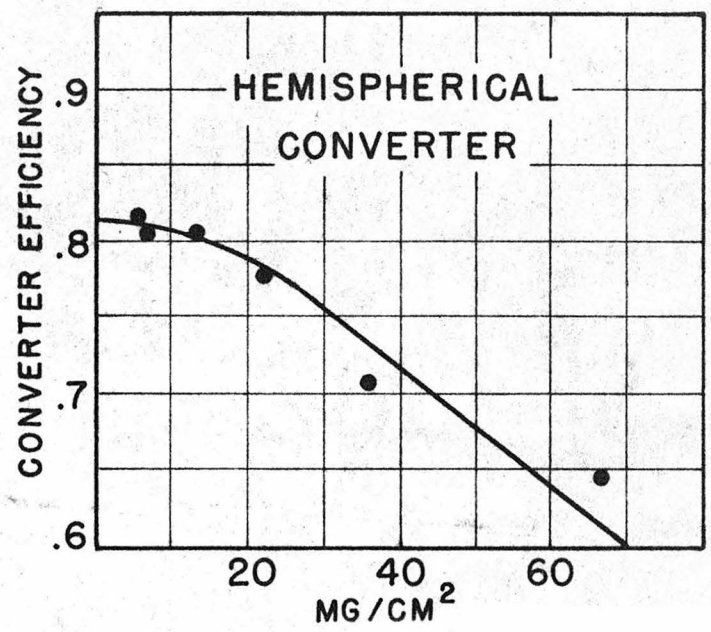
HEMISPHERICAL
CONVERTER
CONVERTER EFFICIENCY
.9
.8
.7
.6
20
40
60
MG/CM²

Fig. 22

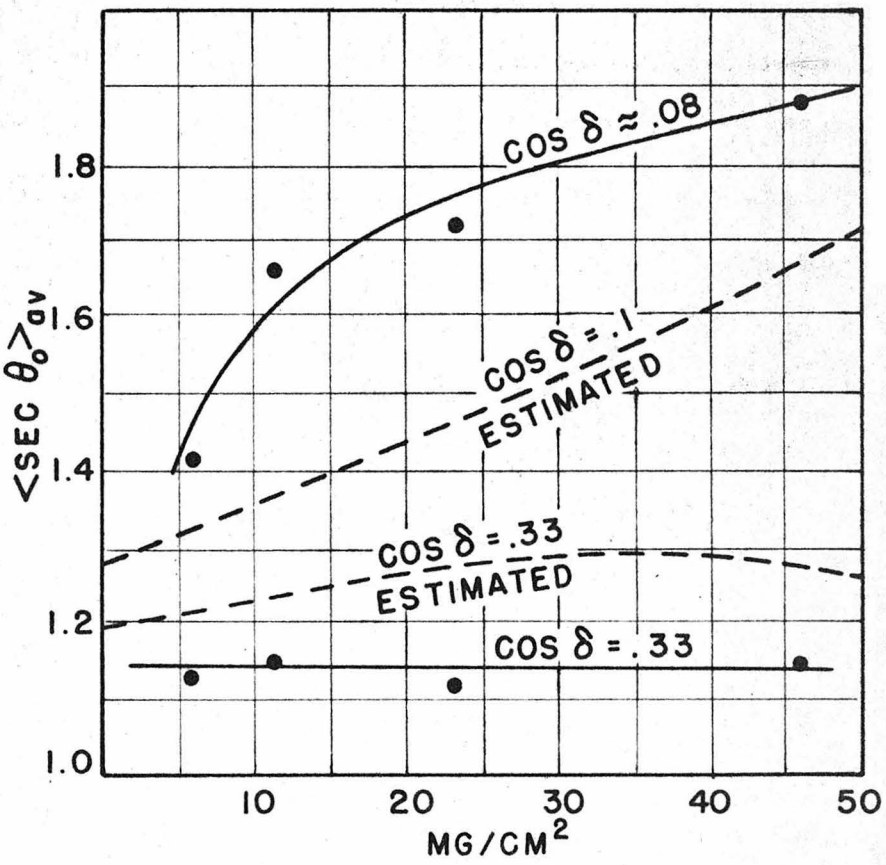
COS δ ≈ .08
COS δ = .1
ESTIMATED
COS δ = .33
ESTIMATED
COS δ = .33
<SEC θ₀>av
1.8
1.6
1.4
1.2
1.0
10
20
30
40
50
MG/CM²

Fig. 21

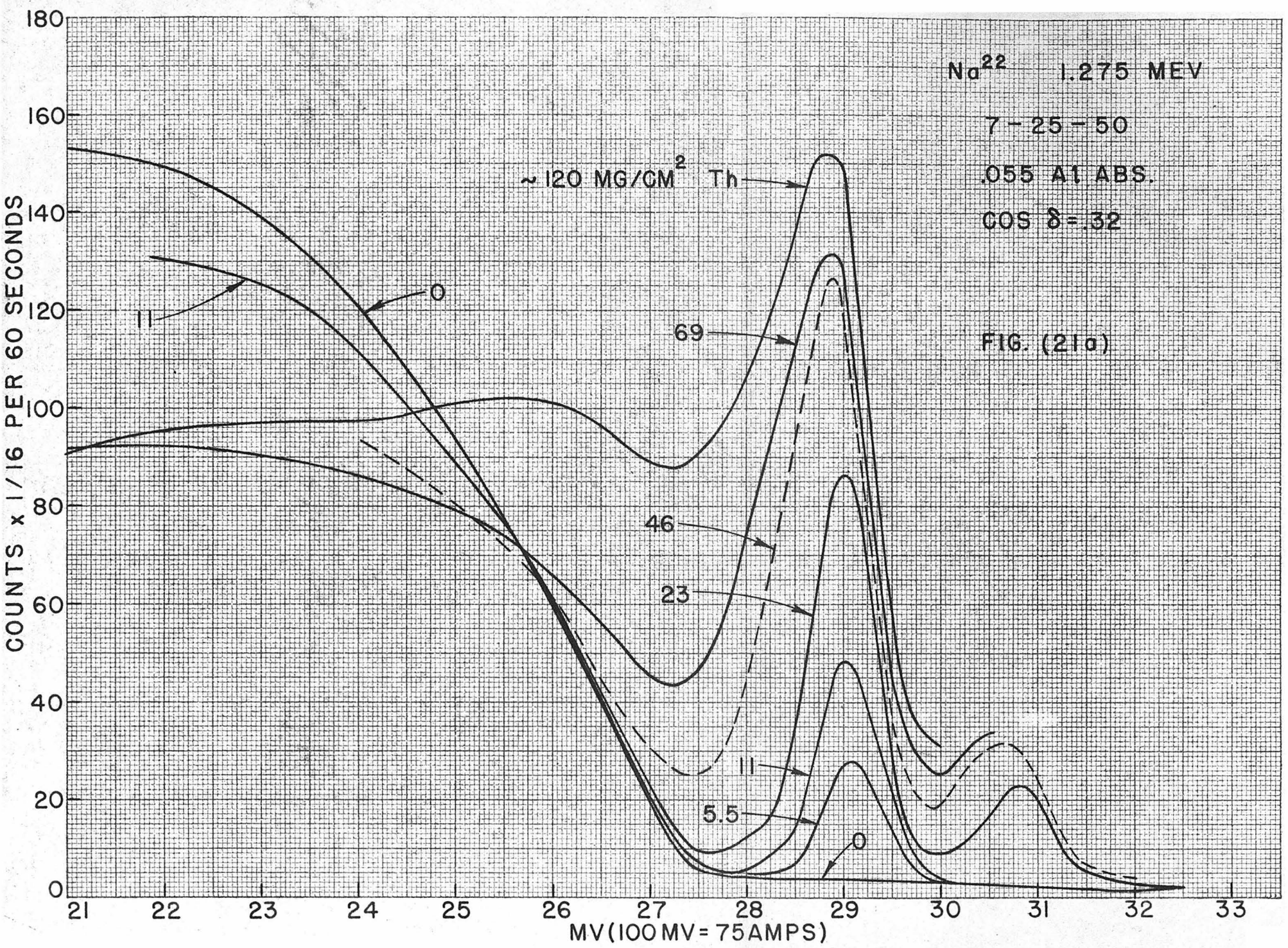
Na^{22} 1.275 MEV
7-25-50
.055 Al ABS.
COS δ=.32
~120 MG/CM² Th
0
11
69
46
23
11
5.5
0
COUNTS x 1/16 PER 60 SECONDS
MV(100 MV = 75 AMPS)
180
160
140
120
100
80
60
40
20
0
21
22
23
24
25
26
27
28
29
30
31
32
33

FIG. (21a)

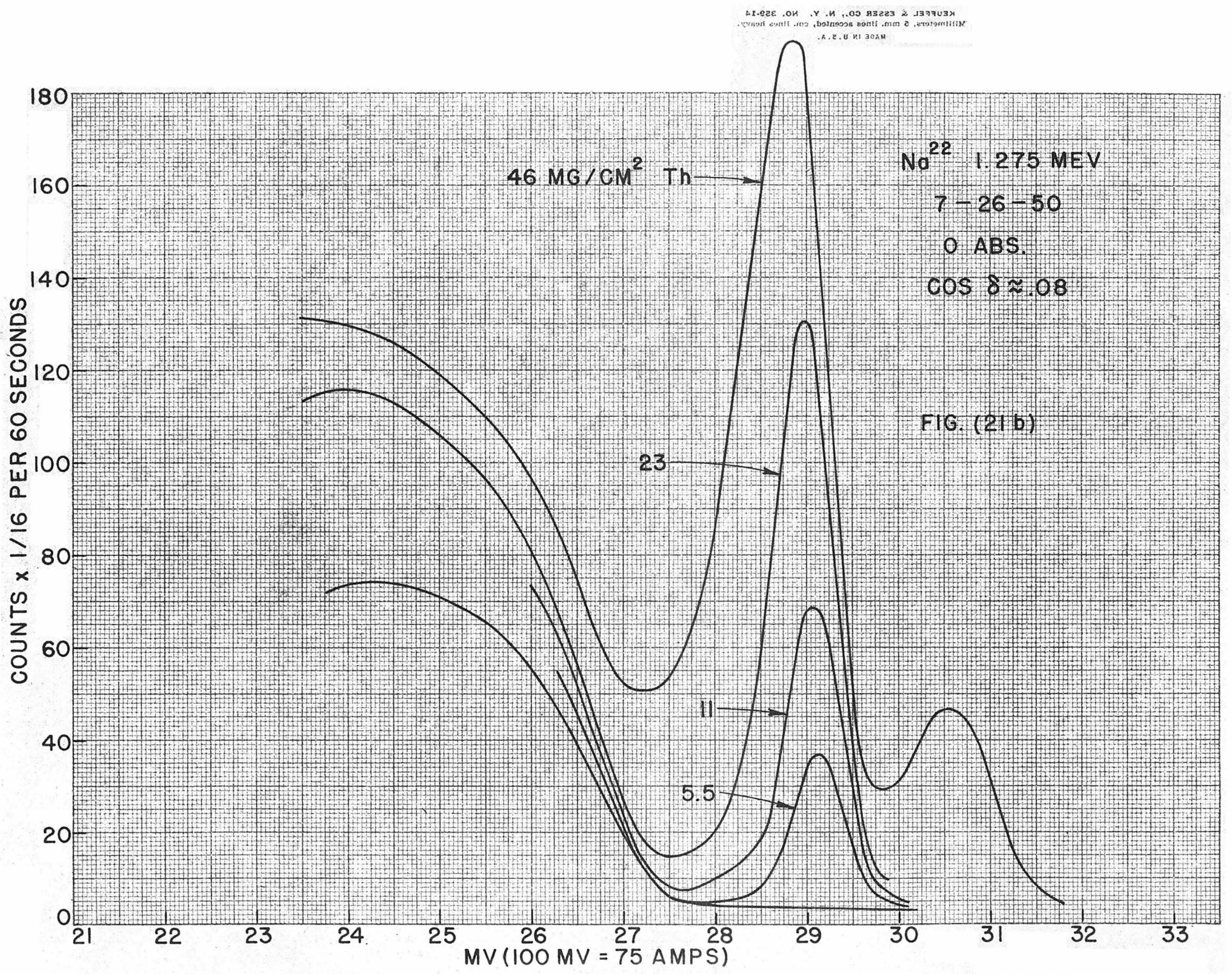
46 MG/CM² Th
Na²² 1.275 MEV
7-26-50
0 ABS.
COS δ ≈ .08
23
11
5.5
COUNTS x 1/16 PER 60 SECONDS
MV (100 MV = 75 AMPS)
0
20
40
60
80
100
120
140
160
180
21
22
23
24
25
26
27
28
29
30
31
32
33

FIG. (21 b)

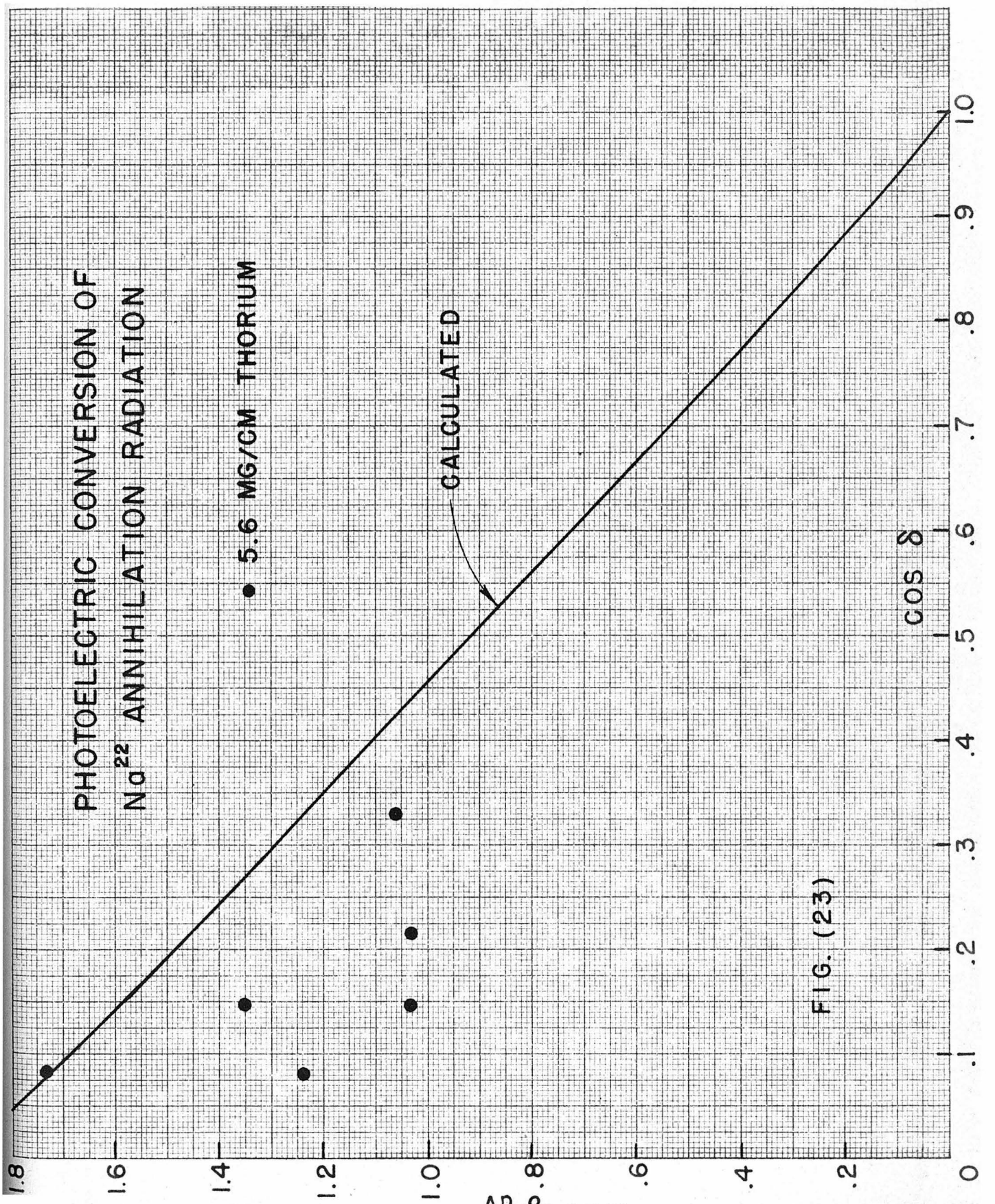
PHOTOELECTRIC CONVERSION OF
Na22 ANNIHILATION RADIATION
5.6 MG/CM THORIUM
CALCULATED
<SEC θo>av
COS δ
1.8
1.6
1.4
1.2
1.0
.8
.6
.4
.2
0
.1
.2
.3
.4
.5
.6
.7
.8
.9
1.0

FIG. (23)

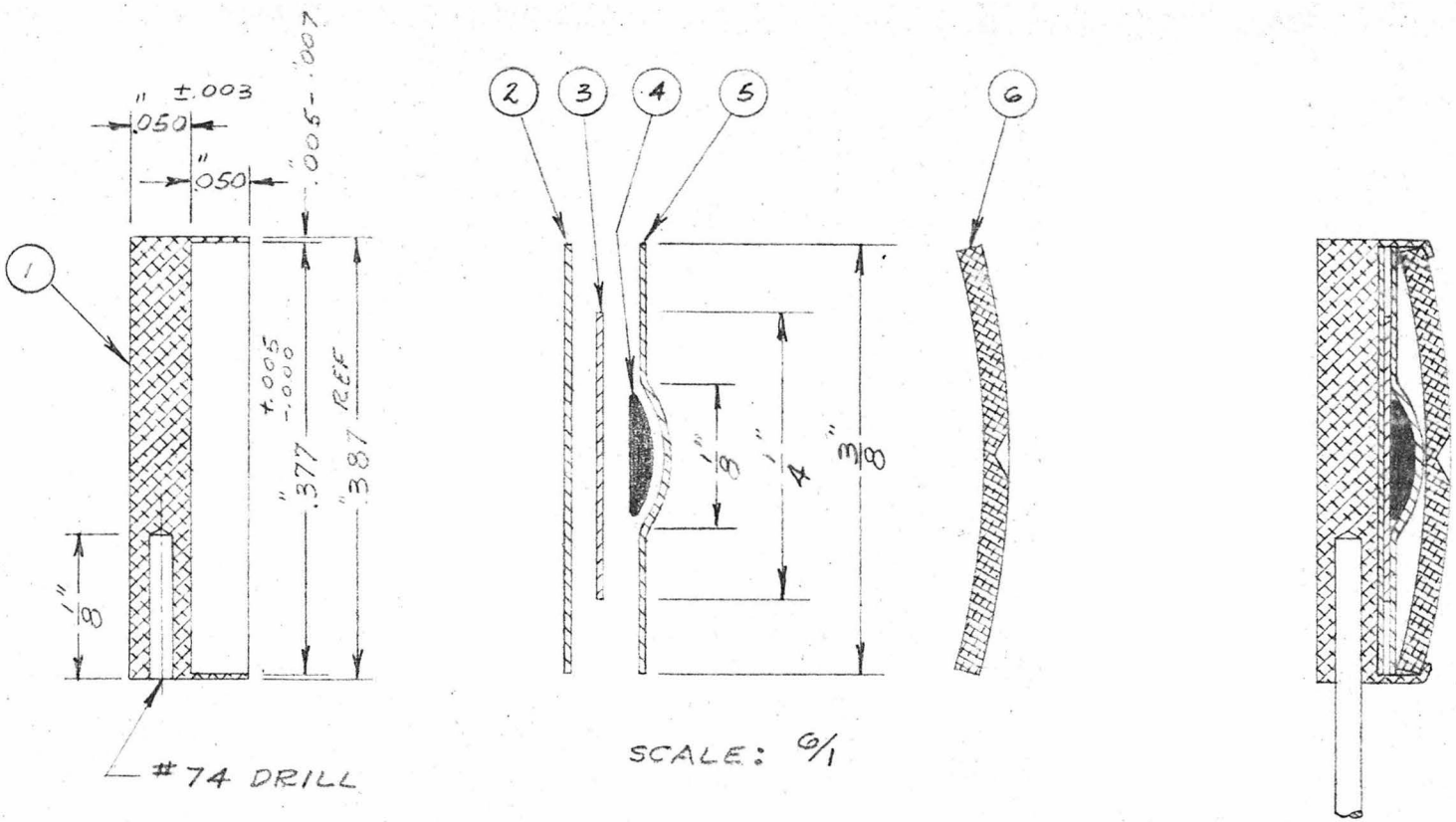

FIG.(23a) GAMMA SOURCE HOLDER

(1) 2S ALUMINUM

(2) ".0015 ALUMINUM FOIL

(3) SCOTCH TAPE

(4) GAMMA SOURCE

(5) ".0015 ALUMINUM FOIL

(6) ".020 ALUMINUM SHEET

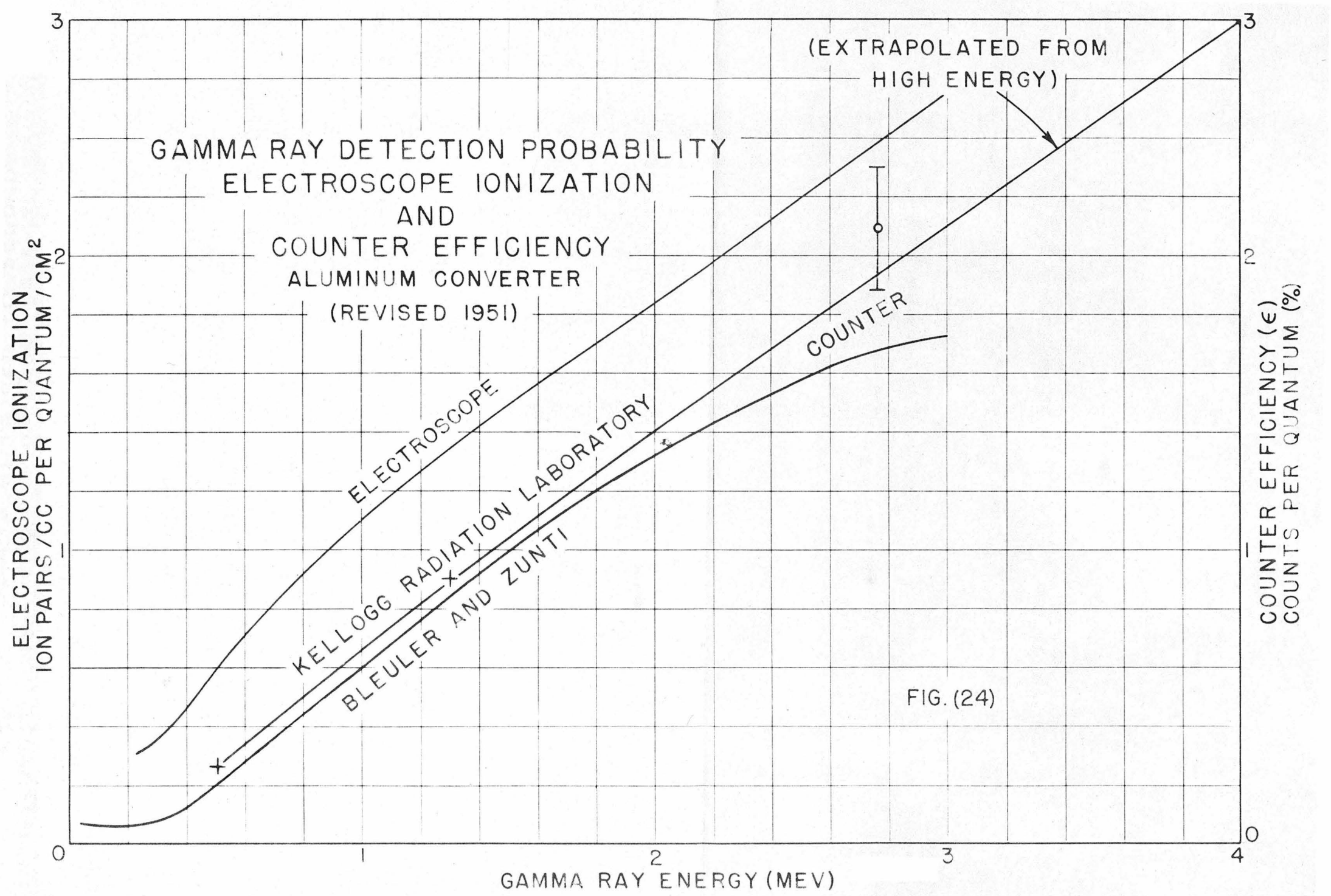
GAMMA RAY DETECTION PROBABILITY
ELECTROSCOPE IONIZATION
AND
COUNTER EFFICIENCY
ALUMINUM CONVERTER
(REVISED 1951)
(EXTRAPOLATED FROM
HIGH ENERGY)
ELECTROSCOPE
KELLOGG RADIATION LABORATORY
BLEULER AND ZUNTI
COUNTER
ELECTROSCOPE IONIZATION
ION PAIRS/CC PER QUANTUM/CM²
COUNTER EFFICIENCY (ε)
COUNTS PER QUANTUM (%)
GAMMA RAY ENERGY (MEV)
0
1
2
3
4

FIG. (24)

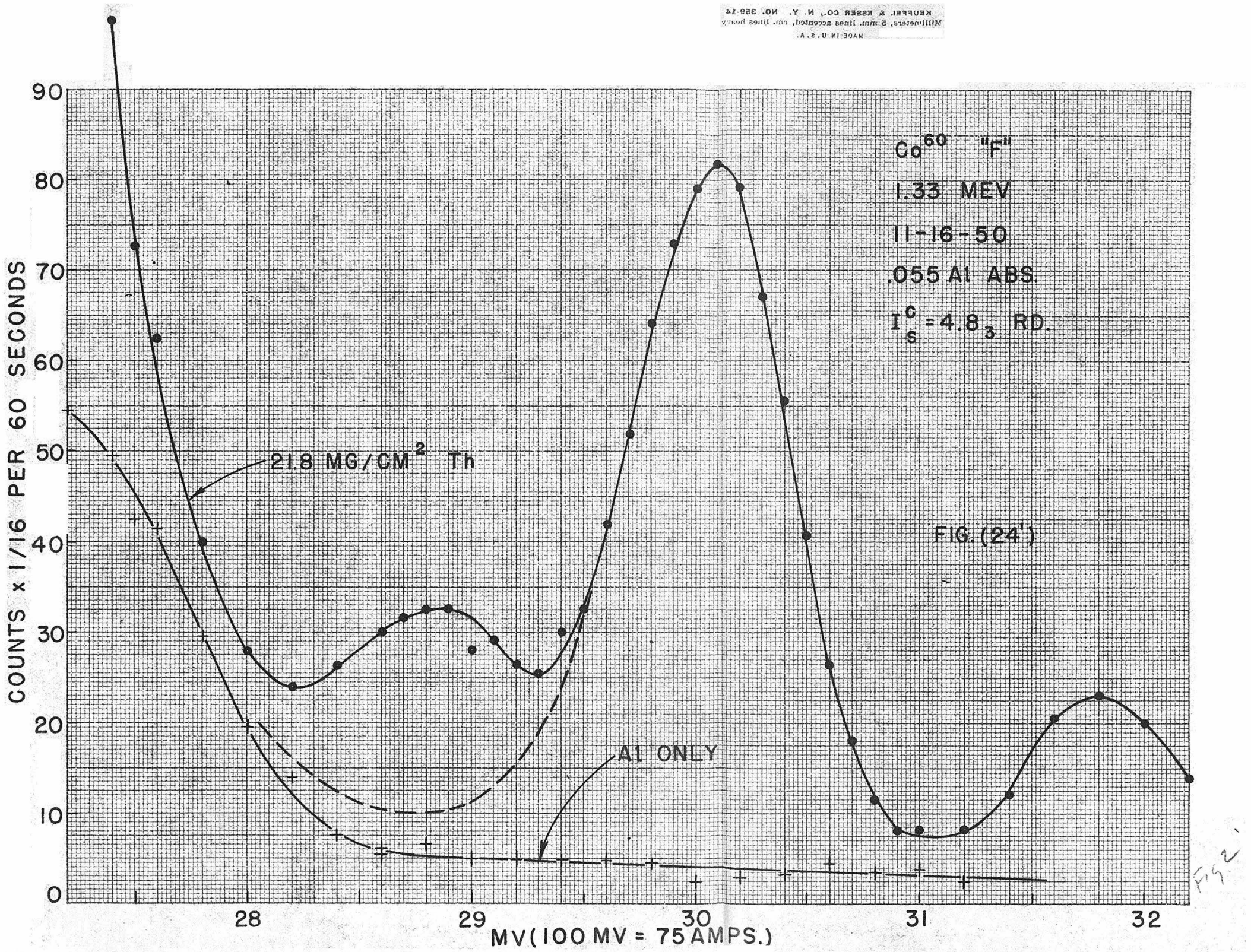

FIG. (24')

Fig 2'

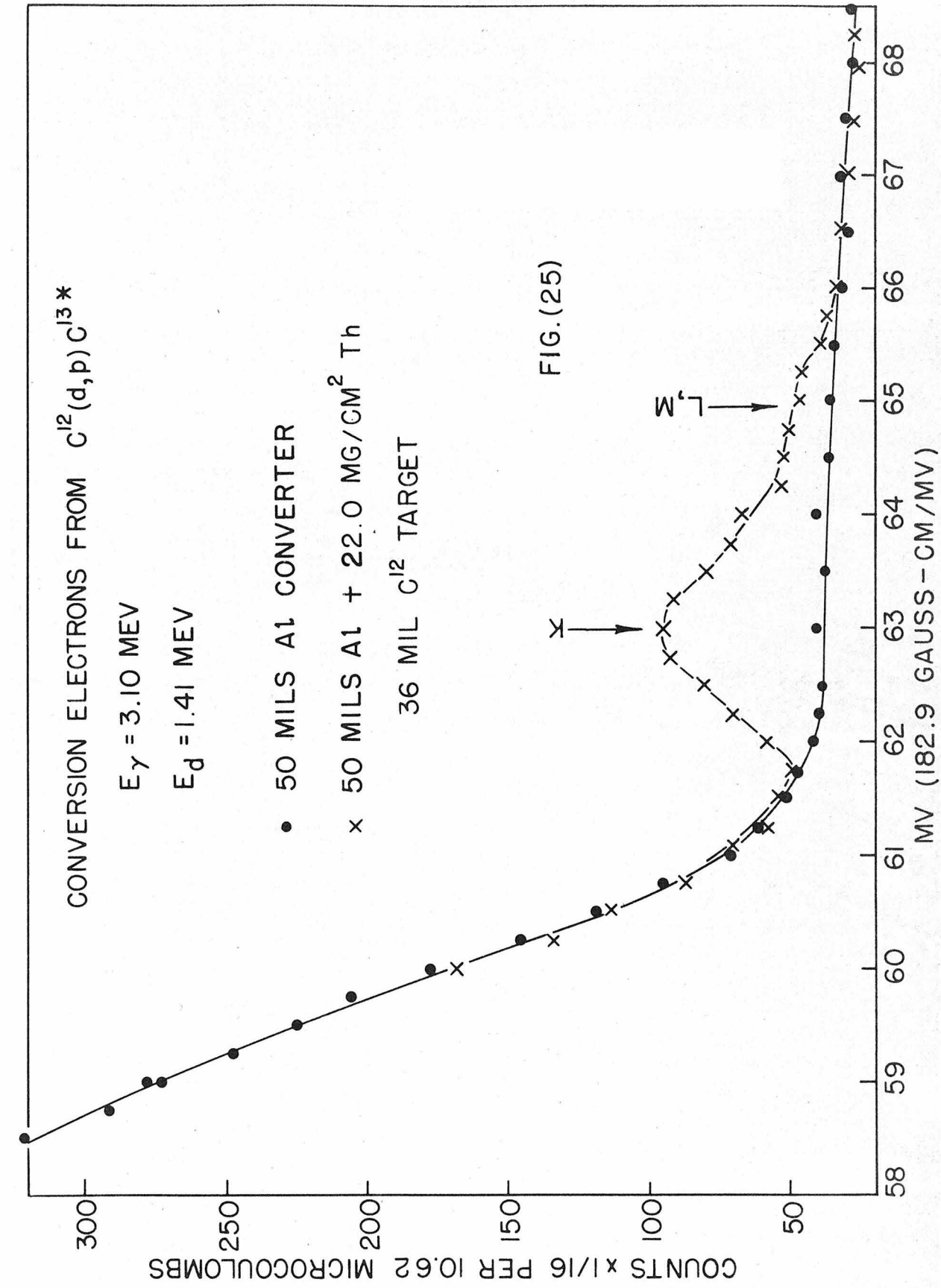
CONVERSION ELECTRONS FROM $C^{12}(d,p)C^{13}$*
E_γ = 3.10 MEV
E_d = 1.41 MEV
• 50 MILS Al CONVERTER
× 50 MILS Al + 22.0 MG/CM^2 Th
36 MIL C^{12} TARGET
K
L,M
COUNTS x 1/16 PER 10.62 MICROCOULOMBS
MV (182.9 GAUSS-CM/MV)
50
100
150
200
250
300
58
59
60
61
62
63
64
65
66
67
68

FIG.(25)

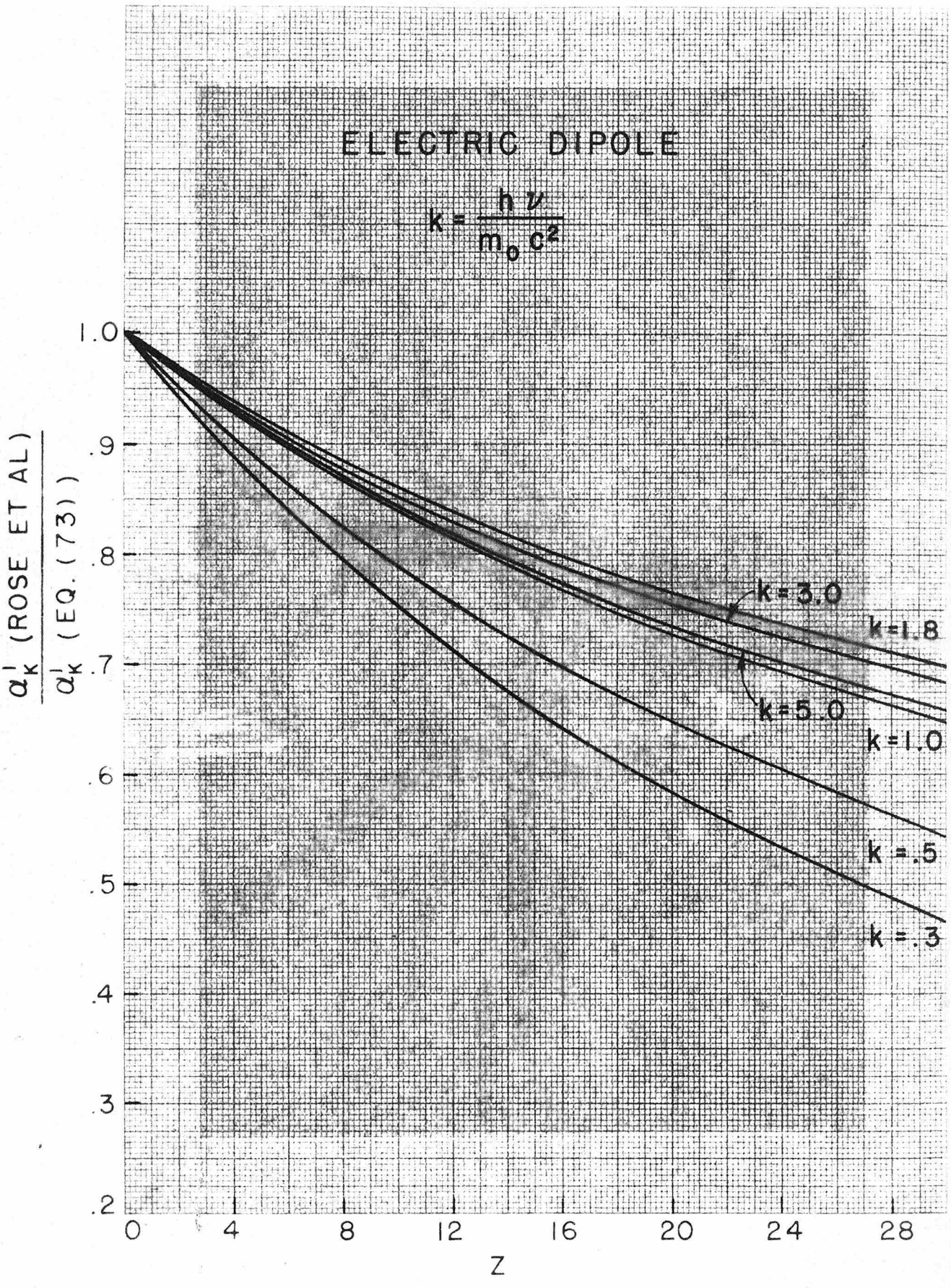
ELECTRIC DIPOLE
$k = \frac{h\nu}{m_0 c^2}$
$\frac{\alpha'_k \text{ (ROSE ET AL)}}{\alpha'_k \text{ (EQ. (73))}}$
1.0
.9
.8
.7
.6
.5
.4
.3
.2
0
4
8
12
16
20
24
28
Z
k = 3.0
k = 1.8
k = 5.0
k = 1.0
k = .5
k = .3

FIG. (26)

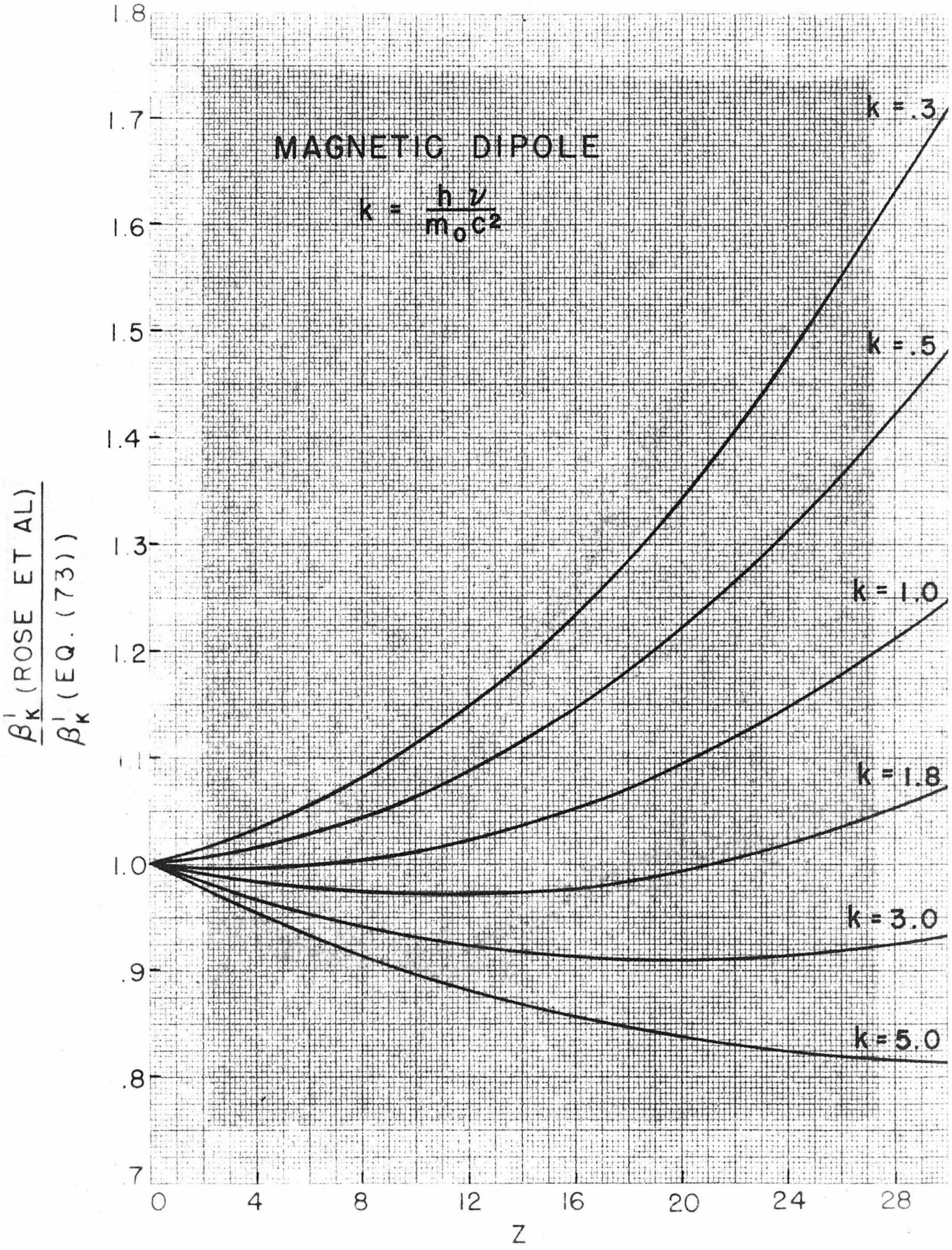
MAGNETIC DIPOLE
$k = \frac{h\nu}{m_0 c^2}$
k = .3
k = .5
k = 1.0
k = 1.8
k = 3.0
k = 5.0
$\frac{\beta_k' \text{ (ROSE ET AL)}}{\beta_k' \text{ (EQ. (73))}}$
1.8
1.7
1.6
1.5
1.4
1.3
1.2
1.0
.9
.8
.7
0
4
8
12
16
20
24
28
Z

FIG. (27)

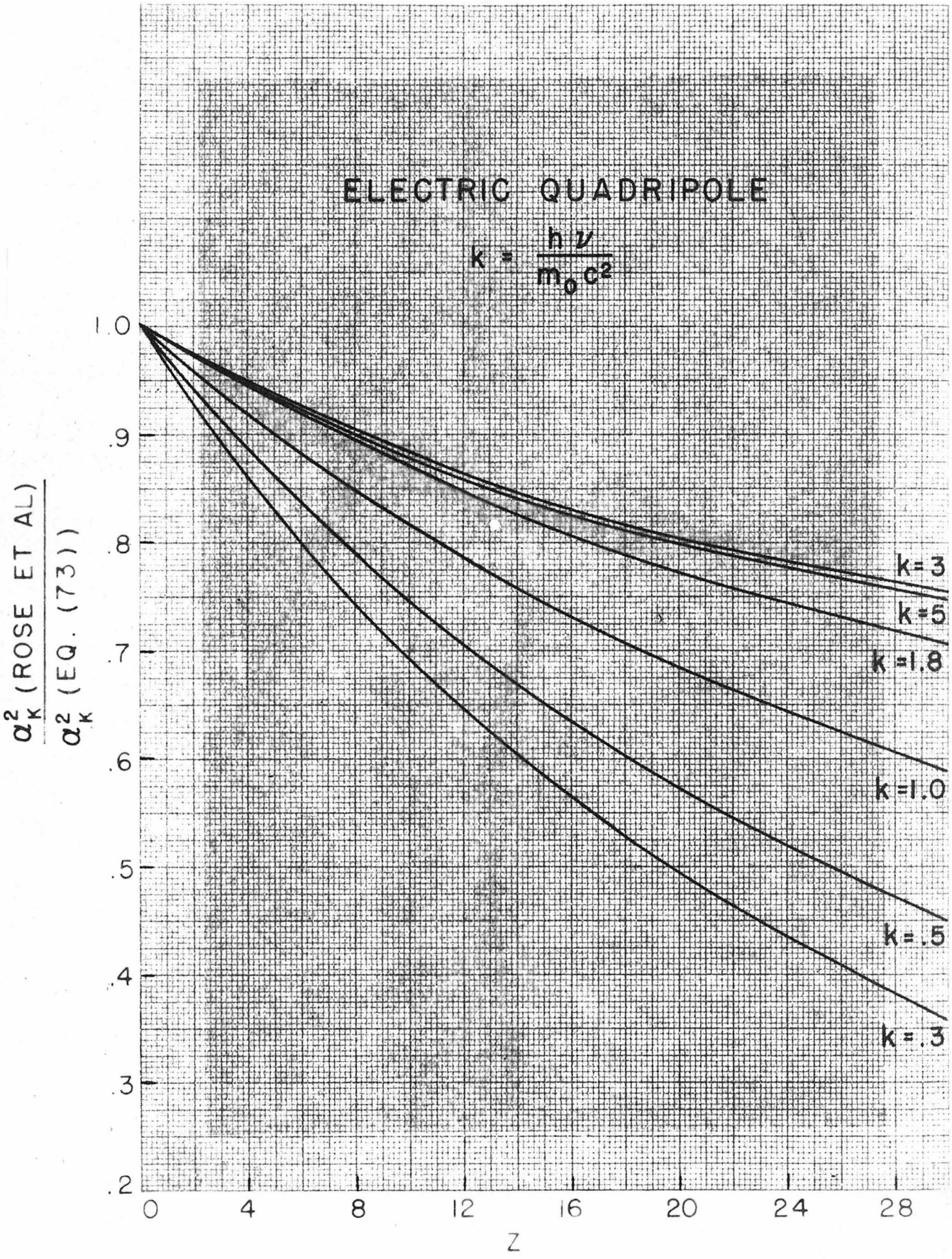
ELECTRIC QUADRIPOLE
$k = \frac{h\nu}{m_0 c^2}$
$\frac{\alpha_k^2 \text{ (ROSE ET AL)}}{\alpha_k^2 \text{ (EQ. (73))}}$
1.0
.9
.8
.7
.6
.5
.4
.3
.2
0
4
8
12
16
20
24
28
Z
k=3
k=5
k=1.8
k=1.0
k=.5
k=.3

FIG. (28)

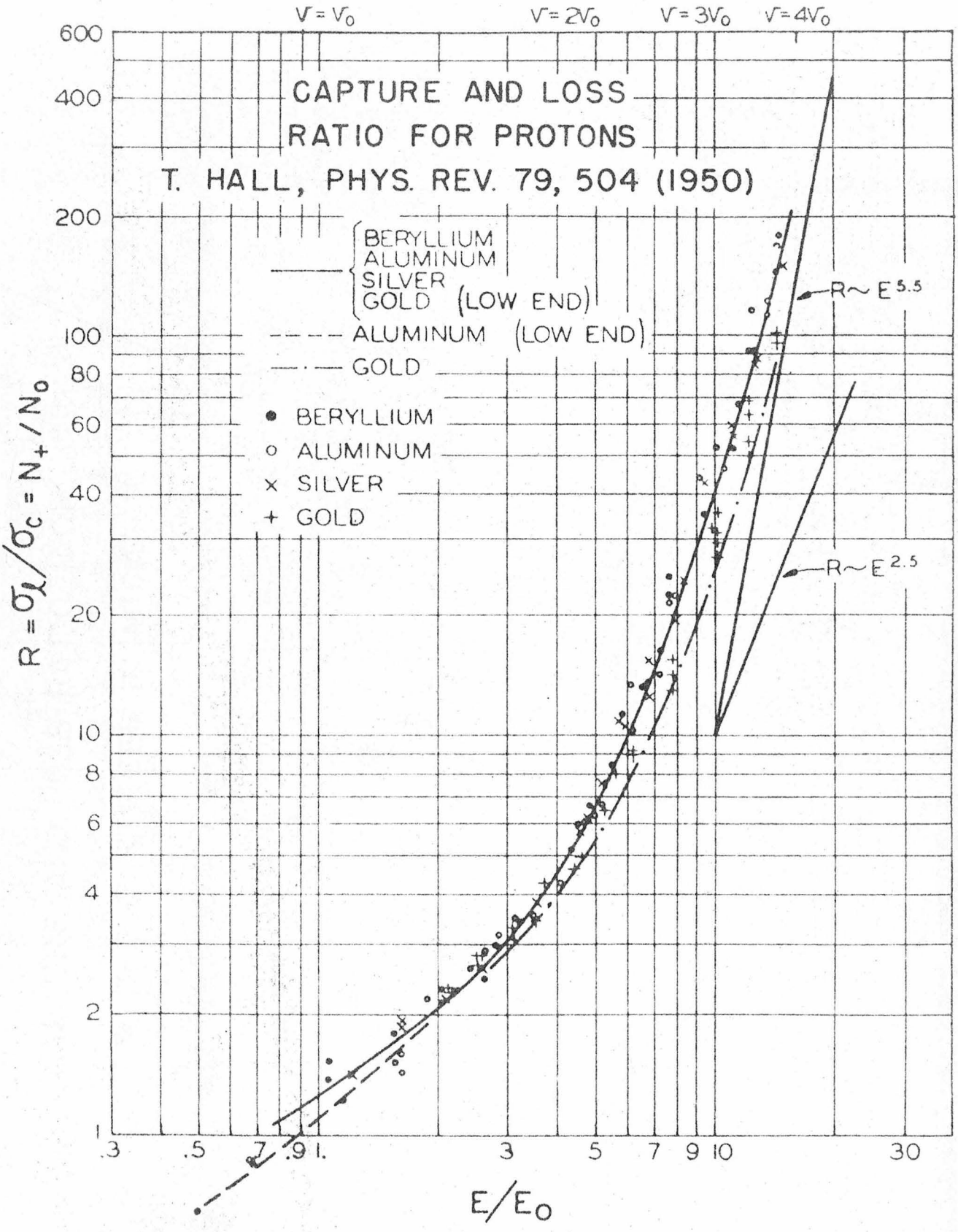

FIG. 29 – RATIO OF LOSS TO CAPTURE CROSS SECTION σ_l/σ_c AS A FUNCTION OF ION ENERGY E. AT ENERGY E_0 THE ION SPEED $v = v_0 = e^2/\hbar$. $E_0 = 24.8$ KEV.

CAPTURE AND LOSS RATIO FOR

ALPHA PARTICLES IN MICA

FIG. (30)

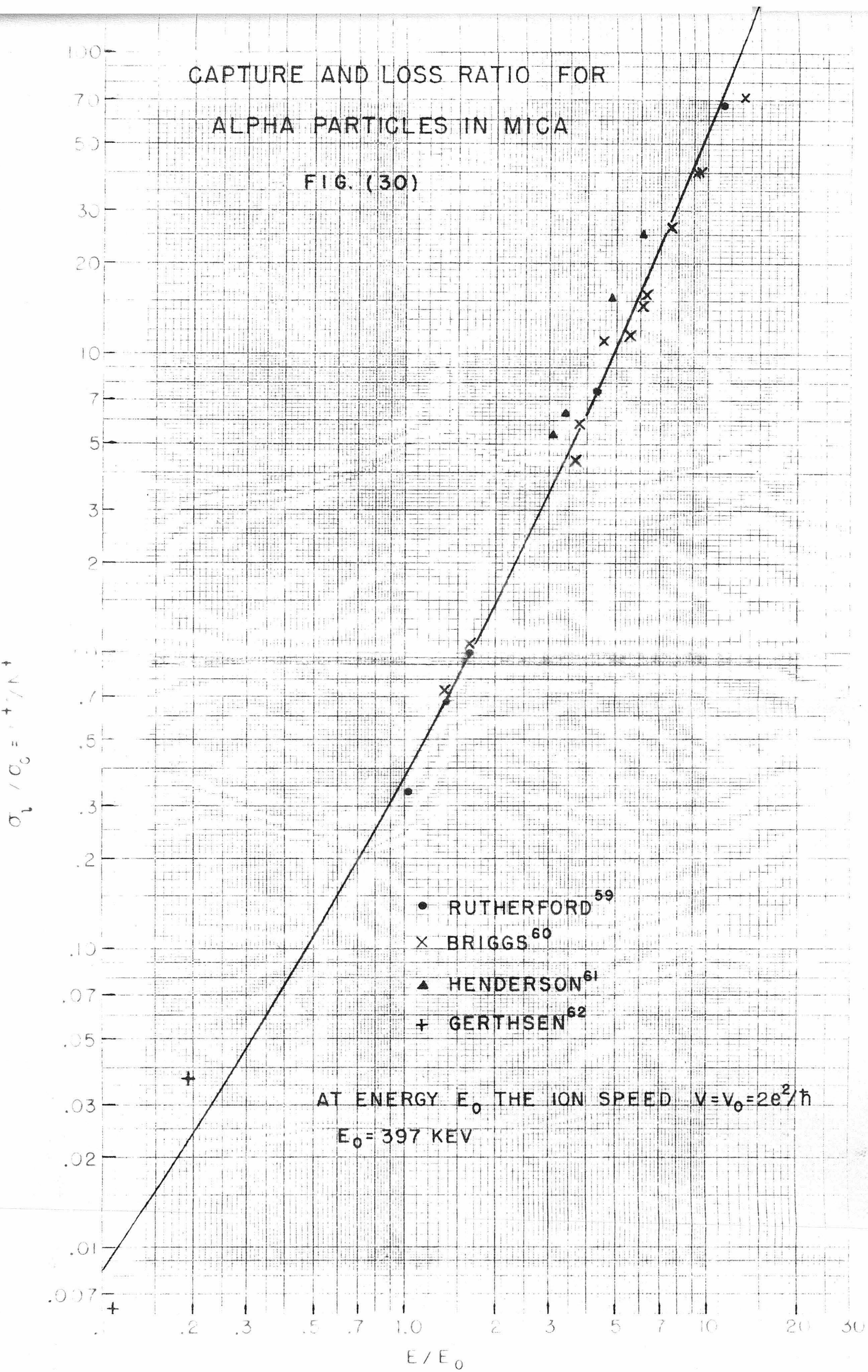

UNCOVERED-SOURCE SPECTRUM FROM $Co^{60}(\beta^-)$ Ni^{60} *

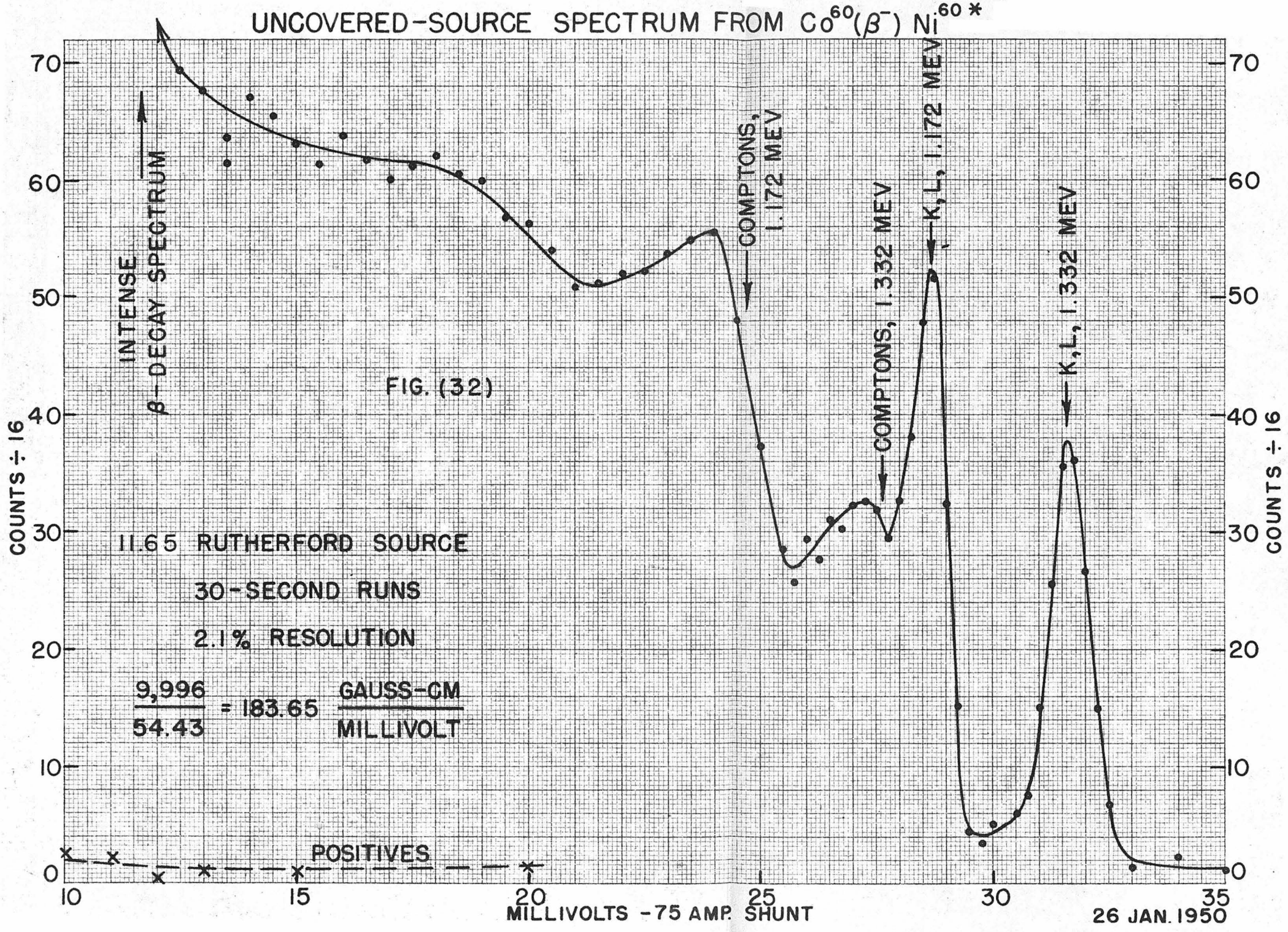

FIG. (32)

SOLID ANGLE DETERMINATION, $C^{60}(\beta^-)Ni^{60*}$

FIG. (33)

11.65 RUTHERFORD SOURCE

20-SECOND RUNS

2.1% RESOLUTION

$\frac{9,996}{54.43} = 183.65 \frac{\text{GAUSS-CM.}}{\text{MILLIVOLT}}$

20 MILS ALUMINUM

8.05 MG/CM^2 THORIUM

20 MILS ALUMINUM

+5.8 MG/CM^2 ALUMINUM

K, 1.172 MEV

K, 1.332 MEV

L, 1.172 MEV

L, 1.332

COUNTS ÷ 16

100

50

25 27 29 31 33 35

MILLIVOLTS - 75 AMP. SHUNT

31 JAN. 1950

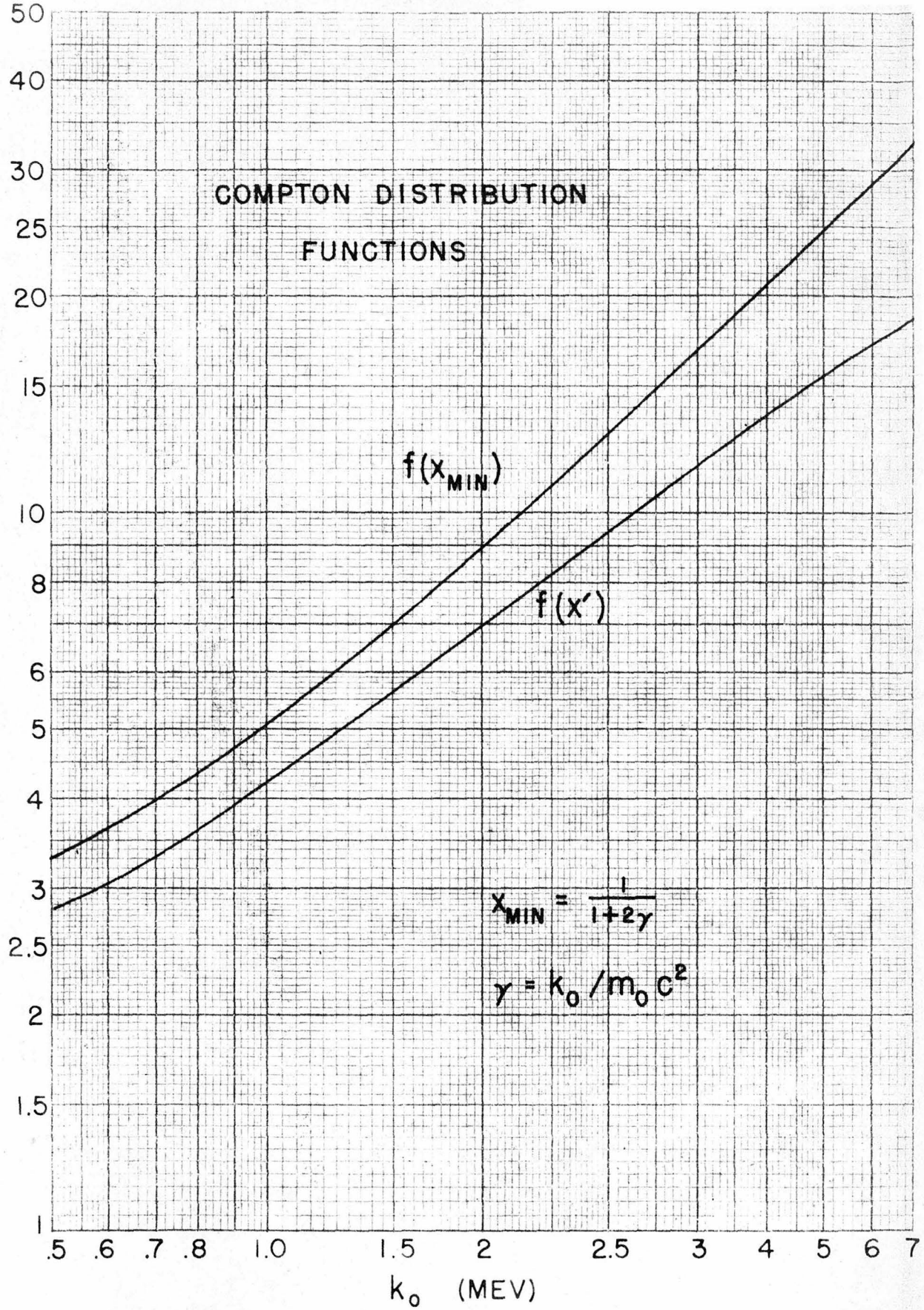
COMPTON DISTRIBUTION
FUNCTIONS
$f(x_{MIN})$
$f(x')$
$x_{MIN} = \frac{1}{1+2\gamma}$
$\gamma = k_0 / m_0 c^2$
50
40
30
25
20
15
10
8
6
5
4
3
2.5
2
1.5
1
.5 .6 .7 .8 1.0 1.5 2 2.5 3 4 5 6 7
k_0 (MEV)

FIG.(34)

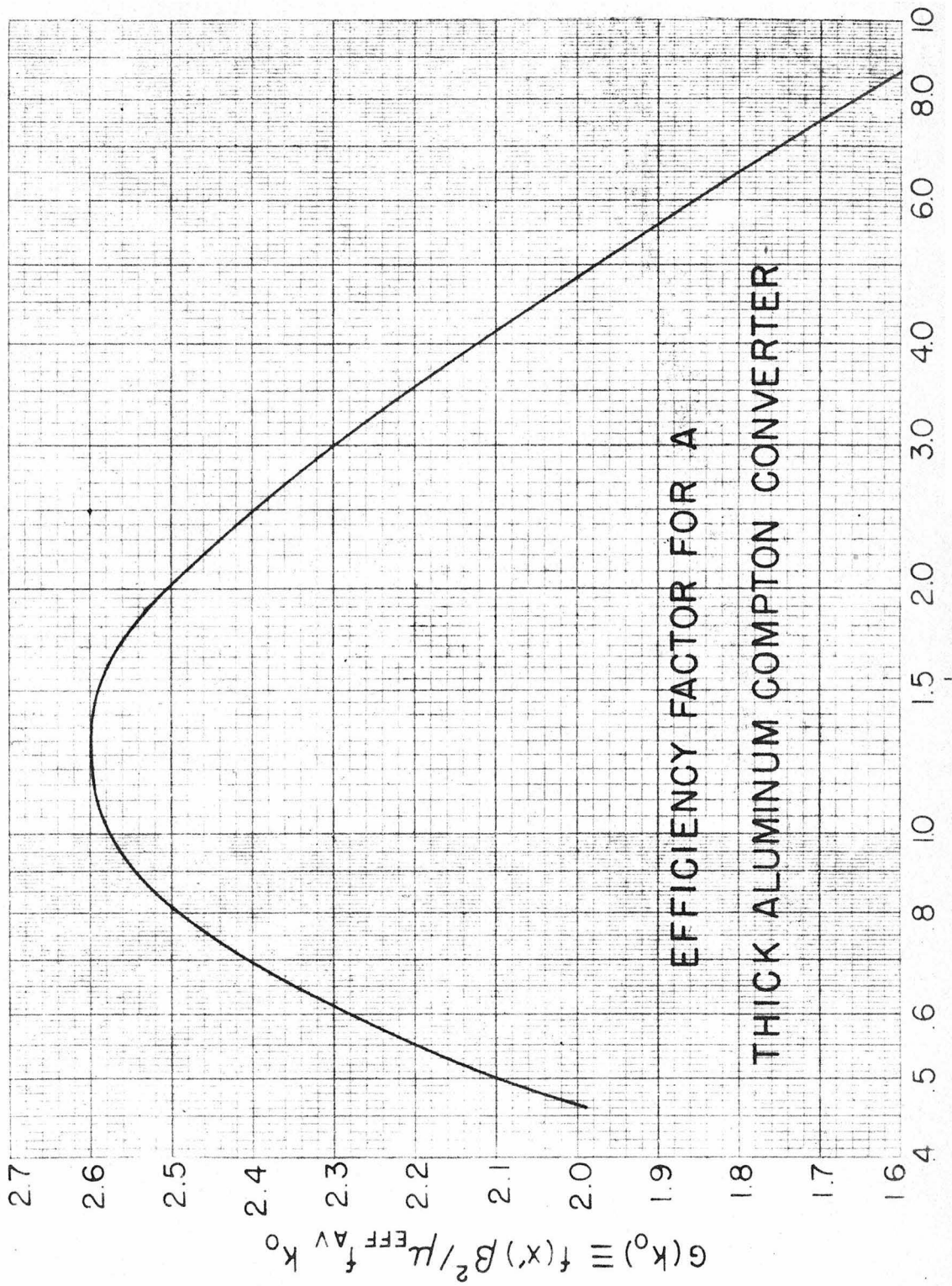
EFFICIENCY FACTOR FOR A
THICK ALUMINUM COMPTON CONVERTER
$G(k_o) \equiv f(x')\beta^2/\mu_{EFF} f_{AV} k_o$
k_o (MEV)
2.7
2.6
2.5
2.4
2.3
2.2
2.1
2.0
1.9
1.8
1.7
1.6
.4
.5
.6
8
10
1.5
2.0
3.0
4.0
6.0
8.0
10

FIG. (35)

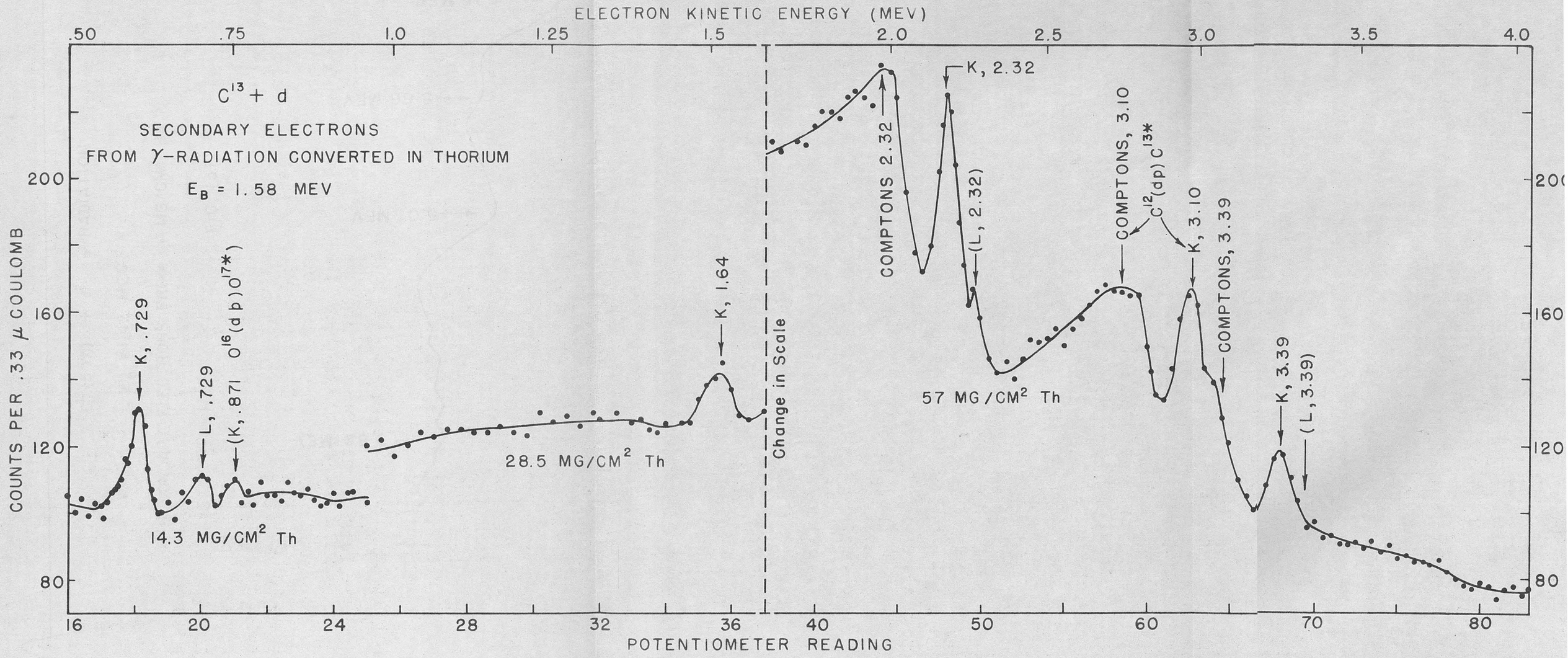
ELECTRON KINETIC ENERGY (MEV)
.50
.75
1.0
1.25
1.5
2.0
2.5
3.0
3.5
4.0
C^{13} + d
SECONDARY ELECTRONS
FROM γ-RADIATION CONVERTED IN THORIUM
E_B = 1.58 MEV
COUNTS PER .33 μ COULOMB
200
160
120
80
K, .729
L, .729
(K, .871 $O^{16}(d\,p)O^{17*}$)
14.3 MG/CM² Th
28.5 MG/CM² Th
K, 1.64
Change in Scale
COMPTONS 2.32
K, 2.32
(L, 2.32)
57 MG/CM² Th
COMPTONS, 3.10
$C^{12}(dp)C^{13*}$
K, 3.10
COMPTONS, 3.39
K, 3.39
(L, 3.39)
16
20
24
28
32
36
40
50
60
70
80
POTENTIOMETER READING

FIG. (36)

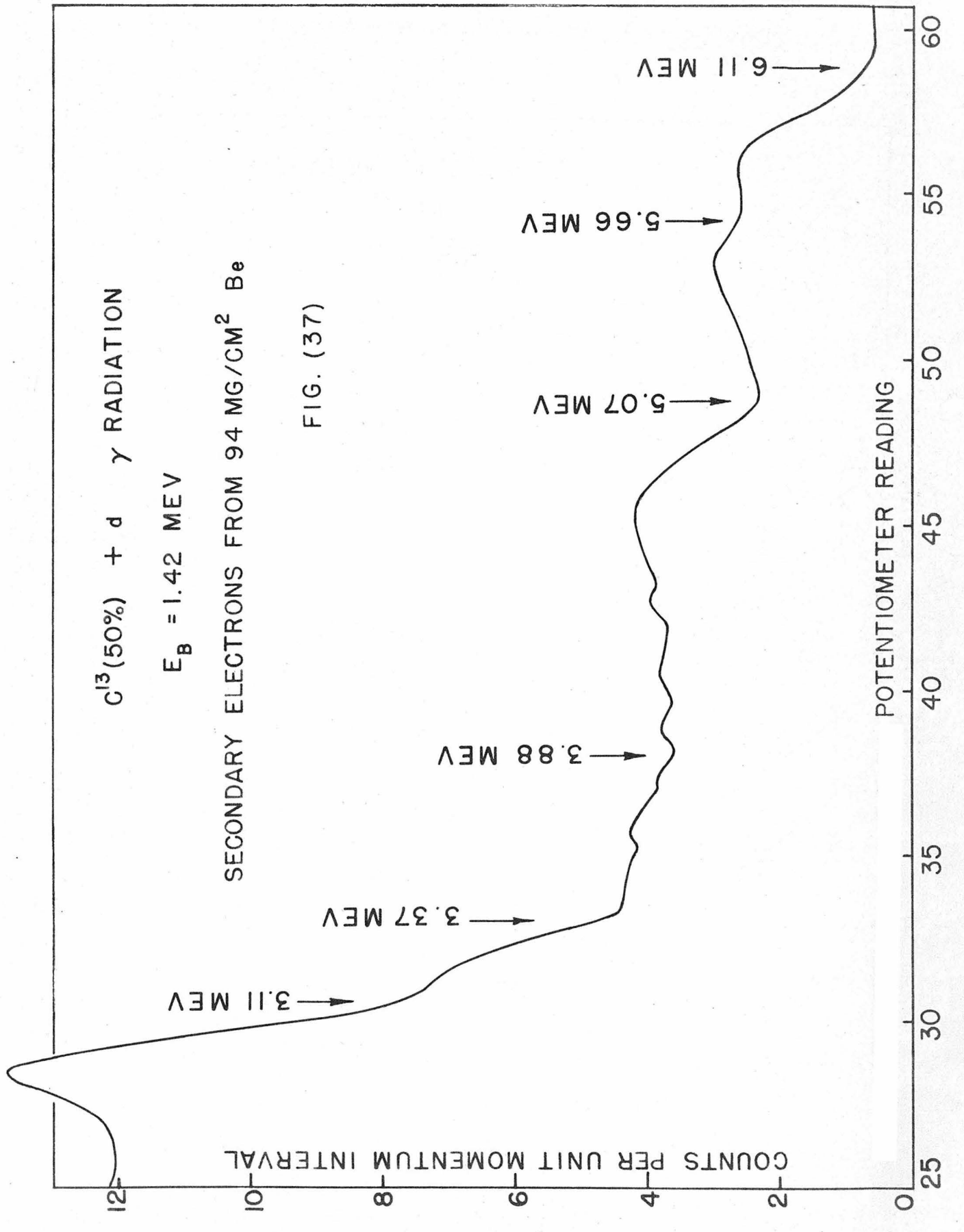
C^{13}(50%) + d γ RADIATION
E_B = 1.42 MEV
SECONDARY ELECTRONS FROM 94 MG/CM² Be
FIG. (37)
3.11 MEV
3.37 MEV
3.88 MEV
5.07 MEV
5.66 MEV
6.11 MEV
COUNTS PER UNIT MOMENTUM INTERVAL
POTENTIOMETER READING
0
2
4
6
8
10
12
25
30
35
40
45
50
55
60

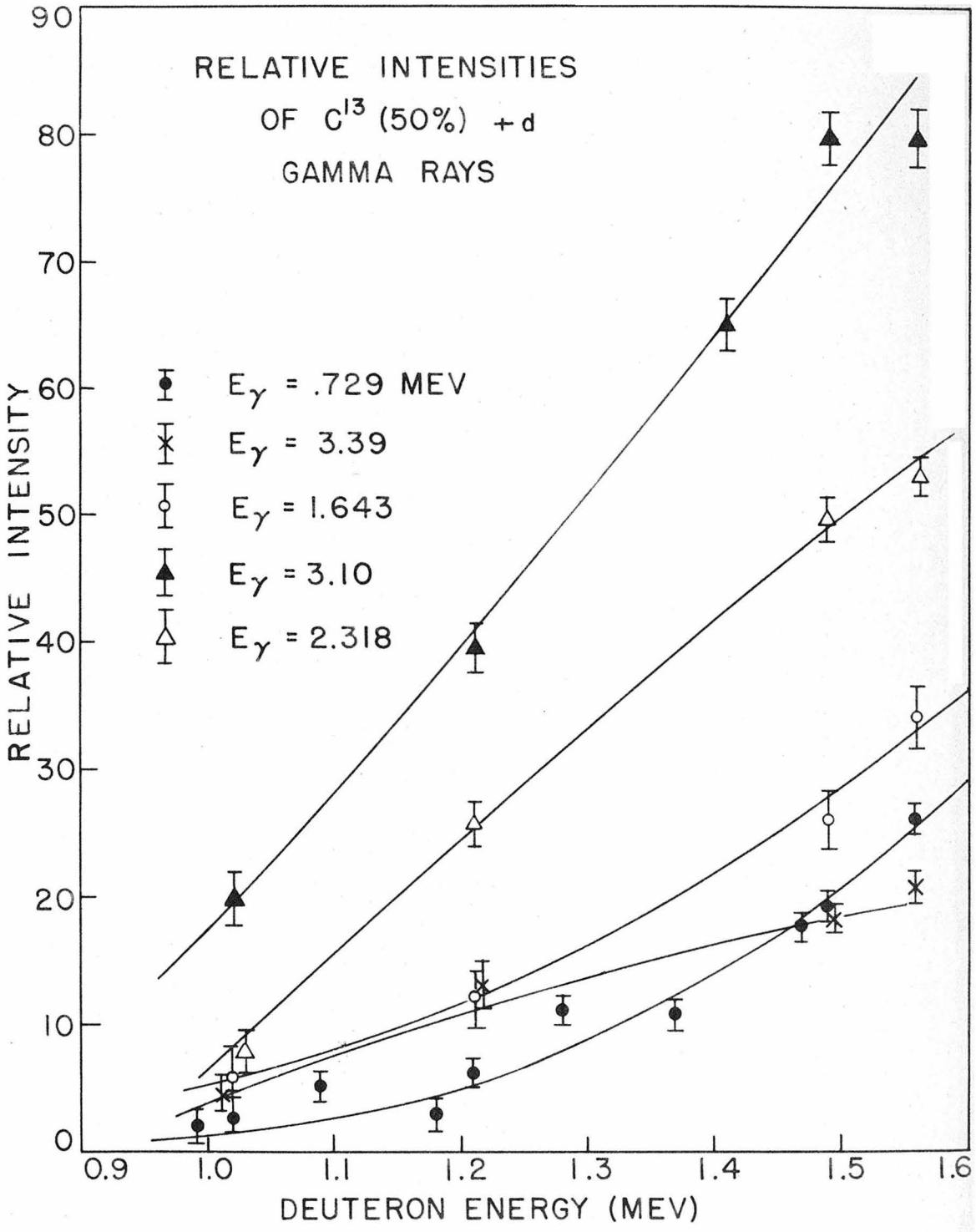
RELATIVE INTENSITIES
OF C13 (50%) + d
GAMMA RAYS
Eγ = .729 MEV
Eγ = 3.39
Eγ = 1.643
Eγ = 3.10
Eγ = 2.318
RELATIVE INTENSITY
DEUTERON ENERGY (MEV)
0
10
20
30
40
50
60
70
80
90
0.9
1.0
1.1
1.2
1.3
1.4
1.5
1.6

FIG.(39)

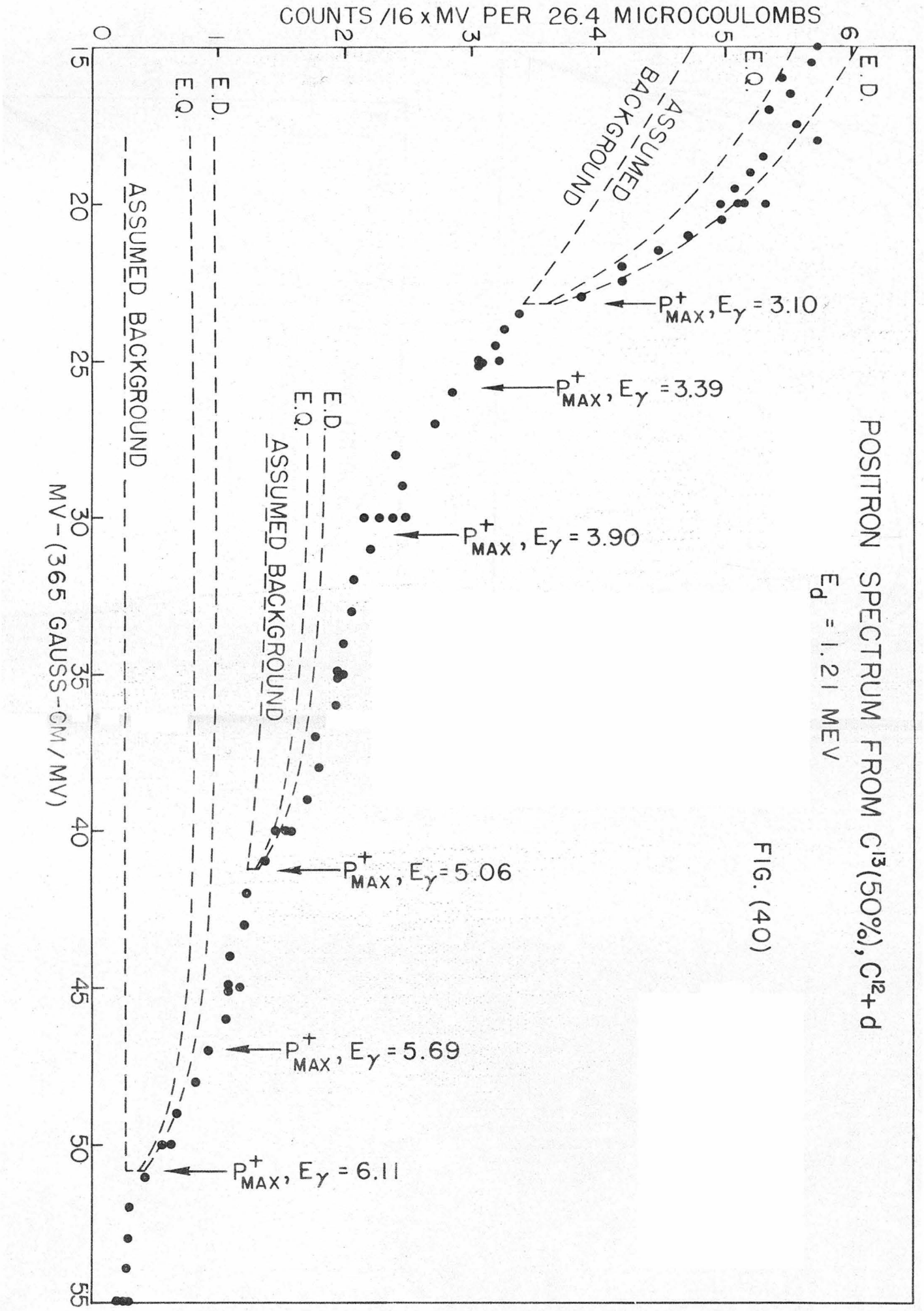
POSITRON SPECTRUM FROM C^{13}(50%), C^{12}+ d
E_d = 1.21 MEV
COUNTS /16 x MV PER 26.4 MICROCOULOMBS
0
1
2
3
4
5
6
E.D.
E.Q.
ASSUMED BACKGROUND
P^+_{MAX}, E_γ = 3.10
P^+_{MAX}, E_γ = 3.39
P^+_{MAX}, E_γ = 3.90
P^+_{MAX}, E_γ = 5.06
P^+_{MAX}, E_γ = 5.69
P^+_{MAX}, E_γ = 6.11
E.D.
E.Q.
ASSUMED BACKGROUND
E.D.
E.Q.
ASSUMED BACKGROUND
15
20
25
30
35
40
45
50
55
MV-(365 GAUSS-CM / MV)

FIG. (40)

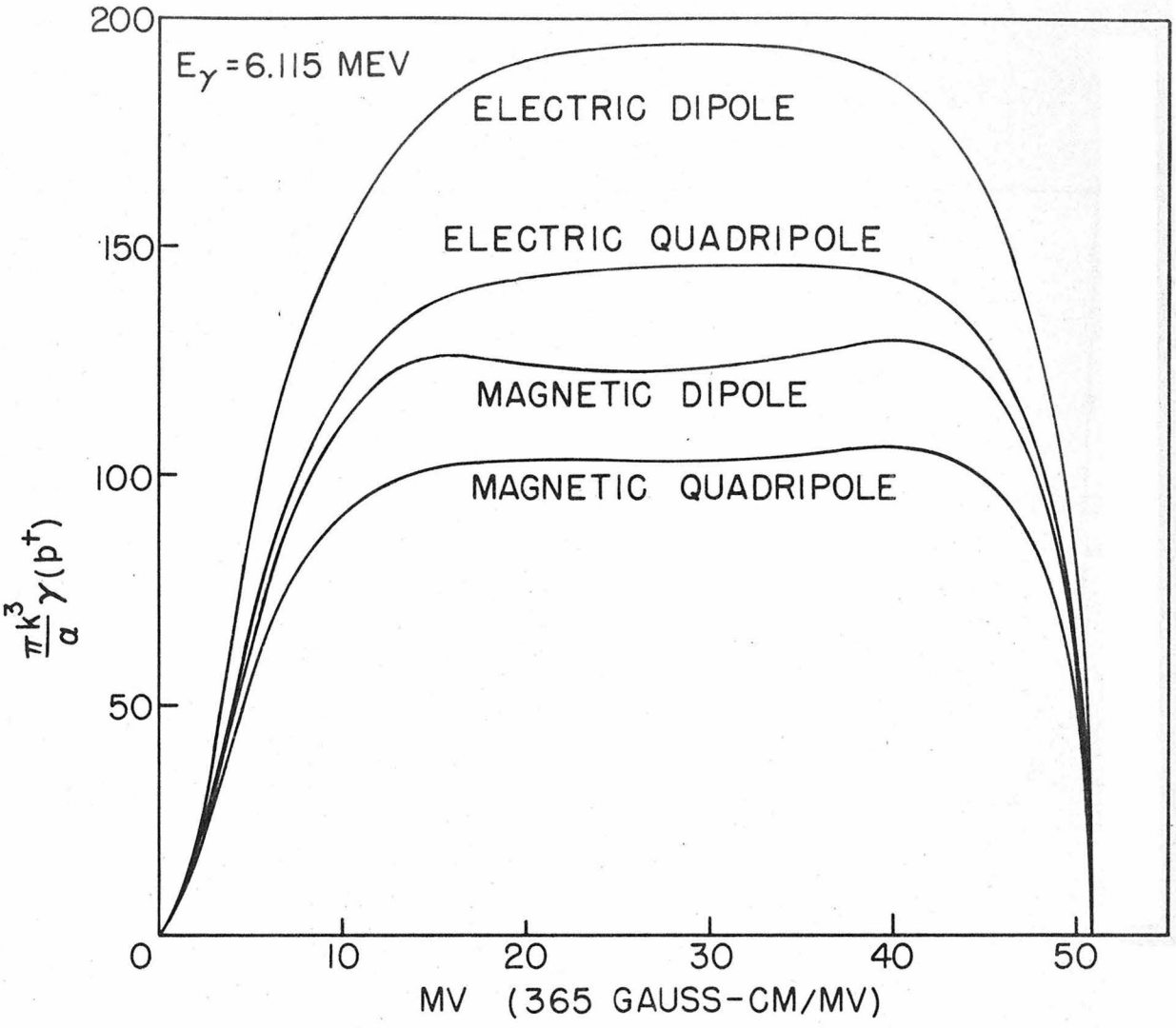

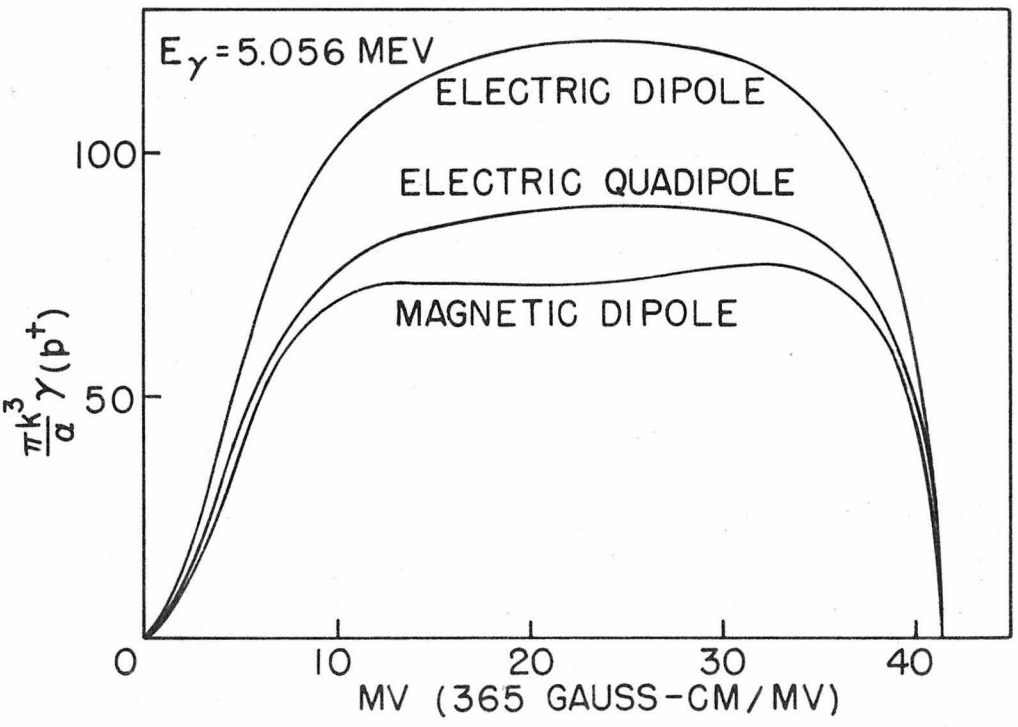

FIG. (41) INTERNAL PAIR-FORMATION MOMENTUM DISTRIBUTIONS

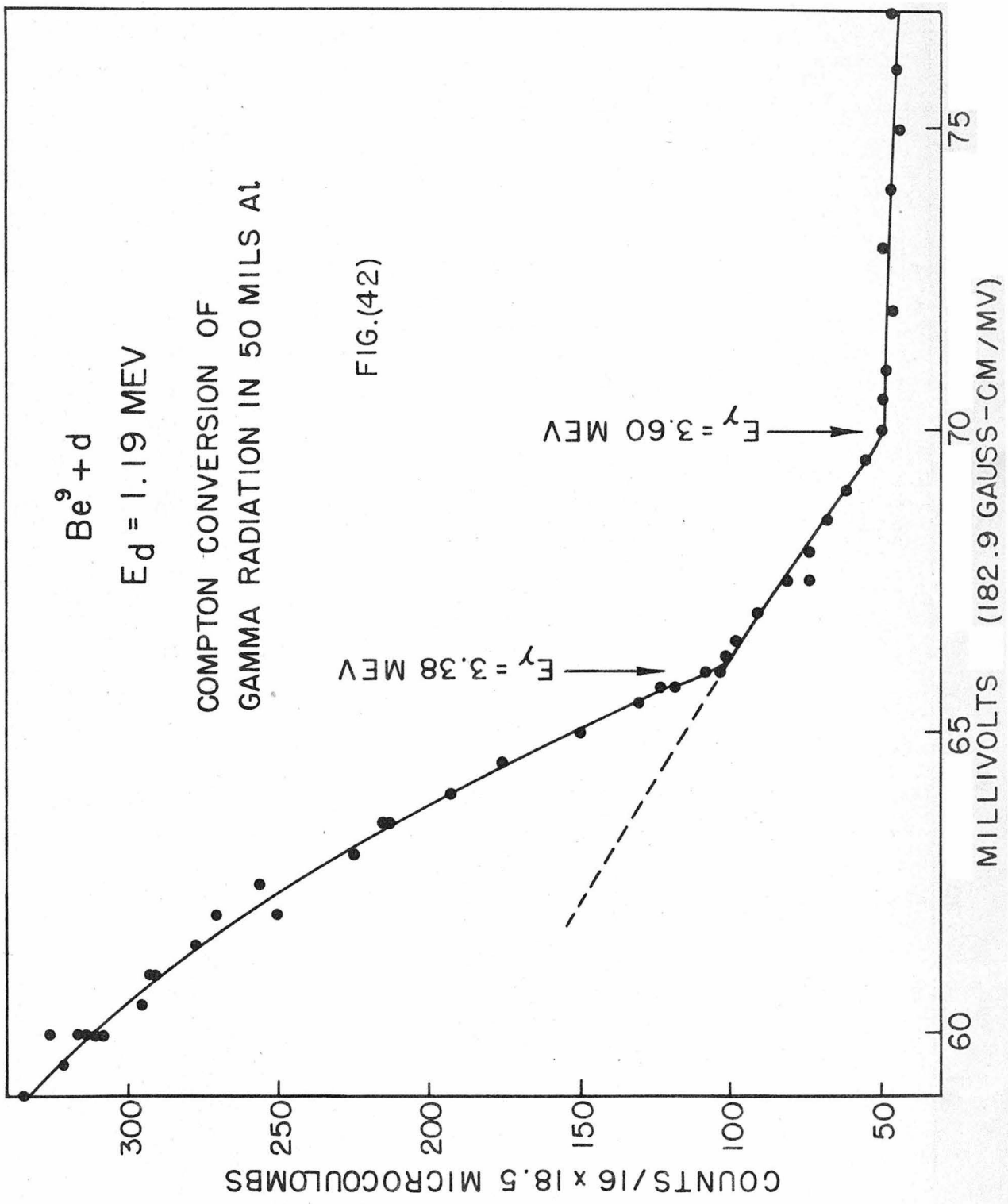
$Be^9 + d$
E_d = 1.19 MEV
COMPTON CONVERSION OF
GAMMA RADIATION IN 50 MILS Al
E_γ = 3.38 MEV
E_γ = 3.60 MEV
COUNTS/16 x 18.5 MICROCOULOMBS
300
250
200
150
100
50
60
65
70
75
MILLIVOLTS (182.9 GAUSS-CM/MV)

FIG.(42)

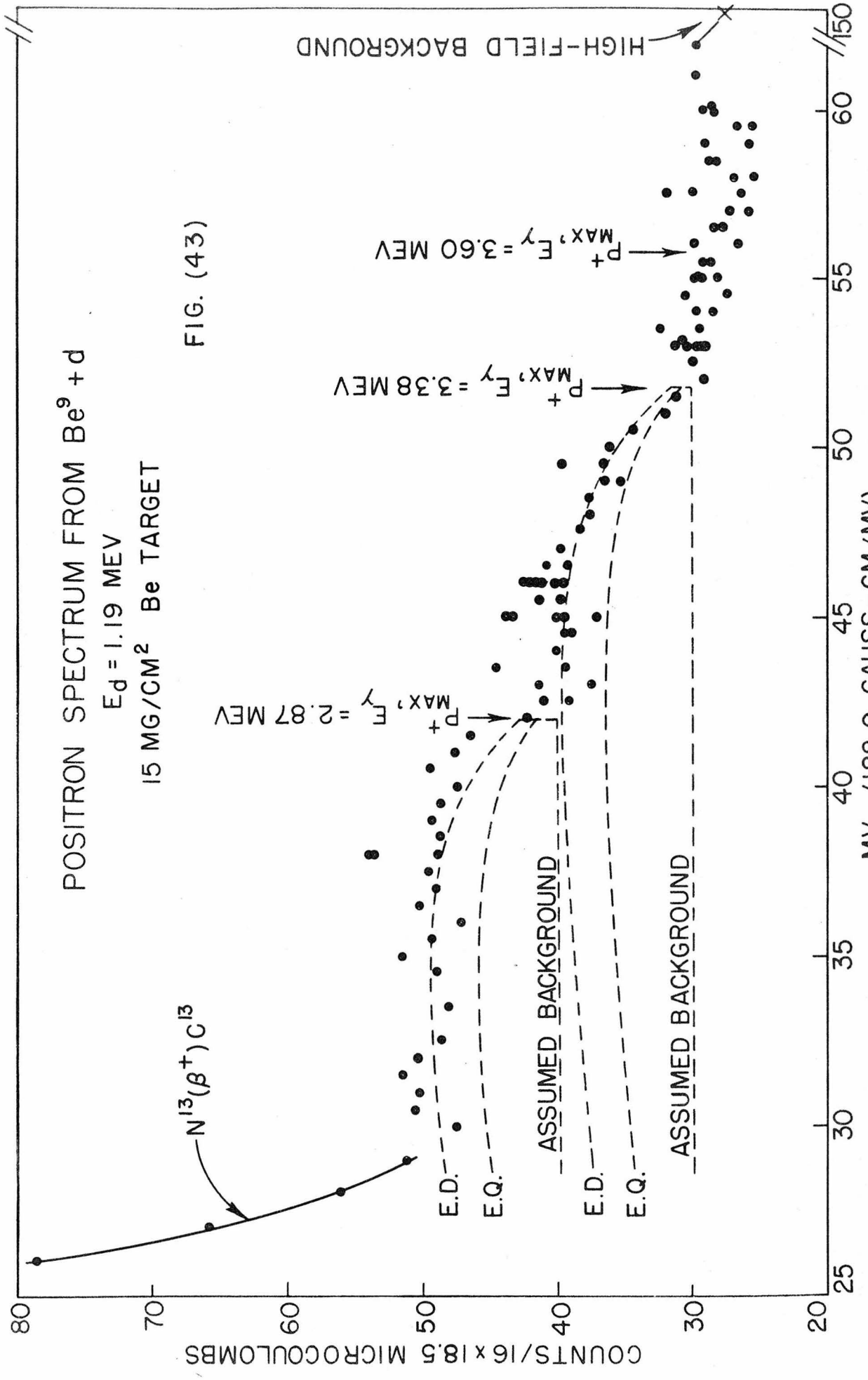
POSITRON SPECTRUM FROM $Be^9 + d$
E_d = 1.19 MEV
15 MG/CM² Be TARGET
FIG. (43)
P^+_{MAX}, E_γ = 3.60 MEV
P^+_{MAX}, E_γ = 3.38 MEV
P^+_{MAX}, E_γ = 2.87 MEV
HIGH-FIELD BACKGROUND
$N^{13}(\beta^+)C^{13}$
E.D.
E.Q.
ASSUMED BACKGROUND
E.D.
E.Q.
ASSUMED BACKGROUND
COUNTS/16 x 18.5 MICROCOULOMBS
MV (182.9 GAUSS-CM/MV)
80
70
60
50
40
30
20
25
30
35
40
45
50
55
60
150

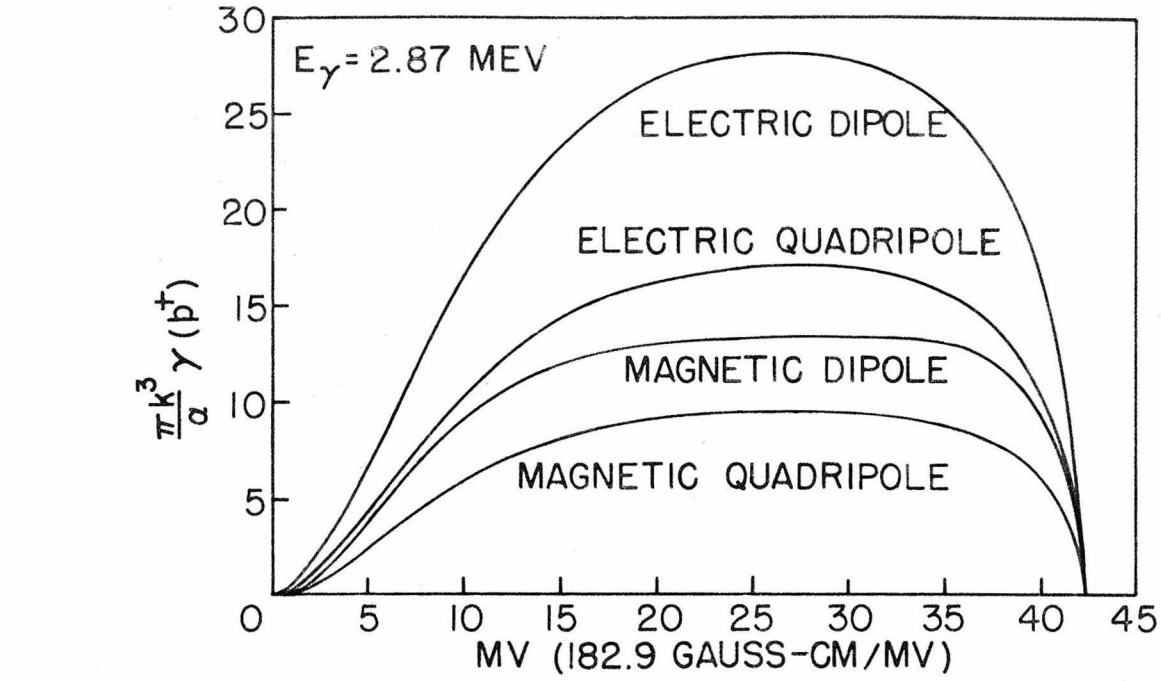

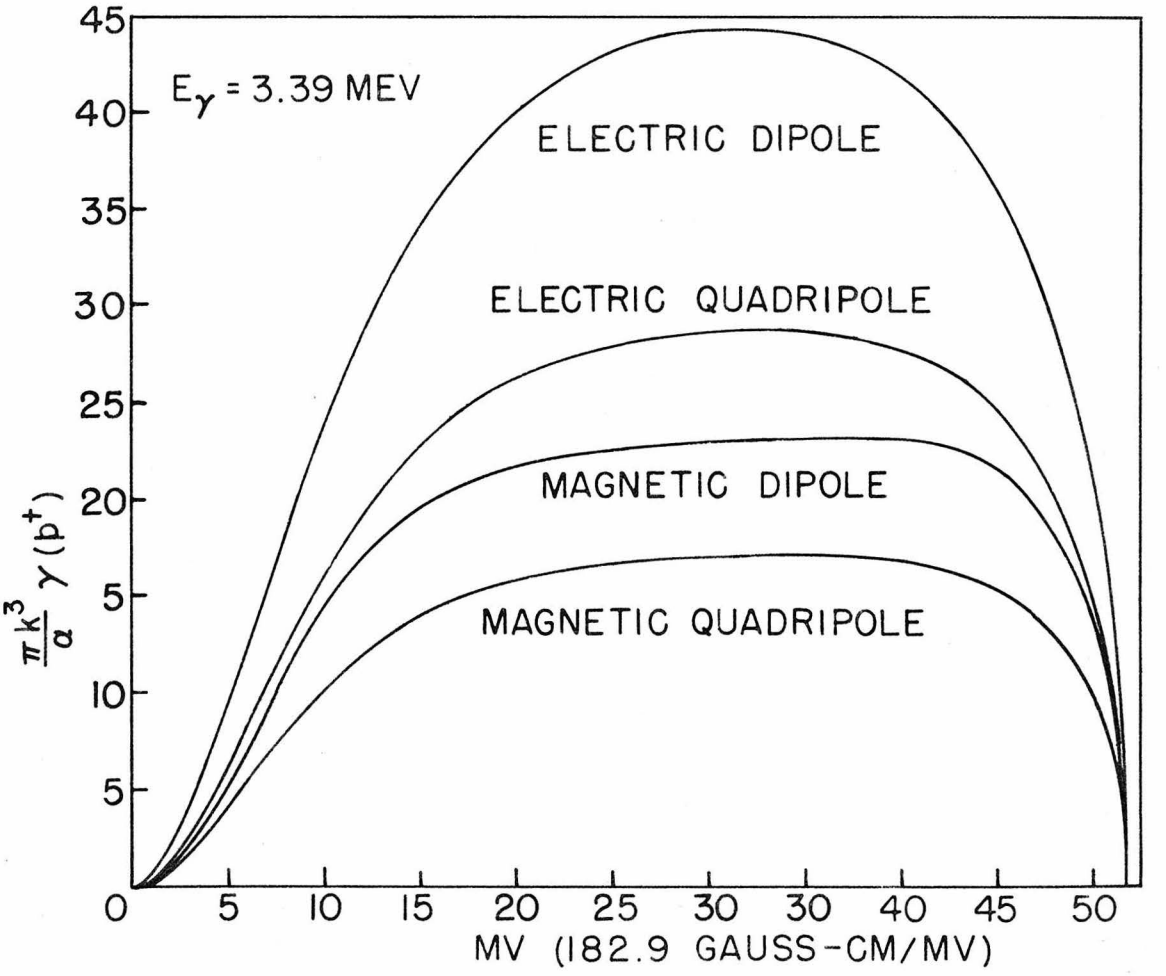

FIG.(44) INTERNAL PAIR-FORMATION MOMENTUM DISTRIBUTIONS

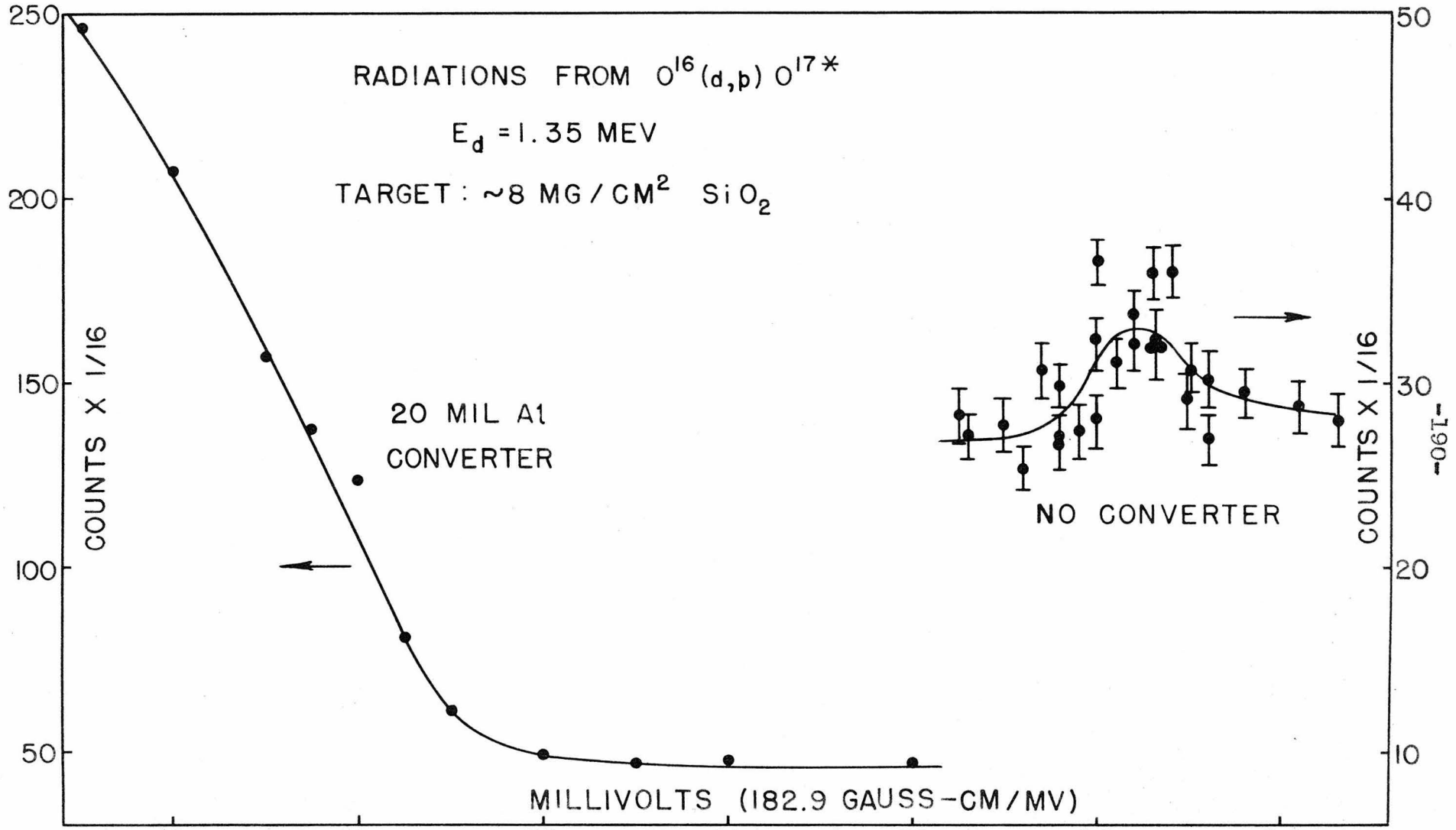
RADIATIONS FROM $O^{16}(d,p)\,O^{17*}$
E_d = 1.35 MEV
TARGET : ~8 MG / CM^2 SiO_2
20 MIL Al
CONVERTER
NO CONVERTER
COUNTS X 1/16
COUNTS X 1/16
MILLIVOLTS (182.9 GAUSS-CM/MV)
250
200
150
100
50
50
40
30
20
10
18
19
20
21
22
23
24

FIG. (45)

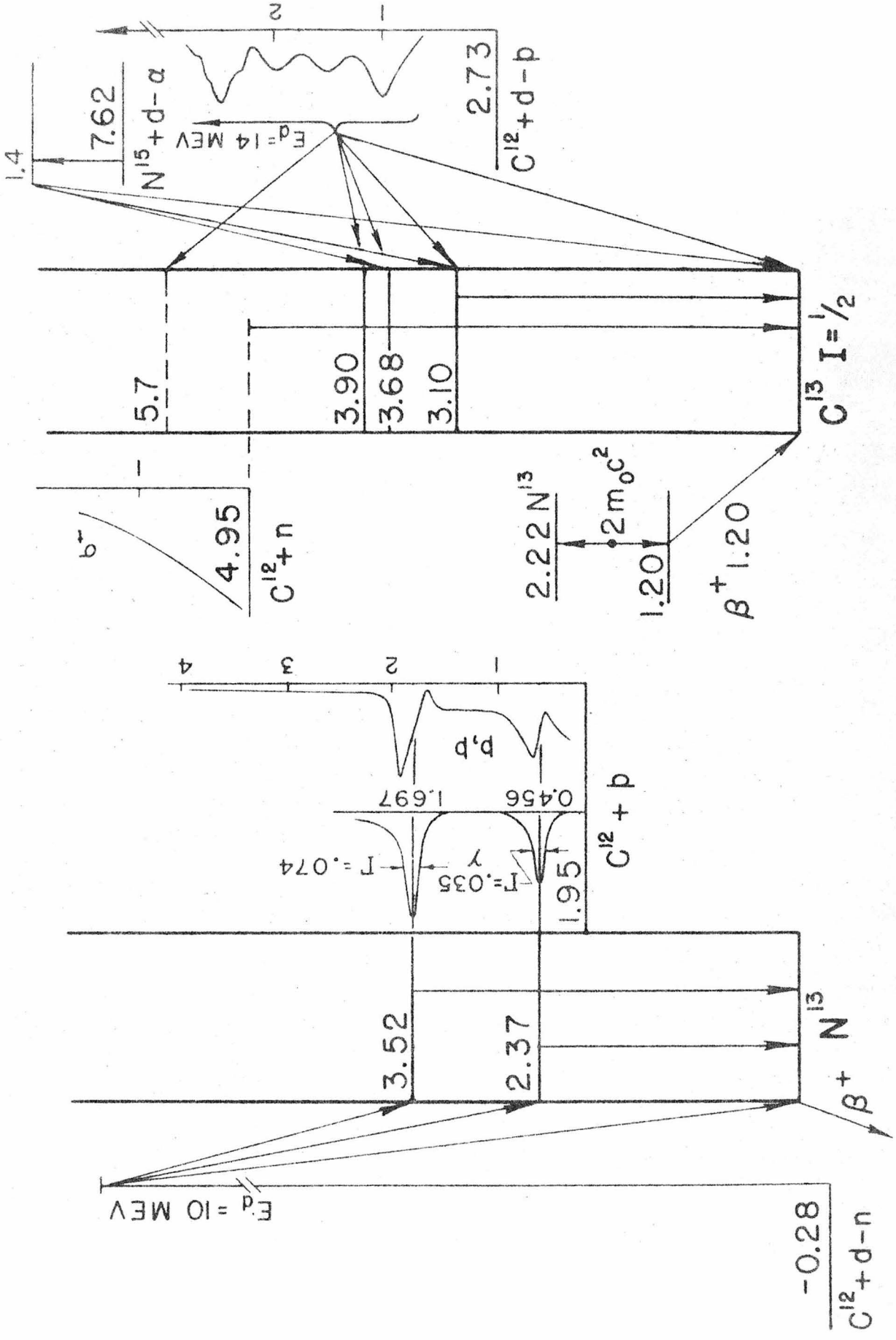

FIG. (I) ENERGY LEVELS OF C^{13} AND N^{13} BELOW 6 MEV

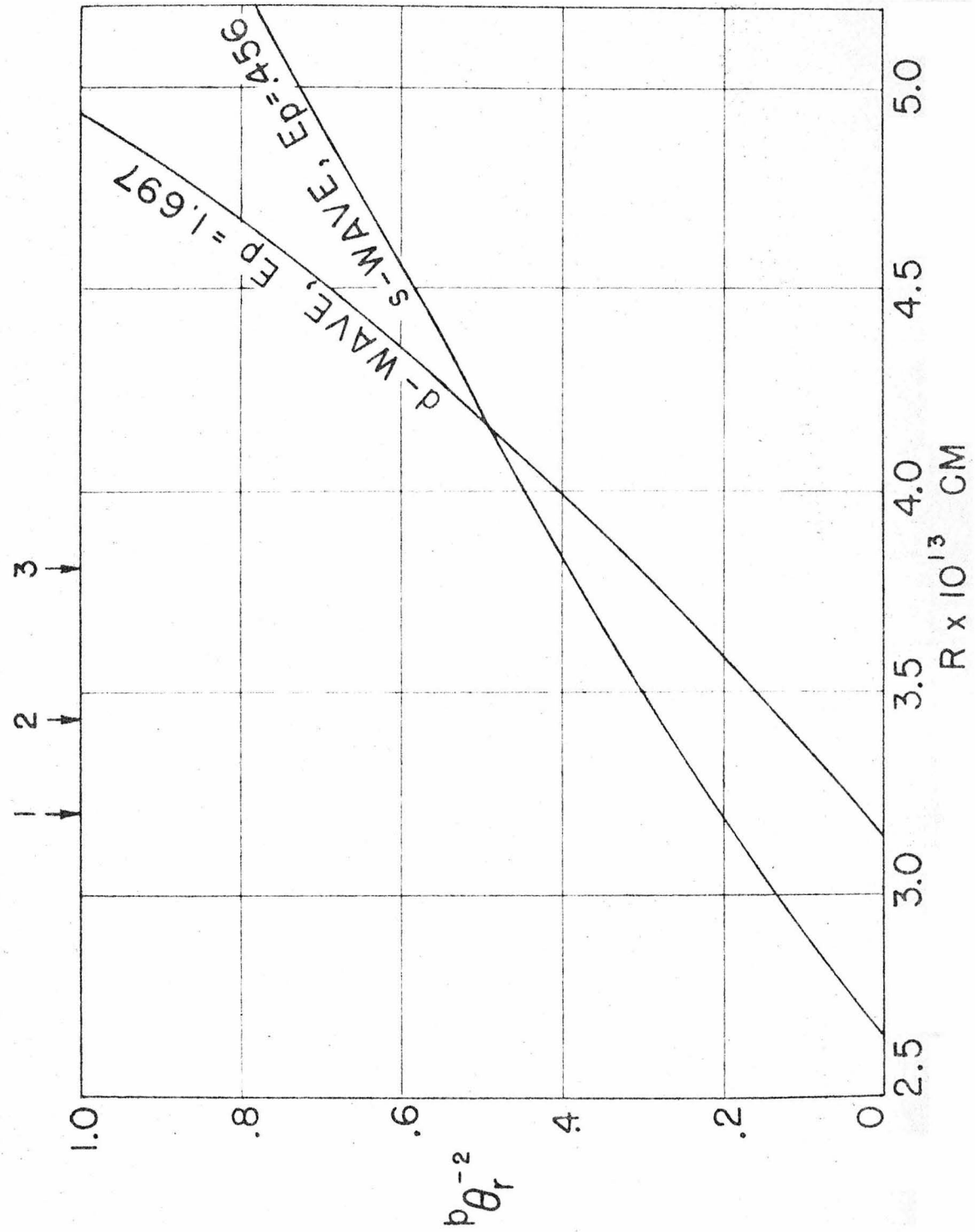

Fig. (2). Reciprocal of the reduced widths as a function of radius of the C^{12} + p resonances. Nuclear radii obtained in various ways are indicated at the top of the graph: 1) Neutron scattering at 95 Mev (DeJuren and Knable, Phys. Rev. 77, 606 (1950)); 2) From the ground-state Coulomb energy difference, $R_c = 1.46\ A^{1/3} \times 10^{-13}$ cm; 3) Neutron scattering at 25 Mev (Feshbach and Weisskopf, Phys. Rev 76, 1550 (1949))

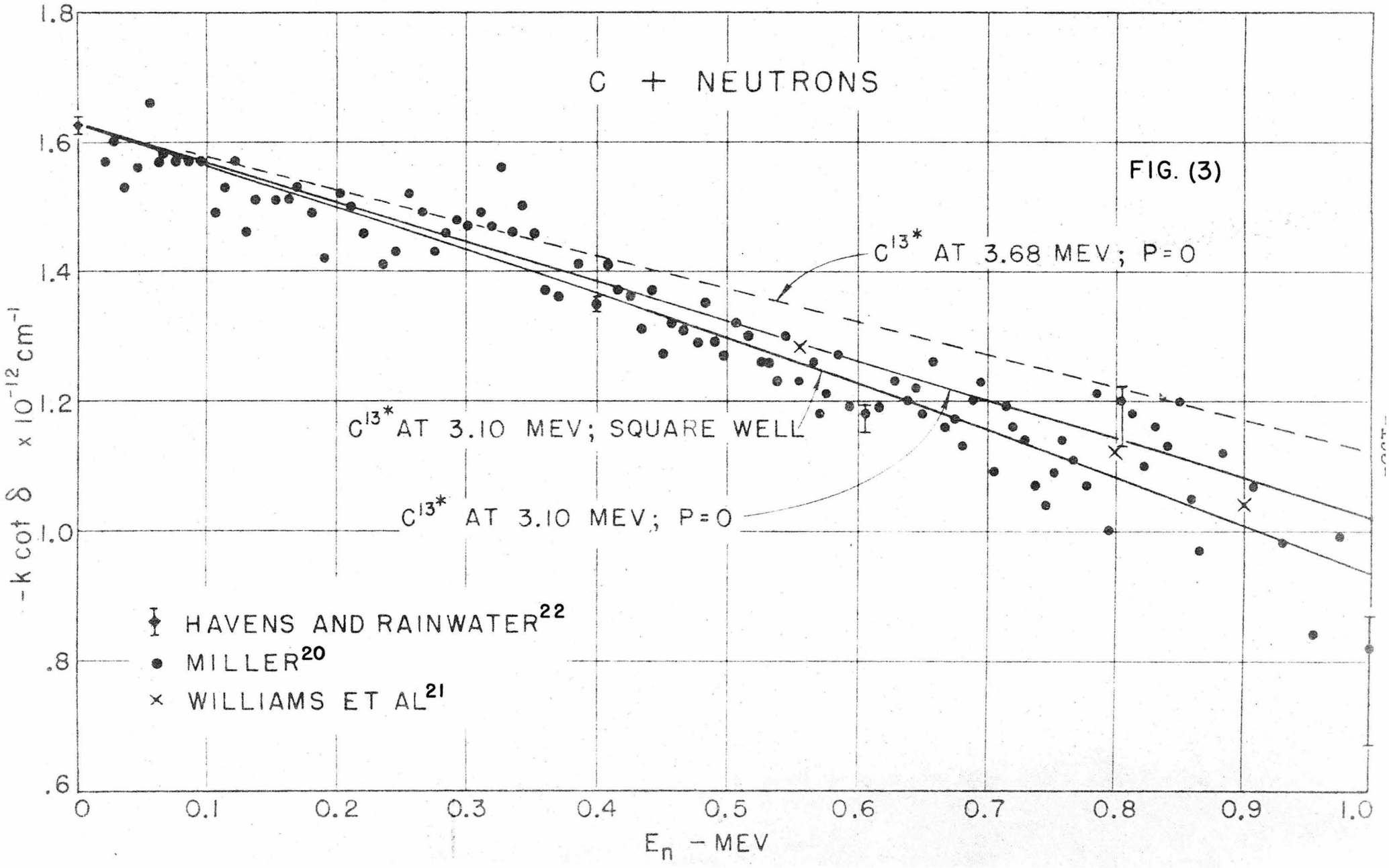
C + NEUTRONS
FIG. (3)
C13* AT 3.68 MEV; P=0
C13* AT 3.10 MEV; SQUARE WELL
C13* AT 3.10 MEV; P=0
HAVENS AND RAINWATER22
MILLER20
WILLIAMS ET AL21
-k cot δ x 10-12 cm-1
En - MEV
1.8
1.6
1.4
1.2
1.0
.8
.6
0
0.1
0.2
0.3
0.4
0.5
0.6
0.7
0.8
0.9
1.0

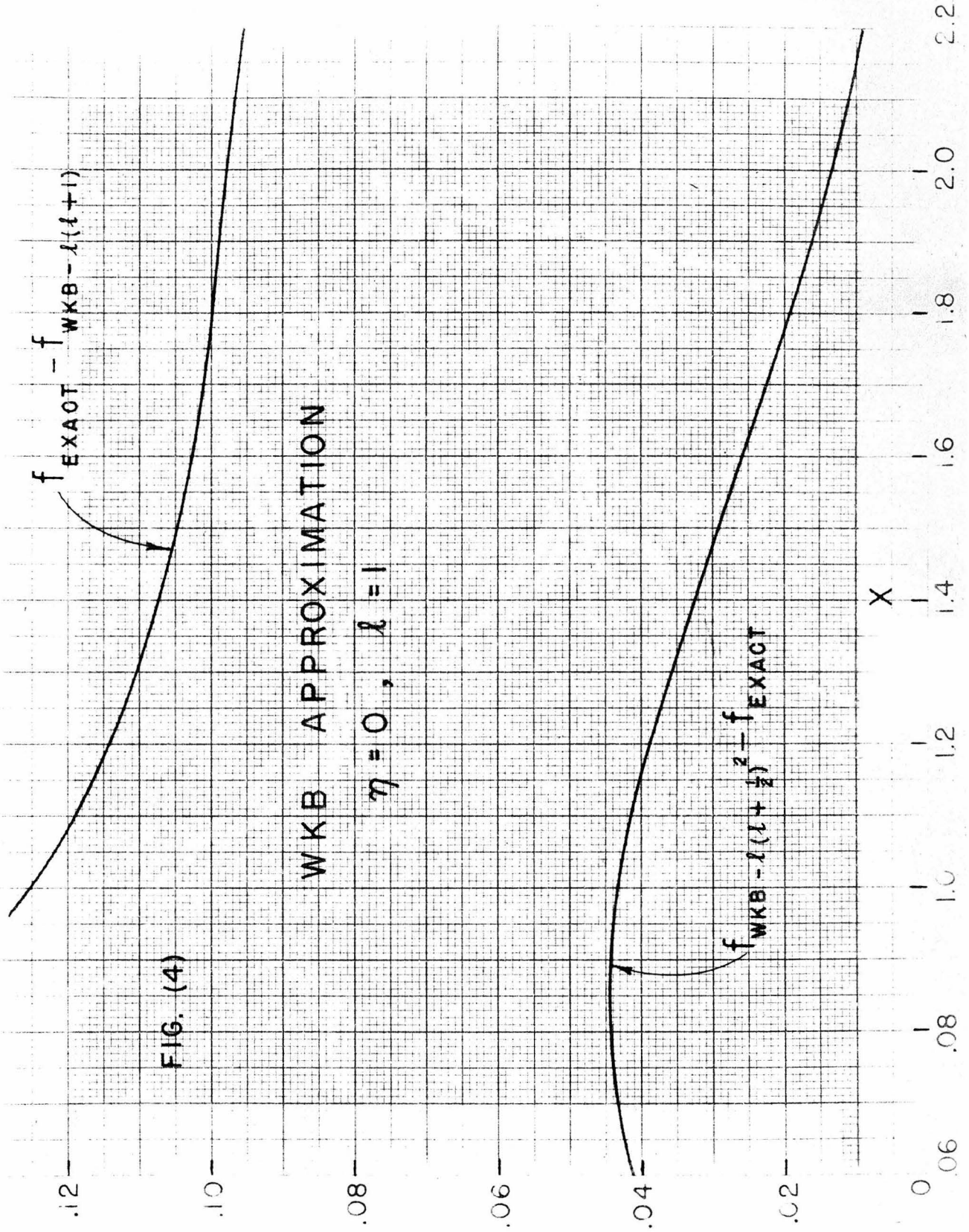
WKB APPROXIMATION
$\eta = 0$, $l = 1$
$f_{EXACT} - f_{WKB - l(l+1)}$
$f_{WKB - l(l+\frac{1}{2})^2} - f_{EXACT}$
X
.12
.10
.08
.06
.04
.02
0
.06
.08
1.0
1.2
1.4
1.6
1.8
2.0
2.2

FIG. (4)

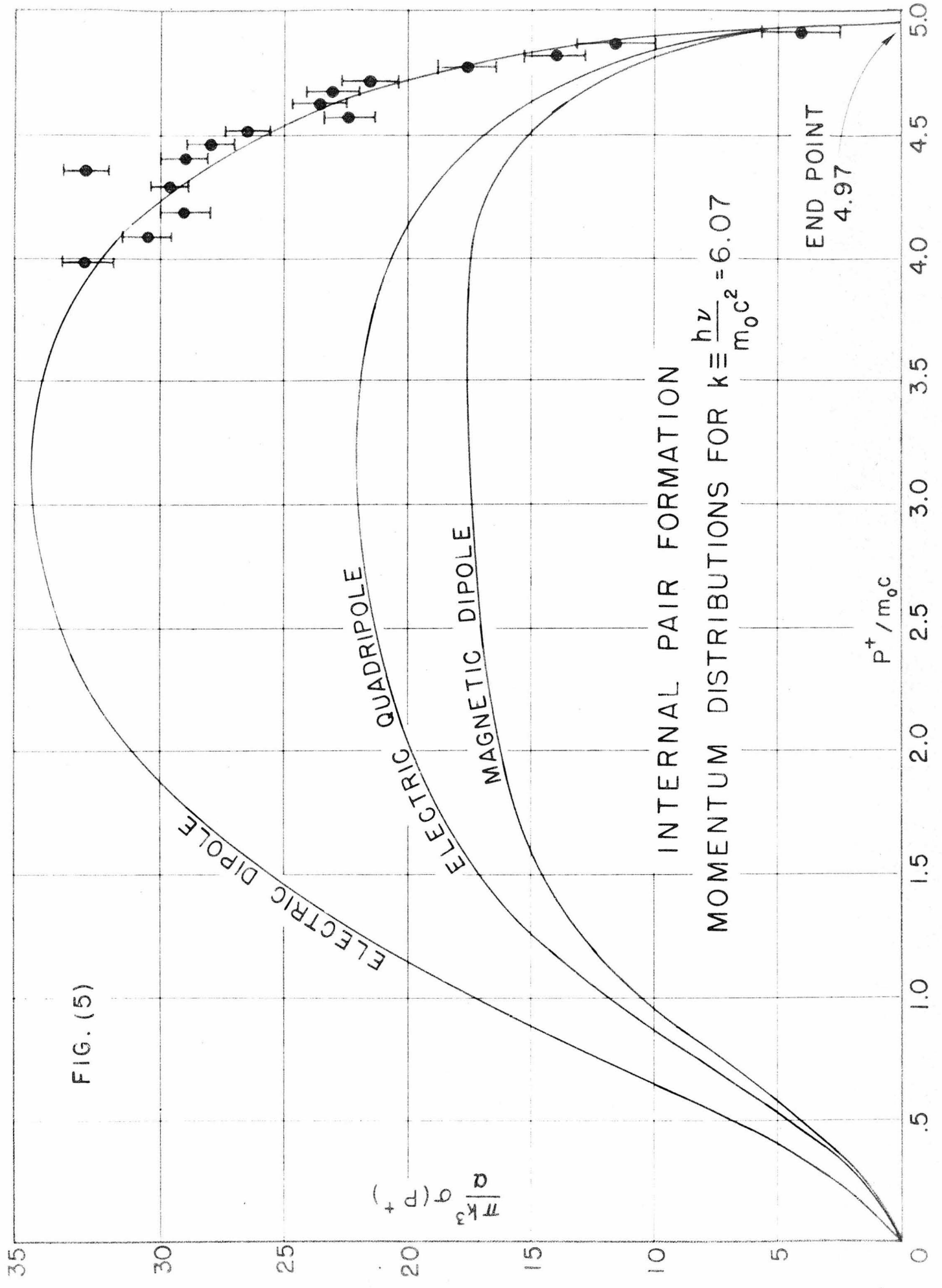
INTERNAL PAIR FORMATION
MOMENTUM DISTRIBUTIONS FOR $k \equiv \frac{h\nu}{m_0c^2} = 6.07$
ELECTRIC DIPOLE
ELECTRIC QUADRIPOLE
MAGNETIC DIPOLE
END POINT
4.97
$\frac{\pi k^2}{\alpha} q(P^+)$
P^+/m_0c
0
5
10
15
20
25
30
35
.5
1.0
1.5
2.0
2.5
3.0
3.5
4.0
4.5
5.0

FIG. (5)

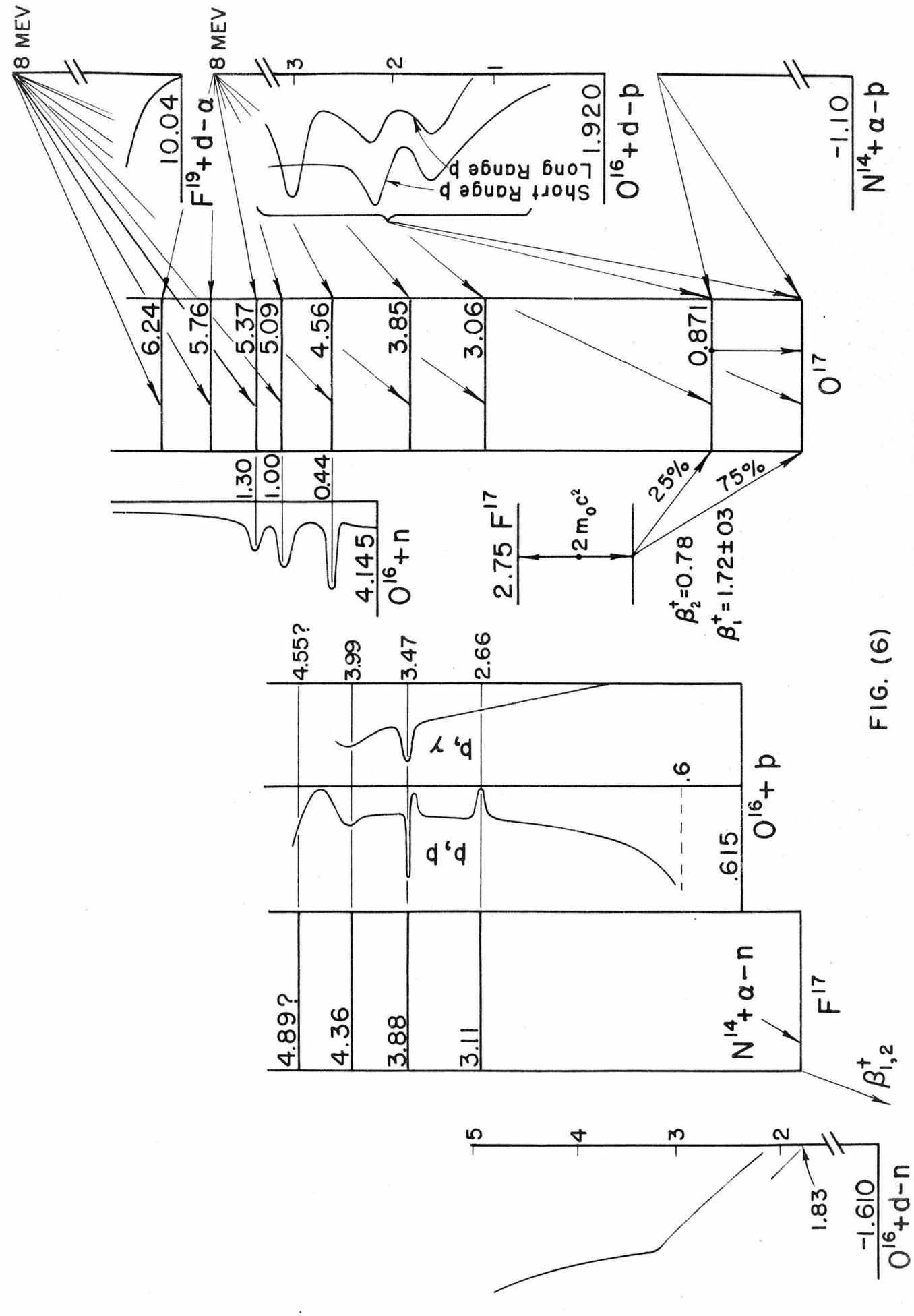
8 MEV
10.04
$F^{19}+d-\alpha$
8 MEV
3
2
1
Short Range p
Long Range p
1.920
$O^{16}+d-p$
-1.10
$N^{14}+\alpha-p$
6.24
5.76
5.37
5.09
4.56
3.85
3.06
0.871
O^{17}
1.30
1.00
0.44
4.145
$O^{16}+n$
2.75 F^{17}
$2m_oc^2$
25%
75%
$\beta_2^+=0.78$
$\beta_1^+=1.72\pm03$
4.55?
3.99
3.47
2.66
p, γ
.6
p, p
.615
$O^{16}+p$
4.89?
4.36
3.88
3.11
$N^{14}+\alpha-n$
F^{17}
$\beta_{1,2}^+$
5
4
3
2
1.83
-1.610
$O^{16}+d-n$

FIG. (6)

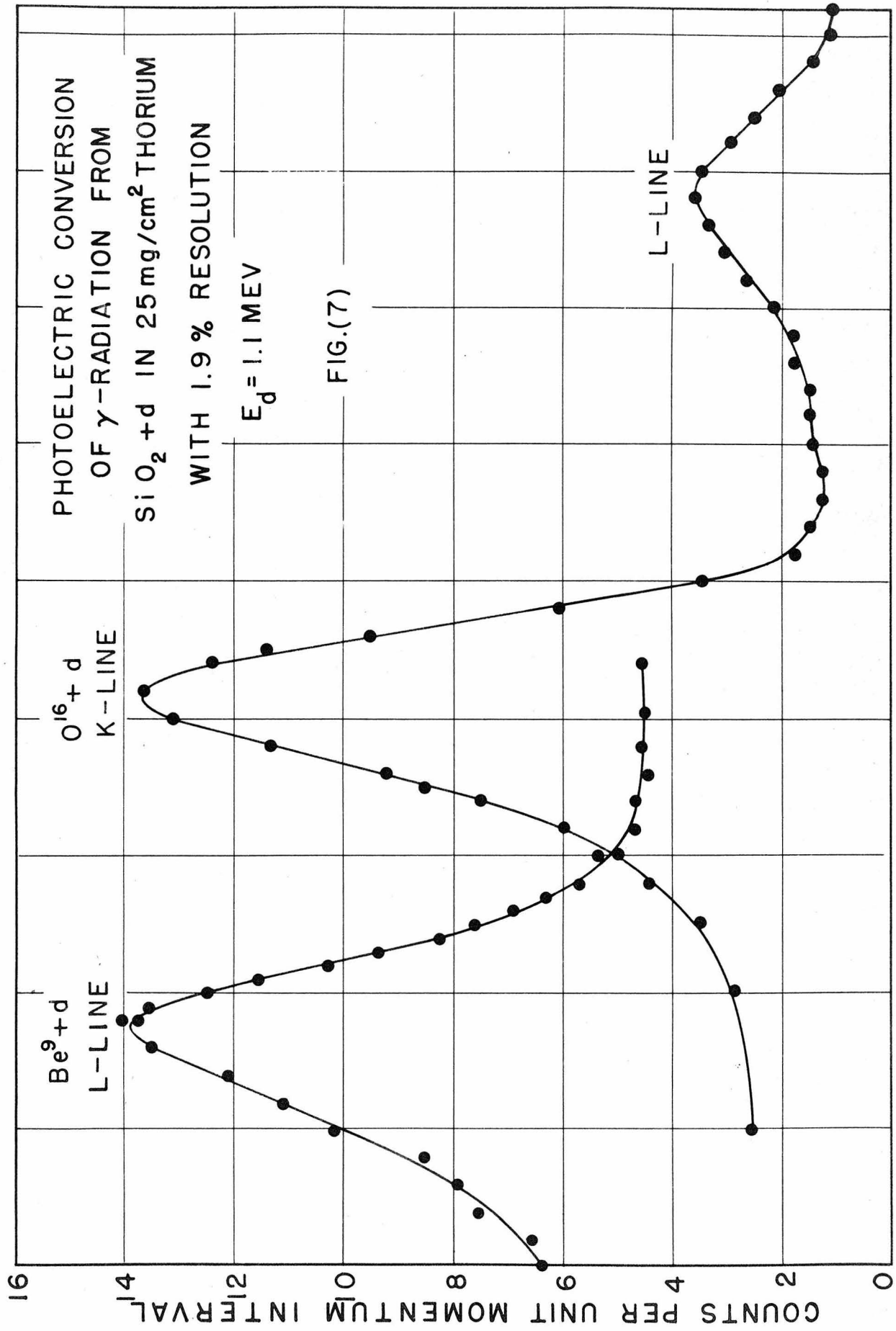
PHOTOELECTRIC CONVERSION
OF γ-RADIATION FROM
Si O2 +d IN 25 mg/cm² THORIUM
WITH 1.9 % RESOLUTION
Ed = 1.1 MEV
FIG.(7)
Be9+d
L-LINE
O16+ d
K-LINE
L-LINE
COUNTS PER UNIT MOMENTUM INTERVAL
POTENTIOMETER READING
0
2
4
6
8
10
12
14
16
19.0
19.5
20.0
20.5
21.0
21.5
22.0
22.5
23.0
23.5

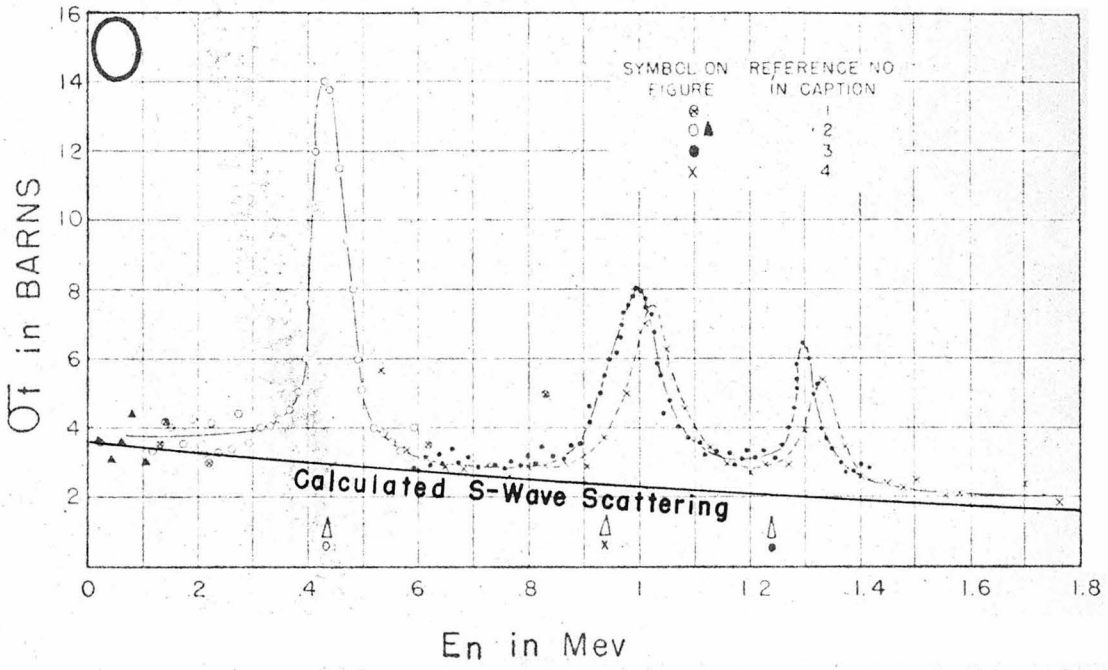

FIG. 8 (1) Fields, Russell, Sachs, and Wattenberg, Phys. Rev. 71, 508 (1947). (2) Adair, Barschall, Bockelman, and Sala, Phys. Rev. 75, 1124 (1949). (3) C. K. Bockelman (unpublished). (4) Freier, Fulk, Lampi, and Williams, Phys. Rev. 78, 508 (1950).

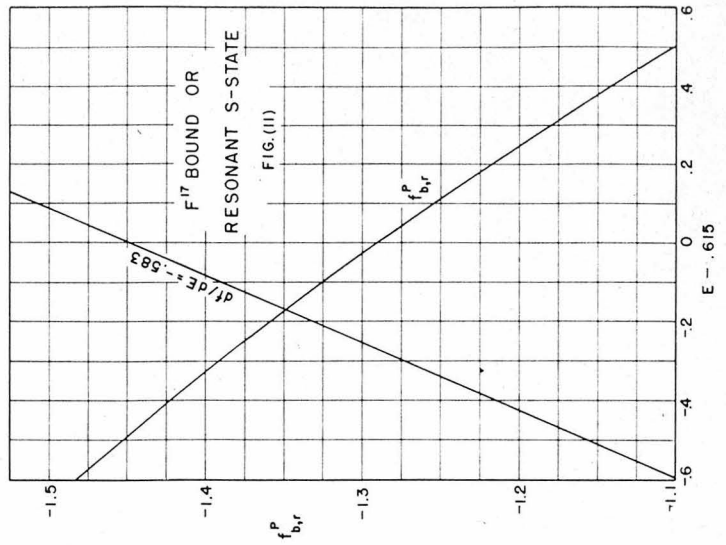
F17 BOUND OR
RESONANT S-STATE
FIG.(11)
df/dE = -.583
$f^P_{b,r}$
E - .615

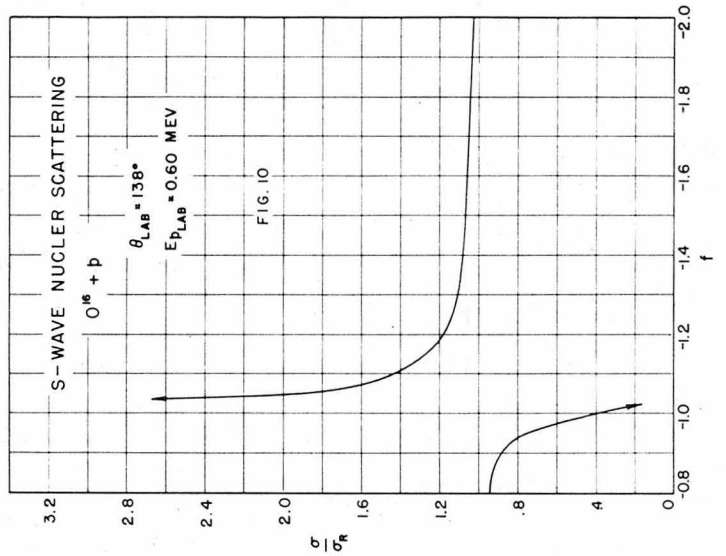
S-WAVE NUCLER SCATTERING
O16 + p
θLAB = 138°
EpLAB = 0.60 MEV
FIG. 10
σ/σR
f

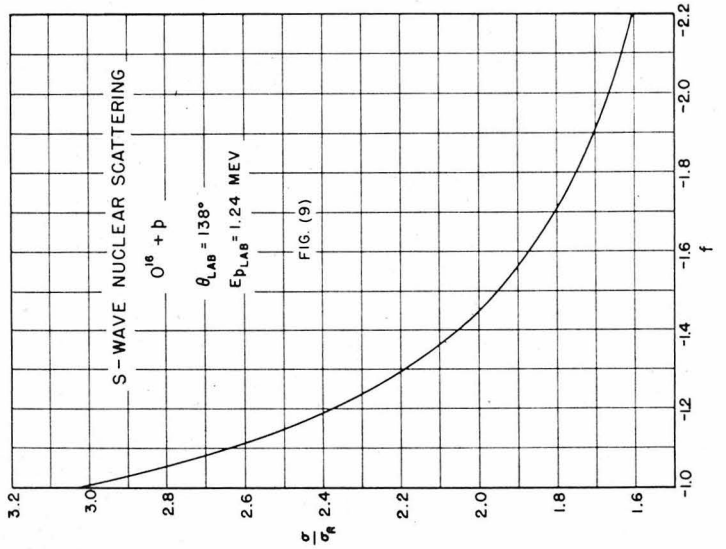
S-WAVE NUCLEAR SCATTERING
O16 + p
θLAB = 138°
EpLAB = 1.24 MEV
FIG. (9)
σ/σR
f